Design of a Sustainable Surveillance UAV Led by a Turbopropeller

Final Report - Group 9

B.P. Dorca	4279115
A. Engelke	4204840
E.M.Fernandez-Santoro	4293967
T. Haex	4217535
L.P.J. Hikspoors	4279670
N.K. Kirov	4278879
R.J. Molenaar	4280814
R.N.M. Riepe	4299604
D. Risselada	4150724
M.M. Smeenk	4282299

Delft University of Technology

TU Delft Delft University of Technology

Challenge the future

PREFACE

This paper is the final report of the DSE project of group 9 of the faculty of Aerospace Engineering at Delft University of Technology. The scope of this project is the design of an unmanned aircraft vehicle propelled by a micro-turbine engine for remote monitoring of power stations and pipelines. Though this report has been done by university students, it would be useful for further research in the ever increasing field of civil UAVs.

The aim of this project is: ***To design a micro-gas turbine propelled UAV with a payload of up to 50kg. As well as having an endurance of 20 hours at a cruise speed of 100km/h, the UAV will be remotely controllable at long distance. Moreover, the socio-economic benefits, the environmental footprint and the sustainability connected to the life-cycle of the UAV will be investigated.***

We would like to thank Dr. ir. M. Pini for his invaluable insight into this topic, as well as Dr. M.D. Pavel, Ir. O. Stroosma and Drs. W. Vogel, for their guidance proved extremely useful.

Delft, June 28, 2016, DSE Group 9

B.P. Dorca 4279115
A. Engelke 4204840
E.M.Fernandez-Santoro 4293967
T. Haex 4217535
L.P.J. Hikspoors 4279670
N.K. Kirov 4278879
R.J. Molenaar 4280814
R. Riepe 4299604
D. Risselada 4150724
M. M. Smeenk 4282299

SUMMARY

Natural resources such as oil and gas are crucial aspects of most of the world's economies. Most countries have extensive networks of pipelines to transport resources as it decreases drastically the freight expenses. Currently, daily manned aircraft are used to monitor pipelines. However, these are expensive and potentially dangerous to human life. Such missions need to be carried out at very low altitudes and only visible effects can be detected. Pipelines are often located in remote areas; missions require experienced pilots that need to be able to fly, in some cases, during extremely challenging atmospheric conditions. Any potential misdetection can result in the rupture of pipelines, with fires that could spread to developed areas, becoming a real hazard for the people nearby. This is especially important in wide countries such as Russia and Canada with a large number of power stations and pipelines. In other words, the current solutions for monitoring pipelines are dangerous and inefficient.

The use of Unmanned Aerial Vehicles (UAV) can improve this process making it more economic, safer, more precise and less fuel consuming. It is for this reason a team of 10 students designed a new UAV, called SCULPTUR (Surveillance Civil UAV Led by Propeller-based Gas Turbines), to perform this pipeline surveillance. Designed to endure a 20 hour mission, with a cruise speed of 100 km/h and a payload of 50 kg, containing a long wave infrared camera, this UAV radically changes the way surveillance of pipelines is done.

The payload, specifically chosen to perform a surveillance mission in Australia, is capable of taking high resolution images of pipelines above and underground, with electro optical and infrared cameras. These are send down linked with a high data rate and stored internally for later analysis. The UAV itself flies autonomously waypoint to waypoint, while monitored by operators on base.

The design focuses on two major goals, being more sustainable and being more cost economic. It is because of this the engine design is done focusing on reducing specific fuel consumption, emissions and noise. With a total fuel usage of 87.7 kg in the whole mission and the engine being in the nose, this indeed succeeded well. Combined with low production costs and very good performance in terms of recycling, due to the thermoplastic composite material chosen for producing the UAV, SCULPTUR succeeds in performing its mission. With a final take-off weight of 403.5 kg, well within the budget with an optimised lightweight structure, and clever layout and design, using slender wings and an inverted Y-tail, SCULPTUR allows for more stable and precise aerial surveillance. The aerodynamic design, the control soft- and hardware and the low vibrating engine ensure stable and remote controlled flight at all times, improving surveillance more than any other alternative. In case of emergency SCULPTUR is always capable of landing safely, by the use of an emergency parachute. This reduces the operating risk and the impact on the environment a lot during an emergency. This all comes for a total price of US$3,341,000, making SCULPTUR the choice in remote pipeline surveillance.

CONTENTS

NOMENCLATURE

α	Angle of attack	[rad]
β	Sideslip angle	[rad]
U_1	Ground speed	$[\frac{m}{s}]$
Γ_{VT}	V-tail anhedral angle	[rad]
$\Gamma_{VT_{scr}}$	Aircraft angle at screen height	[°]
δ_a	Aileron deflection	[rad]
δ_e	Elevator deflection	[rad]
δ_r	Rudder deflection	[rad]
ϵ	Downwash angle at the V-tail section location	[rad]
η_h	Horizontal tail efficiency	[-]
η_p	Propulsive efficiency	[-]
θ	Pitch angle	[rad]
Λ	Wing sweep at 25%	[rad]
λ	Wavelength	[m]
Λ_{ht}	Horizontal tail sweep at 25%	[rad]
Λ_{vt}	Vertical tail sweep at 25%	[rad]
λ	Taper ratio wing	[-]
λ_{ht}	Taper ratio horizontal tail	[-]
λ_{vt}	Taper ratio vertical tail	[-]
ρ	Air density	$[\frac{kg}{m^3}]$
ϕ_1	bank angle at which steady state roll rate is reached	[rad]
A	Aspect ratio	[-]
A_d	Aspect ratio of the diagonal tail	[-]
A_{VT}	V-tail aspect ratio	[m]
B	Transmission bandwidth	$[Hz]$
b_{RV}	ruddervator span	[°]
B_h	Horizontal tail span	[ft]
B_w	Wing span	[ft]
C	Channel capacity	$[\frac{bit}{s}]$
C_{D_R}	rolling drag coefficient	[-]
$C_{D_{0_h}}$	Zero-lift drag coefficient of the tail	[-]
$C_{D_{0_w}}$	wing zero-lift drag coefficient	[-]
C_D	Drag coefficient	[-]
$C_{D_{L_w}}$	Wing drag coefficient due to the lift	[-]
$C_{D_{total}}$	Drag coefficient of the total UAV	[-]
$C_{D_{wing}}$	Wing drag coefficient	[-]
C_ℓ	Stability derivative for the moment in around the X axis direction	[-]
C_{f_w}	Turbulent flat plate friction coefficient of the wing	[-]
C_L	Lift coefficient	[-]
C_ℓ	Rolling moment coefficient	[-]
$C_{L_{design}}$	Average lift coefficient during cruise	[-]
C_{L_h}	Horizontal tail lift coefficient	[-]
C_{L_w}	Lift coefficient of the wing	[-]
C_m	Stability derivative for the moment in around the Y axis direction	[-]
$C_{M_{0_f}}$	Zero-lift moment coefficient of the fuselage	[-]
$C_{M_{0_w}}$	Zero-lift moment coefficient of the wing	[-]
$C_{M_{0_{w+f}}}$	Zero-lift moment coefficient of the wing-fuselage combination	[-]
$C_{m_{airfoil}}$	Moment coefficient of the airfoil	[-]
$\frac{dC_{M_w}}{dCL_w}$	Slope of the moment coefficient of the wing	[-]
$C_{M_{w+f}}$	Combined moment coefficient of wing and fuselage	[-]
C_n	Stability derivative for the moment in around the Z axis direction	[-]
cr	Climb rate	$[\frac{m}{s}]$
C_X	Stability derivative for the force in X direction	[-]
C_Y	Stability derivative for the force in Y direction	[-]
C_Z	Stability derivative for the force in Z direction	[-]
D	Fuselage structural depth	[ft]
$\frac{dC_{M_{w+f}}}{dC_L}$	Slope of the wing-fuselage moment coefficient graph	[-]
e_d	oswald factor of the diagonal tail	[-]
e_w	Oswald factor of the wing	[-]
e_h	Oswald factor of the tail	[-]
F	Noise figure	[–]
H_t	Horizontal tail height above fuselage	[ft]
H_v	Vertical tail height above fuselage	[ft]
L'	Airfoil thickness location parameter	[-]
L_h	Moment around the x-axis	$[N \cdot m]$
L_m	Main gear length	[in]
L_n	Nose gear length	[in]
ℓ_h	Horizontal tail arm	[m]
MAC	Mean Aerodynamic Chord	[m]

N	Noise power at receiver end	[W]
N_{en}	Number of engines	[-]
N_l	Ultimate landing load factor	[-]
N_t	Number of fuel tanks	[-]
N_z	Ultimate load factor	[-]
p	Roll rate	[rad/s]
P	Engine power	[W]
$\dot{P}$	roll acceleration	$[\frac{rad^2}{s}]$
P_{EIRP}	Effective Isentropic Radiated Power	$[\frac{bit}{s}]$
P_{Rx}	Power received	$[\frac{bit}{s}]$
P_{ss}	Steady state roll rate	$[\frac{rad}{s}]$
P_{Tx}	Power transmitted	$[\frac{bit}{s}]$
q	Pitch rate	[rad/s]
q	Dynamic pressure at cruise	[lb/ft^2]
r	Yaw rate	[rad/s]
R	Leading edge suction parameter	[-]
R_{LS}	Lifting surface correction factor	[-]
R_{LS_h}	Tail lifting surface correction factor	[-]
R_{wf}	Wing-fuselage interference factor	[-]
S	Signal power at receiver end	[W]
S	Wing surface area	[m^2]
S_f	Fuselage wetted area	[ft^2]
SFC	Specific fuel consumption	$[\frac{kg}{Ws}]$
S_{ht}	Horizontal tail area	[ft^2]
s_L	Landing distance	[m]
SM	Longitudinal stability margin	[-]
s_{to}	Take-off distance	[m]
S_{total}	Total lifting surface area of the UAV	[m^2]
S_{VT}	Surface area of inverted V-tail section	[m^2]
S_{vt}	Vertical tail area	[ft^2]
S_w	Trapezoidal wing area	[ft^2]
S_{wet_w}	Wing wetted area	[m^2]
T_{TO}	Engine thrust at take-off	[N]
$\frac{t}{c}$	Thickness to chord ratio	[-]
TOP	Take-off parameter	$[\frac{N}{m^2}]$
U_1	Ground speed	$[\frac{m}{s}]$
V_T	Total airspeed	$[\frac{m}{s}]$
V	True airspeed	[m/s]
V_h	Airspeed at horizontal tail	$[\frac{m}{s}]$
V_i	Integral tanks volume	[gal]
V_{s0}	Stall speed	$[\frac{m}{s}]$
V_t	Total fuel volume	[gal]
W_{dg}	Design gross weight	[lb]
W_{en}	Engine weight	[lb]
W_l	Landing design gross weight	[lb]
W_{press}	Weight penalty due to pressurisation	[lb]
W_{uav}	Uninstalled avionics weight	[lb]
$x_{ac_{w+f}}$	Aerodynamic centre of the wing-fuselage combination	[m]
x_{ac_w}	Aerodynamic centre of the wing	[m]
x_{ref}	The point about which the aerodynamic moment is computed	[-]
y_D	distance to drag center	[m]

1 INTRODUCTION

Natural resources such as oil and gas are crucial aspects of most of the world's economies. Most countries have extensive networks of pipelines to transport resources. Pipelines decrease the freight expenses of the transport of petroleum and natural gas drastically. They are out of sight of the general public and are an environmental friendly way to transport these products. There are two main types of energy pipelines: liquid petroleum and natural gas pipelines. Liquid petroleum pipeline networks transport a range of different liquids including crude oils and refined products. In the case of crude oil lines, there are two types of lines: gathering lines and transmission lines. Gathering lines are very small pipelines which can be found in the areas where crude oil is found deep within the earth. On the other hand, transmission lines are larger and bring the crude oil from the producing areas to refineries. Furthermore, refined petroleum products such as jet and diesel fuels or heating oil are brought, through the pipelines, from the refineries to terminals with storage. These are then loaded into trucks that deliver the products to gas stations and homes. Natural gas lines differ from oil lines as they deliver the gas directly to homes through the pipelines. In order to prevent accidents, these types of infrastructure need to be monitored regularly. Corrosion and third party damages can lead to incidents and accidents such as leaks and explosions which have negative impacts on the environment or can generate substantial safety issues, such as a pipeline explosion in Nigeria in 2005 that killed hundreds of people. The most important impact of pipeline failures is the consequence it has on national economies. The economic loss as well as energy loss is very dangerous. Such incidents can paralyse a whole sector of a country. Hence, it is clear that pipeline monitoring missions to ensure safety are vital for both oil and gas companies and governments. Currently, these monitoring missions are mainly performed by manned aircraft. However, they are very expensive and present a potential risk for the safety of the crew. A Need Statement may be found due to the high risk of pipeline leaks and their catastrophic impact on the environment. The need for better surveillance arises from the ageing of current pipelines, both above the ground and buried underneath[1]: ***Pipelines must be monitored to prevent incidents and accidents that may generate substantial safety issues for the environment.***

An opportunity to solve this need is the adoption of an unmanned aerial vehicle (UAV). It would permit these missions to be carried out with no human risk and to have extended endurance leading to cheaper missions. However, current UAV technologies use reciprocating engines which can not support the required endurance. It follows that a new design is needed. To solve this issue, a UAV propelled by a micro gas turbine engine is proposed. This can lead to a higher endurance due to its large power-to-weight ratio. Also, its low noise emissions and low vibrations will allow for better quality of observation. Hence, the aim of this project is:

To design a micro-gas turbine propelled UAV with a payload of up to 50kg. Which can have a range of 1800 kilometres, as well as having an endurance of 20 hours and an altitude of 1000 meters at a cruise speed of 100km/h. The UAV will be remotely controllable at long distance. Moreover, the socio-economic benefits, the environmental footprint and the sustainability connected to the life-cycle of the UAV will be investigated.

The structure of this report is as follows: Chapter 2 is an exploration study on the world of UAVs. This includes, among others, a classification of UAVs, an exploration on propulsion systems and a research into the current certifications available for civil UAVs. Chapter 3 contains the mission definition and design strategy. The possible missions are described and the functions of the UAV are determined; the certification and requirements are included as well. The approach for sustainability, risk, verification and validation is described and the initial budget and resources are allocated. Chapter 4 contains the design of the UAV starting from the conceptual design, the Class I weight estimation to the subsystem designs and finally the Class II weight estimation. Chapter 5 presents the analysis of the UAV. The performance, aerodynamics, materials, structure and the stability and control will be analysed. Chapter 6 deals with the cost estimation. The costs involved in the development, manufacturing and operation stages are evaluated. Also, an estimation of the break even point, return on investment and cost break-down will be made. Chapter 7 contains the description of the operation and logistics of the UAV mission. A summary of the reliability, availability, maintainability & safety will be presented as well as the layout of the software, and the manufacturing, assembly and integration plan. In Chapter 8 will be a summary of the final design, describing all the system characteristics and design lay-out. Chapter 9 elaborates on the project design and development logic and the project Gantt chart as a follow up on Chapter 7. Finally, Chapter 10 and Chapter 11 contain the conclusion of the report and the recommendations for the future of the project.

2 Exploration Study

In the introduction of this report (Chapter 1), the need statement was expressed. In this following section, an insight into the current market of surveillance UAVs that can carry out monitoring missions will be presented. This analysis is vital to find what is missing in the market which can then be translated into an opportunity. This will be achieved by first defining UAVs and classifying them in different categories in Section 2.1. This will be followed by Section 2.2 which will highlight the oil and gas companies that are either developing or already using UAVs for pipeline monitoring purposes. This will give an insight into which aspects to investigate further in the current UAV market. This investigation will be found in Section 2.3. It will look at the performance of current UAVs, the current types of UAV propulsion and finally, it will outline the current emergency situations encountered by UAVs and their mitigation strategies. Section 2.4 will present the current surveillance payloads used, as well as the communication and emergency payloads. Following, a SWOT analysis (Section 2.5) showing the strengths, weaknesses, threats and opportunities of the current UAV market will be presented. This exploration study chapter will be finalised by an outlook on UAV technology (Section 2.6) and a final prediction of the future market (Section 2.7).

2.1. UAV Definition, Classification and Certification

The word UAV is an acronym for Unmanned Aerial Vehicle. Various definitions can be found for such vehicles. Remotely Piloted Vehicles (RPVs), UAVs and drones are defined as vehicles that fly without pilots. As the name indicates, RPVs are controlled from remote locations while UAVs have the possibility of being autonomous or pre-programmed[2]. Drones, on the other hand, are vehicles which have limited flexibility for their missions. They fly in a monotonous fashion, such as target drones. Finally, another variation of the definition is Unmanned Air Systems (UAS). This definition is more general as it includes the sophisticated payloads, ground control systems and other components. The Department of Defence [3] defines UAVs as: *"Powered, aerial vehicles which are designed or modified not to carry a human operator/pilot, use aerodynamic forces to provide vehicle lift, can fly autonomously or be piloted remotely, can be expandable or recoverable, and can carry one or multiple designated payload(s)"*. It is clear that, with such definitions, a wide array of vehicles can be called UAVs. The following section highlights the main categories of current UAVs.

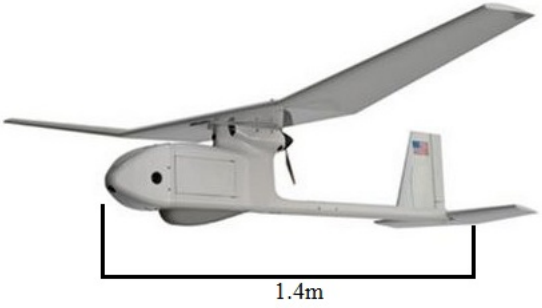

Figure 2.1: The AeroVironment RQ-20 Puma

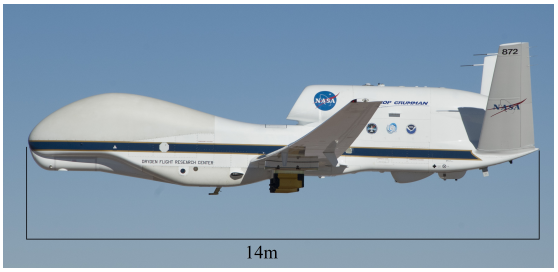

Figure 2.2: Northrop Grumman RQ-4 Global Hawk

Overall UAV Classification

Currently, the UAV market consists mainly of UAVs designed for military applications. These are mainly for security, search and rescue, monitoring, impact and disaster management, communications and munitions [1]. The UAVs with tasks concurrent with surveillance are the ones used for Search and Rescue, monitoring and impact and disaster management. All terrain Search and Rescue UAVs have the ability to mark rescue points as well as deploying life rafts[1]. Moreover, UAVs may be used to monitor chemical, radiological, biological and nuclear deployments. Finally, impact and disaster management UAVs are able to perform damage estimations. An example of such UAV is the AeroVironment RQ-20 Puma (Figure 2.1). In November 2015, the United States Marine Corps made a US$13 Million order of RQ-20 Puma UAVs[2], one unit of the RQ-20 Puma is priced at US$250,000. When comparing it to the average military drone, on the one hand it is lighter, on the other it has a shorter range, a lower ceiling and reaches lower cruise speed [3]. It is planned to be deployed in Alaska to support oil spill response crews. Another UAV that is used for surveillance is the Northrop Grumman RQ-4 Global Hawk (Figure

[1] URL https://www.uavs.org/military [cited 20 April 2016]
[1] URL http://ftnews.firetrench.com/2012/04/u-s-marine-corps-first-to-procure-four-different-aerovironment-small-unmanned-aircraft-systems-with-5-5-million-rq-20a-puma-order/ [cited 21 April 2016]
[2] URL https://www.avinc.com/.../aerovironment-receives-13-million-rq-20a-puma-ae-small-unmanned-aircraft-sy [cited April 21 2016]
[3] URL http://planes.axlegeeks.com/l/958/AeroVironment-RQ-20-Puma [cited April 21 2016]

2.2). Including the development costs, each unit is priced at US$222.7 Million. This US$16 Billion program[4] started in 1998 and has seen over 50 different airframes. It is operated by the United States Air Force, NASA and NATO. Potential operators include Australia, Canada, Japan and South Korea.

Table 2.1[2] shows six different categories in which UAVs can be classified. One can clearly see that only one of these classifications deals with civil and commercial UAVs while the other five categories deal with military UAVs. This indicates that the civil market has a lot of room for growth.

Table 2.1: Classification of UAVs in the market

Classification	Description
Target and Decoy	Provides a target to ground and aerial batteries
Reconnaissance	Used for battlefield intelligence
Combat	Provides attack capability
Logistics	Used to deliver cargo
Research and Development	Used to improve technologies used by UAVs
Civil and Commercial	Used in different fields such as Agriculture, Earth observations, Energy sensors, etc

This last category is researched upon and the classifications of civil UAVs are expanded in the following subsection. The different applications require different requirements for the UAV in terms of range, endurance, flight altitude, speed and vertical take-off and landing (VTOL). In Table 2.2[2] the definition of the different classification terms for the requirements of the applications can be found.

Table 2.2: UAV classification terms

Range (km)	Endurance (hr)	Altitude (m)	Speed (km/h)
Short = 0 - 70	Short = 0 - 3	Low = 0 - 3,000	Low = 0 - 100
Medium = 70 - 500	Medium = 3 - 12	Medium = 3,000 - 5,000	Medium = 100 - 350
Long = 500 - 20,000	Long = 12 - 48	High = 5,000 - 20,000	High = >350
Ultra long = 20,000 - ∞	Ultra long = 48 - inf		

According to these requirement classification, SCULPTUR can be classified as a long range, long endurance, low altitude, medium speed and non-VTOL UAV.

CIVIL UAV CLASSIFICATIONS

As stated previously, civil UAVs are a very small part of the global UAV market. Nevertheless, this part of the market has a very high potential for growth. In fact, a study conducted in 2007 identified that there are six principle sectors in which UAVs could be used (Table 2.3[5]).

Table 2.3: Classification of civil UAVs in the market

Classification	Description
Government	Law Enforcement; Boarder Security; Coastguard
Fire Fighting	Forest Fires; Emergency Rescue (e.g Mountain Rescue)
Energy Sector	Oil and gas industry distribution infrastructure; Electricity grids/distribution networks
Agriculture; Forestry and Fisheries	Environmental Monitoring; Crop Dusting; Optimising use of resources
Earth Observation and Remote Sensing	Climate Modelling; Aerial Photography, mapping and surveying; Seismic events, and Major incident and pollution monitoring
Communications and Broadcasting	VHALE platforms as proxy-satellites; MALE/S/MUAS as short-term, local communications coverage

It is clear that this report is directed to UAVs in the energy sector as the SCULTPRU UAV is aimed at surveing oil and gas pipelines. Hence, it is important to research what the current usages of UAVs by oil and gas companies are. This is outlined in Section 2.2.

UAV CERTIFICATION

In order to be allowed to perform missions with civil, commercial UAVs will need to obtain certification from the governing organisation in the country of operation. Currently, little countries have a fully developed set of

[3] URL http://www.nasa.gov/centers/armstrong/news/FactSheets/FS-098-DFRC.html [cited April 21 2016]
[4] URL http://www.northropgrumman.com/capabilities/globalhawk/Pages/default.aspx [cited April 21 2016]
[5] URL http://www.qi3.co.uk/wp-content/uploads/2014/02/Qi3-Insights-White-Paper-UAVs-Growing-Markets-in-a-Changing-World-2014021903.pdf [cited 20 April 2016]

regulations for the operations of UAVs and clear certification is missing. Due to the increasing growth of civil UAVs, the need for these regulations is growing to ensure a safe airspace in which both aircraft and UAVs can operate. An overview of the current state of certification regulations of the 5 countries with the largest length of pipelines located in remote areas, namely the United States (2,225,032 km), Russia (259,913 km), Canada (100,000 km), China (86,921 km) and Australia (34,612 km), is given in [4].

2.2. EXISTING ENERGY PIPELINE SURVEILLANCE MISSIONS

Currently, monitoring missions are carried out by manned aircraft that are forced to fly very low. Moreover, these missions can only detect visible effects. In other words, the current solutions for monitoring pipelines are dangerous and inefficient. Present methods do not allow for the search of gas or oil leaks in the pipelines. Pipeline failures are very common occurrences, for instance, in Russia there are 0.11 to 0.14 pipeline breaks per kilometre per year [5]. This section shows the current surveillance missions carried out by oil and gas companies. This includes helicopters, satellites and optical fibres. Also, such companies are either developing or using UAVs to carry out these missions. These are also highlighted.

2.2.1. CURRENT SURVEILLANCE MISSIONS

Oil and natural gas companies mainly use helicopters to carry out the pipeline surveillance missions. However, these companies are not shy to try to innovate. They have also used different methods such as using optical fibre distributed acoustic and temperature sensors. These sensors enable leak detections along the whole length of the optical fibre. The company explains that *thermal leak detection works by detecting a localised change of temperature at a point along the pipeline induced by a release of the contents of the pipeline into the surrounding soil. For liquids, such as oil, this is usually a rise in temperature whereas for high pressure gases this is a drop due to the Joule-Thompson effect*[6]. It is very common for these oil companies to hire surveillance companies to carry out these missions. Table 2.4 shows one example for each of the three main methods used by mainstream oil and natural gas companies. For instance, Indian oil companies will hire GAIL India[7] to survey pipelines using their satellite. Air Lloyd[8] uses helicopters and SILIXA[9] lay optical fibre distributed accoustic and temperature sensors with new pipelines.

Table 2.4: Current Detection strategies

Company	Mission	Method
Air Lloyd, OGE, Adlares and the German Aerospace Centre (DLR)	*Gas Leakage Detection*	BO 105 Super 5 Helicopter
GAIL India	*"Pipeline Surveillance"*	Satellite
SILIXA	*"Temperature based leak detection"*	Optical Fibre Distributed Acoustic and Temperature Sensor

2.2.2. CURRENT OR PLANNED UAV SURVEILLANCE MISSIONS

Table 2.5 shows the current oil and gas companies that are either developing or already using UAVs for pipeline monitoring purposes. From these monitoring missions, one can see that they have one main interest in common: to detect leaks in pipelines. For instance, British Petroleum[10] wants to be able to spot oil leaks and detect buried metallic objects using its UAV. Other companies such as ENGIE[11], China Petroleum[12] and Kinde Morgan[13] can also be found in the following table.

[6] URL http://silixa.com/pipeline-surveillance/leak-detection/ [cited June 10 2016]
[7] URL http://articles.economictimes.indiatimes.com/2015-11-26/news/68582400_1_gas-pipeline-network-dahej-vijaipur-gail-india [cited June 10 2016]
[8] URL http://www.airlloyd.de/alnew/ueberwachung.php?lang=english [cited June 6 2016]
[9] URL http://silixa.com/pipeline-surveillance/leak-detection/ [cited June 6 2016]
[10] URL http://www.fastcompany.com/3031725/fast-feed/oil-giant-bp-is-first-company-approved-to-use-commercial-drones [cited May 4 2016]
[11] URL http://dronelife.com/2015/04/03/french-energy-company-invests-in-drones/ [cited May 4 2016]
[12] URL https://en.wikipedia.org/wiki/CPPC_UAV [cited May 4 2016]
[13] URL http://www.upi.com/Business_News/Energy-Industry/2015/04/29/Pipeline-companies-probe-aerial-leak-monitoring/4161430303477/ [cited May 4 2016]

Table 2.5: Market analysis of current missions carried out by UAVs and their on-board equipment

Company	Mission	Technology
Kinde Morgan, Enbridge and TransCanada	*Discover crude oil or other hydrocarbon leaks*	Infrared camera-based systems, laser-based spectroscopy systems and flame ionisation detection systems
ENGIE	*Monitoring of natural gas infrastructure, survey topography and monitor "security for public institutions"*	Infrared camera
British Petroleum	*Integrating photographs and sensor information into 3-D models of roads, pads, and pipelines, along with precision volumetric measurement, and topographic analysis of the company's gravel pits*	Sophisticated electro-optical and infrared sensors
China Petroleum Pipeline College	*Aerial patrol, surveillance, and survey missions for petroleum pipelines*	Infrared Camera Electro-optical Camera

In the present, at Prudhoe Bay, Alaska, BP (British Petroleum) uses UAVs to conduct monthly surveys of 2090 km (1300 miles) of pipeline. The pipeline infrastructure in the area makes manual inspection difficult, especially when considering the harsh weather conditions. A 3 km section of pipeline can be checked in 30 minutes by a PUMA AE UAV, an activity which would take a human up to seven days. BP is also conducting tests at its offshore installations with multi-rotor UAVs.

With the introduction of monitoring UAVs for such missions, a new market has been opened, full of opportunities. One can now use cameras and radars to find leaks or other type of failures even in pipelines beneath ground. However, as Brian Wagg, director of business planning for C-FER Technologies says, *"The challenge with airborne leak detection systems is not with the aircraft, but with selecting appropriate sensors to detect liquid hydrocarbon leaks before they reach the surface"*. Furthermore, current UAVs at altitudes lower than 5 kilometres have low range (10-200 kilometres) and endurance (1-10 hours) capabilities [6].

It is clear that there is room for improvement for current UAV technologies. Two possible improvements stand out: better range and endurance, and improved surveillance technologies. This would allow a longer and continuous surveillance of pipelines. The more time the UAV is in the air, the more efficient the missions can be. Moreover, better quality from the sensors makes it easier to detect leaks. The cruise speed of the UAVs is also an important factor as the quality of the surveillance depends on it. If the UAV flies too fast, the quality of the images may be jeopardised. Furthermore, the type of engine is also important. An engine that makes the UAV vibrate too much will also be an obstacle to high quality surveillance data. Hence, the following sections will highlight the main UAVs in the market by looking at range, endurance, cruise speed and maximum altitude. Also, the current UAV propulsion will be presented which will be followed by a discussion of the current emergency situations and mitigations. Finally, the current payload market will be highlighted.

2.3. CURRENT UAV MARKET

The analysis of current missions has shown the aspects which need to be investigated for this UAV. These are, for performance: the range, endurance and cruise speed. This will be followed by an exploration on UAV propulsion. Moreover, an analysis of current emergency situation encountered by UAVs and their mitigation procedures will be presented.

2.3.1. PERFORMANCE

As stated in Chapter 1, the performance requirements are to have a range of 1800 km, to have an endurance of 20 hours and to have a cruise speed of 100 km/h. Reference UAVs are compared using these three requirements as a basis.

RANGE

In the previous section it is shown that SCULPTUR is classified as a long range UAV. Table 2.6 [14] shows UAVs with similar range classification as SCULPTUR. Looking at Table 2.2 it can be seen that the maximum altitude is higher. The reason behind this is that at higher altitudes, there are lower air densities. This allows the UAVs to be more efficient.

[14] URL https://insitu.com/information-delivery/unmanned-systems [cited June 2016]

Table 2.6: Comparison - Similar Range

UAV	Range (km)	Endurance (hours)	Cruise Speed (km/h)	Max Altitude (km)
Boeing Insitu SeaScan	1500	15	130	-
Kestrel Aerospace Lancer	1667	12	290	-
Elbit Hermes 900	2500	36	113	9.145
Pterodactyl I	4000	20	150-180	5.000

ENDURANCE

Table 2.7 [15] shows UAVs with similar endurance. Their endurance is in the range 20-24 hours. This can be classified using Table 2.2 (Section 2.1) as long endurance UAVs. One can see 3 relationship for these long endurance UAVs: they are all long range UAVs and are classified as having medium speed. A mistake often made is to multiply the cruise speed by the endurance to get the range. The endurance and range Breguet equations are dependant on different inputs (SCULPTUR for example has an endurance of 20 hours and a range of 1800 km at a cruise speed of 100 km/h). Finally, the 5 of them have high altitude. One can see that the AirStrato Explorer and the Denel Dynamics Bateleur UAVs have a smaller range but similar endurance. However, their maximum altitude differ by approximately two times.

Table 2.7: Comparison - Similar Endurance

UAV	Range (km)	Endurance (hours)	Cruise Speed (km/h)	Max Altitude (km)
MQ-1 Predator	1100	24	135-165	7620
Denel Dynamics Bateleur	750	24	250	8.000
AirStrato Explorer	837	20	153	18.288
TAI Anka	4896	24	204	9.144
Chengdu Pterodactyl I	4000	20	75-220	5.000

CRUISE SPEED

SCULPTUR is classified as a medium speed UAV. Table 2.8 [16] presents medium speed UAVs in the market.

Table 2.8: Comparison - Similar Cruise Speed

UAV	Range (km)	Endurance (hours)	Cruise Speed (km/h)	Max Altitude (km)
Yabhon-N	-	3	107	6.000
Hermes 450	300	20	130	5.486
DRDO Rustom-H	1000	9	125	10.668
Rui Ying (Sky Saker)	4000	30 hours (unarmed) 14 hours (armed)	150-180	7.500

2.3.2. EXPLORATION UAV PROPULSION

Power systems in UAVs differ only slightly from aircraft systems. Their main difference is found in output power/thrust and the physical size of the engine. It is therefore important to not only investigate the propulsion systems currently used by UAVs, but to also investigate current developments and future possibilities. In this section the properties of electrical, reciprocating and turbine engines are discussed.

Before investigating the different types of propulsion systems, an overview showing the current distribution of propulsion types is given in Figure 2.3. From this piechart it can be seen that the main propulsion of UAVs is provided by the use of electrical motors. Together with the use of reciprocating engines, they account for more than 50% of all propulsion systems used. As seen in the figure, a large portion of more than a third of the UAVs uses an unknown propulsion system. This large gap of information is mainly due to the large percentage of military UAVs, as shown in Figure 2.4, of which little information is available.

[15] URL http://www.military.com/equipment/mq-1b-predator [cited June 2016]
[16] URL http://www.israeli-weapons.com/weapons/aircraft/uav/hermes_450/Hermes_450.html [cited June 2016]

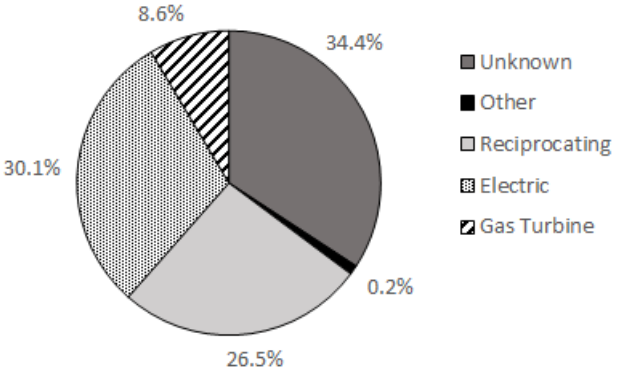

Figure 2.3: Propulsion systems emplyed by existing UAVs [7]

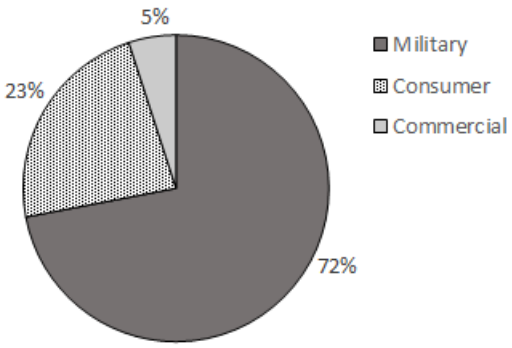

Figure 2.4: Current UAV market areas [7]

ELECTRICAL MOTORS

Electrical motors are used as main propulsion system in small UAVs and model aircraft. In this type of propulsion, electrical energy is converted into mechanical energy used to drive a propeller, fan or rotor. The electrical power required can be supplied through the use of different sources. Currently available sources include batteries, solar-powered photovoltaic cells or fuel cells [8].

Multiple advantages of electrical motors over gas turbine or reciprocating engines are described by [8] and [9]. The main advantage is that no consumables are required in order to drive the electrical motor, hence its emission level is reduced to zero. Another advantage of the electrical motor is that contrary to internal combustion engines, little maintenance is required. The performance of an electrical motor is independent of the altitude of operation, making it an appropriate engine for UAVs with different purposes and mission profiles. An electrical motor is the quietest engine of the three, with the smallest thermal signature [9]. Aside from these performance aspects, they are also most easy to design, implement and test. It is for this reason that electrical motors are often used in small projects and/or small UAVs.

The most significant limitation imposed by the use of electrical motors on UAVs is the energy-storage capacity, which limits the endurance of the UAV to 0.5-3 hours [9]. Since the power source of the electrical motor has to provide electrical power to both the motor as well as the payload and communication system of the UAV, the endurance and speed of flight is limited. Current research is performed extensively into batteries with higher energy densities (over 350 Wh/kg)[10], in order allow a wider range of application areas by elongating the endurance. Other means of obtaining a continuous electrical power supply are being researched and developed in order to extend this endurance, and with this also the range. Promising results have been found with tests of solar-powered photovoltaic and fuel cells, but these options are not yet available on the market and are still under development. At the moment, only small UAVs with a mass of less than 9 kg are powered by batteries and electrical motors that deliver a power output of less than 1 kW. Examples of UAVs propelled by an electrical motor are the Desert Hawk and Skylight [8].

RECIPROCATING ENGINES

The majority of engines used in the current operational UAVs are internal combustion engines, with most of them having reciprocating engines. Because of its high popularity, reciprocating engines are commercially off-the-shelf engines with a rated power output between 1-150 kW [9] used to power UAVs with a maximum take-off weight (MTOW) between 10-1100 kg. One of the reasons behind the current popularity of reciprocating engines in the current UAV market is the lack of suitable alternatives [2].

Reciprocating engines can be divided into two-stroke, four-stroke and rotary engines. The two-stroke engine produces twice the power of a four-stroke engine when operating at the same rotational speed, at the cost of a higher operation temperature and increased weight [9]. Rotary engines offer a long life and low specific fuel consumption compared to the two- and four- stroke engine, but limited information is available on them, therefore they are not often used on UAVs. Reciprocating engines used in UAV applications are often scaled versions of existing engines from a variety of sources, ranging from model aircraft to general aviation. They are often preferred over electrical or gas turbine engines when considering slow, low altitude flight with a power output below 150 kW.

Difficulties are found when using reciprocating engines in surveillance UAVs, as they generate more vibrations than an electrical or gas turbine engine. This vibration reduces the pointing accuracy of the payload and required the UAV to be designed with appropriate materials. Along with the increased vibration, the rotational speeds of the engine generates high-frequency noise [8].

GAS TURBINE ENGINES

The last type of engines are the gas turbine engines, which are, as seen in Figure 2.3, only used on 8.6% of the currently existing UAVs. This low percentage is caused by the lack of existing gas turbines with an appropriate power output for UAV application. Two generic types of gas turbines can be distinguished, namely turbojet and turboshaft engines. The general lay-out of both types is similar, however the method of thrust generation differs. Turbojets produce thrust from its high-velocity jet stream for direct propulsion, where turboshafts produce power using in an output shaft, which then drives a propeller to provide thrust. Within the generic types of turbojets and turboshafts, another subdivision is made into the groups of turboshafts, turboprops, turbojets and turbofans. An overview of the area's in which civil UAVs are used with these types of gas turbine engines is given in Figure 2.5. From this it can be seen that for mapping and reconnaissance missions, turboprops are the preferred option.

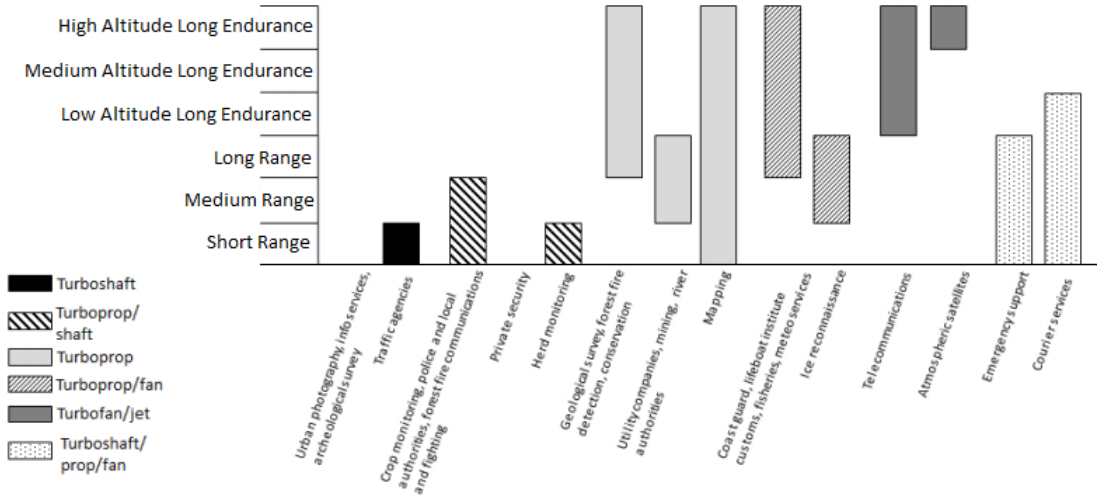

Figure 2.5: Civil UAV type - Propulsion System relationship [11]

The advantages of using gas turbine engines over using reciprocating engines for the functions shown in Figure 2.5 are their smooth power production at high power-to-weight ratio with low noise emission. Since little moving parts that can fail are present in a gas turbine engine, long mean times between overhauls can be reached, making it less maintenance intensive than a reciprocating engine. Most current day gas turbine engines are fuel by "heavy" fuels, like JetA, making them suitable for both civil and military use.

Turbojet Units

The first type of gas turbine currently used in UAV applications is the jet engine. Main features of these engines are their property to maintain thrust at high airspeeds and high altitudes. This trait makes them suitable for UAVs cruising at a mach number greater than 0.6 [8]. Two different engine lay-outs are considered to be categorised as jet engines, turbofans and turbojet. Turbojets accelerate the oncoming air making use of a series of compressors and turbines stages, whereas turbofans follow the same principle with the addition of a second turbine driving a ducted fan.

Turbojet units are often found to produce high thrust levels, well above the required output for UAV applications. At the smallest end of the jet-thrust spectrum are the ones designed for model aircraft, with a thrust below 0.13 kN. Due to the low number of available engines in the correct thrust spectrum, jet engines often have to be built specifically for UAVs. However there is rarely budget available for these kind of designs, therefore only mature jet-units are selected for UAV programs [9].

Turboshaft Units

The other type of gas turbine are the turboshaft units, which are further divided into turboshafts and turboprops. Turboprops have a similar engine lay-out as turbofan units, as described above, only the second turbine now drives a propeller. In order for this propeller to match the speed of the low-pressure turbine a reduction gearbox is added. Turboshafts follow the same principle as turboprops, only the shaft is available for other uses than driving a propeller. They are often used to provide VTOL propulsion to UAVs.

Many favourable attributes are present in turboprop engines. Compared to reciprocating engines, they have a low vibration level and are highly reliable. Additionally, they operate at higher power to weight ratios (3.5-4.8 kW/kg) [9] than reciprocating engines, thus allowing a lighter engine to be installed on the UAV. Manned aircraft turboprop engines have a mean overhaul time of 3,000 to 4,000 hours, which is more than twice that of reciprocating engines. The flight speed of turboprop engines is limited to below 0.6 Mach due to propeller tip compressibility constraints.

The reason for the low number of turboprop engines currently installed on UAVs is the lack of available turboprop engines in the desired power class [2]. Most turboprop engines are used in large general-aviation aircraft, with an output power larger than 200 kW. Smaller aircraft, as well as UAVs, would benefit from the high power-to-weight ratio of turboprop/turboshaft engines if available with the right power output. A major disadvantage is the increase in fuel consumption of turbine engines when operated at part-load [8]. It is for this reason that it is unfavourable to fly with an overpowered engine, as both the engine weight and fuel weight increase.

Since the lowest turboprop engine currently available for small UAVs is the TP100 engine with an output power of 180 kW[17], a new market has yet to be explored. The application of turboprop/turboshaft engines with their relatively low fuel consumption and high power-to-weight ratio makes them a suitable engine for long endurance UAVs. The low vibration level of the engines makes them specifically suitable for missions requiring high accuracy observation equipment. This is thus chosen to be the market to further explore in this DSE project, as described before in Chapter 1.

MICRO-GAS TURBINE (TURBOPROP)

The development of micro-gas turbines (MGT) is focused on filling up the gap of low power output gas turbine engines. The low power output of micro-gas turbines makes them suitable for implementation on smaller UAVs, granting them the advantages as described above. Current research project have been performed mostly on engines with a power output lower than 100W [2] for intended use on small UAVs. Promising results in this power class are shown by *UAV Turbines inc.*, who are in the process of developing several turboprop engines specifically intended for UAV application with a power range of 20-110 kW [18]. Larger turbofans and jets are developed mainly for military operations.

According to Pilavachi [12], micro-gas turbines offer multiple advantages compared to other small-scale power generation methods. The main advantage lies in its high energy density potential, which ensures that even with a relatively low system efficiency the power to weight ratio exceeds the ratios achieved by alternative methods. This means that a compact system can be used with a relatively low weight, leading to reduced engineering costs and favourable properties for long endurance missions.

Additional advantages of micro-gas turbines compared to other technologies are the small number of moving parts, therefore increasing the mean time between overhauls and corresponding maintenance costs. Also low noise emission and multi-fuel capabilities are part of the possible advantages, offering opportunities in terms of emission levels [12]. Current technologies offer possibilities of using natural gases and bio-based liquids as alternative fuels, resulting in reductions of CO_2 and NO_x emissions up to 40% [13].

Before micro-gas turbines can become widely available for UAV applications, present technical difficulties have to be solved. The main technical barrier is the low overall efficiency of the engine, which is lower than a reciprocating engine of similar power output [12]. In addition, the efficiency drops even further when the engine is operated at partial load, making it an unfavourable choice. Increasing the efficiency of micro-gas turbines can only be done operating at high pressure and temperature conditions, imposing a challenge on materials engineers around the world [14] [12].

2.3.3. EMERGENCY ANALYSIS AND CURRENT MITIGATION

In this subsection the current emergency/accident occurrence in UAVs is discussed. For this reason a report regarding UAV accidents and incidents of a total time span of 15 years is used, particularly taken from years 1989 to 2004 [15]. The sample UAVs taken for the accident analysis are the IAI RQ-5 Hunter, AAI RQ-7 Shadow, AAI RQ-2 Pioneer and the General Atomics MQ-1 Predator (see Figure 2.6). It can be observed that the accidents are divided in four categories.

The category 'Maintenance' includes accidents for which there was a contribution from the maintenance personnel. Those averaged to around 8.5% of the sample UAV accidents, noting that for aircraft that have been developed and have flown for years, this number was extremely small. This is mainly because of the development of these maintenance procedures through the years, for instance, only 2% of the RQ-2 Pioneer accidents occurred due to improper maintenance [15].

The human factor accidents, defined as being caused by either the UAV operator, the airport ground crew or the air traffic control accounted for approximately 35.5% of the sample. Regarding this type of accidents/emergencies, it has been found that approximately 41% have originated from decision errors, followed by skill-based errors of 26%, perceptual errors of 20%, while violations were only a source for 13% [15].

The category 'Aircraft' includes problems associated with the failure of a mechanical or electrical component of the airframe. These were approximately 45% of the total sample UAV accidents for the period of time.

Lastly, 'Others' accounted for all accidents that are not related to any of the previously discussed criteria. Fur-

[17] URL:http://www.pbsvb.com/customer-industries/aerospace/aircraft-engines/tp-100-turboprop-engine[cited June 3 2016]

[18] URL: http://www.uavturbines.com/ [cited June 3 2016]

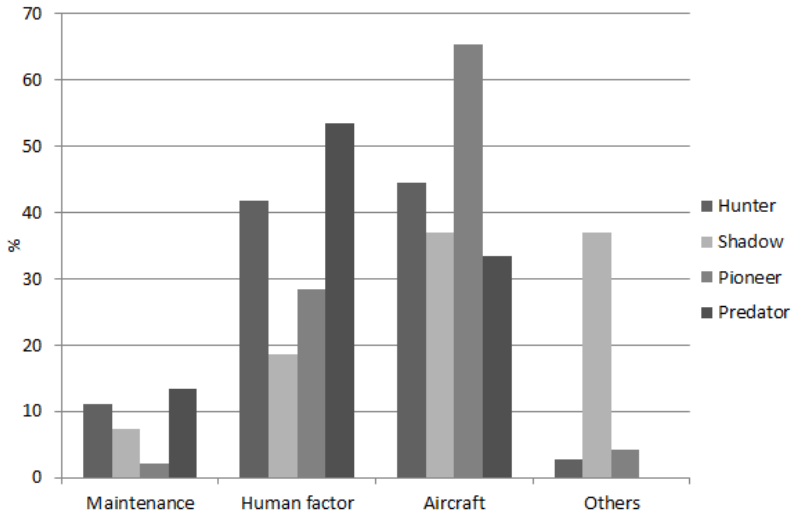

Figure 2.6: Sample UAV accidents 1989-2004 [15]

thermore, this category includes the accidents/incidents for which no information was available, and it can be imagined that for military Unmanned Aerial Systems (UAS) such as the ones listed, such unavailability of data is common.

All these emergency situations and accidents have occurred during different phases of the flight itinerary of the UAVs. Subsection 2.3.3 will consider most of the probable emergencies that have been confronted by different UAS. The following 2.3.3 will provide different available techniques to prevent these emergency situations and cope with them in case they do occur.

EMERGENCY SITUATIONS ENCOUNTERED BY AERIAL VEHICLES

As discussed, the emergency situations/incidents can occur in several phases of the flight itinerary, particularly during start-up, taxi, take-off, cruise & surveillance and landing.

Starting with the possible emergency situations during the initial stand-by mode when the UAV is being started-up, the first scenario considered, a relatively common hazard through history amongst aircraft, is a starter-system flaw that inflames the engine compartment, adjacent systems and/or electrical harness [15].
During taxi, examples of emergency situations are miscommunication with Air Traffic Control (ATC) which causes a runway collision with aircraft or other objects. Moreover, over-increased runway temperature or surface roughness, especially during acceleration or deceleration, may cause further structural damage to UAS components, e.g. a tire puncture which may result in a loss of control, roll-over or further component failure.
Typical emergency during take-off acceleration is again a tire puncture that causes the UAV to become initially unstable, skid on the ground and lose speed [16]. Another accident scenario is an engine malfunction during acceleration that causes loss of speed and lift generation; in such a case a decision has to be made to either continue or abandon the take-off. During rotation a roll-over may occur given a stronger elevator input. Considering the high speed during rotation, a roll-over can also lead to substantial structural damage to the UAV. At lift-off, the control surface inputs are crucial for maintaining a stable climb - an over-increase in angle of attack may lead to separation and stall which at this take-off stage is almost impossible to recover from [17]. Still concerning this flight stage, many unfortunate incidents have resulted from wild life encountered on the runway and mid-air, especially bird-strikes.

The take-off, cruise and landing phases, in general, include risks of any structural, mechanical or software failure that may result in loss of UAV control, disturbance in the communication with ground station, system (e.g. engine) failure, fuel leakage, etc. Other emergency scenarios include a mid-air collision and complete loss of fuel [16].

Strictly regarding the approach phase of the flight itinerary, emergencies that are typically encountered are aerodynamic stall due to over-decreased speed and/or over-increased angle of attack [15]. At landing, structural or mechanical damage may occur in case of severe weather conditions or improper operation. Examples of a mechanical failures during landing are inoperative/jammed control surfaces or failure to deploy the landing gear in case the UAV uses a retractable type [17]. Common structural failures include strut or tire failure during touch-down. Last but not least, interactions with wild life, people or other vehicles on the runway have caused many UAV incidents as they may cause structural damage and may even result to be fatal.

EMERGENCY MITIGATION

The emergency mitigation deals with the reduction of further emergency/incident risk that is currently performed at the UAV market. These mitigation strategies are given for the previously discussed emergency situa-

tions at each flight phase.

Visual inspection and pre-flight checking

Prior to engine start-up, a visual inspection is carried out to closely observe for any obvious structural, mechanical or electrical harness failure. These include observations of the propeller blades, fairing and hub, fuselage, wing, tail, landing gear structural failures (especially visual cracks or any visible plastic deformation). It is also examined if there is a flat tire by observing if the tire rolling radius has rapidly decreased while the aerial vehicle is at a stand-by mode on the ground[19].

Only after it has been ensured that no visual flaws are detected, the UAV is started-up and the pre-flight checklist is performed. This procedure first involves a check on whether the payload that will be installed is damaged in any way or has any functionality flaws. Following, the functionality of the on-board avionics, remote control, data link and ground station software are tested. If a problem is encountered, the flight is most probably postponed or cancelled, as the components may either require repair or replacement by experienced specialists. Furthermore, all control surfaces are checked for required deflection, and the functionality of the propulsion system is tested by adjusting the rotational rate and blade-pitch settings of the propeller. If any weakness is observed or overheard, the flight is either cancelled or delayed until the appropriate sub/system is repaired by the aircraft mechanic or engineer in charge.

Emergency prevention during taxi & take-off

To begin with the UAV taxi phase, if any communication with the ATC or ground crew is unclear, the same information is requested again. However, there is little that can be done if an air traffic controller makes a mistake and does not realise it on time. In case of any structural or mechanical defect is observed or overheard from the UAV, the flight is delayed while the severity of the flaw is examined.

During take-off acceleration there are several factors to be considered before the best decision is made in case of a defect, for example any structural failure. It is examined whether the take-off can continue and whether the speed required for lift-off can be reached safely for the given remaining runway length. Moreover, in case the decision speed V_1 is already reached, most of the times it is safer to continue the take-off procedure, depending on the type of problem that is encountered. This decision speed is provided by regulations according to the UAV take-off performance and the runway distance available. In a situation at which the failure is severe enough so that a safe take-off and go-around is not possible, even if the decision speed has passed, the take-off is still attempted to be abandoned.

Emergency prevention during cruise & surveillance

In almost any aircraft failure during cruise & surveillance, UAVs enter an emergency mode. First of all the severity of the failure is established and then it is determined whether the UAV may continue the flight or attempt an emergency landing procedure. In case of an engine failure, for instance, the required settings for the most optimal glide-slope are estimated using UAV operation manuals. If a runway cannot be reached, the closest plain field with the least amount of obstacles is chosen for the emergency landing. In case of a complete loss of control of the UAV, such as a critical structural or mechanical failure (e.g. jammed control surface causing instability), some aircraft employ usage of a parachute for UAV recovery. These are also used in a situation of a lost communication found the ground station and/or satellite[20].

Emergency prevention during landing

Most aerial vehicle accidents throughout history have occurred during the landing phase. As discussed previously, reasons for that are component failure, meteorological conditions, pilot error, air traffic control misguidance.

Common action taken by pilots given an incorrect approach UAV attitude, cross-wind or over-speed is to perform a go-around. This way the risk of a possible accident is further decreased. The lower sides of the fuselages of some UAVs are optimised to cope with the landing weight in case the landing gear fails to deploy or the strut breaks during touch-down. Furthermore, safety factors are typically used on all calculated static and dynamic loads when designing these UAVs.

A fully stalled wing can be used for descent using the phenomenon known as deep stall, a steep but steady stall. Deep stall is initiated through a steep nose-down angle of incidence relative to the wing and aft horizontal stabiliser. This leads to a pitch-up manoeuvre followed by a conventional stall; the fixed stabiliser prevents any possibility of recovery. As the UAV starts descending, there is a large drag vertical component, acting similarly in a way to a parachute. Deep stall is mainly used in UAVs with a conventional configuration but this procedure was also tested with canard configurations, in the latter case both the canard and wing being fully stalled. This technique is used on the AeroVironment FQM-151 Pointer, a UAV that is used by the United States Army for battlefield surveillance.

[19] URL http://www.experimentalaircraft.info/flight-planning/aircraft-preflight.php [cited June 1 2016]
[20] URL https://fruitychutes.com/uav_rpv_drone_recovery_parachutes.htm [cited June 1 2016]

The main drawback is that the descent speeds are usually much higher than for conventional landing techniques, thus most of the impact energy needs to be absorbed by the airframe. Shock absorbers can be used to decrease the impact energy on the airframe. A very interesting alternative that the AeroVironment RQ-11 Raven uses is to detach the wing and tail right before impact with the ground [18].

2.4. CURRENT PAYLOAD MARKET

The main task of the UAV is to carry out surveillance missions. The most important part of the payload for such missions consists of cameras and radars. Furthermore, the UAV needs to communicate with ground control, hence the communication payload is needed. Finally, in case of emergencies, special payloads need to be used.

2.4.1. SURVEILLANCE

Aerial detection of fluid and gas leaks in pipelines is generally done by the use of electro-optical (EO) imaging, infrared (IR) sensing or synthetic aperture radars. Each of these methods offer distinct advantages. Optical images can be analysed by human operators to not only detect leaks, but also to detect other anomalies. Infrared sensing detects changes in surface temperature due to the thermal conductivity of the gas or fluid, which makes it a very powerful tool for detecting leaks in particular (above or below ground). Lastly, a synthetic aperture radar is used to create a detailed 3D image of the environment and is used to spot geometric anomalies such as buckling of pipelines.

CLASSIFICATION OF UAV SENSORS

Four types of sensors are currently being used by both civil and military UAVs: Wide area, Spot, Targeting, and Weather effect sensors. For surveillance missions only the first 2 sensor types need to be used namely, Wide area and spot sensors. Sensors are typically expressed in terms of National Interpretability Rating Scale (NIIRS) and Ground Resolved Distance (GRD). There are 9 NIIRS that define the nominal capabilities of the different sensors. For instance, NIIRS 1 (over 9.0 meters GRD) defines an infrared sensor that can "*Detect large ocean-going vessels (e.g. aircraft carrier, super-tanker, KIROV) in open water*[21]". It defines a radar that can "*Detect, based on presence of piers and warehouses, a port facility*". Furthermore, NIIRS 9 (less than 0.10 metres GRD) defines an infrared sensor that can "*identify access panels on fighter aircraft*" and a radar sensor that can "*Detect major modifications to large aircraft (e.g. fairings, pods, winglets)*".

[19] shows which NIIRS type you need to choose for the wanted GRD. This allows the user to choose a sensor that is appropriate for the mission that needs to be carried out. For the chosen mission, a GRD of 0.20 - 0.40 meters is needed. This corresponds to a NIIRS 7 which can "*detect mooring cleats or bollards on piers*" for infrared sensors and can "*detect road/street lamps in an urban residential area or military complex*".

EO/IR SENSORS

EO/IR sensors cover a wide range of sensor types such as TV cameras or sophisticated thermal imaging. They are usually mounted in gimbaled "turrets" and some of these sensors, especially for military applications, have integrated lasers for target designation and range measurement. Despite their limitations with bad weather, they are often preferred because of their high resolution and ease of interpretation.

Infrared Cameras

Infrared cameras operate in a similar way to optical cameras. However, instead of electromagnetic waves in the optical spectrum, IR cameras are designed to detect waves in the infrared spectrum. Infrared radiation is emitted by all bodies and is a function of only the body temperature. The wavelength of the IR radiation determines the behaviour of the waves and consequently measuring different parts of the IR spectrum provides different information about the environment. Long wavelength IR (LWIR) radiation is not absorbed by the atmosphere and is therefore very useful for thermal imaging of the earth surface. Since gas plumes and oil spills originating from pipeline leakages change the thermal conductivity of the soil, changes in surface temperature can be detected near a leak. In the case of a gas leak the surface cools and in case of an oil spill the surface heats. This technique is also used for detection of subterranean leaks at depths up to 30 metres and corrosion voids caused by erosion, deteriorated pipeline insulation, and poor backfill (Figure 2.7[22]). One disadvantage of this technique is that substantial amounts of measurements and data analysis are required to correct for temperature fluctuations due to environmental conditions.

[21] URL http://www.fas.org/irp/imint/niirs.htm [cited May 30 2016]
[22] URL http://www.smartleakdetection.co.za/index.php/services [cited May 4 2016]

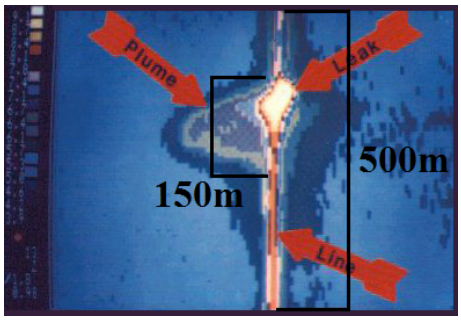

Figure 2.7: Leak detection with Infrared Radiometric testing

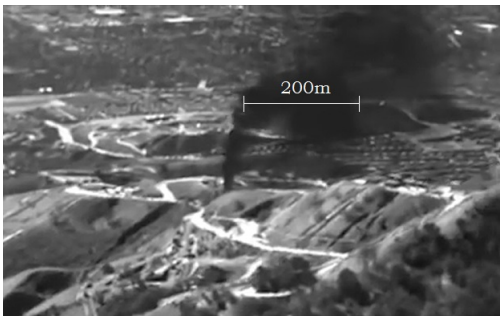

Figure 2.8: Methane leak detection with SWIR testing - The Telegraph

Short wavelength IR (SWIR) radiation is located nearer to the optical spectrum. SWIR waves do get reflected or absorbed by certain objects. While oil spills and gas plumes are not visible using optical imaging, petroleum and natural gas have a characteristic reflectance and absorbance for light in the SWIR spectrum, making above ground oil spills and gas plumes very easy to detect using SWIR sensing as can be seen in Figure 2.8 [20].

Table 2.9: Market analysis of infrared cameras for UAVs

Camera	Price ($)	Resolution (pixels× pixels)	Power (VDC)	Size (mm× mm×mm)	Weight Range (g)	Zoom (Digital)	Field of View	Operating Temperature Range (°C)
Tau 2 336	2,750	336×256	4.0 - 6.0	44.45x 44.45x29.97	72-150	2x, 4x	6.5°x5°	-40 to +80
Tau 2 640	7,350	640×512	4.0 - 6.0	44.45x 44.45x29.97	72-150	2x, 4x, 8x	12.4°x9.9°	-40 to +80
Quark 2 336	4000	336×256	3.3+/-0.1	22x22x12	18 - 28	2x, 4x	13°x10°	-40 to +80
Quark 2 640	9,500	640×512	3.3+/-0.1	22x22x12	18 - 28	2x, 4x, 8x	25°x20°	-40 to +80

Electro-optical Cameras

Electro-optical systems measure or detect radiation in the optical spectrum. Parts of the electromagnetic spectrum which can be detected include infrared radiation, visible light and ultra-violet radiation[23]. Electro-optical cameras provide visual imaging in a similar way to the human eye and therefore results in videos and images that can be analysed by human operators (Figure 2.9). Because there is little interaction between visible light and gas plumes or oil spills, electro-optical cameras are less suited for direct detection than for example SWIR cameras. However, electro-optical cameras are very suited for human inspection of the environment and spotting (structural) anomalies that indicate leaks or other hazards. A disadvantage is that the EO camera can be used only when daylight is available. The CM202 is equipped with a HD (1280x70 picture elements) EO camera that provides detailed visual imaging of the environment.

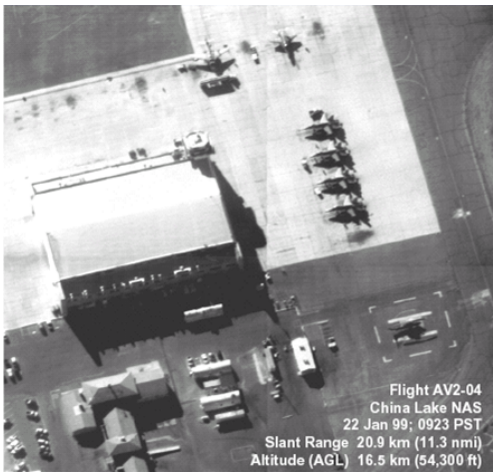

Figure 2.9: Global Hawk EO Image[19]

Table 2.10[24] shows the difference between 3 types of electro-optical cameras. In the research carried out for this

[23] URL http://www.unmannedsystemstechnology.com/category/supplier-directory/cameras-imaging-systems/electro-optical-systems/#intro [cited April 27 2016]

[24] URLhttp://uavvision.com/[cited 20 June 2016]

analysis, it was very hard to find a price for the Hitachi DISC120R, the reason being there are no official prices. It was found at 2 or 3 instances that the price of this camera could be bargained. Hence, the price could only be estimated based on the research carried out.

Table 2.10: Market analysis of EO cameras for UAVs

Camera	Price ($)	Resolution (pixels× pixels)	Power (VDC)	Size (mm× mm×mm)	Weight Range (g)	Zoom (Optical)	Field of View	Operating Temperature Range (°C)
Sony H11	700	1920×1080	6.0 to 12.0	43.1x 47.2x72.2	120	10x	44° wide - 1.5° tele	0 to 45
Hitachi DISC120R	Estimated: ≈ 800	1280×720	9 to 12	50 x 60 x 89.5	260	30x	44° wide - 1.5° tele	-10 to +60
Sony EV7500	750.00	1920×1080	6.0 to 12.0	50.0 x 60.0 x 89.7	260	30x	45° wide - 1.6° tele	-5 to +60

Gimbal with EO and IR Cameras

Electro-optical imaging and infrared sensing are achieved through the use of cameras detecting optical and infrared electromagnetic waves. For the detection of small leakages from 1000m altitude both high resolution and high stability cameras are required. To achieve a high level of stability a gimbal should be used. Table 2.11[19] shows the current market for EO/IR gimbals used in UAVs of the United States Army.

Table 2.11: EO/IR Gimbal used in military UAVs

Sensor	Power [W]	IR Detector (µm)	Diameter [in]	Height [in]	Weight [lbs]
WESCAM Versatron 12DS200	210	3-5	12	14.6	47
Star Safire AN/AAQ-22C	360	3-5	15.1	17.55	92
MicroStar	28VDC	3-5	9	13.5	26
SeaFlir Family	28VDC	3-5	9	15.2	26
Ultra 7000	450	3-5	9	13.5	26
AN/AAS-44(V) Lamps Flir	200	3-5	16.7	18.6	11.4
Baseline MMP	310	3-5	15.0	19.6	70.5
BriteStar	800	3-5	16.1	19.3	113
SAFIRE II AN/AAQ-22	-	8-12	15.1	17.55	88

Table 2.12: EO/IR Gimbal used in civil UAVs

Sensor	Power [W]	IR Detector [µm[	Diameter [cm]	Height [cm]	Weight [kg]
CM100	12	3-5	9.91	12.7	0.82
CM160	12	3-5	16.0	23.6	1.45
CM202	55	3-5	18.8	29.5	3.63

Table 2.12[25] shows the CM family of gimbals currently used for civil UAVs. It can be seen that these turrets used by civil UAVs are much lighter and smaller than military ones. Nevertheless, when comparing these values with the ones found in Table 2.11, one can see that these results do make sense. As the turret diameter decreases, the height, weight and power decreases.

2.4.2. COMMUNICATION

The communication payload and ground station are required for the operation and control of the UAV. There needs to be a ground station from which the operators can control the UAV and monitor what the sensors receive. The communication data link will be performed via satellite, for which the ground station and UAV need a antenna.

GROUND STATION

The ground station usually consists of two consoles; one for the control of the aircraft and one for the payload. The UAV has a small payload that needs to be controlled, only the gimbal camera needs direct control from the operator. But all the received data needs to be analysed by the ground station. When there is an issue detected by the payload, the operator can make a change in the mission to make the UAV fly back and do more surveillance on the specific point.

[25] URL http://uavvision.com/product/cm202-3/ [cited 20 June 2016]

There are two main ground control stations (GCS); the portable GCS is a station that is packed in a case which makes it easy to move, or a container based GCS that includes all the equipment inside a container where the operators can sit inside. Table 2.13 shows example ground stations that are currently available on the market (where NI stands for not included).

Table 2.13: Ground Stations

Unit	Data link	Displays	Control inputs	Features
UAV Factory GCS [26]	NI	17" and 13" touch screen	Keyboard, mouse, joystick	Portable; battery provides 2h operation, can be hot-swapped without restarting
UAV Solutions Portable GCS [27]	NI	3x17" TFT LCD	Mouse	Portable
Bluebird Portable GCS [28]	NI	3x17" TFT LCD	Mouse	Portable
IMOC [29]	customisable	6 monitors	customisable	complete, mobile, self-contained, climate-controlled work environment

REMOTE CONTROL

The remote control will be performed with small commands to give directions to the UAV, which then autonomously has to fly to the provided direction. This kind of control has less hard requirements for the communication channel, because it does not need a continuous connection. The autopilot payload needs to be selected for this control system. Table 2.14 shows the available autopilots for UAVs.

Table 2.14: Autopilots

Unit	Power	Size [cm×cm×cm]	Weight in UAV [g]	Control
MicroPilot's MP2x28g2 [30]	140mA @ 6.5V	4.0x10.0x1.5	28	GPS waypoint navigation; independent operation
wePilot 300 [31]	450mA @ 12V	16.5x11.6x6.1	300	GPS waypoint navigation; independent operation
VECTOR [32]	2.5W	4.5x6.8x7.45	180	Auto flight plan execution (waypoints); independent operation
SC2 [33]	160mA @ 5V	12.3x7.8x4.3	285	
U Pilot [34]	4W	8.9x3.5x15.5	280	independent operation

COMMUNICATION

The communication should be performed with a satellite link, since a line of sight communication is not possible for the long range mission. For the satellite communication, two options are available: optical or radio communication. The optical communication requires a smaller antenna, half the mass and power for the same data rate. However the optical provides wider coverage, multitasking services and can be applied in omni-directional applications [21]. On the market there are currently no commercially available optical communication units. Therefore radio communication is the preferred option. A short overview of available communication units for the UAVs is shown in Table 2.15.

Table 2.15: Market analysis of communication units for UAVs

Unit	Power [W]	Size [cm× cm×cm]	Weight in UAV [kg]	Data transmission [kbps]	Frequency
RockBLOCK [35]	5V 100mA	7.60x5.15x1.90	-	340bytes downlink 270bytes uplink per message	Iridium Antenna 1621Mhz tuned patch antenna
Gilat BlackRay 1000[36]	350	25.4x46x46	13.6	4000	Receive 10.95-12.7 GHz Transmit 14.0-14.5 GHz
Cobham SATCOM AVIATOR UAV 200[37]	28	24 x 16 x 6	1.45	200	-
GNOMAD SR-3000/20[38]	≤ 700	114 x 89 x 18	38.6	Receive: ≥ 2000 Transmit: ≥ 512	Receive: 10.95 – 11.7 GHz or 11.7 – 12.75 GHz Transmit: 14.0 –14.5 GHz
Ku-band SATCOM Data Link (KuSDL)[39]	50	Diameter: 76	-	Receive: 200 Transmit: 3200 or 1600	Forward: 12.75 GHz Return: 14.50 GHz
ROCKWELL COLLINS SAT-2100[40]	395	20 x 26 x 32	13.2	500	-
ViaSat Models 2540 / 2532[41]	395	Diameter: 80.8 Height: 20.6	38.6	Forward: 70-100 Mbps Return: 2.5-20Mbps	Transmit: 28.1-30.0 GHz Recieve: 18.3-20.2 GHz
ViaSat Aero Mobile Terminal 5230[42]	335W	20.3 x 27.9 x 8.64 37.1 x 12.4 x 19.4	17	Forward: <42000 Return: <4200	Transmit: 29.5-31.0 GHz Recieve: 19.7-21.2 GHz

2.4.3. EMERGENCY

This section is a continuation of Section 2.3.3 where all the possible emergency circumstances were considered. Possible proven solutions to increase the safety of UAV and reduce operational risks will be discussed below.

PARACHUTE

A far safer method of making an emergency landing than a belly landing is achieved through the usage of a parachute. The first ballistic parachutes (make use of a small explosion to eject the parachute) were used on the Cirrus SR20 in 1998 as standard equipment. A ballistic parachute is preferred over a conventional parachute because it ejects the parachute canopy, causing it to open rapidly. This makes them a very interesting option in the case of small aircraft, especially when they are close to the ground. Nowadays, several other well known aircraft such as the Piper PA-28, Cessna 172 and the Cessna 182 make use of a similar system. In the case of the Cessna 172, a 35-foot diameter parachute known as the BRS-172 which can carry around 12500 pounds is used.

Investigations concerning the use of ballistic parachutes in the case of larger and faster aircraft is ongoing already. Ballistic Recovery System (BRS) is investigating the use of a two stage chute. In the case of the SCULPTUR mission, the initial stage would slow the aircraft to a speed of around 90 m/s while the final stage would manage the actual descent by bringing the aircraft to a stand still. This can be seen in Table 2.16. In this table, two BRS systems are shown as well as a Magnum recovery system. These 3 systems have a maximum deployment speed higher than the SCULPTUR cruise speed. In fact, these are the parachutes with the lowest speed values. Furthermore, this table indicates how the parachute is packed. Either in a canister (CAN) or in a soft pack (SP). Finally, the Magnum is made for Special Light-Sport Aircraft (S-LSA) type aircraft.

Table 2.16: Ballistic Parachutes for UAVs

Ballistic Recovery System	Weight [kg]	Maximum Load [kg]	Maximum Deployment Speed [km/h]	Size [cm x cm x cm]	Price [US$]
BRS-6-1050-CAN[43]	26	475	252	55x18	5170
BRS-6-1350-SF[44]	30.1	612	252	41x25x15	4700
Magnum 601 S-LSA[45]	27.3	620	220	43x25x21	-

There are also certain changes on the configuration of an UAV that have to be undertaken in the case a parachute is included. There must not be any interference between the airframe/propulsion system and the parachute. The parachute must stay clear of the propeller or be located to the side especially in the case of a pusher propeller. A way to solve this is the use of ducted propellers which could protect the propeller from the parachute.

FLIGHT DATA RECORDER

A flight data recorder, informally known as a black box, is used in aircraft to facilitate the investigation of aviation accidents and incidents. This recorder preserves the recent recording of dozens of parameters collected several times per second. This allows to view the aircraft in any condition of flight. The box is designed in such a way that it is capable of surviving the conditions that are likely to occur with such aircraft. Furthermore, in the case of manned aircraft, the flight data recorder is coupled with a cockpit voice recorder which records the recent sounds in the cockpit. Both these recorders give an insight on the aircraft's history before the accident or incident.

Table 2.17 shows light-weight flight recorders that are available on the market and other available options for flight data storage. The usual flight data recorders used in civil aviation are too heavy for the UAV. The lightest option would be the Curtis Wright Fortress, which is still 2.6 kg. The other option for a flight data recorder would be an more simple data storage unit which has less protection then the usual flight recorders, but has the data storage availability. The options could be a Parrot AR.Drone 2.0 Flight Recorder, which is used in a quad-copter. SLICE Micro is produced by DTS, a company that specialises in data storage for testing applications for which the data storage needs a focus on survivability. A last option is a light data acquisition unit also from Curtis Wright.

Table 2.17: Market analysis of flight data recorders

Sensor	Power [W]	Data storage	Weight [g]	Length [mm]	Width [mm]	Height [mm]
Curtis Wright Fortress [46]		25 hours	2600			
Parrot AR.Drone 2.0 Flight Recorder [47]	5V TBC	4GB	31	77.7	38.3	12.5
SLICE Micro [48]	12V 70mA	16GB	28	42	42	8
Curtis Wright microKAM [49]			260	125	51	47

2.5. SWOT ANALYSIS

In Figure 2.10, a SWOT analysis is presented, with which the competitive position of UAVs on the market can be further analysed. UAVs are easy to install; due to their lightweight structure and small size, they can easily be transported from one place to another. They can be used in a variety of missions, with multiple purposes: communication, payload, computation, propulsion, material and manufacturing and military. UAV pilots require a different training procedure than airline pilots, which could lead to additional costs. Payloads that can be taken on board the UAV are rather limited in number and size: communication payloads are also susceptible to cyber attacks, one of the main reasons UAVs have not taken a larger portion of the civil market. Due to the ever growing market, there are many new and established companies. A threat, especially for the SCULPTUR project, is that the design team is not familiar with design procedures for UAVs so the end result is very unpredictable. This at the same time could be an advantage since the group is open to multiple options while the competitors always follow a certain procedure of doing things. Strong willpower is necessary establish to a solid ground in order for the market to grow. The main factor for commercial and civil UAVs that will determine how the market will develop in the near future are the uncertain legal and regulatory constraints.

2.6. OUTLOOK ON UAV TECHNOLOGY

The expansion of UAVs into public, private and commercial applications has increased the amount of such vehicles using the national airspace. This ever increasing presence of UAVs requires authorities to devise new legal and regulatory policies and procedures to assure the safety of future air-traffic.

Operators of UAVs will need to acquire various certifications from authorities such as, vehicle airworthiness, maintenance, pilot license, etc. Moreover, the implementation of these policies and procedure are long, tedious and costly. Hence, they will possibly hinder the growth of UAVs.

In addition to the policies, the future designs of UAVs need to take into account this congested airspace. Systems to automatically detect, predict and avoid incoming traffic need to be developed. The various types of UAVs will also require authorities to find a way to let each UAV use their specific functions while still safeguarding the rest of the air-traffic and public in general.

After the operational procedures have been implemented and the safety and guidance issues for UAVS are resolved, civil UAVs can be used for a wide range of missions. Two types of UAVs are currently considered for pipeline inspection (Table 2.5) [22]:

- Small and lightweight low-altitude UAV - Fly at low altitudes (100 m), carrying a payload of less than 25 kg and have an endurance of around 5-6 hours. An optical/IR sensor system is satisfactory in this case. Identifying the important features from the images is relatively easy because the processing is related to only one sensor. The main drawback is the fact that there are currently no set regulations for safe low

airspace automatic operation.

- Medium-size and medium-weight mid-altitude UAV - Fly at medium altitudes (>1000 m), carrying a payload of typically 200 kg and have an endurance of up to 30 hours. In general, it does not operate below the clouds therefore a Synthetic Aperture Radar (SAR) is required which could be used together with an optical/IR sensor system. There are multiple sensors used, making the image processing more time-consuming and computationally intensive. This UAV would operate in an ATM/ATC environment for which regulations regarding automatic operation still have to be developed and implemented.

Figure 2.10: SWOT Analysis - UAV

2.7. PREDICTION OF FUTURE UAV MARKET

In 2013 a five year forecast study (Figure 2.11) was conducted concerning the financial investments for UAV technology. A rise from $7bn to $8.2bn is expected, with the biggest growth being attributed to the increase in the number of UAVs used for civil applications. The technical capabilities of UAVs are rather limited in the present, photography and filming being the main uses for UAVs. Where human life cannot be risked, in areas that are dangerous or difficult to access, drones are a good option. Around 41800 land- and sea-based unmanned systems worth about 10.5 billion are forecast for production during the 2014-2023 forecast period. From this amount, the value of production for yet-undetermined manufacturers is nearly $1.3 billion.

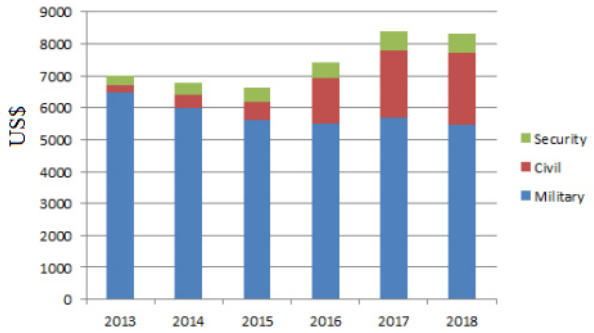

Figure 2.11: Market forecast for Security, Civil and Military UAVs[23]

3 Mission Definition & Design Strategy

In the previous chapter, the missions that are currently carried out by oil and gas companies are presented. The following chapter goes one step forward and presents the mission that SCULPTUR has to accomplish (Section 3.1). This consists of a need statement as found in the introduction of this report (Chapter 1) followed by a mission statement. Moreover, a country is chosen for where the mission can be carried out. This choice allows the investigation of the oil and natural gas pipelines in the country which, in turn, allows the creation of a specific mission. Also, knowing the country is needed for the UAV certifications (Section 3.3). When the specific mission is known, the functional diagrams can be made (Section 3.2). Once these are finished, the sustainability strategy is discussed in Section 3.4. All the aforementioned sections are needed in order to be able to set the requirements for this mission (Section 3.5). The design of the UAV is based on these requirements. From these, one can then do a risk assessment (Section 3.6). A general overview of the verification and validation strategy used throughout the rest of the report is given in Section 3.7 and finally, the initial budget and resources is presented in Section 3.8.

3.1. Mission Analysis

The SCULPTUR mission is provided by a need expressed from companies and governments with an extensive pipeline network. Due to this need, an opportunity rose from which SCULPTUR will profit. The need and opportunity found resultes in a specified mission for SCULPTUR. The mission of SCULPTUR is defined by formulating a mission need statement and a mission statement.

Need Statement

In the introduction of this report (Chapter 1), the need statement is expressed. This need arises from the impact that pipeline leaks have on the environment.

Pipelines must be monitored to prevent incidents and accidents that may generate substantial safety issues for the environment.

Mission Statement

The mission statement communicates the main purpose of this system. As mentioned previously, the UAV has to detect leakages of oil and natural gas pipelines. Furthermore, detecting leaks with a minimum mass flow rate of 1% of the total pipeline mass flow rate is the competitive industry standard for surveillance UAVs [24].

An Unmanned Aerial Vehicle will provide a sustainable, safe and economically viable solution for oil and natural gas pipeline surveillance in remote areas to detect leaks.

Furthermore, in Chapter 1, the main requirements that this UAV needs to comply with are stated. One can clearly see that the UAV needs to be designed to be able to carry out the missions in very remote areas with long distances for long periods of time. A country in which this UAV could be very useful is Australia. The country choice will be further expanded in the next section.

Country Selection

Australia is the 13^{th} largest economy in the world. Its economy is highly dependent on imported crude oil and petroleum products (around 80%). There are over 9000 kilometres of natural gas and crude oil pipeline systems across Australia. Moreover, as seen in Figure 3.1, very long pipelines can be found in the driest and most remote parts of Australia. Its population has one of the lowest densities in the world. In fact, most of Australia's population lives on the south-eastern coastline. Due to its very dry climate, long distances, very remote and uninhabited locations, the use of a UAV would benefit pipeline companies in Australia enormously. In case of emergencies, it could be very complicated to help the pilots and crew of normal surveillance aircraft. This risk can be limited by introducing the use of UAVs. Furthermore, said country has a very important wild life that would be negatively affected by leaks in oil and gas pipelines. Finally, the distances that need to be covered are very long, thus, a UAV with high endurance and range would allow to carry out long surveillance missions without having to land and refuel, making it more efficient. It was therefore decided to design the UAV for operations in the remote areas of Australia. Furthermore, there are thousand of kilometres of pipelines available. Hence, the next section will explain a possible mission for a specific pipeline.

Possible Mission

Figure 3.1[50] shows a map of the main oil and natural gas pipelines in Australia. The red lines are natural gas pipelines while the green lines are oil pipelines. Hence, one can clearly see that most of Australia's pipelines are

[50] URL http://www.theodora.com/pipelines/australia_new_zealand_and_papua_new_guinea_oil_gas_products_pipelines_map.html [cited May 18 2016]

used to transport natural gas. Furthermore, in this figure, one can see 6 black diamond shaped spots. These show domestic airports near these pipelines and their respective ICAO codes[51]. A particularly interesting area is the one where Alice Springs (YBAS) airport is located. It is very near the G4 oil pipeline and the G2 natural gas pipeline. Hence, this mission can test the SCULPTUR UAV for both types of pipeline it is designed to survey. This is chosen as an exemplary mission to test the design of this UAV. This missions consists of taking off at Alice Springs, carrying out the surveillance travelling 200 km west over the G4 pipeline and then 1000 km north on the G2 pipeline. Finally, the SCULPTUR UAV will land at YTNK, 400 km away. The choice of taking off and landing in an airport is to facilitate the choice of landing gears. Otherwise, the UAV would need special landing gears to take off and land in hard terrain.

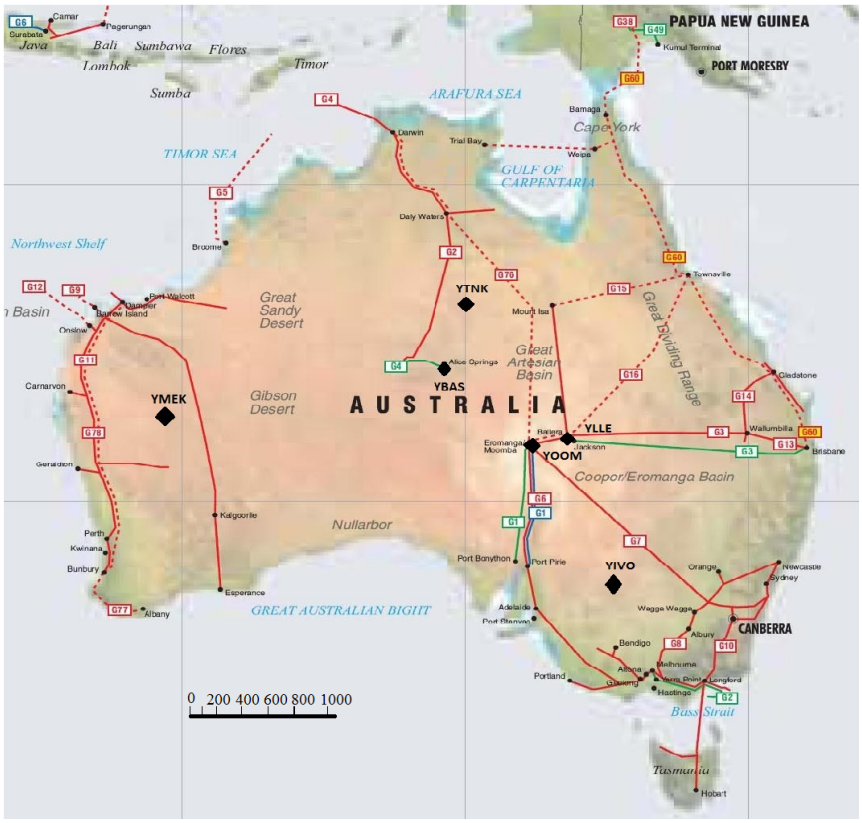

Figure 3.1: Pipelines in Australia

3.2. FUNCTIONAL DIAGRAMS

This section presents the Functional Break-Down Structure and the Functional Flow Diagram. These diagrams give the reader an insight into the functions that this UAV follows during operation. The difference between both diagrams is the level of details and the order in which the activities and tasks are stated. The level of detail in the break-down diagram is found to be three levels deep, whereas only two levels of detail appear in the functional flow diagram. A description of the first two levels is given in Section 3.2.2.

3.2.1. FUNCTIONAL BREAK-DOWN STRUCTURE

The functional break-down diagram is an "and" tree visualisation of the functional flow diagram (Figure 3.3). This section will briefly describe the third level activities within the functional break-down diagram. A visualisation of the top level of the functional break down diagram is shown in Figure 3.2, the visualisation of the second and third level of the break-down diagram can be found in Appendix C.

[51] URL https://www.google.com/maps/d/viewer?mid=1P7WCsAI4-C3DI9odSLGwAuR4tg0&hl=en_US [cited May 18 2016]

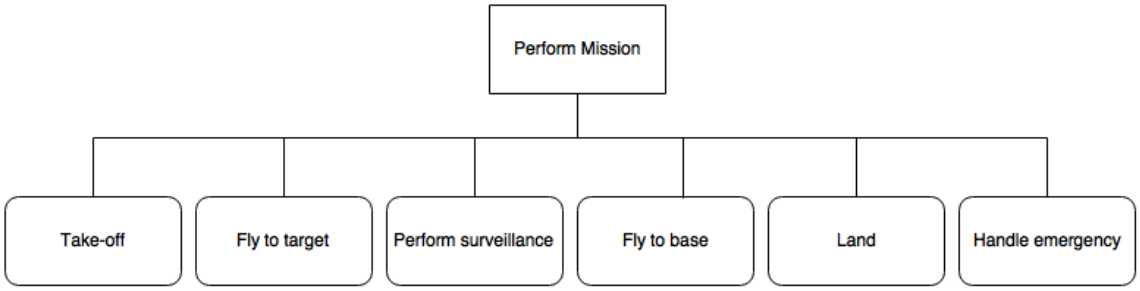

Figure 3.2: Top Level Functional Breakdown Diagram SCULPTUR

The first activity which takes place to start the mission is the visual inspection of possible mechanical and/or structural flaws. After ensuring the inspection has taken place, the systems are started and a pre-flight checklist is carried out to guarantee all software, electronic, hydraulic or mechanical systems and mechanisms function properly. After this, the flight track for the mission and the take-off track of the UAV is determined and uploaded. When this is finalised, the actual take-off of the UAV takes place. The final activity in this phase is to transfer from take-off to cruise mode, an operation performed by adjusting landing gear position, control surfaces and power settings.

The second stage in the mission performance is the flight to target, which is an extended cruise flight. The two main functions of the UAV during cruise flight are to maintain flight path and cruise flight conditions. This is done by first determining the location of the UAV, which is then used for optimising the flight path. The adjustment of this flight path is achieved through control commands from the ground station or by autonomous commands. Maintaining cruise conditions is done by adjusting the appropriate power settings depending on the type of cruise flight the UAV is required to perform (e.g. long-endurance/long-range etc.). Furthermore, states like airspeed and altitude are measured, after which again control commands are given to optimise or alter them.

When the UAV has reached its target location, the surveillance phase begins. This phase is initiated by transferring from cruise to surveillance mode, which includes a change in power, altitude and/or control surface setting. During this phase, the payload is activated, data is obtained and possibly transmitted to the ground station. The phase is concluded by transferring back to cruise mode.

The final stage of the cruise mode is when the UAV returns to base; this procedure includes similar activities as the phase of flying to target. The flight path is optimised according to commands provided by En Route Air Traffic Controllers (ATC).

Finally, the aircraft enters an approach & landing phase. The radio frequency is adjusted and contact is initialised with the appropriate Approach ATC. On the operational side of the UAV, a transformation to landing configuration. Control commands regarding the deployment of the landing gear and control surfaces are provided to ensure that the aircraft can safely approach and land at a lower speed. On touch-down, ground and aerodynamic brakes are deployed to ensure the UAV can safely decrease its speed for taxiing to the allocated ramp. For ground route manoeuvring, the radio frequency is adjusted once again in order to make contact with a Ground ATC. After the aircraft has come to a stand-still, a post-flight checklist is carried out by checking for structural damage and overall performance of the different subsystems. Only after this is performed, the system is shut down.

Aside from the five required phases during the mission performance, an extra phase is added in case of an engine failure. When an engine failure occurs, the UAV shall be able to land safely, hence to accommodate this requirement, several steps are taken. At first the UAV shall be able to determine the severity of the emergency, and whether it is capable to fly back to base or if a direct emergency landing is necessary. When this is resolved, the optimum emergency landing track is determined in order to perform the landing at the decided site. On completion, the UAV transfers to emergency landing mode, which may include the activation of emergency landing systems. After the emergency landing is finalised, a post-emergency landing check is performed, consisting of the regular post-flight checks, together with a more thorough inspection of the failure and how it has occurred. After the completion of the checks, the system is shut down.

3.2.2. FUNCTIONAL FLOW DIAGRAM

In Figure 3.3 the Functional Flow Diagram is shown. This diagram shows the functions during the operation of the UAV in a chronological order. In the first block, the aircraft takes off (1.0). Following, it is flown to target (2.0), which can be a short or long distance. After reaching the target, surveillance is performed (3.0). When surveilling is done, the UAV flies back to the base (4.0). Once it reached the base, it lands safely (5.0). Whenever an emergency situation arises in flight (e.g. engine failure), the UAV immediately goes into an emergency mode, which will ensure the UAV lands safely (6.0).

The first step, concerning the take-off procedure, is to start-up all the systems of the UAV and perform the pre-flight operations check. After these checks are completed, the UAV is set for take-off. Given that the take-off is executed correctly, and the required altitude is reached, the aerial vehicle is transformed to configuration.

Furthermore, in order to shift into surveillance mode, some configuration changes are performed. Subsequently, the payload is activated to perform the surveillance, and when this is done, the actual surveillance data is obtained. Once finished, the payload is deactivated again and the UAV goes back to cruise regime.

Concerning phase 5.0 (landing), the UAV first needs to transform into landing configuration and then it will be set for landing. When it is back on the ground, the post flight operations are performed in which the status of the UAV and data are checked. The last step will be to shut down the system.

In case of emergency, its severity is first determined to check if there is a possibility of reaching base or not. If the emergency is too severe, the UAV goes into emergency landing configuration and performs the emergency landing at a local area. Following, special post-flight operations are performed to ensure the reason for the emergency condition has been resolved. Finally, the system is shut down.

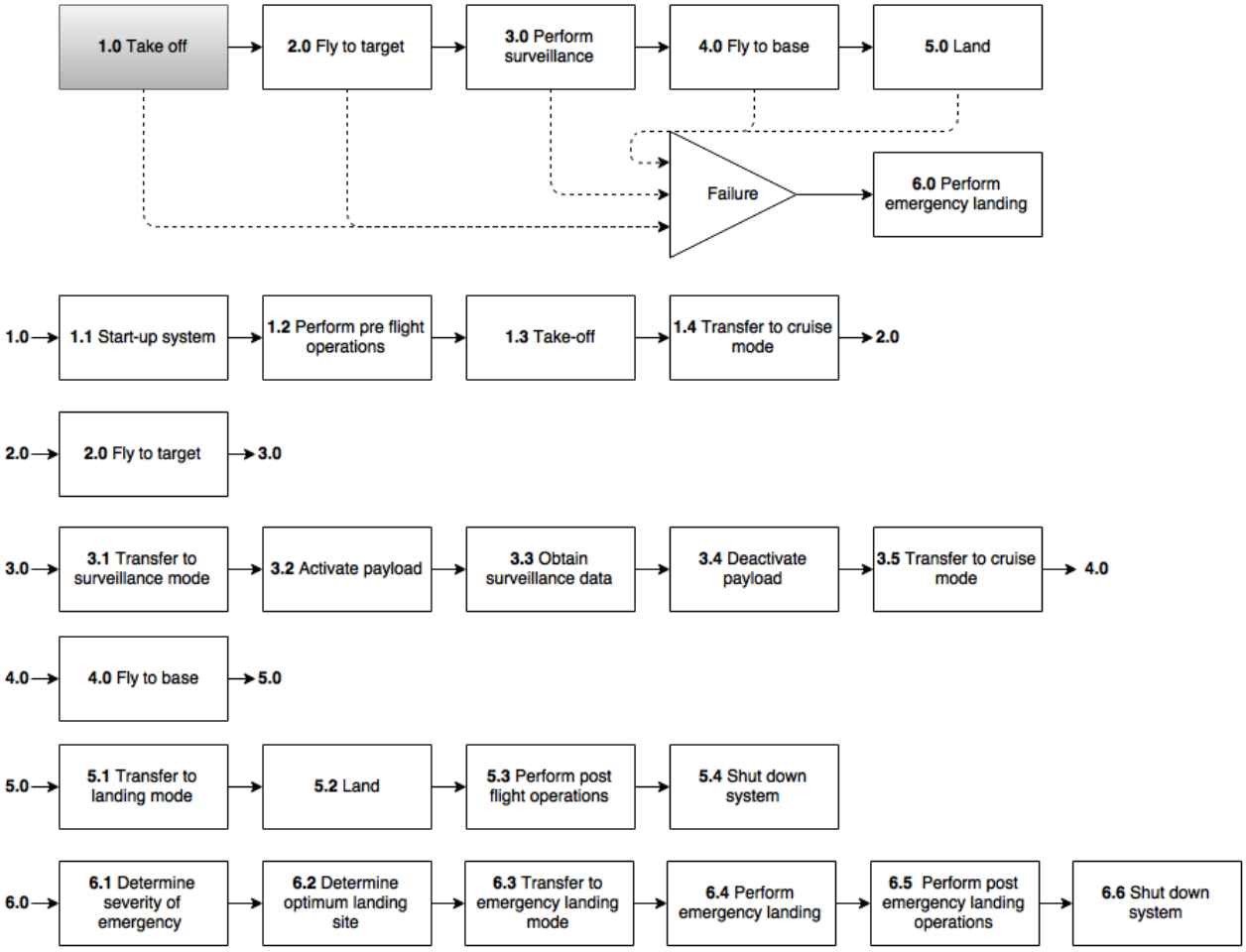

Figure 3.3: Functional Flow Diagram SCULPTUR

3.3. UAV CERTIFICATION

In order to fulfil the mission stated in Section 3.1 the UAV must be certified to fly in the mission state, Australia. This certification has to be approved by all governing organisations influencing the safety of the Australian airspace. Certification therefore does not only include national, but also international organisations of which Australia is registered as a member-state. Certification of the UAV serves several functions in order to sustain the mission. Namely to provide minimal requirements in case of emergency, and to ensure safe flight by requiring minimal redundancy in the system. These functions are ensured through different types of UAV approval, as described in this section. This section furthermore describes the different organisations influencing the certification of the SCULPTUR UAV, and the requirements they impose on the design process.

3.3.1. NATIONAL CERTIFICATION

Rules and regulations in Australia are published by the Civil Aviation Safety Authority, CASA, of Australia[52]. This organisation has been working on revising their regulations concerning the certification process and regulations of aircraft, to separate the UAVs from the aircraft. The need for this separation arises from the limited coverage of the current certification of aircraft with respect to remote equipment required for UAVs. Additionally the current airworthiness standards of aircraft (e.g. Parts 23 and 25) are found to be inappropriate to certify UAVs in relation to the safety of the occupant [25].

Currently, large UAVs (>150 kg) [26] need 4 types of approval to be fully certified and allowed to fly in Australian airspace. Namely, operating area approval, operator approval, aircraft approval (in the form of an airworthiness certificate) and operating approval. These approvals are given based on Part 21 and Part 101 of CASR (Civil Aviation Safety Regulations)[25]. Due to the limited applicability of Part 21 to UAVs, some design standards [27] are given. This is done to give guidance to UAV developers to comply with the regulations and to obtain an airworthiness certificate.

According to the market analysis performed and the resulting weight budget as described in chapter 3, SCULPTUR has to be certified according to these 4 types of approval.

OPERATING AREA APPROVAL

Before the UAV is allowed to operate in a certain area it has to receive an operating area approval. This specific type of approval can be temporary, semi-permanent or a permanent depending on the regularity of flight in the desired area. The aim of this approval is to alert other aircraft in the airspace of the possible presence of UAVs in the particular area. Said approval can be given after consultation between CASA, the UAV operator, air services Australia, the regional airspace users and the advisory committee [26].

As described in section 3.1 the mission of SCULPTUR is performed in remote areas at an altitude of 1000 m, where little aircraft will be present. These airspaces are classified as Class G[53] airspaces, and are considered to be uncontrolled as no ATC clearances are required. The operating area therefore does not imply additional requirements on the UAV during these operations. Restrictions are implied if a controlled civil airport (Class C or D) is used for take-off or when flying within 3 nautical miles of a controlled aerodrome at an altitude above 400 feet AGL. To pursue certification to also fly in these areas, air traffic control clearance is required. In order to obtain this clearance the UAV ground control center should be able to communicate with the local ATC.

OPERATOR APPROVAL

The second type of approval relates to the operator of a commercial UAV which should obtain an unmanned operator certificate (UOC). This certificate is issued by CASA when it is proved that the operator is able to control the UAV safely. This approval can be issued with or without special conditions to the operator. This limits the time, place or type of UAV the controller may get certified for [26].

Applying for an operator certificate at CASA requires the pilot to perform multiple assessments in a time period of approximately 3 months. These assessments consist of following a remotely piloted aircraft system (RPAS) training offered by CASA, a type training offered by the manufacturer, with an additional need for an aircraft radio operators certificate (AROC) for operations outside of line of sight. The costs of this certification process is estimated by CASA to be around 7500$ for each required pilot of the UAV[54]. The issued certificate remains in force until cancelled by CASA.

Due to the long endurance mission of SCULPTUR described in Section 3.1, a total of 4 pilots per location will need to be trained. This is determined keeping in mind shift work and maximum working hours for each pilot. The risks of certifying to few pilots to control the aircraft could lead to long working hours, lack of concentration when observing the images during real time surveillance missions, and therefore missing possible leakages. The total cost for operator certification per location will be around 30,000$.

OPERATING APPROVAL

All large UAVs require operating approval from CASA before it is taken into use. For flights outside of controlled airspace, CASA will base its approval on the proposed mission and other aircraft in the airspace. For flights in controlled airspace or over populous areas, CASA will base its approval on the proposed mission and limitations in the airworthiness certificate and operations manual[26].

Since SCULPTUR performs its mission mainly over non-populous areas, little limitations will be present for it to receive an operating approval. A requirement is present for SCULPTUR to carry a manufacturer's data plate and aircraft registration identification plate on the UAV, which allows the airworthiness authorities to identify each aircraft [25]. Another demand of the SCULPTUR UAV is that, when operating over a populous area, it should fly at

[52] URL https://www.casa.gov.au/ [cited May 26 2016]
[53] URL http://www.airservicesaustralia.com/services/how-air-traffic-control-works/separation-standards/ [cited June 24 2016]
[54] URL http://remotepilot.com.au/uav-controller-certificate-in-australia/ [cited May 26 2016]

a minimum height from which it would be able to clear the area if any of the components fail. This requirement demands a sufficient gliding performance of the UAV, of approximately 2,600 meters for the mission described in section 3.1. This distance is based on the average radius of the city of Alice springs, which is the biggest city after the capital city, Darwin, of the Northern Territory of Australia. Darwin itself was not considered due to its remote location and considerable distance from our exemplary mission.

AIRCRAFT APPROVAL

The UAV is approved by means of a certificate of airworthiness [26]. This airworthiness certificate is issued according to the design specifications as stated in Part 23 and 25 [27]. These parts specify requirements for design, allowable load factors and safety requirements. Approval for the UAV to fly over or in certain areas is dependent upon the conditions imposed on its certificate of airworthiness. To ensure that the SCULPTUR can get fully certified when taken into use, the design standards given by CASA are translated into requirements for the UAV design. An overview of all requirements is described in section 3.5.

3.3.2. INTERNATIONAL CERTIFICATION

Aside from Australia's national certification regulations imposed by CASA, Australia is also a member of ICAO, the International Civil Aviation Organization[55]. ICAO is a UN specialised agency with 191 member states and industry groups, working together to reach consensus on international civil aviation standards and policies to support a safe, efficient, secure, economically sustainable and environmentally responsible civil aviation sector. Member states of ICAO must conform with the standards imposed on them to ensure they conform to global norms [28].

The effects of this additional organisation influencing the regulations are focused on higher-level performance demands of the UAV. It focuses on what the UAV should be able to do, without specifying how it should. Since Australia is a member-state of ICAO, the regulations described above do also satisfy the ICAO standards. Hence, the UAV will comply with regulations for flight by both ICAO and CASA if the approvals described above are given.

Considering the possibility for operation in other countries outside of Australia a comparison was made of the 5 countries with the largest number of kilometers of pipeline, namely the United States, Russia, Canada, China and Australia itself. The differences between their certifications can be found in [4]. From this it can be concluded that difficulties were found considering the certification in China and Russia, but that they were generally found to be less strict than the Australian regulations. The application of SCULPTUR in China and Russia will therefore have a high likelihood of being possible without further modifications. Furthermore the US was found to have different regulations for different states, making it difficult to get approval for UAV pipeline inspection as they would cross state-borders. Lastly the Canadian regulations were well defined, making it slightly more complicated to operate the SCULPTUR UAV without changes in Canadian airspace. For operations in Canadian airspace, small modifications to the UAV are likely to be necessary.

3.4. SUSTAINABILITY STRATEGY

The depletion of fossil fuels and the ongoing climate change has caused the world to realise that in order to maintain our current living standards, our global future will depend on sustainable engineering. To facilitate the changes to sustainable development of current technologies, emission reduction plans are implemented by governments and international organisations. In the aviation industry, a large organisation quantifying these goals is ICAO, who sets design standards for the development of new UAVs [28]. Aside from the reduction of emissions, sustainable engineering covers multiple other aspects of the design process. This section will cover the different aspects to sustainable engineering, and will focus on the implementation of a sustainable development strategy in the SCULPTUR project.

To be able to follow a sustainable engineering approach, a clear definition must be given. In this design process, a product is observed to be sustainable when it meets the needs of the present without compromising the ability of future generations to meet their own needs. Attaining this goal is done by combining the three main dimensions of sustainable development as described by Broers [29]. A visualisation of the three dimensions is given in Figure 3.4 together with the method op application of each dimension in the SCULPTUR design process.

[55] URL http://www.icao.int/MemberStates [cited May 26 2016]

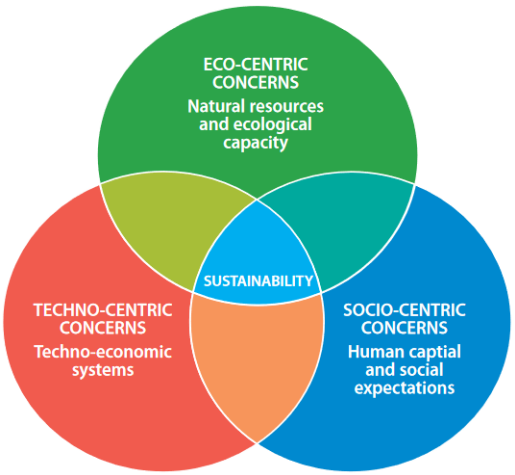

Eco-centric:
- Reduce emissions
- Reduce noise
- Reduce usage fossil fuels

Socio-centric:
- Remove risk to human operator
- Improve safety of population

Techno-centric:
- Reduce operational cost
- Elongate life-time
- Improve reuseability
- Reduce production waste

Figure 3.4: The three dimensions of sustainability and their application to SCULPTUR [29]

3.4.1. ECO-CENTRIC CONCERNS

The first dimension of sustainability are the eco-centric concerns of the design. In this dimension the ability of the planet to sustain us with materials and fuels, as the ability of the planet to accommodate our emissions is discussed. As the Earth is no longer able to sustain the growing emissions of greenhouse gasses, the emissions of SCULPTUR will need to be lower compared to current existing solutions. A second concern is found in the depletion of fossil fuels. Since less fossil fuels are being available on Earth, it is of great importance to reduce the dependency and usage of this product. According to ICAO, the goal for SCULPTUR should be set at reducing the CO2 emissions and fuel consumption to 10% of current small single-engine manned aircraft [28]. Lastly, noise emission is found to be influencing wildlife and its surroundings, and must therefore be limited. The goal for SCULPTUR is to reduce the noise level with 6 to 9 dB compared to a small single-engine manned aircraft [28].

3.4.2. SOCIO-CENTRIC CONCERNS

The second aspect of sustainability is the social matter of the design. To create a design which is accepted and inspires society, it is important that it provides a solution for our current society and future society. The SCULPTURE UAV provides for a better future by reducing the risk to humans involved in surveillance missions, as no human crew is required on board of the UAV. Also the implementation of SCULPTUR improves the living conditions of the future by improving current surveillance accuracy. A higher accuracy is achieved using high performance camera's as described in section 2.4 that together with the reduced vibrations of the implemented gas turbine result in a clearer, higher resolution image [30]. This improved performance will lead to the detection of smaller leaks, therefore decreasing possible environmental impact of leakages. As a result, the safety of wildlife and population near pipelines is improved.

3.4.3. TECHNO-CENTRIC CONCERNS

Lastly the influence of SCULPTUR (technology) on the economic system is considered. To generate a promising market for SCULPTUR, it should be competitively priced compared to current existing solutions. To ensure a market, SCULPTUR will provide for low operational costs by performing long endurance surveillance missions. Aside from its mission profile, also the UAV design and production process is involved. The design of the UAV is focused on elongating the life-time and reducing maintenance needs by selecting proper, durable, materials. During production, additional attention is given to creating a lean manufacturing environment, in which waste will be reduced[56]. The favourable aspects of SCULPTURE will even continue after its end-of-life, as it will be designed using reuseable materials and components. This way parts that are still able to function in different industries can be recycled and sold again. With these approaches kept in mind, a competitive development cost with a maximum of 3,000$ per kilogram operational empty weight is to be achieved [30].

3.5. REQUIREMENTS

Requirements are the basis of the design process as they impose constraints on possible solutions. The source of requirements is diverse, as they come from stakeholders, regulations or simply to ensure competitiveness with the current market. This section will describe the requirements of the design of SCULPTUR, as given in [30], from certification regulations imposed by CASA and ICAO [26] [25] and from the sustainability aims as described in section 3.4. The requirements are grouped into the sections performance, safety and reliability, sustainability, ground control and cost, which cover the main areas of the design process.

[56] URL http://www.sixsigma.nl/lean-manufacturing [cited May 30 2016]

3.5.1. PERFORMANCE

SCULPTUR-SH-01 The UAV shall have an endurance of 20 hours

SCULPTUR-SH-02 The UAV shall be able to carry a payload (e.g. IR and day camera, sensors,etc.) up to 50 kg

SCULPTUR-SH-03 The UAV shall be remotely controlled by a ground crew

SCULPTUR-SH-04 The UAV shall have a cruise altitude of 1000 m

SCULPTUR-SH-05 The UAV shall have a cruise speed of 100 km/h

SCULPTUR-SH-06 The UAV shall have a maximum flight distance of 1800 km

SCULPTUR-SH-07 The UAV shall be powered by a mini-turboprop gas turbine

SCULPTUR-SH-08 The UAV shall have a sufficient climb gradient when taking off or performing a balked landing

- **SCULPTUR-PERF-SH08-1** The UAV shall have a climb gradient of at least 8.33% with take-off power on the engine and a calibrated airspeed of 1.3 V_{s1}
- **SCULPTUR-PERF-SH08-2** The UAV shall have a climb gradient of at least 3% with take-off power on the engine and a calibrated airspeed of 1.3 V_{s0}

SCULPTUR-SH-09 The UAV shall be able to cruise

- **SCULPTUR-PERF-SH09-1** The UAV shall have the ability to climb at a gradient of 3.2% in standard atmospheric conditions at a speed not exceeding 1.3 times the stall speed.

SCULPTUR-SH-10 The UAV shall be able to take-off

- **SCULPTUR-PERF-SH10-1** The UAV shall be able to land on a runway of length as described in the CS-23 regulations

SCULPTUR-SH-11 The UAV shall be laterally statically stable

SCULPTUR-SH-12 The UAV shall be longitudinally statically stable

- **SCULPTUR-PERF-SH12-1** The value of the longitudinal stability coefficient (C_{m_α}) shall be negative

SCULPTUR-SH-13 The UAV shall be dynamically stable

- **SCULPTUR-PERF-SH13-1** Any short period oscillations, not including combined lateral-directional oscillations, shall be damped (UA25.181 a)

SCULPTUR-SH-14 The structure of the UAV shall be able to sustain the aerodynamic loads during all flight conditions

- **SCULPTUR-PERF-SH14-1** The UAV shall be capable to cope with positive (up) and negative (down) gusts of 50 fps at cruise speed which must be considered at altitudes between sea level and 6096 m (20000 ft) as specified in the CS-23 regulations
- **SCULPTUR-PERF-SH14-2** The UAV shall be able to cope with the loads during take-off
- **SCULPTUR-PERF-SH14-3** The UAV shall be able to cope with the loads during landing

SCULPTUR-SH-15 The aircraft shall be able to bank from 30 degrees one wing low to 30 degrees the other wing low in less than 4 seconds

SCULPTUR-SH-16 The aircraft shall be able to perform a cross-wind landing when wind speed is $0.4V_{s0}$ and at a 90 degree angle to the runway

SCULPTUR-SH-17 A single point failure of the propulsion system shall not lead to failure of the complete system

- **SCULPTUR-PERF-SH17-1** Each fuel pump shall be connected to an emergency fuel pump with an independent power source.
- **SCULPTUR-PERF-SH17-2** Each oil system shall have an endurance that exceeds fuel system endurance.
- **SCULPTUR-PERF-SH17-3** Each engine compartment shall be separated from the rest of the airframe by a firewall

3.5.2. SAFETY AND RELIABILITY

SCULPTUR-SH-18 In case of engine failure, the UAV shall be capable of landing undamaged

- **SCULPTUR-SR-SH18-1** The UAV shall make use of an unmanned control system capable of navigating the unmanned aircraft to pre-selected emergency sites when a recoverable failure occurs or performing a controlled crash when an unrecoverable failure occurs
- **SCULPTUR-SR-SH18-2** The UAV shall be certified according to CS-23 regulations regarding emergency

SCULPTUR-SH-19 The engine shall be able to operate at take-off power, without malfunctioning, for at least 30 seconds (UA25.959)

3.5.3. SUSTAINABILITY

SCULPTUR-SH-20 The emissions of the engine, in terms of SFC (specific fuel consumption), shall be comparable to other existing systems (e.g. reciprocating engines)

- **SCULPTUR-SUST-SH20-1** The fuel used by the UAV shall be ten times lower than a small single-engine, manned aeroplane as suggested by ICAO.
- **SCULPTUR-SUST-SH20-2** The CO_2 emissions shall be ten times lower than a small single-engine, manned aeroplane as suggested by ICAO.

SCULPTUR-SH-21 The noise emissions of the UAV shall comply with existing regulations

- **SCULPTUR-SUST-SH21-1** The noise levels of the UAV shall be 6 to 9 dB lower than a small single-engine, manned aeroplane as suggested by ICAO.

SCULPTUR-SH-22 The vibrations of the engine shall be lower than the values of current alternatives, primarily reciprocating engines

- **SCULPTUR-SUST-SH22-1** The maximum vibration stresses of the propeller shall not exceed the endurance limit for the material

SCULPTUR-SH-23 Waste management of the UAV shall comply with existing regulations

SCULPTUR-SH-24 All UAV components shall be able to be recycled and possibly allocated for different uses after decommissioning

3.5.4. GROUND CONTROL

SCULPTUR-SH-25 The UAV shall be able to relay flight data information to the ground control station.

- **SCULPTUR-GC-SH-25-1** A sensor to measure indicated airspeed shall be installed on the aircraft.
- **SCULPTUR-GC-SH-25-2** A sensor to measure altitude shall be installed on the aircraft.
- **SCULPTUR-GC-SH-25-3** A sensor to measure magnetic direction shall be installed on the aircraft.
- **SCULPTUR-GC-SH-25-4** A sensor to measure ground position shall be installed on the aircraft.

SCULPTUR-SH-26 The UAV shall be able to relay power plant information to the ground control station.

- **SCULPTUR-GC-SH-26-1** A sensor to measure engine RPM shall be installed on the aircraft.
- **SCULPTUR-GC-SH-26-2** A sensor to measure temperature shall be installed on the aircraft.
- **SCULPTUR-GC-SH-26-3** A sensor to measure pressure shall be installed on the aircraft.
- **SCULPTUR-GC-SH-26-4** A fuel quantity indicator for each fuel tank shall be installed on the aircraft.
- **SCULPTUR-GC-SH-26-5** A oil quantity indicator for each fuel tank shall be installed on the aircraft.

SCULPTUR-SH-27 The UAV shall be equipped with a system for rebroadcast of two way radio communications.

SCULPTUR-SH-28 The UAV shall be equipped with a programmable transponder with mode C.

SCULPTUR-SH-29 The UAV shall be equipped with two systems for radio navigation.

SCULTPUR-SH-30 The ground control station shall be equipped with a recording device.

- **SCULPTUR-GC-SH-30-1** The recording device shall record all aircraft communications.
- **SCULPTUR-GC-SH-30-2** The recording device shall record all sensor indications available to the operator of the control system.
- **SCULPTUR-GC-SH-30-3** The recording device shall store all recorded parameters for at least the last 30 minutes of operations.

3.5.5. COST

SCULPTUR-SH-31 The development cost of the UAV shall be lower than current empty weight cost per unit mass (≈3000 €/kg)

3.5.6. STRUCTURE

SCULPTUR-SH-32 The aircraft structure shall be able to withstand limit loads without permanent deformations and without deformations large enough to interfere with safe operation

SCULPTUR-SH-33 The aircraft structure shall be able to withstand ultimate loads with a positive margin of safety (analysis), or without failure for at least three seconds (static tests)

SCULPTUR-SH-34 The aircraft shall be designed for load factors between -1 and 2.5

SCULPTUR-SH-35 The landing gear shall be able to withstand the energy of landing with MTOW and an impact vertical load factor of 1.33

3.6. RISK ASSESSMENT

Unmanned Aerial Vehicles is an emerging sector in the aerospace industry. The potential benefits of using UAVs are limitless; they can be used for multiple missions, especially for those that are considered too “dull, dirty, dangerous or demanding” [31]. Even when complying with the existing regulations for UAVs, which are not

as clearly defined as for manned aircraft, accidents can still occur. A good approach to risk management is to compare a new product with an existing, proven product that can accomplish similar tasks. According to RTCA (Radio Technical Commission for Aeronautics):

"UAS must operate safely, efficiently, and compatibly with manned aircraft operation in the airspace so that the overall safety of the airspace is not degraded. The fundamental safety requirement for the UAS is to provide an acceptable level of risk for people and property in the air and on the ground [32]."

3.6.1. RISK IDENTIFICATION

It is important to anticipate and recognise all the risks presented for UAVs. This is why most of the related emergency situations on the market during history, listed in Section 2.3.3, have been closely investigated and considered for the risk identification. Determining the associated root causes will help with finding mitigation options. This is a rather straightforward approach but this can be problematic for UAVs: most of them are used for military purposes thus data available regarding the failures and crashes is scarce. Another thing to consider is that the investigation of UAV crashes is not as comprehensive as for manned aircraft: less time is spent due to no loss of human life and the documents are not made available to the public. When looking at reference data it is also important to look at the specifics of the mission itself because of their differences - area in which they fly, nature of the mission, altitude and speed etc. With that in mind, in Table 3.1, the main subsystems that fail for UAVs are presented together with the percentage of failure.

Table 3.1: Different failure modes for UAV [33]

Failure mode category	Description	% of total mishaps [1] attributed to category [2]
Power/Propulsion	Encompasses the engine, fuel supply, transmission, propeller, electrical system generators, and other related subsystems on board the aircraft	37 %
Flight Control	Includes all systems contributing to the aircraft stability and control such as avionics, air data system, servo-actuators, control surfaces/servos, on-board software, navigation, and other related subsystems. Aerodynamic factors are also included in this grouping.	26%
Human/Ground	Accounts for all failures resulting from human error and maintenance problems with any non-vehicle hardware of software on the ground	17 %
Communications	The datalink between the aircraft and the ground	11%
Miscellaneous	Any mission failures not attributable to those previously noted, including airspace issues, operating problems, and other non-technical factors.	9%
[1] defined as an accident resulting in significant vehicle damage or total loss, loss of human life, or causing more than $1,000,000 in damage. [2] averaged over 100,000 flight hours across five different UAS types.		

Risks can be divided to mission operational risks and UAV development risks. In no particular order, the events that can have a negative impact on the operation of the UAV are listed below.

1. Impact with terrain or objects on the terrain (people, structures)
2. Mid-air collision with aircraft
3. Structural issues
4. Hazardous materials released in the atmosphere
5. Camera/Sensor failure
6. Compromised data link between the aircraft and the ground (e.g. hacking of UAV)
7. Incomplete/inconsistent UAV pilot training

The UAV design development risks are listed as follows:

1. Certification issues (the whole design is not airworthy)
2. Noise risks (do not comply with regulations)
3. Atmospheric emissions (do not comply with regulations, do not comply with sustainable development strategy)
4. Fatigue and fracture analysis (too conservative - "self-fulfilling prophecy", results in structures that are just heavier because they are sized for higher loads; too optimistic - structure cannot cope with loads encountered during flight)
5. Cost and customer risks (infeasible end product price, no customers found for the product)

6. Supplier delivery (supplies not on time, wrong quality)
7. Inspection risks (instruments not accurately calibrated, UAV not dimensionally correct when compared to relevant drawings)
8. Assembly risks (incorrect joining methods due to differences in materials, accuracy of joints is not sufficient)
9. Transportation problems (parts do not arrive on time, damaged products)
10. Killer requirements (if range/endurance/altitude/cruise speed are infeasible)

3.6.2. TECHNICAL RISK ASSESSMENT

Risk is identified as the consequence of an event multiplied by the likelihood of that event. Within systems engineering, the consequences of an event can be categorised as follows (in order of increasing impact):

- Negligible - Little or no impact on the operation of UAV
- Marginal - A small impact on the technical performance of the UAV together with a degradation of the secondary missions
- Critical - A reduction of the technical performance and possibly a danger for the success of the mission
- Catastrophic - The outcome of the main mission is uncertain. Severe degradation of performance is expected; complete failure of the UAV can occur.

Within systems engineering, the probability of occurrence can be categorised as follows (in order of increasing probability):

- Proven Flight Design - almost impossible to occur
- Extrapolated from Existing Flight Design - very unlikely to occur
- Based on Existing Non-flight Engineering - unlikely to occur but still possible
- Working Laboratory Model - likely to occur sometimes
- Feasible in theory - very likely to occur

A very convenient way to visualise the risk of certain events is through a risk map (Figure 3.5 for the in-flight operational risks, Figure 3.6 for the UAV development risks). All the events, taken from Section 3.6.1, are included in the risk map with the highest risks in the top right corner.

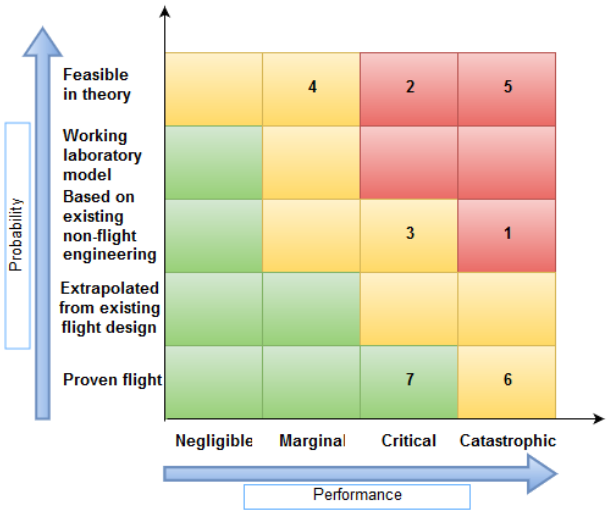

Figure 3.5: Risk map - Operational risks

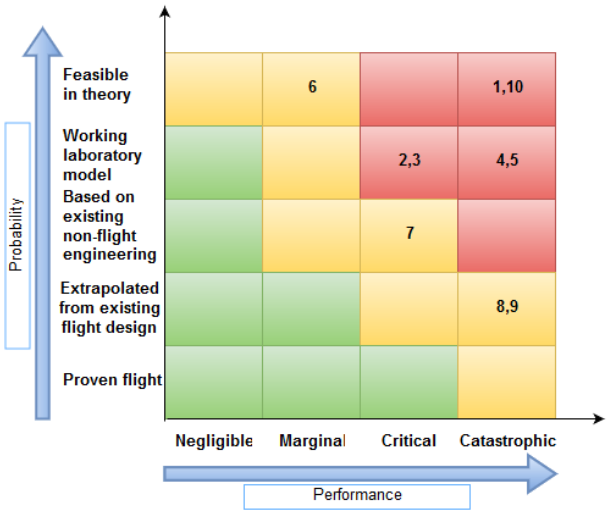

Figure 3.6: Risk map - Development risks

3.6.3. RISK ANALYSIS

For the risks that are not tolerated a plan needs to be developed to reduce the risk. There are several options to reduce risk:

- Remove the hazardous situation
- Reduce the likelihood of the event
- Reduce the impact of a the event
- Sharing the risk

The largest risks are found in the risk map and for these a mitigation strategy is developed. From the operational risks, the collision risks (in mid-air and terrain) and the risk of a camera failure will be analysed. From the design risks the first five and the last one will be analysed, since these events have the highest risks.

CAMERA/SENSOR FAILURE

The reduction strategies for camera and sensor failure risk are given in Table 3.2.

Table 3.2: Mitigation strategies for camera failure

1) Elimination of the hazard	Not conducting the operation; redundancy in the amount of cameras	
2) Reduction in the Probability of a Hazard Occurring	Technical Protection	Selecting a more reliable camera;
		Placing the camera on a strategic spot; Protection against impact; protection against light (direct sunlight or other potentially damaging light);
3) Reduction of the Level of Potential Consequences	Limitation of the dependency of the camera for the mission; Using multiple cameras in the mission, if one fails the consequences are not that high;	

IMPACT WITH TERRAIN OR OBJECTS ON THE TERRAIN

Table 3.3 displays the possible options to reduce the risk of the impact risk.

Table 3.3: Mitigation strategies for aircraft collision with terrain [33]

1) Elimination of the Hazard	Not conducting the operation;	
2) Reduction in the likelihood of a hazard occurring	Operational	Isolating UAS operations to designated and controlled ranges where there are no people or property exposed; Minimising/avoiding the over flight of people and property, or limiting operations to areas of low population density; Operating over the oceans and away from known fishing areas or shipping lanes; Establishing designated recovery or ditching points; ability to operate under more than one mode of operation (e.g., autonomous or manual remote operation);
	Technological	Automated recovery systems capable of flying to pre-programmed recovery sites; Emergency forced landing systems (e.g., Mejias, Fitzgerald et al. 2009); Failure warning systems (e.g., icing or fuel warnings, breach of operational boundaries); Controlled ditching in pre-programmed areas; Containment systems (e.g., automated “fencing”, parachute, ditching or explosive termination systems);
	Strategic	Survey and crew familiarisation with operating environment; Crew training in failure and emergency procedures; General awareness (briefing local population);
3) Reduction of the level of potential consequences	Sheltering of people or assets; Frangible aircraft; Energy dissipating flight profiles (manual or pre-programmed); Air bags; Parachute systems; Avoiding areas with the potential for consequences of “high value” (e.g., areas with hospitals, schools, or areas of high population density); Personal protective equipment (e.g., helmet and eye protection – for micro/small UAS operations); Established emergency procedures; Emergency response equipment (e.g., first aid, environmental spill kits, firefighting and personnel protective equipment for post-accident clean up);	

MID-AIR COLLISION WITH AIRCRAFT

For mid-air collision mitigation, the possible options are given in Table 3.4. The options are divided in the previously described options for risk reduction.

Table 3.4: Mitigation strategies for mid-air aircraft collision [33]

1) Elimination of the hazard	Separation of UAS from other aircraft (e.g. use of prohibited or restricted airspace); not conducting the operation;		
2) Reduction in the likelihood of a hazard occurring		i) Active	ii) Passive
	A) See	Periodic radio broadcasts; Airborne or ground-based systems that employ primary radar, transponder interrogators or lidar sensors; Existing Airborne Collision Avoidance Systems (e.g., TCAS-II);	Chase plane, Radio listening watch; Airborne or ground-based systems that employ electro-optical infrared or acoustic sensors; Automatic Dependent Surveillance Broadcast (ADS-B) In; Ground based visual observers; Subscription to traffic information feeds;
	B) Be seen	ADS-B Out; Transponders; Existing ACAS (e.g., TCAS-II); Inter-aircraft communication systems (e.g., VHF - Data Link); Anti-collision strobe lights;	Chase plane; High visibility paint; Establishment and activation of warning or danger areas;
	C) Staying away	Flying in airspace of known low aircraft activity: Over the oceans, above or below international en-route airspace; At night; Below the CPA minimum safe altitude; Outside peak CPA traffic times;	
	D) Services	Utilisation of third party air traffic services; Flying in controlled airspace;	
	E) Strategic	Survey and crew familiarisation with airspace operating environment; Crew training in procedures; General awareness (briefing local airspace user groups);	
3) Reduction of the level of potential consequences	Established procedures for responding to an emergency; Frangible aircraft; Not flying in areas where there are aircraft with a high consequence “value” (e.g. commercial passenger aircraft);		

DESIGN RISKS

The options for mitigation for the design risks are almost never able to remove the risk completely. However the likelihood and impact can be reduced most of the time by clear communication with the stakeholders, extensive analysis for the design choices and allocating more work time as early as possible to aspects that are statistically known to have high occurrence chance and a high impact. Another good tool to reduce the risk is introducing buffers (for example design the noise level lower than the required noise level from regulations) and safety factors within the design.

- **Certification issues:** The mitigation strategy that could be applied is overdesigning the UAV. This can be achieved by applying buffers for the requirements and safety factors in the design. Another option for mitigation would be the adaption of the schedule for the design choices. When more information is available over time about a certain design choice, the decision moment could be extended to obtain better judgement. Reducing the likelihood of issues with the certification can also be achieved by keeping track of the requirement of the certification. By anticipation on these requirements and take early measures the risk can be reduced.
- **Noise risks:** In order to reduce noise on an UAV, more silent engines (low power setting) can be used or surface operations can be limited. In case the airport is located next to a populated area, efficient runway allocation can lead to less noise annoyance. A reduction of airframe noise (major contributors: high-lift devices, landing gear) is also possible.
- **Atmospheric emissions:** Again for the regulations the same strategies as for the certification apply. When the emissions do not comply with the sustainable development strategy other strategies could be applied. The sustainable development strategy could be changed which could remove the total risk in terms of sustainability.
- **Fatigue and fracture analysis:** Prevention of the fatigue and fracture analysis risks is a hard task, since both depend on a lot of different things. To reduce the risk these factors need to be analysed and accurately predicted. This is very important, since the structure should not be too conservative and not too optimistic. Reducing the risk is again possible by scheduling enough time to make decisions base on a solid analysis.
- **Cost and customer risks:** This risk could be removed or shared with a contract that ensures that a customer buys the UAV, in such a contract the risk for both the cost and customer is covered. It also could

ensure one of the two risks is covered when other requirements are fulfilled (for a certain price of the product the customer will buy the product). Another strategy is to perform a thorough analysis of the potential customers and have requirements to satisfy the potential customers.

- **Supplier delivery:** To avoid this risk, a trustworthy supplier company is chosen to ensure the supplies are of sufficient quality and are delivered on time.
- **Inspection risks:** These risks can be reduced by regularly calibrating the used instruments (sending them to external calibration laboratories, calibration against master instruments, comparing the instrument to a known "faulty" instrument). The calibrated instruments should easily be identified and separated from the faulty ones by marking, labelling etc. Additionally, the quantity of regular inspections can be increased, so that each individual supply/part is checked, rather than only quality controlling the finished product. A system approach would be best: consecutive inspection during each of the production stages in addition to a final inspection in order to reduce waste is not enough; the production equipment used, personnel hired and the accuracy of information available should also be inspected.
- **Assembly risks:** Joining methods in materials and accuracy of joints can be improved by supplying the work force with regularly calibrated measurement tools and manuals on how to properly implement production techniques. To increase the production efficiency and eliminate the waste, additional training may be required for the workers at the expense of slightly higher expenses.
- **Transportation problems:** In order to avoid possible problems with delay or damaged products during transportation, a trustworthy transportation company with a well-built reputation for safety can be chosen.
- **Killer requirements:** The only option for the complete elimination of killer requirements risk would be to not set requirements, which is impossible in practice. For the second option to reduce the occurrence of killer requirements it is necessary to preform a constant analysis for the feasibility of the requirements and adjust the requirements. Besides the adjustment, identification of a killer requirement in early stages can also reduce the impact of the requirement. This identification in early stages can be done by a analysis and comparison with the performance of already existing aircraft. After the identification other measures can be taken, early detection will result in less required change for the design process.

3.6.4. RISK HANDLING

Choosing the mitigation strategy is based on the effectiveness of reducing the risk. The most effective is the removal or decreasing the consequences of the hazard, followed by the reduction of occurrence of the event. The third option would be reducing the impact and the last possible option would be sharing of the risk. Another important factor is the effect of the mitigation has on the system, in terms of performance, but also the limitations of the system has will affect the possibility of mitigation, like maximum weight, available power, etc.

The cost benefits are another important factor in the selection process. The direct and indirect costs need to be taken into account. The cost could be related to a large range of stakeholders, which leads to a wide variety of costs, like planform cost, operational cost, through-life cost, mission costs and market costs. But also reduction or increase of indirect benefits is an important aspect. For example, improvement of reliability can lead to a lower planform attrition rate, a lower insurance, an increase in availability and trust of the customers.

OPERATIONAL RISKS

- **Camera/Sensor failure:** The most effective strategy would be redundancy for the cameras, however for expensive equipment this would not be very cost efficient. From all the mitigation strategies possible, this is the best for the reduction of the risk.
- **Impact with (objects on) terrain:** The most effective strategy would be to avoid exposure for property and people, however since the UAV is for surveillance this may not possible for the biggest part of the mission. The better option is to have a design that limits the possibility for human or in flight failure, by using sense and aviod. The UAV is also designed for emergency situations (like engine failure), but not all failure modes have an automated emergency system.
- **Collision with aircraft in mid-air:** The most effective strategy for the risk mitigation is the segregation of UAS from other aircraft. However this is not always possible and the cost can be too big. Hence more mitigation strategies are necessary. A combination of 'See' and 'Be seen' in combination with 'Staying away' would be effective to reduce the probability of the risk.

DESIGN RISKS

The options for mitigation for the design risks are almost never able to remove the risk completely. However the likelihood and impact can be reduced most of the time by clear communication with the stakeholders and extensive analysis of the design choices.

- **Certification issues:** The most cost-effective option is keeping track of the requirements and regulations. It takes slightly more time in the design process, but it greatly reduces the risk of more time required when there are issues with the certification. This is also the case for adapting and expanding the schedule. In

any case, for certification it is required to apply a safety factor of at least 1.5 to all load calculations.

- **Noise risks:** For the noise, just as for the certification, it will be kept track of the requirements. Furthermore, every subsystem will be designed for reduction of noise emissions so that the regulations are met and the impact of this risk is reduced. To do so, a maximum value will be established in the beginning and an appropriate noise emission budget will be updated after each design iteration; finally, a sufficient margin will be allowed for the remaining development.
- **Atmospheric emissions:** To cope with the regulation risks the requirements will also be constantly checked. When it comes to a sustainable design strategy there are other options, however, changing the sustainable strategy would be a drastic choice that would defeat the purpose of this strategy and would also increase other risks, like customer risk due to the less sustainable design. Therefore the only remaining options to cope with those risks is the aforementioned check whether requirements are met and keeping an appropriate polluting emissions budget, including all substances that are harmful to the environment.
- **Fatigue and fracture analysis:** The most efficient method for the reduction of the occurrence of fatigue/fracture is to perform the analysis, verify and validate it via the usage of established numerical optimisation methods and appropriate fatigue testing machines in order to ensure that the structure and material used can cope with the required number of load cycles. Furthermore, relevant non-destructive tests will be performed as a crucial part of the quality control of the final product. Furthermore, it will be ensured that proper maintenance procedures are applied regularly and critical parts are repaired or replaced on time to avoid any fracture being catastrophic. A downside of these strategies, however, is that they will contribute to additional development, manufacturing and maintenance cost.
- **Cost and customer risk:** The best option would be to have an actual customer in advance of the development, but this is often not possible. Hence the strategy will be to analyse the potential customers throughout the design and manufacturing processes. Additional advertising may be performed to outline all the improvements of the proposed concept with respect to existing technology in terms of performance, cost, sustainability and safety features. Moreover, to reduce the impact of the consequences of not having a customer in the end of the development, the risk may be attempted to be shared with another company.
- **Supplier delivery:** To ensure the supplies delivered are on time and of sufficient quality, the supplier company is chosen only amongst Registered/Certified companies. This way the supplier is proved to have reduced unproductive time, rectification, warranty costs and liability. A way to reduce the occurrence of having been delivered wrong supplies is to regularly contact the company prior to delivery and ensure that the correct products are being sent for transportation. To mitigate the chances of supplier delivery risk to be critical for the development of the UAV, some supplies will be bought in advance and stored conveniently. This can buy extra time in case of a supplier or transportation delay.
- **Inspection risks:** These risks can be reduced by regularly calibrating the used instruments. Additionally, the quantity of regular inspections can be increased, so that each individual supply/part is checked, rather than only quality controlling the finished product. Given that all these measures are executed correctly, this risk is almost impossible to occur.
- **Assembly risks:** Joining methods in materials and accuracy of joints can be improved by supplying the work force with regularly calibrated measurement tools and manuals on how to properly implement assembly techniques. To increase the production efficiency and eliminate the waste, additional training may be utilised for the workers at the expense of slightly higher expenses.
- **Transportation problems:** To avoid problems with delay or damaged products during transportation, a Registered/Certified transportation company with a well-built reputation for safety is chosen. The reasons for using a more expensive company that is certified lay in the importance and cost of the parts being delivered.
- **Killer requirements:** The most efficient way to reduce the risk is based on identifying these killer requirements as soon as possible. This both reduces the occurrence of a killer requirement being a risk and the impact of the killer requirement.

RISK MAP AFTER MITIGATION

After the mitigation strategies are applied, the risk map changes due to the reduction of the risks. In the new risk maps (Figure 3.7 for the in-flight operational risks, Figure 3.8 for the UAV development risks) all the events, again taken from Section 3.6.1, are included with the highest risks in the top right corner.

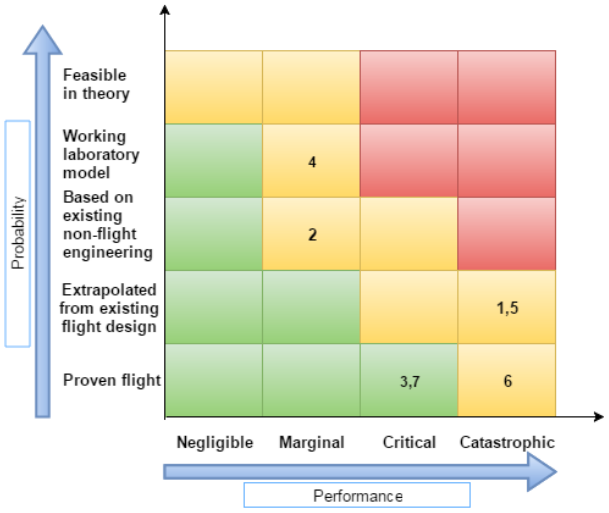

Figure 3.7: Risk map - Operational risks after mitigation

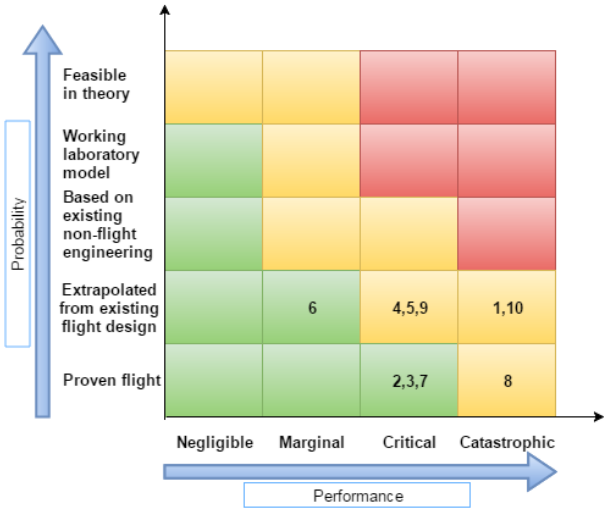

Figure 3.8: Risk map - Development risks after mitigation

3.7. VERIFICATION & VALIDATION STRATEGY

In this chapter the processes which are used to verify the accuracy of the numerical solutions used throughout the report to determine the properties of the UAV are discussed. The process of verification consists of several steps, each of which is discussed. Firstly, Section 3.7.1 focuses on the unit testing of the code blocks. This is followed by an explanation of the system testing in Section 3.7.1. Then, Section 3.7.1 highlights how to address possible errors. Section 3.7.2 deals with the validation strategy and, finally, alternative methods to perform validation are given in Section 3.7.2.

3.7.1. VERIFICATION

The process of verification consists of several steps: unit testing (code verification: finding and fixing the programming errors, either syntax or content errors), system testing (calculation verification: use a simpler solution, an analytical solution, and compare it to the results of the numerical program) and addressing any errors/differences encountered (entire process needs to be repeated afterwards to guarantee correctness).

UNIT TESTING

Unit testing is a method used to test small chunks of code to determine whether or not it performs as expected. The method consists of testing the code using simple and special parameters, such as 0, 1, 10, or multiples of 90° for angles, in order to test both the functionality of the code and the existence of singularities. If the test ends in an error or the result deviates from the expected result, the code is inspected to find the error, and consecutively corrected and reevaluated. The unit test is repeated for different input parameters until there is a certainty that the code behaves correctly. This process is performed for all pieces of code until all the small blocks behave as expected. Unit testing can be split into four parts: Propulsion, Structures & Materials, Stability & Control and Aerodynamics.

There is a clear division between the different students for the coding part within the subgroups. Even though Python will run the code in the right order, each piece of code can be written individually by assuming the necessary inputs from another code block are already known. This can lead to a substantial amount of time being saved that can be used for other parts (e.g. production plan, cost estimation). All code blocks are individually tested by the student responsible before the entire program is assembled.

To demonstrate how unit testing will be performed for the remainder of the project, an example of the unit testing for the Class I weight estimation W/P-W/S diagram is discussed. By using the same inputs as in the slides, the diagram obtained from the Python program can be compared to the results from the "Aerospace Design & Systems Engineering Elements" course. All the lines considered (stall speed, cruise speed, climb rate, climb gradient, take-off distance and landing distance) need to match in order to ensure that the correct design space is obtained, otherwise the wing will be under- or overdesigned due to errors in the program.

SYSTEM TESTING

Once the numerical solution has passed the unit test, it is time to subject it to a system test. This involves comparing the results from the numerical solution to the ones from the analytical solution. This involves comparing interactions between multiple subprograms and seeing if the results are feasible. Often there are iterations needed (e.g. Class I - Class II estimation of the operational empty weight); system testing ensures that these are performed correctly.

ADDRESSING ERRORS

If the results of the test match the expected outcome the code passes the test, but if the results deviate from the expected outcome or fails due to the existence of a singularity, the code is reviewed. During revision, there are different parts of the code in which errors are most likely present. For this reason there are parts of the code which are checked first for errors after obtaining a discrepancy or a failed run from a test. For unit testing, the relevant equations and input variables used are thoroughly checked as the most likely error comes from an erroneous equation or mistyped variable. For system testing, the interaction and relations between the blocks of code is where mistakes can be made, so this is where the focus lies when reviewing the code after a failed system test. The most likely place where mistakes are made in the comparison to a simpler solution (analytical) lies in the made assumptions, so when the analytical solution deviates from the numerical solution, the made assumptions are checked for correctness. If no error is found during these checks the following steps are performed in order to try and find where the mistake in the program lies.

- Check all the assumptions used in the calculation
- Check interaction between blocks of code (where applicable)
- Check the relevant equations, including their derivations
- Check the correctness of the input variables
- Check the analytical solution

Verification is a process repeated throughout the remainder of the report for the individual subsystems (stability & control, propulsion, aerodynamics, structures). This ensures that all possible analysis errors are eliminated.

On a product level, verification can also be used to ensure that SCULPTUR meets the requirements. There are several methods that can be used in this case:

- Analysis - using mathematical approaches or other techniques to estimate if the UAV complies with the requirements (e.g. RAMS analysis - Section 7.2; electrical analysis: electrical performance, worst case scenario, data handling performance - Sections 4.4.9 - 7.5; speciality analyses: human operator, producibility, life cycle cost - Sections 6 - 7.6.1; mechanical analysis: fatigue and fracture mechanics, torque, strength - Section 5.6).
- Testing - using a prototype to show that the product complies with the requirements (e.g. software tests - correct functioning of for example the autopilot in a simulated environment; electrical integration tests; mechanical integration tests; environmental tests - ageing, contamination; calibration tests)
- Review of design - similar to testing, but without the sophisticated instrumentation.
- Inspection - cheapest method of verification, offering visual confirmation that a requirement has been met (e.g. drawing inspection - all components have the right dimensions as in the technical drawings, hardware inspection - all the required equipment is installed)
- Similarity - assuming that a product meets the same performance requirements as another of the same product if they operate in similar conditions. This is useful for the production phase when using off-the shelf components since tests have already been performed on them.

3.7.2. VALIDATION

With verification completed, a validation process has to be performed to quantify the difference between the results from the numerical analysis and actual results obtained either from another valid numerical model or from a model experiment. Only if they are within an acceptable range, the numerical solution can be considered a good approximation of the "real world" scenario. During the detailed design phase, the following stages need to be followed [34]:

- Development - performed on a system, subsystem and component level (tanks, turbopumps, injectors, valves, combustion chamber etc.) for a mock-up/prototype
- Qualification - performed on a model that follows the same drawings, production methods and materials as the actual SCULPTUR. The model is tested under the ultimate design conditions and is discarded afterwards
- Acceptance - performed on the actual flight model, tested under the nominal conditions encountered during the flight. The model is not discarded afterwards as opposed to the qualification phase
- Pre/Post-launch - performed on the actual SCULPTUR itself. It is used to ensure that certain operational aspects are fullfilled at all times

During each phase, there are different test procedures and test facility characteristics that are required.

VALIDATION STRATEGY

After verification is completed successfully, a validation strategy needs to be implemented. For each individual subgroup, a separate validation procedure needs to be implemented. Example strategies for each of the subgroups are shown below.

- Propulsion
  - Phase 0: Detailed design
  - Phase I: Engine validation testing (Endurance, Fan blade out, Bird strike)
  - Phase II: Service readiness (CS certification, UA certification, SCULPTUR first flight)
  - Phase III: Service and support
- Structures & Materials
  - Phase 0: Geometry testing (impact of geometric elements by setting the others to zero (skin, stringers, floor))
  - Phase I: Reaction forces testing
  - Phase II: Normal stress testing (maximum/minimum values, (x y z) location)
  - Phase III: Shear stress testing (maximum/minimum values, (x y z) location)
  - Phase IV: Individual part test
  - Phase V: Assembly test
  - Phase VI: Full system test
- Aerodynamics
  - Phase 0: Airfoil validation testing in wind tunnel
  - Phase I: Subassembly wind tunnel testing for obtaining lift and drag
  - Phase II: Wind tunnel testing of complete profile for obtaining lift, drag and dynamic coefficients
  - Phase IV: Wind tunnel testing of complete design for quantifying noise generation
  - Phase V: Validation of aerodynamic and noise behaviour during flight tests
- Performance & Control
  - Phase 0: Predictive validation for the performance and control
  - Phase I: Controls validation in mission scenario test
  - Phase II: Operations readiness test for the mission performance by a flight test

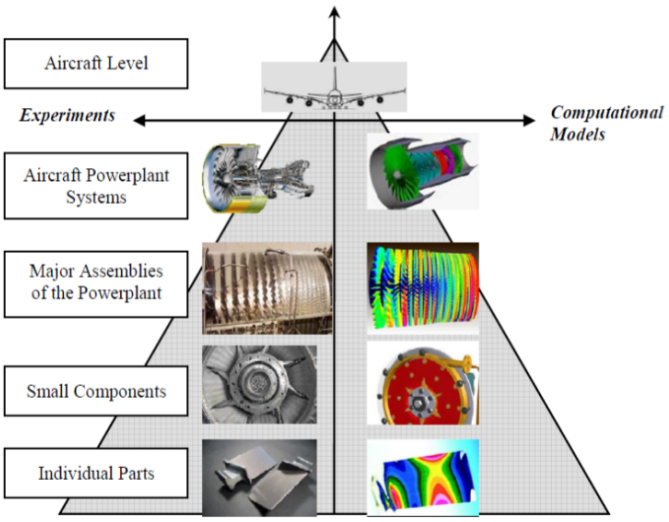

Figure 3.9: Validation strategy pyramid [35]

Figure 3.9 shows how validation will be performed. If the computational model predicts the experimental outcomes within the predetermined accuracy requirements, the model is considered validated for its intended use. It then becomes a simple trade-off between the required accuracy of the analysis, the available time to run the analysis (it is very time consuming to test each individual part) and the available resources (making a prototype model that has the same properties as the design is very expensive). It is always important to relate discrepancies to assumptions and quantify them if possible. Adjustments need to be made accordingly in order to ensure that the UAV performs as expected.

OTHER VALIDATION METHODS

Another way to perform the validation process is comparing the results from the numerical model with another proven model (if available). For the propulsion subgroup for example, the performance of the scaled-down engine is analysed using the GSP (Gas Simulation Program), a program developed by the NLR in coordination with TU Delft. This proven model has already passed the validation test and can be used as a reference. Considering that the two numerical models are based on different assumptions and use different calculation techniques, there will still be differences in the output variables but they should be close and following a certain trend. The already proven numerical model can also be used to validate the results from the test, to ensure that the experi-

mental data is reliable.

3.8. INITIAL BUDGET AND RESOURCES

During the design of an aircraft it is of great importance to determine the allowed values of several technical resources. These allowed values are named budgets and originate from the requirements as described in Section 3.5. Together with the contingency management approach, they allow for tracking of the status of the design process. The budgets of these resources are described in this section together with the reasoning behind them.

3.8.1. WEIGHT BUDGET

The first parameter to be given a budget is the take-off weight of the UAV. To get an estimate of the UAV weight, the statistical data in the Conceptual Design of UAV Systems course from the University of Southampton was used [19]. As a first step, the weight is broken down as shown in Equation (3.1).

$$W_{TO} = W_{OE} + W_F + W_{PL} + W_{MISC} \tag{3.1}$$

where W_{TO} is the maximum take-off weight (MTOW), W_{OE} is the operating empty weight (OEW), W_F is the fuel weight, W_{PL} is the payload weight and W_{MISC} is the miscellaneous weight (trapped fuel and oils, pylons, special mission, equipment). As stated in the requirements, the UAV should be able to carry 50 kg of payload. The payload fraction is a fundamental design driver thus it can be used to determine an initial maximum take-off weight budget estimate. This can be done using actual statistical data for UAVs (Figure 3.10).

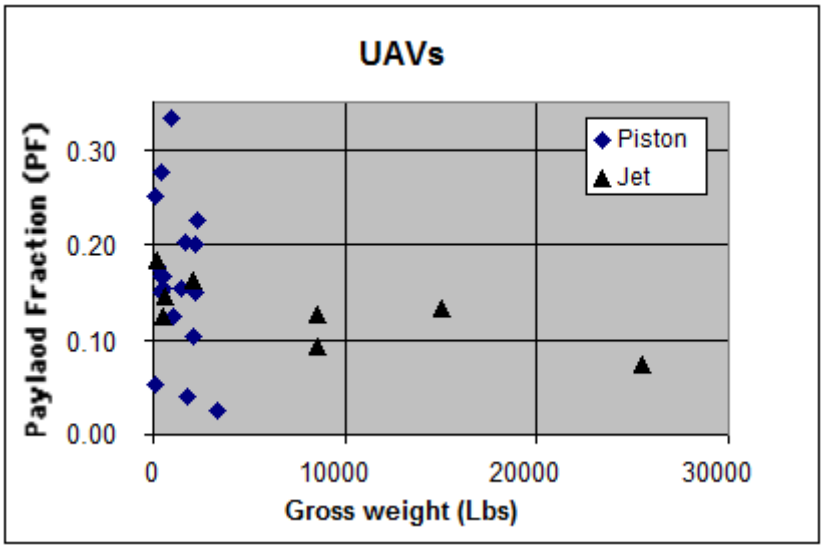

Figure 3.10: UAV Payload fraction - Gross weight [19]

As it can be seen, most of the UAVs have a payload fraction of around 0.13. With a payload of 50 kg, this results in a maximum take-off weight of 385 kg. The budgets for the remaining two major components, the operational empty weight and the fuel weight, can now be determined. The range (1800 km) and endurance (20 hours) requirements can be useful in this regard. It is a known fact that for current UAVs, the design restriction is usually the endurance and not the range hence it is considered more accurate to asses the relationship between the weights and maximum endurance. Empty weight and fuel fractions correlate with the maximum endurance as shown in Figure 3.11 and 3.12 respectively.

The expected behaviour is displayed in the two graphs: with increasing endurance, more fuel is needed and hence a lower operational empty weight. Considering that a turboprop's performance is between the piston and jet engines in the two graphs, a value of 0.58 is chosen for the empty weight fraction and 0.28 for fuel fraction. Based on the maximum take-off weight found earlier, this gives an OEW of 223 kg and a fuel weight 108 kg. Finally, the miscellaneous weight can be estimated to be 1% of the maximum take-off weight according to [19], resulting in a value of 4 kg (insignificant when compared to the others however it should not be ignored).

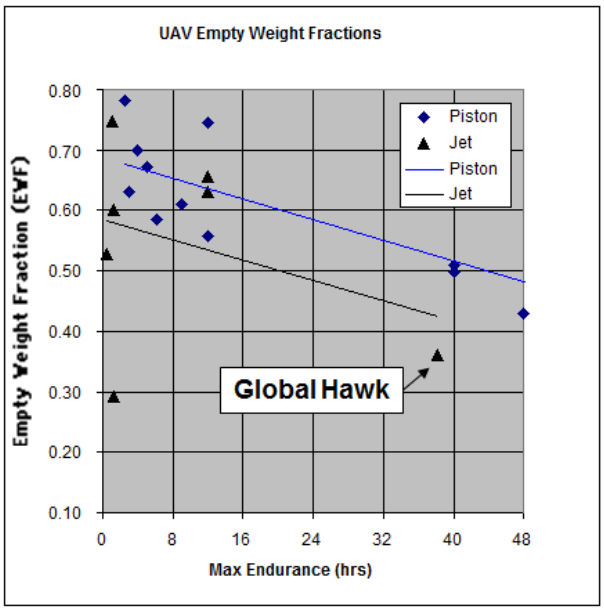

Figure 3.11: UAV Empty weight fraction - Endurance [19]

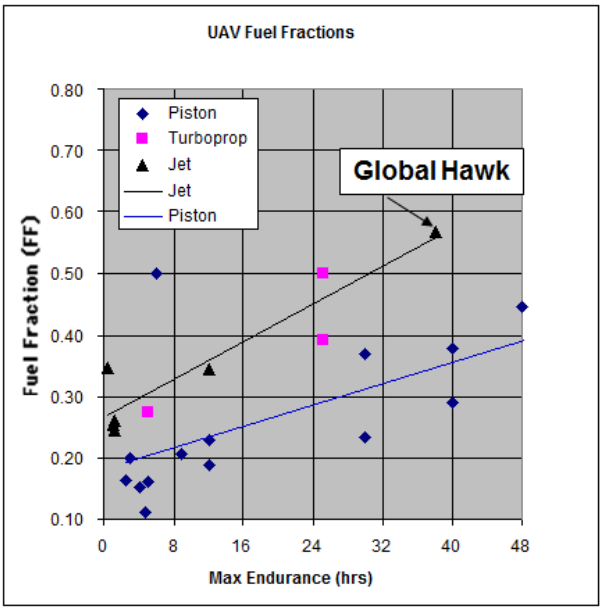

Figure 3.12: UAV Fuel weight fraction - Endurance [19]

The weight budget is summarised in Table 3.5. A margin of 10% is added to the OEW and fuel weight to account for any unforeseen circumstances (mission specific weight increases, erroneous statistical data etc). This margin can not be added to the payload however since the 50 kg is a stakeholder requirement.

Table 3.5: SCULPTUR Weight budget

Budget component	Weight [kg]	Weight (10% margin) [kg]
W_{OE}	223.0	245.3
W_F	108.0	118.8
W_{PL}	50.0	50.0
W_{MISC}	4.0	4.4
W_{TO}	**385.0**	**418.5**

3.8.2. ELECTRICAL POWER BUDGET

There are several subsystems in the UAV that require electrical power:

- Payload
- External lighting
- Flight instruments and avionics systems
- Flight control system
- Engine systems
- Fuel system

For every subsystem there needs to be a electrical power budget. When all the budgets are set a estimation for the total power usage can be made. The required power is used in the design of the power generation of the engine and emergency power systems (batteries and ram air turbine). The payload is already chosen, the required power for all the parts can be found in Figure 3.13. The UAV needs lighting for visibility during night to prevent aircollision and provide information about the position, heading and status. The required lighting and the power usage can be found in Figure 3.14.

Figure 3.13: Payload power usage

Payload	Power [W]
Gimbal camera	55
Communication	350
Autopilot	2.5
Flight data recorder	0.84

Figure 3.14: External lighting power usage

Light	Power [W]
Navigation light (red/green)	14
Strobe lights (wing tips)	14
Tail light	7
Anti collission (top bottom)	14

AVIONICS

For the flight instrumentation a air / inertial / meteorological data system can be used like a ARIM320 [57]. This unit provides information about the pressure, speed, angle of attack, temperature, heading, etc. The power usage of this unit is 6.5W.

The usual collision avoidance system are heavy and use a lot of power[58]. But there are also new systems developed that do not use radar, but optical collision avoidance technology[59]. Such a unit weights only 0.11kg and uses 1W of power.

The navigation system uses the flight instruments and GPS for the position determination [4]. For the GPS a receiver and an antenna is required. The GPS system will have a power usage of 2.5W based on the AT300 antenna[60] and the M300 receiver[61].

FLIGHT CONTROL

In the flight control system are all the actuators for the control of the UAV included. They are described in Section 4.4.6. In Figure 3.15 the power usage of the actuators is shown.

FUEL SYSTEM

The fuel system that will be used is described in Section 4.4.8. The components that use power are the fuel level transmitter, booster pump and high pressure pump. FR37[62] would be a possible option for the transmitter. For the pumps the PX500-TC[63] boost pump can be used. In Figure 3.16 the power usage of the fuel system components is shown.

Figure 3.15: Actuator power usage

Actuator	Power [W]
Aileron	500
Ruddervator	80
Rudder	18
Landing gear	550

Figure 3.16: Fuel system power usage

Component	Power [W]
Fuel level transmitters	0.18 x 2
Booster pump	84
High pressure pump	84

Figure 3.17: Electrical power usage

System	Power [W]
Payload	408.5
Exterior lighting	49
Avionics	11
Fuel	168.5
Flight control	1148
Miscellaneous	0
Total	**1785**

MISCELLANEOUS

The anti icing system can be a mayor system in terms of required power supply typical thermal deicing systems use tens of thousands of watts[64]. Hence IMS-ESS was designed for UAV to use less power, however this system still uses 600-900W. There are also newer techniques developed like heatcoat[65], which is a light and less power consuming solution. For now a ground de-icing procedure and a traditional pneumatic system, which does not require electrical power.

TOTAL POWER BUDGET

An overview of the initial power budged can be found in Figure 3.17.

[57] URL https://www.google.nl/url?sa=t&rct=j&q=&esrc=s&source=web&cd=2&ved=0ahUKEwiV4sL4v5rNAhXKBBoKHWkrAnAQFggvMAE&url=http%3A%2F%2Faventech.com%2Fdocuments%2FARIM320%2FARIM320%2520Technical%2520Brochure.pdf&usg=AFQjCNHePnqwJ23D5W105Ydi60uLI5B5Ag&cad=rja [cited June 9 2016]

[58] URL https://www.google.nl/url?sa=t&rct=j&q=&esrc=s&source=web&cd=1&ved=0ahUKEwii9NjJ1prNAhXKhRoKHeJYAYkQFgglMAA&url=https%3A%2F%2Fwww.rockwellcollins.com%2F~%2Fmedia%2FFiles%2FUnsecure%2FProducts%2FProduct%2520Brochures%2FRadar%2520and%2520Surveillance%2FTraffic%2FTTR-4100%2520data%2520sheet.ashx&usg=AFQjCNH--R6P9r0iCViPTs_J51fDh7JG2g&cad=rja [cited June 9 2016]

[59] URL http://www.sara.com/isr/uav_payloads/oca.html [cited June 9 2016]

[60] URL http://www.comnavtech.com/products-detail.asp?id=6 [cited June 10 2016]

[61] URL http://www.comnavtech.com/products-detail.asp?id=3 [cited June 10 2016]

[62] URL http://www.fozmula.com/product/fuel-level-sensor-with-integrated-feed-return-fr37x/ [cited June 20 2016]

[63] URL http://www.aircraftspruce.com/catalog/eppages/andairfuelpump.php [cited June 20 2016]

[64] URL https://spinoff.nasa.gov/Spinoff2010/ps_2.html [cited June 13 2016]

[65] URL http://www.battelle.org/media/press-releases/battelle-heatcoat-anti-icing-technology-for-drones-passes-milestone [cited June 13 2016]

4 UAV Design Methodologies and System Characteristics

As the missions specifics and requirements have been defined in the previous chapter, it is now possible to start the design process. Section 4.1 gives a general overview of the preliminary design, offering insight into why certain options are picked. In Section 4.2 the payload required to accomplish the mission is discussed. Sections 4.3, 4.4 and 4.5 depict the iterative process between the Class I and Class II weight estimations as well as the preliminary sizing of the main subsystems.

4.1. Conceptual Designs

To start off with the design process of SCULPTUR conceptual designs need to be made that are able to satisfy the requirements as described in chapter 3. For this a system engineering method was followed as described in section 4.1.1. Following this approach one conceptual design was determined which will be further analysed in this chapter. This chosen conceptual design is described in section 4.1.2.

4.1.1. Concept Generation Process

The generation of conceptual designs for the SCULPTUR mission as described in section 3 was performed following a trade-off process. To explore all design options, design option trees were created for all subsystems of the UAV shown in Table 4.1. From these trade-offs the unfeasible options were eliminated, after which a graphical trade-off was made of the feasible options in order to determine the ones most suitable for the mission.

Table 4.1: Subsystems considered during conceptual design phase

Design Option Trees		
Aerodynamic Design	**Propulsion System Design**	**Flight Control System**
Landing methods	Turboprop engine design	Remote control
Lift-generation methods	Power generation	Communication
Take-off methods	Thrust generation	In-flight control
Emergency landing methods		Flight navigation

The next step in the process was the generation of strawman concepts by combining the suitable options in several designs. These concepts were grouped into three different UAV configurations, monowing with empennage, tandemwing configuration, and a flying wing concept. From each category one design was chosen and evaluated for its performance in stability, weight, drag, development risk and design complexity. This lead to a concept trade-off as described in [4], with as most favourable the outcome the monowing with empennage design.

4.1.2. Conceptual Design Configuration

A sketch of the chosen design of a monowing configuration with empennage design is given in Figure 4.1. To complete the sketch a T-tail is added, this is not considered to be a fixed property of the design as tail sizing was not yet performed at the time of conceptual design. Section 4.5 discusses the tail sizing and final empennage design.

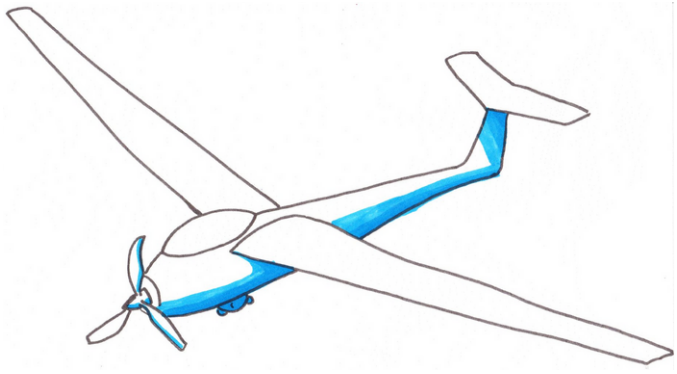

Figure 4.1: Conceptual design: monowing with empennage configuration

The conceptual design features the trade-off options shown in Table 4.2. Additional information about the trade-off method and the graphical trade-off tables can be found in [4].

Table 4.2: Configuration features of conceptual design

Design Configuration			
Landing mechanism	Landing gear	**Engine lay-out**	T.B.D.
Lift generation	Monowing + empennage	**Power generation**	Micro-gas turbine
Remote control	Assisted autopilot	**Thrust generation**	Single propeller
Communication system	Satellite radio communication	**In-flight control**	Control surfaces
Emergency landing	Parachute	**Flight navigation**	INS+GPS
Take-off mechanism	Runway		

The conceptual design takes off and lands using a retractable landing gear on a (semi-) paved runway. In case of an emergency landing, the UAV will attempt to glide to the ground, making a regular landing at a possibly (non-)paved area. If complete control is lost, a parachute installed using a ballistic recovery system can be deployed by the ground controller, which reduces the impact of the UAV crash.

Control of the UAV is provided by the use of simple control surfaces similar to general aviation aircraft. These surfaces are directed by the autopilot, as direct control is eliminated by the 1800 km requirement. The assisted autopilot is controlled by commands from the ground station, and is able to navigate using GPS. To add redundancy to the system, an INS system is also present in the UAV. Ground commands are send to the UAV by satellite communication using radio waves, which was found to be the most reliable and currently available method [21].

Lastly, focus was laid on the propulsion system of the conceptual design, after which it was found that deciding on the engine lay-out was not suitable for the conceptual design phase yet. The engine lay-out will be further discussed in section 5.4. A single propeller is installed on the MGT due to its low noise level [36]. Also it was determined that the most efficient way to power the systems on board of the UAV is by retrieving this power from the MGT. Moreover, the following section presents the choice of payload for this SCULPTUR design.

4.2. CHOSEN PAYLOAD

The previous section presents the choice In Chapter 2 the different payloads that are available for UAVs are discussed. The following section presents the chosen payloads for this SCULPTUR UAV mission. First, the chosen surveillance payload (gimbal, EO and IR cameras) is discussed. Then, the choice of communication payload is presented and finally, the choice of emergency payload is found.

4.2.1. SURVEILLANCE PAYLOAD

The gimbal turret is first chosen with all the possible EO and IR options that accompany it. Then, in accordance with the chosen mission, the appropriate cameras are chosen.

GIMBAL TURRET

The CM202 direct-drive multi-sensor stabilised gimbal by Ascent Vision, was selected as the most suited gimbal since it has very good stability characteristics, high accuracy and contains a high-definition EO camera and multiple long range IR cameras together covering a large part of the IR spectrum. This is critical since different wavelength IR cameras are needed for detection of oil and gas leaks[37]. The gimbal payload contains the sensors listed in Table 4.3 which are discussed in the following sections.

Table 4.3: CM202 gimbal payload sensors [37]

Sensor	Model	Type	Picture elements
EO daylight	DI-SC120R	Electro Optical	1280x720
IR LWIR	Tau 2 640	Long Wavelength IR	640x512
IR MWIR	-	Medium Wavelength IR	640x512
IR SWIR	Tau SWIR	Short Wavelength IR	640x512

IR CAMERA

The CM202 gimbal payload consists of three different (640x512 picture elements) infrared cameras one for SWIR sensing, one for MWIR (medium wavelength) sensing and one for LWIR sensing that is paired with a long range optical zoom for sensing at large distances 4.3. This provides the UAV with the ability of both accurate thermal as well as accurate visual detection of oil spills and gas plumes. For the mission chosen in Section 3.1, the pipelines are underground. Hence, the best choice is an IR LWIR camera such as the Tau 2 640. This camera has a field of view of 12.4° wide and 9.9° tele and a digital zoom of 8. More specifications of this camera can be found in Table 2.12.

EO CAMERA

Table 4.3 shows that one EO Camera can be installed in the gimbal: the Hitachi DI-SC120R EO camera. This camera has a size of 50 x 60 x 89.5 mm^3, it weighs 0.260kg and has a power required ranging from 9 to 12 VDC. Furthermore, it has an optical zoom of 10, a field of view of 44° wide and 1.5° tele and an operating temperature ranging between -10 to 60°.

4.2.2. COMMUNICATION PAYLOAD

As stated in the requirements in Section 3.5, the UAV shall be able to relay flight data information to the ground control station as well as being equipped with systems of radio navigation. Moreover, the ground control station shall be equipped with a recording device. In this part, the chosen communication payloads which comply with these requirements are presented.

GROUND CONTROL

The ground station that will best suited for SCULPTUR is a container based GCS, because the mission will be performed for a long duration of time. The operators need a relaxed environment where they can focus on their job for a such periods of time. Hence, a climate-controlled environment will be preferred.

REMOTE CONTROL

For the remote control payload, an autopilot needs to be chosen. In Chapter 2 five autopilots are presented and the VECTOR autopilot is chosen. This system is an advanced, lightweight (0.180 kg) solution that does not require much power (2.5 W). Moreover, this autopilot has all the build in functions that are required for the surveillance mission. It has a protective enclosure and, complying with the requirements, has redundancy in the control processor included.

COMMUNICATION

The communication unit that is chosen is the Gilat BlackRay 1000, since the camera payload requires a large data transmission for the downlink. The most efficient in terms of downlink from the UAV with a reasonable weight is the Gilat BlackRay 1000. However the required communication link still needs to be analysed and compared to the communication unit, this can be found in Section 4.4.10.

4.2.3. EMERGENCY PAYLOAD

Chapter 2 presents a thorough overview of all the possible risks the current UAVs encounter and their mitigation strategies. Two of these mitigation strategies consist of specific payloads that need to be added to the UAV. A ballistic recovery system is needed for safe emergency landings. This is a main requirement listed in Section 3.5 which this UAV needs to comply with. Furthermore, a flight data recorder is needed. When an emergency situation arises, this recorder gives an insight into the flight of the UAV. This allows to learn what caused the incident/accident.

BALLISTIC RECOVERY SYSTEM

The chosen parachute is the BRS-6-1050-CAN ((Figure 4.2 [66])). It weighs 22.6 kg and has a canister height of 55 cm and a diameter of 18 cm. It uses a solid fuel rocket (BRS-460) and has a minimum total impulse of 400 N-sec. The mechanical igniter consists of redundant primers with pyro booster. It complies with the requirements of SCULPTUR as it can has a maximum deployment speed of 250 km/h which is higher than this UAV's cruise speed (100km/h). Moreover, this parachute can sustain a load of 475 kg which, as can be seen in Section 3.8, is more than the MTOW found in the weight budget (418.5 kg).

Figure 4.2: Cirrus SR20 Ballistic Parachute

[66] URL http://golfhotelwhisk.wpengine.netdna-cdn.com/wp-content/uploads/2010/10/image.png

FLIGHT DATA RECORDER

The chosen flight data recorder is the SLICE Micro. It is selected due to its low weight (0.028 kg). It is still capable of performing the required data storage and is designed to withstand high loads that can occur during a crash.

4.2.4. SUMMARY CHOSEN PAYLOADS

Table 4.4 shows a summary of the final payloads that are used in this SCULPTUR UAV to carry out the mission chosen in Section 3.1.

Table 4.4: Summary of chosen payloads

Payload Type	Chosen Model	Weight [kg]	Power [W]	Size [cm]
Gimbal	CM202	8	55	29.5 Diameter = 18.8
EO Camera	Hitachi DISC120R	0.26	11 VDC	5 x 6 x 9
IR Camera	Tau 2 640	0.15	5 VDC	4.4 x 4.4 x 3
Autopilot	Vector	0.180	2.5	4.5 x 6.8 x 7.45
Communication Unit	Gilat BlackRay 1000	13	350	25.4 x 46 x 46
Ballistic Parachute	BRS-6-1050-CAN	22.6	-	55 Diameter =18
Flight Data Recorder	SLICE Micro	0.028	12V, 70mA	4.2 x 4.2 x 8

4.3. PRELIMINARY CLASS I ESTIMATIONS

SCULPTUR is currently in the Early conceptual phase, when almost nothing about the UAV is known, apart from its requirements and the mission it has to perform. The next step in the design process is the class I weight estimation. The inputs required are all currently available: payload (17.46 kg, Chapter 2.4), performance requirements (range, speed) and reference data (statistic based fuel fractions estimation, statistic based OEW/MTOW estimation).

The sizing-for-performance process, is based on the generation of the so called W/P – W/S diagram. All the given performance constraints based on either the stakeholder requirements or reference data restrict the design space. In this section, the weight estimates from the baseline report are used to compute a preliminary wing surface area and power estimate. A Class I weight estimation is useful since without knowing anything about the geometrical properties and positioning of the wing, fuselage, landing gear, tail, etc. it is still possible to obtain an estimation of the wing surface area.

4.3.1. W/P-W/S

This section will elaborate on the different lines in the W/P-W/S graph in Figure 4.3. An explanation about the method and the equations will be given.

CLEAN WING STALL

The cruise stall speed requirement is not dependent on W/P, therefore it is represented as a straight vertical line in the W/P-W/S graph. The wing loading can be calculated by using the lift equation (Equation (4.1)) and since the conditions are the ones for cruise, it is possible to assume that L=W:

$$\frac{W}{S} = 0.5 \cdot \rho \cdot V_{s0}^2 \tag{4.1}$$

The mission requires a maximum value of the stall speed V_{s0}, which should not be exceeded. According to CS 23.49, the stall speed must not be higher than 61 kts (113 km/h).

The 330 N/m^2 does not restrict the design area since the landing distance requirement will not be met with such a wing loading.

CLIMB GRADIENT AEO (ALL ENGINES OPERATING)

The climb gradient requirement is dominated by the certifications specifications. For AEO conditions, the CS23 Sec. 65a states that the steady gradient of climb may not be less than 8.3% for landplanes or 6.7% for seaplanes and amphibians. The weight-to-power ratio in the case of propeller aircraft is dependent of wing loading; therefore this requirement will be expressed as a curved line in the diagram.

The weight-to-power ratio can be calculated as follows:

$$\frac{W}{P} = \frac{\eta_p}{\sqrt{\frac{W}{S}}\left(\frac{cr}{V} + \frac{C_D}{C_L}\right)\sqrt{\frac{2}{\rho \cdot C_L}}} \tag{4.2}$$

as proved by [38].

LANDING REQUIREMENT

The certification requirements do not allow the effect of thrust reversers to be taken into account. The wing loading is constant, therefore a straight vertical line can be seen in the graph for this requirement.

The amount and type of parameters is such that, similarly to the take-off case, it is extremely difficult to make accurate estimations of the landing field. Purely based on statistics, a relationship between the landing distance and the landing speed has been found [39]:

$$s_L = 0.5915 \cdot V_{s,land}^2 \tag{4.3}$$

$$\frac{W}{S} = \frac{C_{L_{max}} \cdot \rho \cdot \frac{s_L}{0.5915}}{2\frac{W_L}{W_{TO}}} \tag{4.4}$$

where the statistical coefficient (0.5915) above accounts for the relation between stall speed and approach speed.

TAKE-OFF REQUIREMENT

Take-off requirements are expressed in terms of the take-off distance s_{TO}. There are several different statistical relationships between the take-off field length and the TOP (take-off parameter). For the purpose of this report, the method taught in the Aerospace Design and System Engineering Elements course was used to calculate the TOP in N/m^2:

$$s_{TO} = 0.0577 \cdot TOP^2 + 8.6726 \cdot TOP \tag{4.5}$$

The value found for the TOP is 37.0 N/m^2. After the determination of this parameter, the following formula is used to determine a relationship between W/P and W/S for propeller aircraft:

$$\frac{W}{P} = \frac{TOP \cdot C_{L_{max}} \cdot \frac{\rho_0}{\rho}}{\frac{W}{S}} \tag{4.6}$$

The airport is assumed to be at sea level thus the $\frac{\rho_0}{\rho}$ ratio is 1. Margins are added further on in the report to take into account taking-off from airports at different altitudes. The design point is chosen such that it accounts for some margin of error. The above relation is a linear equation which means that the take-off requirement is represented in the W/P-W/S diagram by a straight line starting from the origin.

CRUISE REQUIREMENT

The most fuel intensive portion of the flight phase is cruise. Equation (4.7) describe the cruise portion of the flight phase.

$$\frac{W}{P} = \eta_p \left(\frac{\rho}{\rho_0}\right)^{0.75} \cdot \left(\frac{0.5 C_{D_0} \rho V^3}{\frac{W}{S}} + \frac{W}{S}\frac{1}{0.5\pi A e \rho V}\right) \tag{4.7}$$

CLIMB RATE REQUIREMENT

The climb rate requirement for the aircraft in this design process is set at a minimum of 3 m/s at a cruise altitude at 1000 m. From theoretical analysis on aircraft dynamics, the following equation for a propeller aircraft gives a relationship between wing loading, thrust over weight ratio, climb rate, air density, C_L and C_D:

$$\frac{W}{P} = \frac{\eta_p}{c + \frac{\sqrt{\frac{W}{S}}\sqrt{\frac{2}{\rho}}}{1.345 \cdot \frac{(Ae)^{0.75}}{C_{D_0}^{0.25}}}} \tag{4.8}$$

4.3.2. DESIGN POINT

Now that the W/P-W/S diagram has been constructed, one of the most essential parts in the preliminary design process can be conducted: choosing the design point.

To select the design point, it is essential that all the possible outcomes are contained within the available design space as indicated on the diagram. This design space is limited by regulations and physical restrictions of the clean wing stall, take-off distance, landing distance, climb rate and climb gradient. While designing an aircraft, it is required to make the design as light and efficient as possible. From this follows that a high wing loading and a high weight-to-power ratio are essential to achieve this goal (top right point in the diagram), since a high wing loading results in small wings and a high weight-to-power ratio results in small engines which, again, result in a light and efficient design. The W/P-W/S diagram with the design point can be seen in Figure 4.3.

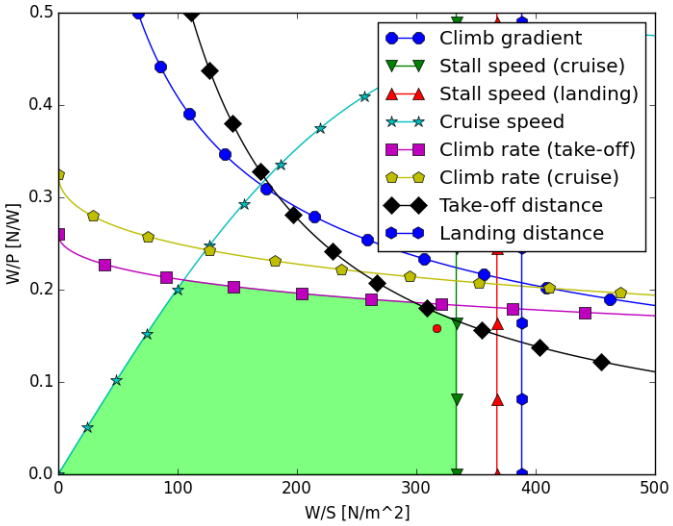

Figure 4.3: W/P-W/S diagram with design point

The design point has a power loading of 0.165 N/kW and a wing loading of 333.5 N/m^2. Using the estimated weight of 250 kg, this results in a required power of 14.9 kW and a wing area of 7.4 m^2. The power loading is limited by the climb rate during take-off, cruise speed and the take-off distance while the wing loading is limited by the stall speed requirement in cruise configuration.

4.3.3. FUEL WEIGHT ESTIMATION

Now that the power required has been calculated, an estimation for the fuel usage can be made. Reference data from 192 engines with power less than 1000 kW[67] was used to set up a quadratic equation relating engine power and specific fuel consumptions (SFC), by means of a least squares method. Since the power is known to be 14.9 kW and the endurance to be 20 hours, the total fuel required can be calculated to be 102 kg.

A very important parameter of an aircraft is the maximum take-off weight (MTOW). It is the weight that all the airworthiness parameters have to meet. It is valuable to investigate further the components that make up the MTOW. Namely, the operational empty weight (OEW), the maximum payload weight and the fuel weight. In Figure 4.4, a summary of the relevant weights from the Class I weight estimation is shown.

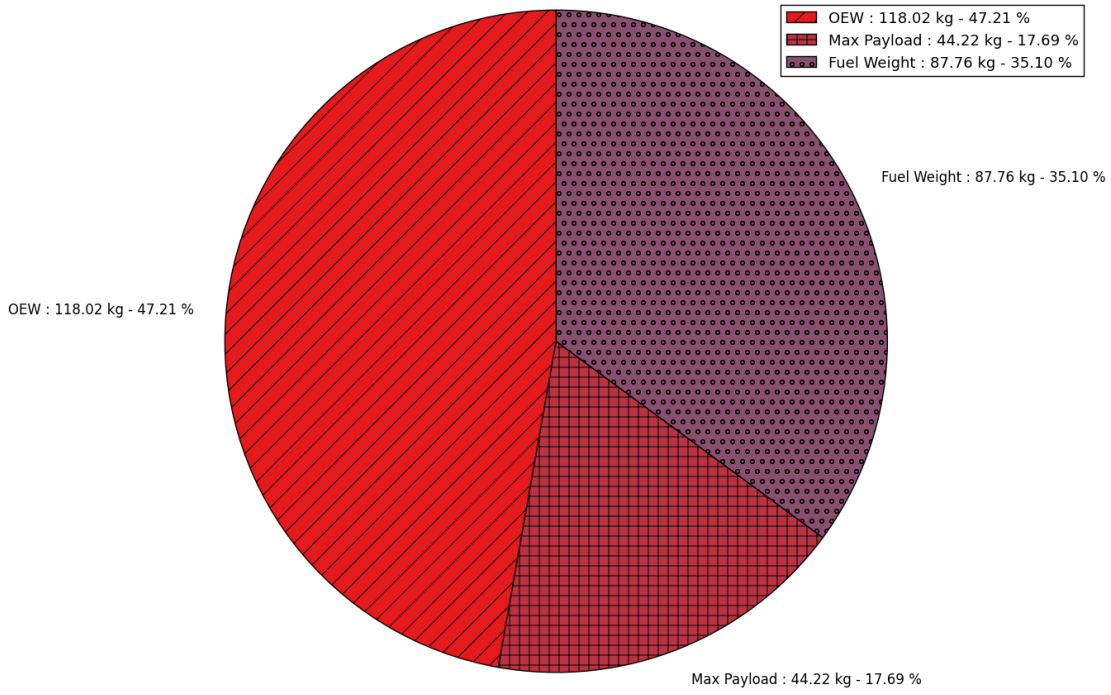

Figure 4.4: Class I: Weight division

[67] URL http://www.jet-engine.net/civtsspec.html [cited May 11 2016]

The results of Class I are summarised in Table 4.5.

Table 4.5: Summary - Class I results

Parameter	Symbol	Value	Units
Maximum take-off weight	MTOW	250.00	kg
Operational empty weight	OEW	118.02	kg
Fuel weight	W_{fuel}	87.76	kg
Payload weight	$W_{payload}$	44.22	kg
Wing surface area	S_{wing}	7.40	m^2
Power required	P	14.90	kW

4.4. PRELIMINARY SUBSYSTEM DESIGN

The preliminary sizing of the main aircraft components is an intermediary step between the Class I and Class II weight estimations. As presented in the N2 chart from the Midterm report [4], the dimensions of the wing (Section 4.4.1), fuselage (Section 4.4.2), tail (Section 4.4.3), control surfaces (Section 4.4.4) and landing gear (Section 4.4.5) are inputs for the Class II. The actuators, fuel, electrical and communication subsystems are presented in Section 4.4.6, Section 4.4.8, Section 4.4.9 and Section 4.4.10 respectively.

4.4.1. WING DESIGN

A comparison between the wing planform design from the mid-term report and from the final report is shown in Table 4.6. All the relevant explanations and motivations have remained the same as in [4]. Regarding the differences between the two, they are mainly due to the fact that the aspect ratio changed from 25 to 15 which directly also affects the other wing parameters (wingspan, chord, aerodynamic centre location). It was found that with an aspect ratio as high as 25, the negative effect on the wing weight (and cost) is too great. Also, with a high aspect ratio wing, it is difficult to accommodate the fuel and the required structural elements (stiffeners, ribs etc) to cope with the higher loads. The incidence angle marginally increased since the required C_L for cruise became larger, meaning that the UAV needs to fly at a larger angle of attack. In order for the fuselage to maintain level during normal cruising flight, it had to be increased.

Table 4.6: SCULPTUR UAV Wing planform sizing

Parameter	Symbol	Mid-term	Final	Units
Wingspan	b	13.31	12.50	m
Root chord	c_{root}	1.41	1.19	m
Tip chord	c_{tip}	0.57	0.48	m
Mean aerodynamic chord	MAC	1.05	0.88	m
Spanwise position of MAC	Y	5.30	2.68	m
Aspect ratio	A	25	15	-
Taper ratio	τ	0.4	0.4	-
Sweep angle	Λ	0.0	0.0	°
Dihedral angle	Γ	5.0	5.0	°
Incidence angle	i_w	3.5	3.56	°

4.4.2. FUSELAGE DESIGN

Since at this stage of the design there is limited information about the actual structural and aerodynamic loads that would be exhibited throughout the fuselage section, the initial sizing of diameter and length will mainly be based on reference UAV data.

In conventional aircraft the main design parameters are the regulations concerning the safety, comfort and weight of the passengers, crew and cargo. Obviously, for unmanned aerial systems, however, these are not an issue as the only external weight the fuselage has to support are the avionics, communication and surveillance systems. Based on the statistical analysis estimated in [19], it can be found that for a UAV with a cruise speed of 100 km/h, the ratio of fuselage length to wingspan is approximately equal to 0.4. It follows that $L_{fuselage} = 0.4 \cdot 12.50m = 5.0m$. This value was based on statistical data and taken for preliminary design purposes, using [2] for propeller parameters and related UAV tail sizes obtained from Raymer [40].

To continue with the diameter of the fuselage, it is important to define the fineness ratio as $D_{fuselage}/L_{fuselage}$. This ratio has been taken to be rather low - 0.1, again, based on statistical data in [19] and [40]. Even though such a small value would impose a relatively higher friction drag, it has been chosen because of its low pressure (form) drag low characteristics [41]. The diameter of fuselage is estimated as $D_{fuselage} = 0.1 \cdot 5.0m = 0.50m$.

An important parameter for the Class II weight estimation in the case of the fuselage is the wetted area. Using Figure 4.5 and Equation (4.9), where the parameters fe_1 and fe_2 describe the curvatures at the ends, it is possible to determine the fuselage wetted area.

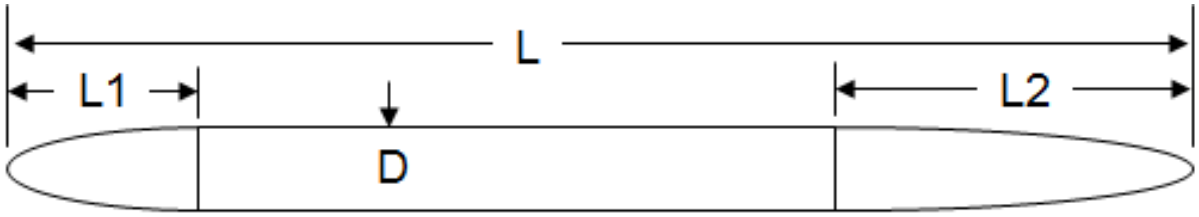

Figure 4.5: Fuselage model [19]

$$S_{wet-fuse} = \left[\left(\frac{\pi}{2}\right) \cdot D^2\right] \cdot (1 + (L/D) * \left(k1 * \left(fe_1 - 2\right) + k2 * \left(fe_2 - 2\right) + 2\right) \tag{4.9}$$

The final dimensions of the fuselage are summarised in Table 4.7:

Table 4.7: SCULPTUR UAV Fuselage dimensions

Dimensions	Value	Units
L	5.0	m
D	0.5	m
L_1	0.7	m
L_2	1.4	m
$S_{wet,fus}$	7.2	m^2

4.4.3. EMPENNAGE DESIGN

As can be found in section 3.5 the UAV should posses longitudinal and lateral stability. An unswept wing aircraft in combination with an airfoil with a negative pitching moment coefficient, as is the case for the SCULPTUR UAV, is both virtually untrimmable as well as unstable. Therefore, an empennage is required to provide the required trim capability and stability. However, during the design of the empennage not only stability and controllability have to be considered, the effect on aircraft weight, structural complexity, drag and safety also have to be taken into account. The empennage design for the SCULPTUR UAV consisted of the following steps:

1. Empennage configuration selection
2. Empennage area determination & positioning
3. Empennage airfoil selection
4. Empennage sizing

During each step both longitudinal as well as lateral stability was taken into account.

EMPENNAGE CONFIGURATION

The first step in the design of the empennage was the selection of the configuration. Below the advantages and disadvantages of different tail configurations are described [42].

- **Conventional tail** A large amount of data and literature is available on the conventional tail making it a safe choice with a low development risk. It has a reasonably low weight and a low complexity. A disadvantage is that the horizontal stabiliser is in the wing wake
- **T-tail** Compared to the conventional tail the advantage of the T-tail is that the horizontal stabiliser is above the wing wake reducing drag. However this comes at the cost of increased weight. Also, a T-tail has the added risk of a deep stall when AoA is too high
- **Cruciform tail** The cruciform tail is in between the conventional and the T-tail. It largely eliminates the risk of deep stall but has higher drag than a T-tail and higher weight than a conventional tail
- **Dual tail** A dual tail has increased vertical stabiliser effectiveness because the vertical stabilisers are not in the wing wake. Also the vertical stabiliser serve as winglets reducing horizontal stabiliser drag. However this comes at the cost of a very large increase in weight and complexity
- **V-tail** For a V-tail the stabilisers are out of the engine exhaust jet as well as the wing wake and fewer connections to the fuselage, both leading to improved efficiency and lower drag. However, the omission of a vertical stabiliser leads to decreased yaw stability and in turning the ruddervators produce an adverse rolling moment, which lead to a need for larger ailerons. A V-tail will also result in a small increase in the control software complexity
- **Inverted V-tail** Has largely the same performance as the non-inverted V-tail, but has the advantage that the ruddervators produce a proverse rolling moment during in turning, which lead to a smaller required aileron size. Additionally, the anhedral angle provides safer operation by keeping stabiliser tips out of the

wing wake during stall and increases the dutch roll damping, however this comes at the cost of the roll stability. One huge drawback however is that a large amount of ground clearance is required which lead to a very high and heavy landing gear

- **Y-tail** The Y-tail is similar to the V-tail in most regards. However, drag is higher than for the V-tail since more connections to the fuselage are needed, and an even larger ground clearance is necessary. Weight on the other hand is lower and an important advantage with respect to the V-tail is the increased yaw stability
- **Inverted Y-tail** The inverted Y-tail performance is comparable to the performance of the non-inverted Y-tail, i.e. it has both lower weight and higher yaw stability compared to V-tails. Compared to a inverted V-tail, it produces a smaller proverse rolling moment, though still a significant amount, and the anhedral angle still provides beneficial stall behaviour and dutch roll damping, but it doesn't require nearly as much ground clearance, though some clearance is still required. It also shares a lot of similarity with a conventional tail reducing the development risk
- **Boom tail** Boom tails heavier and more complex than other tail configurations, without any large performance benefits. Therefore only used in configurations where a conventional tail or fuselage would be too obstructive

As mentioned, the requirements Section 3.5 state that the UAV should be longitudinally and laterally stable. This is necessary to comply with regulations but also because a higher stability reduces the motion of the aircraft during flight which has a positive impact on the image quality during surveillance. At $1000m$ altitude, the flight altitude according to requirements, there is a significant amount of turbulence due to convection and irregularities in the surface of the earth with leads to gusts and other disturbances. Therefore a tail configuration that provides the required stability and reduces overall aircraft motion as much as possible is necessary. Also, turbulence could lead to stall. To comply with the high safety standards and requirements, the tail configuration should be able to cope with stall. Lastly, due to the limited weight budget available 3.8 weight and complexity should be as low as possible.

This eventually led to selection of the inverted Y-tail configuration. The inverted Y-tail has high longitudinal stability performance. For the lateral stability the yaw and roll stability should be considered separately. The yaw stability performance of the inverted Y-tail is comparable with the yaw stability of a conventional tail and very high compared to the longitudinal stability of V-tails. The roll stability is slightly less than the roll stability of a conventional tail due to the anhedral angle. However, the anhedral angle does provide very good dutch roll damping. It was determined that a high dutch roll damping was preferable since the dutch roll motion has a short period and therefore results in a lot of motion compromising image quality. A diverging roll is a very slow eigenmotion (due to roll damping by the wings) that is very easily counteracted by the autopilot and therefore causes only small disturbances. Due to the anhedral the inverted Y-tail has better stall performance than a conventional tail and much better stall behaviour than a T-tail. Since the engine exhausts located at the side of the UAV, the anhedral angle has the added benefit that none of the inverted Y-tail surfaces are in the engine exhaust jet increasing efficiency. Another characteristic of the inverted Y-tail is an increase in the effectiveness of the control surfaces, which is very beneficial since large control surfaces are required due to low speeds, and consequently dynamic pressure, at landing and take-off [42].

The inverted Y-tail has a weight comparable to a conventional configuration, lower than a T-tail and slightly higher than a V-tail. However, the upright V-tail leads to added complexity because an increase in the ailerons is required. The inverted V-tail (as well as the upright Y-tail), would require a very high landing gear leading to a large amount of added weight and complexity.

EMPENNAGE AREA & POSITIONING

From the class two weight estimation the fuselage dimensions were determined as can be read in section 5.2.4. It was decided to position the empennage at the rear end of the fuselage, $5.0m$ from the nose, as this would result in the largest possible moment arm with respect to the c.g. location and consequently the minumum required tail area. Using the method it was found that the required tail areas for a conventional tail would be $2.58m^2$ for the horizontal stabiliser and $1.46m^2$ for the vertical stabiliser. The resulting areas and dimensions for the inverted Y-tail are calculated in Section 4.4.3.

EMPENNAGE AIRFOIL

For selection of the tail airfoils, first the $C_{L_{des}}$ has to be determined for all stabilisers. Since the most fuel intensive stage of the mission is the cruise phase, the $C_{L_{h_{des}}}$, the design lift coefficient for the horizontal stabilisers (technically the stabilisers are diagonal but for convenience called horizontal), was taken as the required horizontal stabiliser lift coefficient required for trim during cruise. This value was determined applying longitudinal moment equilibrium as can be seen in Equation (4.10), or written in dimensionless form as in Equation (4.11). The moment due to the propeller and the horizontal stabiliser pitching moment coefficient were assumed very small and therefore neglected.

$$L_h \ell_h = M_{w+f} \tag{4.10}$$

$$C_{L_h} \cdot \frac{1}{2}\rho V_h^2 S_h cos\Gamma_{VT} \ell_h = C_{M_{w+f}} \frac{1}{2}\rho V^2 S\bar{c} \tag{4.11}$$

Where L_h is the lift generated by the tail, M_{w+f} is the moment generated around c.g. by the wing and fuselage, C_{L_h} is the horizontal tail lift coefficient, ρ is the air density, V_h is the airspeed at the horizontal stabiliser, S_h is the horizontal tail surface (as calculated in 4.4.3, Γ_{VT} is the tail anhedral angle and l_h is the distance between the c.g., the aerodynamic center of the horizontal stabiliser, $C_{M_{w+f}}$ is the moment coefficient due to wing and fuselage and V and S are the airspeed and wing surface respectively. Here, V_h was calculated using Equation (4.12).

$$\eta_h = \left(\frac{V_h}{V}\right)^2 \tag{4.12}$$

where η_h is the horizontal tail efficiency. From reference it was determined that η_h for an approximately conventional tail is on average 0.9, which was assumed for the SCULPTUR UAV. Lastly, Γ_{VT} was taken as calculated further on in Section 4.4.3. Solving these equation for $C_{L_{w_{cruise}}}$ his ultimately resulted in a design lift coefficient $C_{L_{h_{des}}}$ for the horizontal tail of -0.091. From reference it was found that the horizontal stabiliser thickness is usually around 12% of the chord length to facilitate enough space for both structural support as well as actuators for control surface, but not larger since an increase in the thickness results in an increase in drag. Using the XFLR5 software package an analysis was done to quantify the effect of a camber increase. It was found that an uncambered airfoil resulted in both less drag and a less complex structure. Therefore, the NACA0012 airfoil was selected. The airfoil properties can be found in Figure 4.6.

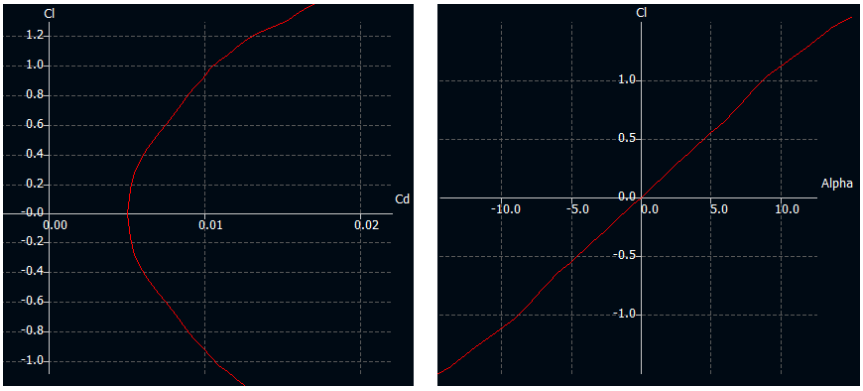

Figure 4.6: $C_l - C_d$ curve (left) and C_{l_α} curve (right) for the NACA0012 airfoil - XFLR5

Since the UAV is symmetrical in the XZ-plane when the aircraft has no sideslip angle, as is the case for cruise, the design lift coefficient for the vertical tail $C_{L_{des_v}}$ is zero. This means that a symmetrical airfoil should be selected. From reference it was found that the thickness of a vertical tail airfoil is typically around 12%. Based on this information, the NACA0012 airfoil was also selected for the vertical tail. The NACA0012 properties can be found in Figure 4.6[41].

EMPENNAGE SIZING

The final dimensions of the horizontal and vertical tails were determined by selection of the aspect ratio A,the chord length c, the span b, the horizontal tail dihedral angle Γ_{VT}, the quarter-chord sweep angle Λ and the taper ratio λ.

The aspect ratios of both horizontal and vertical stabilisers were determined. For the horizontal stabilisers an apect ratio of 4 was selected. This is intentionally much lower than for the wing, since a low aspect ratio greatly increases the angle of attack at which stall occurs. Therefore, having a low horizontal tail AR and high wing AR results in wing stall before horizontal tail stall and therefore a negative pitching moment when wing stall occurs counteracting the stall. Extrapolating the change in lift curve with aspect ratio as shown in Figure 4.7 it was determined that a horizotal tail with an AR would not stall at an angle of attack below approximately 22° with provides sufficient safety during flight. The aspect ratio was not chosen lower than 4 because at 4 stall safety margins are already sufficient and a further increase would lead to decreased roll stability, less available space for ruddervators and decreased effectiveness of the ruddervators during roll. Lastly, a lower aspect ratio would increase the chord length shifting the aerodynamic center forward, consequently reducing the tail moment arm. This would result in a larger required surface. From reference it was also found that most aircraft have an aspect ratio of 4 to balance out the positive and negative effects of low and high aspect ratios [43].

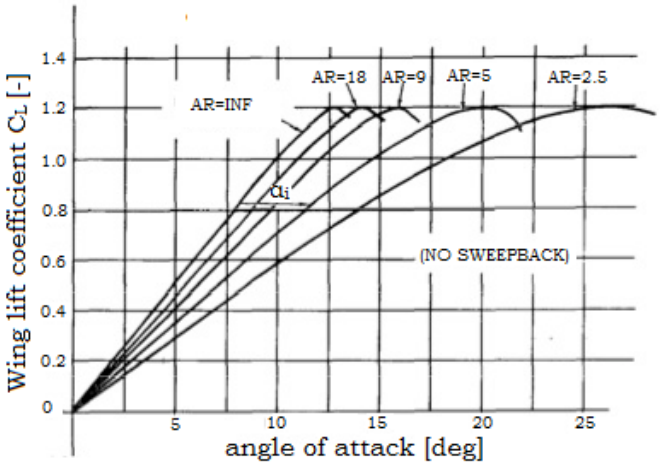

Figure 4.7: Lift curve of an unswept wing for several Aspect Ratios [68]

For the vertical stabiliser an aspect ratio of 4 was selected as well, since a high aspect ratio would only be beneficial for a reduction of the induced drag, which is already zero for the horizontal stabiliser during operating conditions. Conversely, a lower AR reduces the tail cross section perpendicular to the airflow and increases the Reynolds number, both reducing the part of the drag that is not lift related. Again the aspect ratio was not chosen lower than 4 because it would result in reduced roll stability, a more forward vertical stabiliser aerodynamic center and less available space for the rudder.

As stated in Section 4.4.3 a large anhedral angle has several desirable effects, in particular an increase in stall recovery behaviour, increased dutch roll stability and the generation of a proverse rolling moment in turning. It is therefore preferred to have a significant anhedral angle. However, the allowed anhedral angle is limited by the UAV dimensions since regulations require a clearance of $18cm$ between the tail and the ground during take off. Assuming maximum pitch angle at take off to be 15 ° as described in Section 4.4.5, and taking the attachment point for the horizontal stabilisers to be at the height of the fuselage centerline, this results in an allowed height difference of $41cm$ between the root of the horizontal stabiliser and the downward pointing tip of the horizontal stabiliser.

Using the aspect ratios, the required conventional tail surfaces and the allowed downward tip deflection determined above, the inverted Y-tail dimensions were determined using the following method: the inverted Y-tail was divided into two sections, an inverted V-tail as a substitution for performing the function of the horizontal stabiliser and part of the vertical stabiliser, and a conventional dorsal vertical stabiliser providing the additional required rudder authority to ensure equal yaw control as for a conventional tail. Equation (4.13) gives the required surface area S_{VT} required for a V-tail having the same rudder and elevator authority as a conventional tail with horizontal stabiliser area S_h and vertical stabiliser area S_v [44].

$$S_{VT} = S_h + S_v \tag{4.13}$$

Now assuming an initial Y-tail vertical stabiliser area $S_{v_{new}}$, the inverted V-tail area can be calculated using Equation (4.14).

$$S_{VT} = S_h + S_v - S_{v_{new}} \tag{4.14}$$

Where S_h and S_v are taken as stated in Section 4.4.3. The anhedral angle can then be calculated using Equation (4.15).

$$\Gamma_{VT} = atan\left(\frac{S_v - S_{v_{new}}}{S_h}\right) \tag{4.15}$$

Lastly, the inverted V-tail single sided stabiliser length $b_{VT_{single}}$ was calculated using (4.16) to determine the downward deflection δ of the inverted V-tail tips using Equation 4.17.

$$b_{VT_{single}} = \sqrt{0.5 A_{VT} S_{VT}} \tag{4.16}$$

$$\delta = b_{VT_{single}} sin\Gamma_{VT} \tag{4.17}$$

Using an iterative approach, repeating the above calculations for different values of $S_{v_{new}}$ it was found that for a $S_{v_{new}}$ of $0.82m^2$ the optimum downward tip deflection δ of $41cm$ was obtained with a inverted V-tail surface S_{VT} of $6.43m^2$ and an anhedral angle of 8.75°.

For the taper ratio λ a value of 0.5 was chosen for both the horizontal as well as the vertical stabiliser resulting in a semi-elliptical lift distribution, reducing the induced drag.

Finally, it was checked whether the empennage satisfies the longitudinal stability requirement that the stability margin SM should be above 0.05. This was done using Equations (4.18) and (4.19) for the change in the aircraft moment coefficient with angle of attack α C_{m_α}.

$$C_{m_\alpha} = C_{L_{w\alpha}} \frac{x_{cg} - x_w}{\bar{c}} + C_{L_{h\alpha}} \left(1 - \frac{d\epsilon}{d\alpha}\right) \left(\frac{V_h}{V}\right)^2 \frac{S_h}{S} \frac{x_{cg} - x_h}{\bar{c}} \tag{4.18}$$

$$C_{m_\alpha} = C_{L_\alpha} \cdot SM = (C_{L_{w\alpha}} + C_{L_{h\alpha}}) \cdot SM \tag{4.19}$$

Where $C_{L_{w\alpha}}$ is the change in moment coefficient of the wing with α, x_{cg} is the longitudinal location of the center of gravity measured from the nose, x_w is the longitudinal location of the wing aerodynamic center measured from the nose, $\bar{c}$ is the Mean Aerodynamic Chord (MAC) length, $C_{L_{h\alpha}}$ is the change in moment coefficient of the horizontal tail with α, $\frac{d\epsilon}{d\alpha}$ is the change of downwash angle at the tail with α, which can be calculated using (4.21) and x_h is the location of the aerodynamic center of the horizontal stabiliser. Equating these two equation and rearranging results in the expression for $C_{L_{h\alpha}}$ show in Equation (4.20).

$$C_{L_{h\alpha}} = \frac{C_{L_{w\alpha}} \left(SM - \frac{x_{cg} - x_w}{\bar{c}}\right)}{\left(1 - \frac{d\epsilon}{d\alpha}\right) \left(\frac{V_h}{V}\right)^2 \frac{S_{VT} cos\Gamma_{VT}}{S} \frac{x_{cg} - x_h}{\bar{c}} - SM} \tag{4.20}$$

$$\frac{d\epsilon}{d\alpha} = \frac{2C_{L_{w\alpha}}}{\pi A_w} \tag{4.21}$$

Inserting the parameters of the design in this equation resulted in a required value of $0.025\frac{1}{deg}$ for $C_{L_{h\alpha}}$. Using Equation (4.22) from the DATCOM method, the $C_{L_{h\alpha}}$ could be calculated[41].

$$C_{L_{h\alpha}} = \frac{2\pi A_{VT}}{2 + \sqrt{4 + \left(\frac{A\beta}{\eta}\right)^2 \left(1 + \frac{tan^2 \Lambda_{0.5C}}{\beta^2}\right)}} \tag{4.22}$$

Where $\beta = \sqrt{1 - M_\infty^2}$ is assumed to be one and the half-chord sweep $\Lambda_{0.5C}$ of the tail was chosen to be zero for maximum stability. The Airfoil efficiency factor η was assumed to be 0.95 which is a good approximation for virtually all airfoils [41]. It was found that $C_{L_{h\alpha}}$ for the inverted Y-tail is equal to $0.066\frac{1}{deg}$ which means that the stability margin is much higher than required, which is beneficial for payload performance. Using Equation (4.22) it could also be determined that, taking into account the wing downwash that an incidence angle of −3.48° was required at the root of the inverted V-tail to generate the required lift at cruise speed when the fuselage is at 0° angle of attack [45].

As stated above, the static longitudinal stability margin is much larger than required resulting in a very stable aircraft. While this is beneficial when flying in turbulent weather, which is often present at low altitudes, it should in the future be considered whether it would be beneficial to reduce the static stability margin to increase the maneuverability of the aircraft. This would allow either faster maneuvers or smaller control surfaces, reducing the complexity and weight of the UAV.

The final tail parameters are showed in Table 4.8

Table 4.8: SCULPTUR UAV Tail dimensions

Parameter	Symbol	Value	Unit
Inverted V-tail surface	S_{VT}	6.43	m^2
Vertical stabiliser Surface	S_v	0.82	m^2
Inverted V-tail aspect ratio	A_{VT}	4	-
Vertical stabiliser aspect ratio	A_v	4	-
Inverted V-tail anhedral angle	Γ_{VT}	13.82	°
Vertical stabiliser span	b_v	1.81	m
Inverted V-tail span	b_{VT}	3.59	m
Inverted V-tail projected horizontal surface	S_{VT_h}	6.24	m^2
Inverted V-tail projected vertical surface	S_{VT_v}	1.54	m^2
Inverted V-tail projected horizontal span	b_{VT_h}	3.48	m
Inverted V-tail projected vertical span	b_{VT_v}	0.86	m
Inverted V-tail taper ratio	λ_{VT}	0.5	-
Vertical stabiliser taper ratio	λ_v	0.5	-
Inverted V-tail half-chord sweep	$\Lambda_{0.5C_{VT}}$	0	°
Vertical stabiliser half-chord sweep	$\Lambda_{0.5C_v}$	0	°
Inverted V-tail airfoil	-	NACA 0012	-
Vertical stabiliser airfoil	-	NACA 0012	-
Inverted V-tail incidence angle	i_{VT}	-3.48	°

4.4.4. CONTROL SURFACE DESIGN

For safe operation the UAV should have sufficient controllabiliy. This implies two things. Firstly it should be possible to trim the UAV for it's entire c.g. range. Secondly the UAV should have enough control authority to perform the required maneuvers. This resulted in the performance requirements stated in Section 3.5. The design phase for the control surfaces consisted of the following steps:

1. Ruddervator design for longitudinal control
2. Aileron design for roll control
3. Rudder design for yaw control
4. Verification of trim requirements

RUDDERVATOR DESIGN

Since the ruddervators are the only surfaces that can be used for longitudinal control, they were designed first using the longitudinal control requirements. Using reference it was determined that for safe and efficient Take-Off an angular acceleration of approximately $8\frac{deg}{s^2}$ is required, therefore this was selected as the driving requirement for the design of the longitudinal control [46]. From the same literature, a method was selected for design of the ruddervator. First it was determined along what fraction of the inverted V-tail span the elevator would run. Since the elevator section inside or behind the elevator would have a very small efficiency but would still add to the design complexity, the elevator span fraction was determined as shown in Equation (4.23).

$$\frac{b_{RV}}{b_{VT}} = \frac{b_{VT} - D_{fus}}{b_{VT}} \tag{4.23}$$

where b_RV is the span of the inverted V-tail equipped with ruddervators, b_{VT} is the total inverted V-tail span and D_{fus} is the fuselage diameter. The second parameter to be determined for the ruddervators are the maximum deflection angles upward and downward. These deflection angle restrictions result from flow separation at high ruddervator deflection angles. From reference it was found that these angles can be assumed 25° for the upward deflection and 20° for the downward deflection.

Before determination of the final ruddervator dimensions, an analysis of the moments acting on the aircraft at take-off has to be performed to determine the tail lift needed to obtain the required angular acceleration. For the moment diagram, the take-off speed of $85\frac{km}{h}$ was taken as determined in Section 5.1. The diagram is Shown in Figure 4.8.

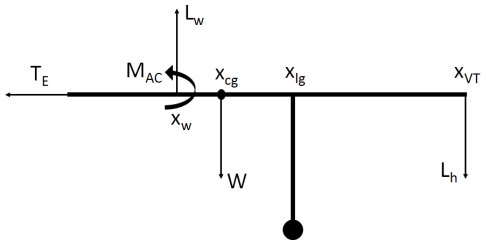

Figure 4.8: Moment diagram of UAV at take-off

Where T_{TO} is the take-off thrust, W is the weight, L_w is the wing lift, M_w is the wing moment, L_h is the vertical component of the lift generated by the inverted V-tail stabilisers, xlg is the aft landing gear location and h_{lg} is the aft landing gear height, with all forces in N and all the distances in m. Using Newton's second law and summing all the moments results in Equation (4.24).

$$I_{yy} \cdot \dot{\omega} = L_w(x_{lg} - xw) + L_h(x_{VT} - x_{lg}) - T_{TO} \cdot h_{lg} - W(x_{cg} - x_{lg}) \tag{4.24}$$

From which L_h can be determined using the required angular acceleration $\dot{\omega}$ for take-off and the moment of inertia I_{yy} which was determined from reference [47].

To calculate the required lift coefficient for the ruddervator the anhedral angle Γ has to be taken into account as shown in Equation (4.25).

$$C_{L_{VT}} = \frac{L_h}{\frac{1}{2}\rho \cdot V_{VT} \cdot S_{VT} \cdot cos\Gamma} \tag{4.25}$$

where $C_{L_{VT}}$ is the required V-tail lift coefficient, V_{VT} is the speed at the inverted V-tail and S_{VT} is the inverted V-tail surface. To prevent oversizing of the ruddervators the $C_{L_{VT}}$ necessary to satisfy landing condition was taken as the $C_{L_{VT}}$ at the maximum upward ruddervator deflection of 25°. For determination of the required $C_{L_{VT_{\delta_{RV}}}}$, the change in lift coefficient with a change in ruddervator deflection angle δ_{RV} Equation (4.26) can then be used.

$$C_{L_{VT}} = C_{L_{VT_{cr}}} - \delta_{RV} \cdot C_{L_{VT_{\delta_{RV}}}} \tag{4.26}$$

where $C_{L_{VT_{cr}}}$ is the lift coefficient of the inverted V-tail due to the incidence angle, while the UAV is driving on the runway with the fuselage at 0° angle of attack. To determine the final dimensions of the ruddervator Equation (4.27) can be used.

$$C_{L_{VT_{\delta_{RV}}}} = C_{L_{\alpha_{VT}}} \cdot \tau_e \tag{4.27}$$

where τ_e is a parameter that relates directly to the ratio $\frac{C_{RV}}{C_{VT}}$ which is the ratio between the ruddervator chord length and the chord length of the entire inverted V-tail. This relation is shown in Figure 4.9. The final ruddervator dimensions are shown in Table 4.9.

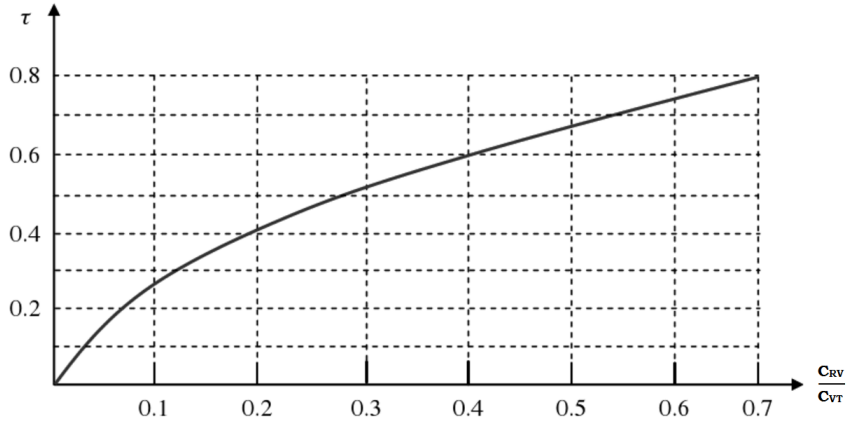

Figure 4.9: relation between τ_e and $\frac{C_{RV}}{C_{VT}}$ [46]

Table 4.9: Ruddervator dimensions

Parameter	Symbol	Value	Unit
Inboard Ruddervator edge	$y_{i_{RV}}$	0.25	m
Outboard Ruddervator edge	$y_{o_{RV}}$	1.79	m
Ruddervator chord length over inverted V-tail chord length	$\frac{c_{RV}}{c_{VT}}$	0.56	–

It can be noted the surface area of the ruddervator takes up a large part of the inverted V-tail part of the Y-tail. This is because the pitch acceleration requirement has to be fulfilled for take-off speed, which is very low for the SCULPTUR UAV resulting in low dynamic pressure.

AILERON DESIGN

Regulations state that the UAV should be able to bank from an angle of 30° to one side to an angle of 30° to the other side in less than $4s$ during take-off conditions (i.e. $V = 85\frac{km}{h}$) to ensure safe operation 3.5. The primary means for providing roll control are the ailerons. However, using differential control for the ruddervators also provides a combination of pro-verse yaw and pro-verse roll in turning. For design of the roll controls, first the total required rolling moment coefficient was determined. Afterwards, the contribution of the ruddervators was evaluated. Using this information the required aileron dimensions could be calculated.

For determination of the required a similar method to the method for the ruddervator design was used [46]. An estimate of the required performance was made using three equations: Equation (4.28), Equation (4.30), Equation (4.31) and Equation (4.32).

$$P_{ss} = \sqrt{\frac{2 \cdot L_A}{\rho \left(S_w + S_{VT} + S_v\right) C_{D_R} \cdot y_D^3}} \tag{4.28}$$

Where P_{ss} is the steady state roll rate, L_A is the UAV rolling moment due to the control surfaces, C_{D_R} is the UAV rolling drag coefficient, which was estimated to be 0.9 using reference data[46], and y_D is the average distance from the x-axis to the drag center of the wing and tail surfaces, assumed to be at 40% of the half-span as measured from the root. The total y_D can be calculated using Equation (4.29).

$$y_D = \frac{S_w \frac{b_w}{2} + S_{VT} \frac{b_{VT}}{2} + S_v \frac{b_v}{2}}{S_w + S_{VT} + S_v} \tag{4.29}$$

$$\phi_1 = \frac{I_{xx}}{\rho y_D^3 \left(S_w + S_{VT} + S_v\right) C_{D_R}} ln\left(P_{ss}^2\right) \tag{4.30}$$

Where ϕ_1 is the bank angle over which the aircraft rolls before reaching the steady state rolling moment P_{ss}, I_{xx} is the mass moment of inertia around the x-axis.

$$\dot{P} = \frac{P_{ss}^2}{2\phi_1} \tag{4.31}$$

Where $\dot{P}$ is the angular roll acceleration.

$$t_{roll} = \sqrt{\frac{2\phi_{des}}{\dot{P}}} \tag{4.32}$$

Where t_{roll} is the time necessary for the roll. Using an iterative approach the value for L_A was found for which the roll time was below the required time of $4s$. To transform L_A to a dimensionless performance coefficient, Equation (4.33) was used.

$$C_\ell = L_A \frac{1}{2} \rho V^2 S \tag{4.33}$$

Where C_ℓ is the UAV rolling moment coefficient. Since the rolling requirement stated above should be fulfilled at take-off condition, the dynamic pressure at take-off should be used for obtaining the required C_ℓ To calculate the change in rolling moment coefficient with a change in the deflection angle for a differential control surface, Equation (4.34) can be used.

$$C_{\ell_{\delta_A}} = \frac{2 C_{L_\alpha} \tau C_r}{Sb} \left[\frac{y^2}{2} + \frac{2}{3} \left(\frac{\lambda - 1}{b} \right) y^3 \right]_{y_i}^{y_o} \tag{4.34}$$

Inserting the ruddervater parameters in this Equation, the rolling moment coefficient contribution of the ruddervators at max deflection can be calculated using Equation (4.35).

$$C_l = C_{\ell_{\delta_A}} \cdot \delta_A \tag{4.35}$$

Where δ_A is the average of the absolute value of the deflection angles for both control surfaces (left and right ruddervator). Subtracting the maximum rolling moment coefficient contribution of the ruddervators from the total required C_l gives the C_l that the ailerons should be able to deliver.

Considering the maximum upward and downward deflection angles of the aileron as found in literature, 25° and 20° respectively, it can be calculated what value of $C_{\ell_{\delta_A}}$ is required for the ailerons so that the required rolling moment can be delivered at maximum deflection angle of the ailerons using Equation (4.34). There are then still three unknowns in this equation: τ, y_i and y_o. Therefore values of y_i and y_o were selected to be $0.1 \cdot \frac{b_w}{2}$ and $0.95 \cdot \frac{b_w}{2}$ respectively, spanning the maximum possible fraction of the trailing edge to minimise the required $\frac{C_a}{C_w}$, the ratio between the aileron chord length and the wing chord length. With these parameters the required value for τ and consequently the ratio $\frac{C_a}{C_w}$ could be determined using Figure 4.9. The required value for τ was found to be 0.71 which corresponds to a $\frac{C_a}{C_w}$ value of 0.55. However, as described in Section 5.6 only a fraction of 0.4 of the wing chord is available for ailerons due to the presence of the wing box. Therefore $\frac{C_a}{C_w}$ was selected to be 0.4 which resulted in the final aileron dimensions as shown in Table 4.10.

Table 4.10: Aileron dimensions

Parameter	Symbol	Value	Unit
Inboard Aileron edge	y_{i_A}	1.25	m
Outboard Aileron edge	y_{o_A}	5.93	m
Aileron chord length over wing chord length	$\frac{c_A}{c_w}$	0.4	–

The requirement for the roll rate discussed above has to be fulfilled at take-off speed which is only $85\frac{km}{h}$ for the SCULPTUR UAV. This also results in a very low dynamic pressure as was already mentioned in the discussion on the ruddervator design 4.4.4. It was found that the minimum obtainable rolling time from 30° on one side to 30° to the other side during take-off with the aileron dimensions stated in Table 4.10 was $5.3s$, not sufficient to fulfill the requirement of $4s$ It was decided to continue with these aileron dimensions since no rolling time regulations exist for UAVs at present. However, it might be necessary for the design team to keep track of future changes in regulation to ensure that certification is possible. If an increase in rolling authority is necessary, possibilities to increase the obtainable deflection angle should be investigated.

RUDDER DESIGN

The rudder provides the UAV with a means to control spin, control direction in turns and function in cross-winds. Since the UAV is not designed for performing high load factor maneuvers, spin control and directional control are not critical parameters during design [46]. However, regulations state that the UAV should be able to perform a landing when a cross-wind of at least $0.2 \cdot V_{s0}$ is present at an angle of 90° to the runway 3.5 [28].Here, V_{s0} is the UAV stall speed, which is $20.4\frac{m}{s}$ for the SCULPTUR UAV. However, since the approach speed of the SCULPTUR UAV is very low, it is expected to encouter cross-winds greater than $0.2 \cdot V_{s0}$ during operation. Therefore the requirement was set that the UAV should be able to land safely with cross-winds of at least $0.2 \cdot V_{s0}$ at a 90° angle to the runway. The approach speed of the UAV is again assumed to be $85\frac{km}{h}$.

For the design of the rudder, aircraft methods from the flight dynamic course were used [45]. First the total airspeed magnitude V_T was calculated combining the wind speed and aircraft speed as shown in Equation (4.36).

$$V_T = \sqrt{U_1^2 + V_2^2} \tag{4.36}$$

where U_1 is the magnitude of the speed in the direction the aircraft is heading and V_w is the magnitude of the wind speed. The directions of these vectors are shown in Figure 4.10.

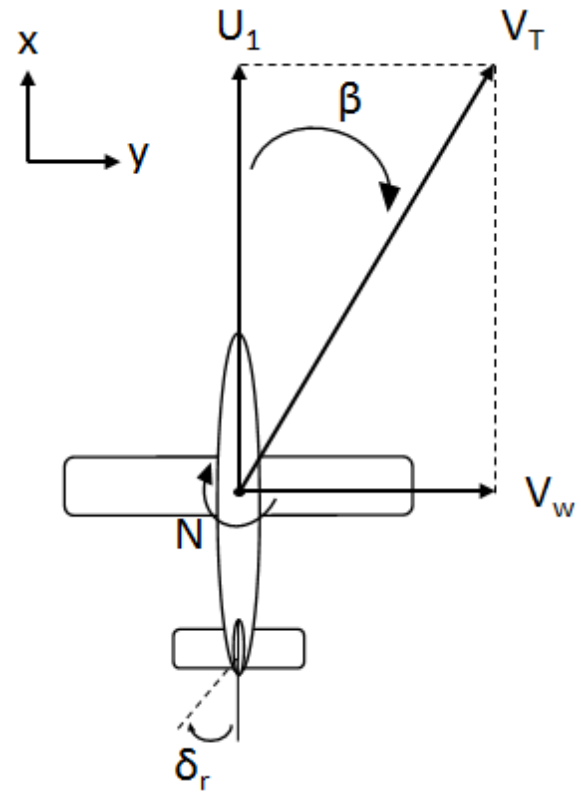

Figure 4.10: Schematic representation of an aircraft landing in cross-wind conditions

To counteract the cross-wind and keep its heading, parallel to the direction of the runway, the UAV has to bank to a certain angle ϕ and fly with its nose in the direction of the total airspeed at a sideslip angle β as can also be observed from Figure 4.10. Here the sideslip angle is calculated using Equation (4.37).

$$\beta = \tan^{-1}\left(\frac{V_w}{U_1}\right) \tag{4.37}$$

This is called a sideslipping landing. To calculate the rudder authority required to sustain a cross-wind landing as described above the equilibrium equations for steady, straight sideslipping flight: (4.38) for sideslip, (4.39) for roll and (4.40) are considered.

$$C_L \cdot \phi + C_{Y_\beta} \cdot \beta = 0 \tag{4.38}$$

$$C_{\ell_\beta} \cdot \beta + C_{\ell_{\delta a}} \cdot \delta a = 0 \tag{4.39}$$

$$C_{n_\beta} \cdot \beta + C_{n_{\delta_r}} \cdot \delta_r = 0 \tag{4.40}$$

These equations are only valid for a small bank angle ϕ which is assumed here. For determination of $C_{n_{\delta_r}}$ we must solve Equation (4.40) whith C_{n_β} as found in Section 5.2.6, β as determined by Equation (4.37). To prevent oversizing of the rudder, it was determined that equation (4.37) should be satisfied at maximum rudder deflection angle, which was determined to be 30° from reference [46].The final dimensions of the rudder could then be derived from the value for $C_{n_{\delta_r}}$ using Equation (4.41).

$$C_{n_{\delta_R}} = -C_{L_{v\alpha}} \frac{l_v S_v}{bS} \eta_v \tau_R \frac{b_R}{b_v} \tag{4.41}$$

where η_v, the ratio between the dynamic pressure at the vertical tail over the dynamic pressure of the undisturbed air, was assumed to be 1 since the vertical tail is not in the wing wake. The ratio $\frac{b_R}{b_v}$ was determined equal to the fraction of the vertical tail span not within the wake of the fuselage as described in Equation (4.42).

$$\frac{b_R}{b_v} = \frac{b_v - \frac{1}{2}D_f}{b_v} \tag{4.42}$$

The ratio between the rudder chord and the vertical tail chord $\frac{C_R}{C_v}$ could again be determined from Figure 4.9. This resulted in the final values for the rudder as found in Table 4.11.

Table 4.11: Rudder dimensions

Parameter	Symbol	Value	Unit
Inboard Rudder edge	y_{i_R}	0.25	m
Outboard Rudder edge	y_{o_R}	1.81	m
Rudder chord length over vertical tail chord length	$\frac{c_R}{c_v}$	0.65	–

With these rudder dimensions it is possible to perform a cross-wind landing as stated in the requirements. When a cross-wind more severe than described in the requirements is present at the airport, the flight should be rescheduled. If this not possible or the UAV is already in the air and the landing route cannot be changed, it should be considered using a higher approach speed. If the runway does not allow a higher approach speed, braking using the parachute should be considered.

4.4.5. LANDING GEAR DESIGN

The landing gear mechanism serves several functions such as supporting the weight of the UAV, transmitting loads partially to the airframe, taxi control, shock absorbing during roll-out, landing, towing and braking. The trade-off concerning landing in [4] already discussed that the most optimal design option is to use landing gear comprising of wheels, brakes, a strut and a shock-absorbing device per wheel. This has been done mainly because of the configuration's relatively high manoeuvring, accelerating and decelerating capabilities, impact resistance, and load damping.

Firstly, the type of landing gear configuration is determined as either tricycle or conventional (taildragger). They both have their advantages and disadvantages, however, the widely used tricycle configuration is preferred based on its relatively high stability during ground manoeuvring which is crucial for landing at unpaved runways for which the UAV will be designed. In addition, the tricycle essentially has higher resistance against a nose-over and a ground loop which could occur due to heavy braking and/or base excitation in rough conditions [48]. Most importantly, the tricycle allows for a better control during crosswind landing because of its relatively large 'crab' angle capabilities (i.e. nose not aligned with runway) due to the supporting main landing gears located behind the nose gear [40].

Further on, because of the relatively low weight and size of the UAV, a retractable solid-spring strut that is mounted on the fuselage is chosen for the main landing gear design. The solid-spring concept is relatively simple, inexpensive, and it has a lower weight with respect to alternatives such as the oleo-pneumatic shock-absorber-strut. The landing gear has been chosen to be retractable, even though it will require a heavier and more complex retraction mechanism design, because in the long run it will prove to be more efficient when compared to fixed-position gear as large amounts of aerodynamic drag can be avoided, especially at the specified altitude of 1000 m. Concerning the lateral positioning, given the rather complex retraction mechanism required and the fuel tank positioning in the wings, there are further limits on the available space in the wings. For these reasons, a decision followed to use long externally-retractable struts coming at a lateral angle from the fuselage, similarly to other reference UAVs such as the Predator MQ-1[69].

The longitudinal positioning of the landing gear requires the determination of both the forward and aft center of gravity locations, corresponding to full fuel mass at the time of take-off and the weight of the aircraft during landing, respectively. This is precisely why this positioning has been done simultaneously with the weight estimation of the subsystems, as several iterations were performed to calculate the c.g. shift (see Figure 4.11).

To begin, the longitudinal position of the main landing gear has been taken to be at 50% of the MAC leading edge [40] [41]. Estimating the Leading edge MAC position as 25% of the UAV longitudinal length ($LE_{MAC} = 1.25m$) after several iterations, it was estimated that the main landing gear will be positioned at $1.70m$ from the nose tip. Furthermore, reference values for $\frac{M_a}{B}$ and $\frac{M_f}{B}$ were taken 8% and 15%, respectively as suggested by Raymer [40]. Obtaining the most aft c.g. location on an iterative basis simultaneously with the Loading diagrams presented in Section 5.2.1, it has been determined that the $M_a = 12.2\% MAC = (12.2\%) \cdot 0.89m = 0.108m$. Using this value it has been estimated that the wheel base $B = 1.35m$, therefore the nose landing gear will be located at $0.35m$ from the nose tip. Moreover, it is positioned at a forward angle of 7° with respect to the vertical to lower axial loads by introducing slight bending stresses (allowing for deflection during bending).
The vertical distance from the ground to the center of gravity location is taken to be a value of $H_{cg} = 1.15m$ (scaled with respect to MTOW), based on [48] and the Predator MQ-1 for preliminary design purposes. This value is rather high for the size of the UAV being developed, however, it is necessary to allow for ground clearance during rotation. A margin of 5 inches from the ground to the tail surface at the maximum take-off angle has been considered and the value for the height was verified to be reasonable.

[69] URL: http://www.airforce-technology.com/projects/predator-uav/ [cited May 28 2016]

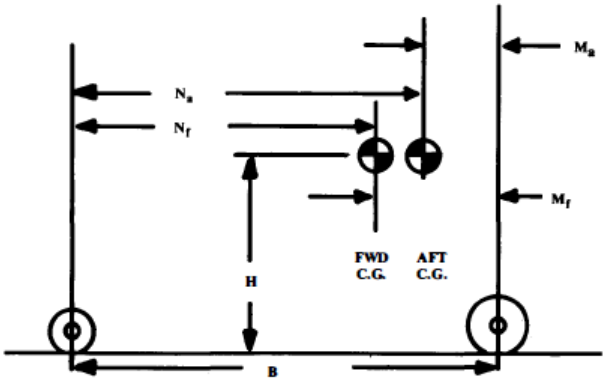

Figure 4.11: Wheel load geometry [40]

These fractions are used to determine the maximum static loads of the nose and main landing gears (see Equations (4.43) and (4.44)). For all of these values a margin of $N_{FAR} = 1.07$ has been accounted for as set by FAR 25 regulations [40].

$$F_{m,max} = \frac{W}{2}\left(\frac{1-M_a}{B}\right)N_{FAR} = \frac{889.6lbm}{2}(1-0.08)1.07 = 437.9lbm = 198.6kg = 1948.3N \tag{4.43}$$

$$F_{n,max} = W\frac{M_f}{B}N_{FAR} = (889.6lbm)(0.15)(1.07) = 142.8lbm = 64.8kg = 635.7N \tag{4.44}$$

Moreover, the nose landing gear has to be able to withstand the dynamic loads during braking, especially at touchdown, according to Equation (4.45):

$$F_{dyn,braking,nose} = \frac{10H_{cg}W}{gB}N_{FAR} = \frac{10\cdot 1.15m\cdot 889.6lb}{32.2ft/s^2 1.35m}1.07 = 251.8lbm = 114.0kg = 1118.3N \tag{4.45}$$

Having determined the longitudinal and vertical landing gear position, it is now time to estimate the lateral location of the main gears, especially the angle at which the gears have to be positioned relative to the fuselage vertical. This estimation depends on the turn-over angle $\theta_{turn-over}$ and the c.g. height. Based on the Predator MQ-1 and [48], a value of $\phi_{WT} = 40°$ has been acquired for the lateral position of each main landing gear with respect to the vertical. This value is acceptable according to Raymer's turn-over angle criteria [40]. This results in a wheel track (lateral distance between the two main gears) of $WT = 2\cdot tan(40°)\cdot H_{cg} = 1.93m$.

It must be noted that a more thorough analysis with exact estimation of the positioning of the landing gear is beyond the scope of this report, as it involves detailed structural & vibrational analysis, as well as ground stability calculations. Therefore, all values have been based on reference aircraft.

The next step in the landing gear design is to estimate the size of the tires. This is done by determining the critical loading cases, particularly the maximum static loads on the main and nose landing gear.

$$D_{main} = 1.51\cdot W_{main}^{0.349}\cdot 1.3 = 1.51\cdot(437.9lbm)^{0.349}\cdot 1.3 = 16.40in \tag{4.46}$$

$$Width_{main} = 0.715\cdot W_{main}^{0.312}\cdot 1.3 = 0.715\cdot(437.9lbm)^{0.312}\cdot 1.3 = 6.20in \tag{4.47}$$

The nose tire parameters were taken to be 70% of the nominal diameter and width of the main tires, particularly $D_{nose} = 70\%15.65in = 11.48in$ and $Width_{nose} = 70\%5.95in = 4.34in$ as specified by Raymer [40]. These results impose the selection of type III tires. In order to estimate the stroke of the main tires on landing, the rolling radius is determined from reference tire data; specifically, the Goodyear-aviation type III 6−6 (ply rating 8) tire has been considered, which has a nominal outside diameter of $17.5in$, minimum diameter of $16.8in$, minimum outside width of $6.2in$, uses a rim diameter of $6in$ and has a rated inflation of $P = 55psi$, values that comply to the calculated ones [49]. It is found that the braking and bottoming load capabilities are well above the calculated forces [49]. Equations (4.48) and (4.49) show the estimation of the contact area with the pavement A_p and then the calculation of the rolling radius R_r [40].

$$A_p = \frac{W_m}{P} = \frac{437.9lbm}{55psi} = 7.96in^2 \tag{4.48}$$

$$R_r = \frac{D_{main}}{2} - \frac{A_p}{2.3\sqrt{(D_{main})(Width_{main})}} = \frac{16.8in}{2} - \frac{6.97in^2}{2.3\sqrt{(16.8in)(6.2in)}} = 8.06in = 20.5cm \tag{4.49}$$

Now that the rolling radius is known, the stroke of the tire S_T is estimated as $S_T = \frac{D_{main,nom}}{2} - R_r = \frac{17.5in}{2} - 8.06in = 0.69in = 0.058ft$ according to Raymer [40].

In order to size the solid-spring stroke, it is needed to know the average total load during deflection L_{load}, the tire and the shock-absorber efficiencies. Statistically, the tire efficiency is $\eta_T = 0.47$, the solid-spring efficiency is $\eta_{ss} = 0.62$ and the load factor $N_{gear} = 3$, values provided by [40]. The maximum landing weight is estimated using Equation (4.50) according to Raymer [40], while Equations (4.51), (4.52) and (4.53) show the estimation of the shock-absorber stroke. The values for $V_{vertical}$, N_{gear} and N_{safety} were taken $15 ft/s$, 3 and 1.5, respectively, according to FAR-25 and CS-23 regulations [40].

$$W_{landing} = 90\% MTOW = (90\%)403.5kg = 363.15kg = 3562.5N = 801.7lbm \tag{4.50}$$

$$N_{gear} = \frac{L}{W_{landing}} \tag{4.51}$$

$$KE_{vertical} = KE_{absorbed,shock-absorber} + KE_{absorbed,tire} = \\ = \left(\frac{1}{2}\right)\left(\frac{W_{landing}}{g}\right) V^2_{vertical} = (\eta_{ss} LS)_{shock-absorber} + (\eta_T LS_T)_{tire} \tag{4.52}$$

$$S = \frac{V^2_{vertical}}{2g\eta_{ss} N_{gear} N_{safety}} - \frac{\eta_T}{\eta} S_T = \frac{(15 ft/s)^2}{2 \cdot 32.2 ft/s^2 \cdot 0.62 \cdot 3.0 \cdot 1.5} - \frac{0.47}{0.62} 0.058 ft = 1.21 ft = 36.9 cm \tag{4.53}$$

It follows that the solid-spring strut will have to do at maximum a $36.9cm$ vertical deflection on heavy landing. Finally the strut length is calculated based on simple geometry as $L_{strut} = \frac{WT}{2 \cdot sin(\phi_{WT})} - R_r = \frac{1.93m}{2sin(40°)} - 0.205m = 1.30m$. This is approximately 3.5 times larger than the deflection of the strut, which is deemed reasonable according to Raymer - for structural reasons the overall strut length is typically between 2.5 and 3.5 times the value of the stroke deflection [40].

All values obtained in this landing gear preliminary design are recommended to be re-iterated even further in a design optimisation process. It is suggested that appropriate FEM and Multi-Body Dynamic analyses is performed to calculate the exact bending, axial and torsional static & dynamic loads of the strut and wheel assembly. Upon performing these analyses, a material can be chosen that is not only capable of carrying the loads but also allowing appropriate stroke deflection during touchdown.

4.4.6. ACTUATORS

The control surface and the landing gear need actuators for the control and deployment. It is important that the actuation system is reliable and accurate for a safe operation. Electronic actuators will be designed, since they reduce complexity, thereby also the weight of the actuator system and the required maintenance with respect to a hydraulic system [50]. For every control surface different actuators need to be designed, because every control surface has a different size, deployment and required actuator force. The choice for actuators are made to give an estimation on the parameters of the actuators (weight, size, power usage).

AILERON ACTUATOR

For the design of the actuator the required control force needs to be calculated. This can be done using Equation (4.54) from [45].

$$F_a = -\frac{d\delta_a}{ds_a} \frac{1}{2} \rho V^2 S_a \bar{c}_a (C_{h_\alpha} \Delta\alpha_a + C_{h_\delta} \frac{\delta_a}{2}) \tag{4.54}$$

In this equation $\frac{d\delta_a}{ds_a}$ is the gear ratio, so the amount of actuator deflection to deflect the aileron. Usually the value is around 1.25 - 1.5 $°/cm$, this gives also the maximum required deflection of the actuator: 37.5cm. For the coefficient part of the equation it is important to select them for the most critical case, this is for largest accumulated angles of angle of attack and aileron deflection angle. The maximum aileron deflection is 25° and the angle of attack for maximum lift is 12.5°. The C_{h_α} and C_{h_δ} can be taken from the control surface design, for now the trim tab is not included. The force with a trim tab will be less, hence the force calculated now will be the maximum force that can occur during operation. This force will be 3399N. In combination with the required aileron deflection the actuator can now be chosen. The choice will be a E-SEMA[70].

RUDDERVATOR ACTUATOR

For the ruddervator the actuator force calculation is less straightforward, since this actuator needs to work for both roll and pitch. The equations for elevator and rudder force are given by Equations (4.55) and (4.56) [45].

$$F_e = -\frac{d\delta_e}{ds_e} \frac{1}{2} \rho V_h^2 S_e \bar{c}_e (C_{h_\alpha} \alpha_h + C_{h_\delta} \delta_e) \tag{4.55}$$

[70] URL https://www.google.nl/url?sa=t&rct=j&q=&esrc=s&source=web&cd=1&ved=0ahUKEwi575n2l7XNAhWDZpoKHVX6B60QFggnMAA&url=http%3A%2F%2Fwww.sener.es%2FEPORTAL_DOCS%2FGENERAL%2FSENERV2%2FDOC-cw53cd2ec89270e%2Felectro-mechanical-actuators-for-aerospace-applications.pdf&usg=AFQjCNHbxWcdVQ82JRXnC7DFXAOhumTUBw&cad=rja [cited June 19 2016]

$$F_r = -\frac{d\delta_r}{ds_r}\frac{1}{2}\rho V_v^2 S_r \bar{c}_r (C_{h_\alpha}\alpha_v + C_{h_\delta}\delta_r) \tag{4.56}$$

These equations are in analogy with the equation for the aileron actuator force. The required force can be calculated by combining the equations using the contribution of the ruddervator for yaw control. The required ruddervator force is calculated to be 748N. A suiting actuator would be a Thomson Max Jack [71].

RUDDER ACTUATOR

The rudder actuator force can be calculated in a similar way, using the same equations as for the ruddervator and the already performed yaw control. The resulting rudder force has to be able to bear a force of 64N. This will require a very light actuator, e.g. M1-D012-0050 [72].

LANDING GEAR ACTUATOR

The landing gear needs to be retracted in flight. The mechanism for retracting will be a simple actuator that extends and retracts directly connected to the landing gear. The actuator will be attached at the half of the landing gear strut. With a landing gear height of 1.15m the actuator needs to be 1.7 extended and 1.0 retracted. The actuator that will be sufficient is a Rolaram B050/R050[73].

4.4.7. PROPULSION DESIGN

During the design of the micro-gas turbine for the SCULPTUR UAV several requirements had to be met as described in section 3.5. These requirements imposed limitations on the specific fuel consumption (SFC), the noise and emission level of the UAV. Furthermore limitations and constraints were created during the design, consisting of the required maximum power of the UAV, the required thrust and the maximum turbine inlet temperature. This section describes the required values of the above named parameters. Implementation of these parameters into the design of the engine is shown in section 5.4.

Specific Fuel Consumption

The first parameter to be analysed is formed by requirement SCULPTUR-SUST-SH20, which describes the need for a SFC comparable with current existing systems. These systems include both gas turbine engines and reciprocating engines with approximately the same power output. Generally it is found, according to [8] that 2-stroke reciprocating engines have a SFC between 0.45-1.2 kg/kWh. The transition from 2 to 4-stroke engines is accompanied by a decrease in SFC to about 0.3-0.4 kg/kWh. The final type of reciprocating engine often used in UAV applications are rotary engines, having an average SFC of 0.35 kg/kWh. Gas turbine (turboprop) engines often operate at a higher power output than reciprocating engines, and therefore have a higher power to weight ratio [9]. Their specific fuel consumption is similar to the 4-stroke reciprocating engines, and can vary between 0.3-0.5 kg/kWh. With the eye on designing a competitive engine, the aim of the engine design is terms of specific fuel consumption was set at 0.35 kg/kWh.

Emission level

Requirement SCULPTUR-SUST-SH20-2 considers the CO_2 emissions of the UAV. Although no official regulations exist around the maximum emission level of a UAV, ICAO has issued a circularly with advices for UAV design. This circularly states a recommended CO_2 emission 10 times lower than a small single-engined manned aeroplane. For general aviation aircraft, approximately 10% of the emissions consist of CO_2, and about 0.04% of NO_x[74] [51]. These percentages are mass percentages of the fuel burned, hence a reduction in emission level is achieved through the reduction of fuel mass flow rate. For general aviation aircraft with a turboprop engine, an average fuel consumption of 0.094 kg/s was determined through a survey by the FAA in 2009 [52]. Assuming a similar engine exhaust composition, the aim for the SCULPTUR engine fuel consumption is to get below 0.0094 kg/s.

Noise level

The noise level of an aircraft is determined under 14 CFR Part 36 and is measured in dBA, these A-weighted sound levels account for the relative loudness perceived by the human ear as humans are less sensitive to frequencies below 1000 Hz. An estimation of the noise levels of general aviation aircraft was retrieved from the FAA database[75], and showed values between 60 and 52 dBA for single-manned aircraft. In order to comply with the ICAO advisory circularly of reducing the aircraft noise by 6 to 9 dB, an estimated noise level of 46-51 dBA is found to be suitable for the SCULPTUR UAV.

Vibrations

Engine vibrations are defined in frequency and amplitude. The amplitude of the vibration is a direct indication of the balance of the part, and corresponding of the wear and life-time. Vibrations in engines are measured using accelerometers, which are often mounted on the bearing housing closely representing the shaft vibrations[53].

[71] URL http://www.thomsonlinear.com/website/com/eng/products/actuators/maxjac.php [cited June 19 2016]
[72] URL http://www.warnerlinear.com/LightDutyActuators.asp [cited June 19 2016
[73] URL http://www.powerjacks.com/products/rolaram/ [cited June 17 2016]
[74] URL: http://aviationbenefits.org/environmental-efficiency/aviation-and-climate-change/ [cited June 17 2016]
[75] URL: http://www.faa.gov/documentLibrary/media/Advisory_Circular/Appx1_pg1A-19A.pdf [cited June 17 2016]

Main vibrations present in the engine come from unbalance of rotating components, such as the turbine and compressor stages, and the propeller. To reduce the vibrations of gas turbines with respect to reciprocating engines conform requirement SCULPTUR-SH-22, multiple actions can be taken. These action include increasing the quality and accuracy of dynamic equilibrium in the different rotating components of the engine, but also include damping existing oscillations by the addition of balancing weights [54]. Accurately estimating engine vibrations however required complicated analysis, and is different for each produced engine considering the frequency and amplitudes. It is therefore not possible to quantify the "vibration" level of general aviation aircraft.

Turbine Inlet Temperature

One of the challenges during the design of a micro-gas turbine, as described in section 2.3.2, are the high temperatures within the gas turbine. The highest temperature encountered in the micro-gas turbine is found at the turbine inlet, which makes it the critical point of the engine. To ensure that the engine is able to operate, the materials of the engine, with emphasis on the turbine blades, should be adjusted to maintain strength and avoid creep at these elevated temperatures and high rotational speeds. Increasing the TIT is favourable during designs with high pressure ratios, and leads to an increased thermal efficiency of the overall engine [55]. For large (>200 kW) turboprop engines, temperatures at the turbine inlet are often found in the region of 1200-1400 K[76].

Beneficial to the development of a MGT with a relatively high thermal efficiency is thus a high TIT combined with high pressure ratios, which leads to a challenge for material engineers. Promising research is currently performed by the Wadley Research Group of the University of Viginia[77] into the application of thermal barrier coatings and environmental barrier coatings to turbine blades, in order to increase component life and reduce the surface temperature of the metallic component to below its maximum use temperature. Figure 4.12 visualises the current research performed and the expectations of allowable TIT according to the Wadley Research Group.

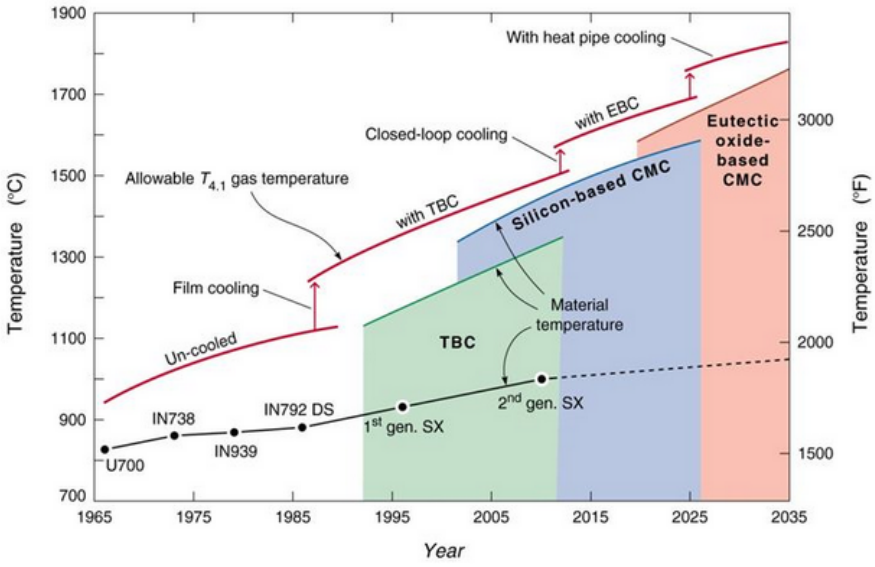

Figure 4.12: The past and (predicted) future evolution of propulsion materials, coatings, cooling concepts and TIT with year of entry [78]

Concluded from this figure is that with current research being done, TIT up till 1450 K are able to be reached if the required budget and development time is available. Other possible solutions to the required high TIT are the development of micro ceramics and Ni-based superalloys, both allowing the TIT to go up to around 1500 K [56][57].

The application of these materials and thermal coatings in micro-gas turbines is still in research phases, as increased accuracies are required and higher rotational speeds are present in the turbine stages [58]. To ensure high reliability and safe operations of the engine, it was chosen to apply a safety margin of 10% to the approximate maximum temperature of 1450-1500 K. This margin has to reduce the chances of mechanical failure due to increased creep or rotational stresses of the blades. This resulted in a maximum turbine inlet temperature of **1350 K** used throughout the engine design.

[76] URL: http://www.wartsila.com/energy/learning-center/technical-comparisons/gas-turbine-for-power-generation-introduction [cited June 19 2016]

[77] URL: http://www.virginia.edu/ms/research/wadley/high-temp.html [cited June 19 2016]

ENGINE WEIGHT AND SIZE ESTIMATION

Aside from the engine performance determination as described in section 5.4, also an estimation of the physical size of the engine was made in order to perform the Class II weight estimation. This estimation is based on the data of 97 reference turboprop and turboshaft engines with varying power outputs[79]. From these reference data regression curves were found to fit the data points as closely as possible, resulting in two different distributions for the engine length, diameter and weight. Figure 4.13 shows the data points with the regression lines used to determine SCULPTUR's engine dimensions.

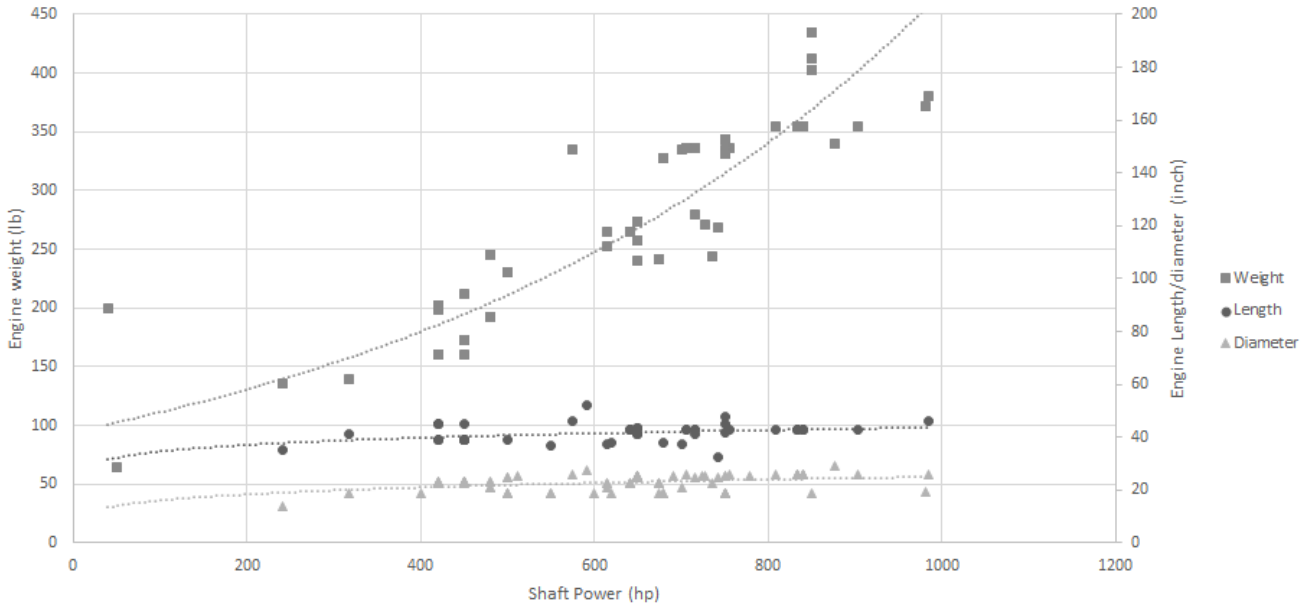

Figure 4.13: Statistical analysis of engine size and weight[80]

From Figure 4.13 it can be seen that two different distributions were chosen to fit the statistical data with the regression lines. For the engine weight an exponential regression line was used, whereas for the engine length and diameter the best fit was found when using a power function. Using these regression lines, together with the maximum power output of **24.61 kW (33 hp)**, an engine weight of **45.3 kg**, an engine length of **65.5 cm** and an engine diameter of **33.5** cm were found.

These dimensions were validated against current available information on MGT and scaled down values of larger engines using Raymer's scaling method as described in [4]. It was determined to not use the Raymer's scaling method for the actual estimation but only for validation purposes, as this method only produces accurate results for scaling factors smaller than 4. Using a scaling factor larger than 4 would, according to [59], lead to unrealistically small values. The scaling factor used to validate the results of the statistical approach is based on the scale-down of the TP100 engine with a power output of 180 kW (SF=7.3). Using the values of the TP100, Capstone C30 and the currently researched UAV Turbine[81], it was found that competitive engine weight would be in the range of 18.4-72.5 kg, with 18.4kg resulting from the extreme Raymer's scale-down, and the 72.5 kg from the modified Capstone C30 generator. The estimated 45.3 kg of engine weight for the SCULPTUR UAV is right in the middle of this weight range, and therefore found to be sufficiently accurate to use further in this conceptual design phase.

4.4.8. FUEL SYSTEM

In order to provide the engine with fuel at all times, a complex fuel system is required. For a conceptual overview of the system implemented in the SCULPTUR UAV, schematic overviews of the (engine) fuel distribution system are shown in Figures 4.14 and 4.15. This section describes the several components present in the designed fuel system.

[79] URL: http://www.jet-engine.net/civtsspec.html [cited June 17 2016]
[81] URL: http://uavturbines.com/ [cited June 17 2016]

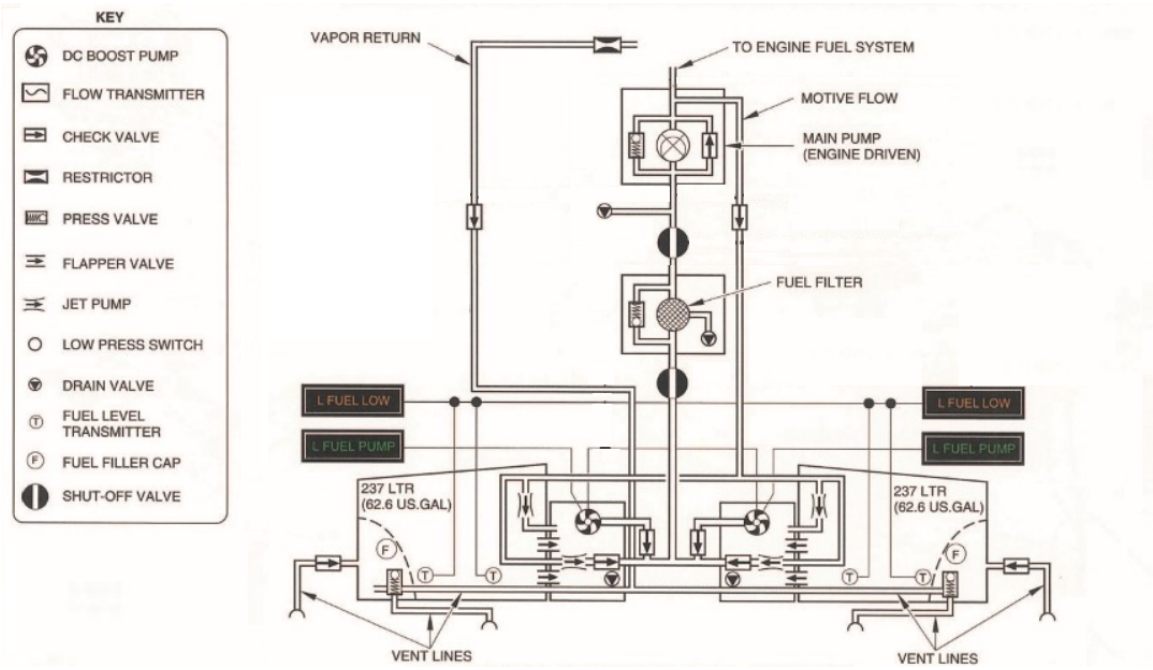

Figure 4.14: Fuel distribution system [60]

The first component of the fuel system are the fuel tanks in which the fuel is stored. The SCULPTUR UAV stores the fuel required to perform its mission in two integral wing tanks from wing root till 80 percent of the wingspan, with a total volume of 117 liters. To ensure "breathing" of the fuel tanks during climb and descent an open vent system is used to connect each tank to the outside air [61]. Two different types of vents are used in each wing tank, one float vent valve and one pressure operated vent valve. Since only small pressure differences are found for operations up till 1000 meters, small venting lines were found to be sufficient. Larger pressure differences are expected to be present during fuel operations of the UAV, hence the pressure operated vent valves get opened during refueling of the UAV for additional venting. This is done to prevent the tank pressure from exceeding the limits, and ultimately by avoiding overfueling [62]. Next to the vent valves, one fuel filler cap is placed towards the outer end of the wing fuel tank. Two fuel level transmitters are placed in each fuel tank for redundancy, which transfer information on the fuel level of each tank back to the controller.

Flapper valves are used to allow one way flow from the fuel tanks to the fuel feed chamber[82], this transfer is done making use of gravity and the dihedral angle of the wings [62]. In the fuel feed chamber a booster pump is located which is used for engine start up, as a backup for the primary jet pump, and when fuel pressure becomes lower than a set, yet to be determined, value. The booster pump is an electric pump of 84 W (as described in Section 3.8), which injects fuel into the fuel feed lines towards the engine. Part of the fuel injected in the fuel feed lines will eventually be re-routed through the motive flow line to power the primary jet pump, which becomes the primary fuel feed once the engine is started[60].

To keep the motive flow pressurised, one transfer jet pump is placed in front of the fuel feed chamber. This pump is a low-pressure device used to transfer energy from high velocity low mass fluid streams to induce a low velocity to a high mass fluid streams [61]. The jet pump in front of the fuel feed chamber received motive flow from the boost pump, where it accelerates the flow and injects it back into the fuel feed chamber where it is used to power the booster pump. During normal operations, fuel is fed to the engine by the primary jet pump. Motive flow for the primary jet pump is provided by the engine driven fuel pump through the motive flow line.

From the fuel feed lines the fuel is guided through a shut-off valve, giving the UAV operator the option to shut down all fuel flow towards the engine. This measure is implemented in case of an engine fire, or in case of a possible engine malfunction which requires engine shut-down. Next in the fuel distribution system is the fuel filter to reduce contaminants in the fuel before it reaches the engine. To ensure safe operations of the fuel system, a pressure valve is added to allow bypass of the fuel in case of a clogged filter or alarming pressure difference over the filter[62]. After the filter a second shut-off valve is added for redundancy purposes.

The last component of the fuel distribution system is the main fuel pump. A low-pressure mechanical pump operating solely as a function of the engine turning. In order to pressurise the fuel, a centrifugal pumping element is used. Similar to the fuel filter, a pressure valve is added in parallel to the pump, to prevent overpressure of the component which might cause failure of the system. Part of the fuel will return as motive flow back to the fuel

[82] URL http://www.airforcecontroller.com [cited June 20 2016]

feed chambers after the main pump, the main flow however continues to the engine fuel system, where it will be further pressurised [60].

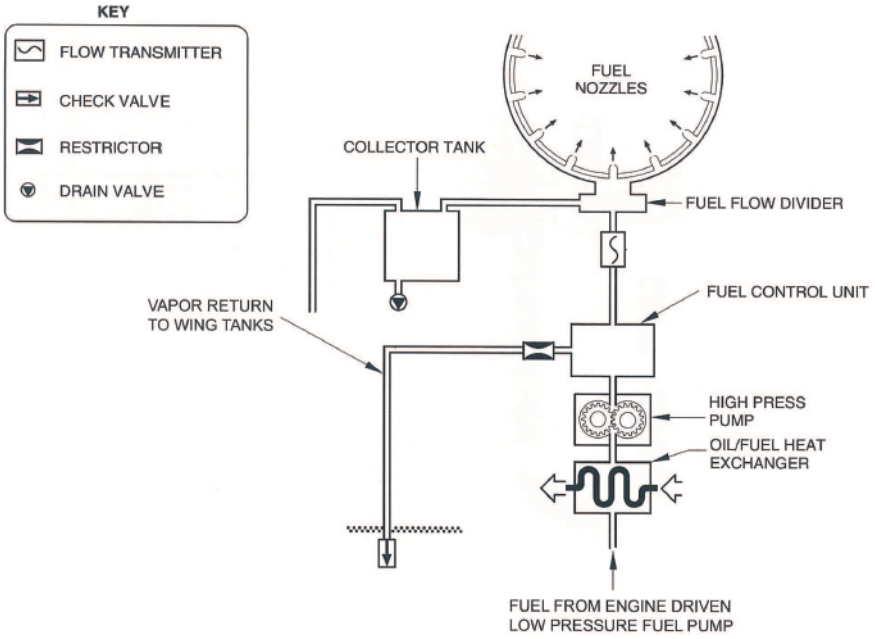

Figure 4.15: Engine fuel system [60]

After the low pressure fuel pump the fuel enters the engine fuel system as shown in Figure 4.15 [60]. Firstly the fuel flow needs to pass the oil/fuel heat exchanger which heats the fuel and cools the oil accordingly. To achieve the required fuel pressure by the engine, the fuel is compressed by two gears in a high pressure pump which rises the pressure above the combustor pressure levels before it continues into the fuel control unit. Inputs for the control unit depend on the performance and power setting of the UAV which are determined by the autopilot with respect to the wanted settings as described in Table 5.12. The control unit furthermore includes a restrictor to return the fuel vapor developed before back to the wing tanks. Which enables the control unit the change the power settings of the engine. After the control unit a flow transmitter transfers the information about the fuel flow to the autopilot of SCULPTUR. In case of a overflow of fuel the flow will be divided into two streams where one flows to the nozzles and one into the collector tank to store excess fuel [62]. From the collector tank the unused fuel is redirected to the fuel tanks in order to enter the fuel system again. Finally the fuel enters the nozzles with the right temperature and pressure.

Aside from the general components of the fuel distribution system, additional drain valves and check valves are present in the design of the fuel system. These valves are added to ensure one directional fuel flow (check valves) and the ability to remove any trapped or leaked fluids from the system. According to requirement SCULPTUR-PERF-SF17-3 consideration was given to implementing a firewall to separate the engine from the other airframe. After extensive research into the background of this requirement, it was found that this is required for manned flight with the purpose of aircrew protection[83]. Since our UAV does not meet this need, it was decided to not add a firewall to the system with the eye on expected weight increase.

4.4.9. ELECTRICAL POWER DESIGN

Figure 4.16 shows the electrical block diagram of the UAV. The required power is generated by the engine by a starter-generator system. This system will start the engine, and when the engine is running will power the complete UAV. The power converted from the engine by the starter-generator system will be directed to the main bus. The main bus distributes the power to all the subsystems. The cabling between the different electrical parts is installed with redundancy, since cables are placed along different sides of the UAV to prevent failure when one part of the UAV is damaged.

A battery is installed in the UAV to assist the starter-generator during start-up. Moreover, the battery will act as a transfer power system in an emergency situation, when the electrical power generation has to switch from the starter-generator to the emergency power system. This set-up is used in multiple engines in the market [63] [64]. The battery is charged by the starter-generator. The emergency power system consists of a Ram Air Turbine; a RAT. When the starter-generator or the main bus fails, the RAT and the emergency bus can be used to provide power to the critical systems to keep the UAV powered to return to base or execute an emergency

[83] URL http://www.experimentalaircraft.info/articles/aircraft-firewall-preparation.php [cited June 20 2016]

landing[84]. When the engine itself fails, the RAT will not be used, since it will cause much drag and therefore make the UAV lose speed fast. Instead, the battery will be used for emergency communications and deploying the parachute.

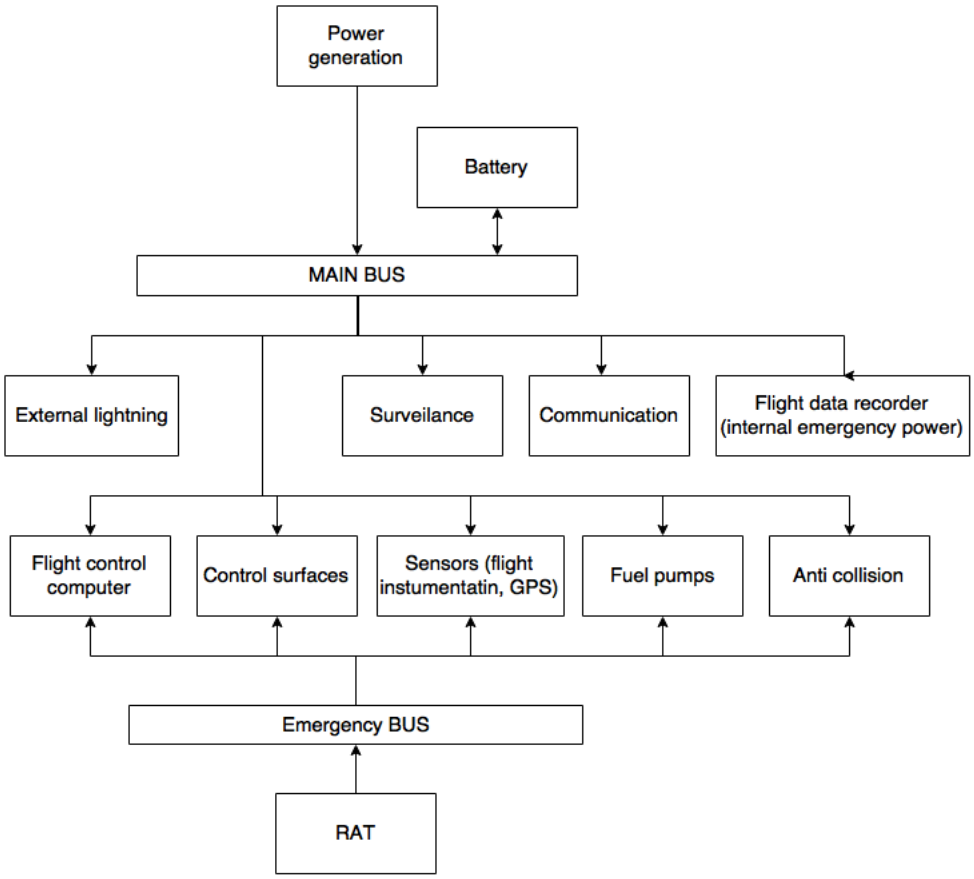

Figure 4.16: Electrical flow diagram

THE STARTER-GENERATOR

The starter-generator is a small generator that converts power received from the engine to Direct Current power for the UAV subsystems. The starter-generator is connected to the main bus on one side, and to an accessory gear box on the other [64]. The accessory gear box transfers the engine power to the starter-generator. The starter-generator will start the engine while making use of the power provided by the installed battery [63].

When the starter is started, it switches on the power supply of the ignition device and switches on the power supply of the fuel valve. It furthermore ensures the start of the fuel-oil pump [64]. The starter provides more detailed actions as well, but a complete description of the workings of the starter is beyond the scope of this report.

THE RAT

The RAT is a small ram air turbine that is embedded within the fuselage. In case of a loss of power, the RAT will deploy into the airstream and provide power by using the speed of the air. The RAT that is used for this UAV is the smallest RAt avaible, the same RAT used in the Hawk and Tornado fighter jets. This RAT can provide 1.5 kW of power at a speed of 100 km/h[85], which is enough for the emergency situation of the UAV. During emergencies, only flight controls will be running, and communication for a small amount of time. The most criticial systems during emergencies are the communication subsystem and the autopilot. Therefore the main purpose of the RAT during an emergency is to sustain the communication subsystem and autopilot at any time.

4.4.10. COMMUNICATION DESIGN

For the communication it is relevant what kind of data should be sent and received and how this should be done. There are two systems that use the communication link; the control system and the payloads. A communication flow is made to display all the ongoing communication in the UAV system. The datalink is designed according to the required communication flow.

[84] URL http://www.skybrary.aero/index.php/Aircraft_Electrical_Systems
[85] URL http://ieee.rackoneup.net/rrvs/06/Emergency%20RATs%20Presentation.pdf

DATA COMMUNICATION

The control is performed with an autopilot that uses waypoint navigation for the flight path. The waypoints are selected by the operator, this is the main input that needs to be sent to the UAV. The other things that will be sent to the UAV are commands for the mission, e.g. abort the mission, change in mission or control for the payload.

For the downlink the sent data consists of the payload data, subsystem performance and the flight instruments data. The payload data will include the IR and EO cameras, which produce a lot of data. The subsystem data are all the status updates of the specific parts, e.g. deployment of control surfaces, failure of a component, etc. The flight data that needs to be sent to the ground control is specified by the requirements also a some data of the engine performance is required, the required information can be found in the list below:

- Indicated airspeed
- Altitude
- Magnetic direction
- Ground position
- Temperature
- Pressure
- Fuel quantity indication
- Oil quantity indication
- Engine RPM

COMMUNICATION FLOW

The communication flow is displayed in Figure 4.17, this diagram shows all the communication channels that are required for the UAV operation. The communication that is required starts with the commands that are the input from the operator. The data is sent to the UAV using the chosen communication channel. The message that is sent needs to be encrypted and decrypted to prevent hacking. The message is received and processed by the data handler, which also receives the data from the sensors (airspeed, altitude) and payload (cameras). The data handler uses the data to sent commands to the subsystems, e.g. control units. The subsystems then give feedback about the status of the subsystem, which is used to check if the command is executed or whether there are failures. The data from the data handler is also sent to the operator. This data includes the payload and flight data. This communication channel also needs encryption to protect the UAV from hacking.

Besides the operator, also the air traffic control and other aircraft need data from the UAV and will send data to the UAV. This is mainly to prevent collision and it is also required to have a mode C transponder, this transponder report range position information and pressure altitude. The other ways for doing this communication is using Very High Frequency (VHF) communication or satellite communication. The main communication channel for this is via Future Air Navigation System (FANS-1/A) datalink communication environment, in combination with the Aircraft Communications Addressing and Reporting System (ACARS) [65].

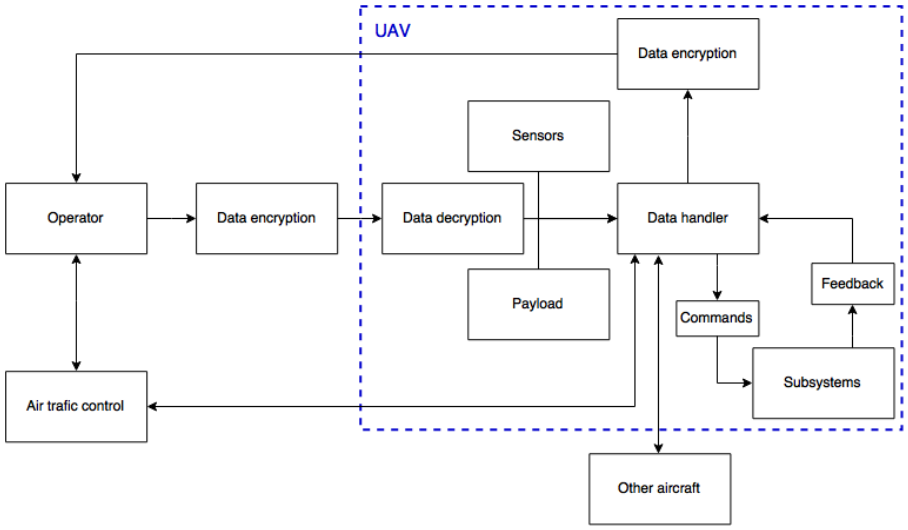

Figure 4.17: Communication flow diagram

LINK BUDGET CALCULATION

Before a communication system can be selected, first an assessment has to be done to determine what the power and bandwidth should be for establishing a reliable satellite communication link. Using reference data, it was determined that a forward (Ground station to UAV) bit rate of 323 $\frac{kbit}{s}$ and a return (UAV to ground station) bit rate of 10.52 $\frac{Mbit}{s}$ are required to facilitate both vehicle and payload operation as can be seen in Table 4.12

[66].

Table 4.12: Required satellite communication bit rate for SCULPTUR UAV

Data link		Type	Thoughput	Delay Sensitive
Mission data link	**Forward**	Data	200 kbps	No
	Return	Data	10 Mbps	No
Safety data link	**Forward**	ATC	16kbps	Yes
		C2	107kbps	Yes
	Return	C2 (data)	107kbps	Yes
		C2 (RT video)	256kbps	Yes
		ATC	16kbps	Yes
		S&A	141kbps	Yes

Total	**Forward**	323kbps
	Return	10.52Mbit

In this table, the communication link is divided into two separate segments, the mission data link and the safety data link. The mission data link is the link used to transfer surveillance data to and from the UAV, which consists mostly of the data from IR and EO cameras which produce $10\frac{Mbit}{s}$. The impact of a delay in this link is not very large, since the surveillance does not necessarily have to be observed in real-time. The safety data link is used for C2 (control and command), for relay of the Air Traffic Control communication line to and from the UAV and for the S&A (Safety and Avoidance) communication with other aircraft. From the table it is obvious that the return communication link is the limiting factor that the communication system should be designed for.

The two factors that have the largest impact on the amount of information that can be transmitted over a channel are the frequency bandwidth and the signal-to-noise ratio. Shannon's equation, shown in Equation (4.57), gives the theoretical maximum information rate C in $\frac{bit}{s}$ that can be obtained on a channel given a certain Bandwidth B in Hz and Signal-to-Noise ratio $\frac{S}{N}$ at the receiver side where signal power S and noise power N are both in Watt.

$$C = B \cdot log_2\left(1 + \frac{S}{N}\right) \tag{4.57}$$

However, the actual capacity of a channel will always be below the ideal value because of bandwidth loss during detection. This loss can be reduced by selection of the optimum detection method. To calculate how much power will be available at the receivers end and how much noise is present, a link budget analysis has to performed to assess all the losses and noise sources on the channel. Three main gains are considered: the transmitting antenna gain, the free space gain and atmospheric attenuation gain (always less than 1) and the receiving antenna gain, which can be related to ratio of the received power to the transmitted power as shown in Equation (4.58).

$$\frac{P_{Rx}}{P_{Tx}} = G_{AT} G_{FS} G_{AA} G_{AR} \tag{4.58}$$

Where G_{AT} and G_{AR} are the antenna gains of transmitting and receiving antennas respectively, which depend on both the shape and the pointing accuracy of the antennas. Antenna gain can be expressed as the ratio between the power transmitted in the direction of maximum radiation to the power that would be radiated by an isentropic antenna transmitting a signal at the same power as shown in equation (4.59).

$$G_{AT} = \frac{P_{Tx_{max}}}{P_{EIRP}} \tag{4.59}$$

Antenna gain is an antenna property and is generally indepent of whether an antenna is receiving or transmitting a signal [67]. The free space gain is the parameter that accounts for signal loss due to the fact that the signal energy is spread over an increasingly large area after transmission and is calculated using Equation (4.60).

$$G_{FS} = \left(\frac{\lambda}{4\pi d}\right)^2 \tag{4.60}$$

where λ is the wavelength of the signal in m. The last gain that has to be evaluated is the gain that accounts for loss is signal due to the absorption properties of the atmoshpere. This parameter can be estimated using Figure 4.18.

Using these equations the signal power at the receivers end can be calculated as a function of the antenna gains, the distance between the antennas, the wavelength and the transmitted signal power.

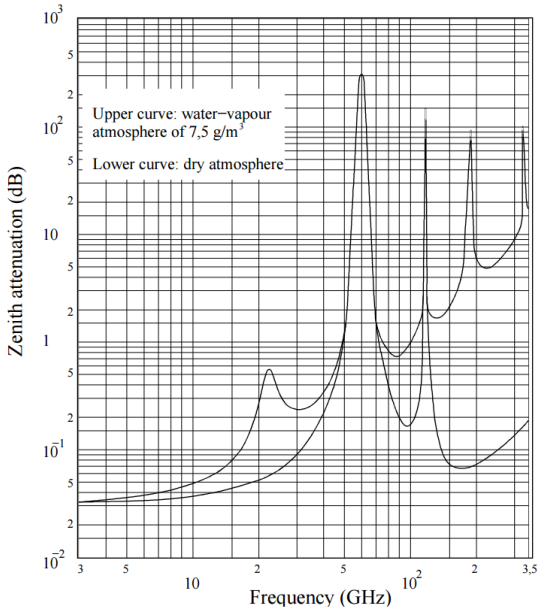

Figure 4.18: The atmospheric attenuation gain as a function of the signal frequency [68]

To evaluate the channel capacity, a figure for the noise power is also required. The noisiness of a certain object is usually expressed using noise temperature T in Kelvin. This parameter, derived from the relation between the temperature and noise in a simple resister, should not be confused with the actual temperature of an object. From the noise temperature the produced noise can be calculated using Equation (4.61).

$$N = kTB \tag{4.61}$$

Where N is the noise power, k is the Boltzmann constant and B is the signal bandwidth in Hertz. The significant contributors to the noise on a certain link are the receiving antenna, which not only receives the transmitted signal but also a certain amount of background radiation and atmospheric noise, and the receiver hardware, the line and pre-amplifier at the antenna output. The antenna noise is a function of the transmitted signal frequency and the satellite elevation angle and can be determined using Figure 4.19.

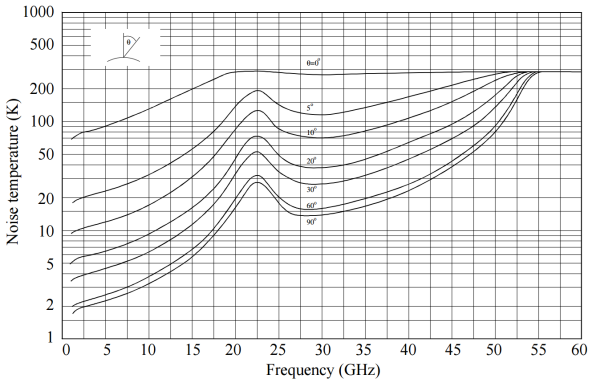

Figure 4.19: Antenna noise as a function of signal frequency and elevation angle [68]

Lastly, an estimation can be made of the noise produced by the receiver. The influence a receiver has is commonly expressed as the noise figure F which is defined as shown in Equation (4.62).

$$F = \frac{SNR_{in}}{SNR_{out}} \tag{4.62}$$

Where SNR is the signal-to-noise ratio of the signal. From this noise figure the noise temperature can be calculated as shown in Equation (4.63).

$$T = (F-1) \cdot T_0 \tag{4.63}$$

where T_0 is a constant with a value of $290K$.

Because the UAV to satellite data rate is critical, an estimate has to be made of the receiver properties of a satcom satellite which can then be used to evaluate whether a certain UAV communication device meets the requirement. Using reference, geostationary satellite, 35,786 km altitude, was assumed at an elevation of 2° [86]. A low-noise receiver was assumed with a noise figure of 2. The antenna gain was assumed to be $37dB$ from reference [69].

Equation (4.57) gives the capacity of a channel. However, this capacity will in practice never be reached. To account for additional external noise sources and other constraints that limit the achievable data rate, the maximum achievable bit rate should be assumed to be 0.5 times the calculated channel capacity.

CHOSEN COMMUNICATION PAYLOAD

The Gilat BlackRay 1000 was chosen for the communication payload [70]. Using the specification sheet and the link budget analysis described in Section 4.4.10 it was calculated that with a signal bandwidth of 1kHz it would be possible to achieve the required bit rate of $10\frac{Mbits}{s}$, therefore fulfilling the requirement. Compared with reference data, this required signal bandwidth is relatively low. It is therefore recommended to perform verification of the data link analysis method during the next phase of the design, taking into account modulation and coding. Validation should be performed by requesting company data on the performance of the Gilat Blackray 1000. If future results indicate that the required bandwidth is significantly higher, a trade-off should be made between increasing the signal bandwidth and compressing the surveillance data to reduce the bit rate required, since hiring more communication bandwidth would increase operational costs.

4.5. PRELIMINARY CLASS II WEIGHT ESTIMATION

When results from Class I are available, as well as a simplified geometric definition of the UAV, a Class II weight estimation can be performed. The inputs are formed by initial estimate of OEW, MZFW, MTOW, and take-off thrust, as well as initial three-view drawings. The limited amount of conceptual design optimisation will also require some information on weight component sensitivity to variation of basic design variables such as wing area, aspect ratio, angle of sweep, type of high lift devices, etc. Results of these conceptual weight prediction methods are the weight of the main aircraft components, as well as an educated guess of the c.g. location of each component.

4.5.1. WEIGHT ESTIMATION SUBSYSTEMS

For an initial weight estimation of the UAV's subsystems, the statistical methods from [40] (Equations 4.64 4.74) are used for each individual subsystem. The results are presented in Figure 4.20. The corrective coefficients and formulas have been derived on the base of extensive databases of actual aircraft weights. Designs that do not differ significantly from general aviation aircraft (i.e. most applicable to SCULPTUR) will provide acceptable estimations. It is important to keep in mind that UAV design is based on different principles than the ones used in Raymer for designing an aircraft. This is most likely the cause of the large discrepancy between the Class I and Class II weight estimations (the result of the MTOW of the Class II are 19.58% higher than the ones of the Class I). It is assumed that the Class II weight estimation is more accurate than the Class I, especially when considering the wing plan form sizing; however it is still important to acknowledge the differences between UAV and aircraft design. An iterative procedure between the Class I and Class II is used to get an even better estimate. If the difference between the initial and the revised weight is small enough, few iterations will be sufficient to bring the difference to a sufficiently low value and allow proceeding with the design. This means that some iteration is generally required to guarantee consistency to the overall process (Section 4.5.3). Also, the accuracy of single component weights (e.g. main landing gear, wing ribs, tail rudder) is not as high as their summation (OEW, MTOW), mainly because most Class II weight estimations have been calibrated to give results at a group level. This is also the main reason Raymer suggests that weight estimates from one method should never be combined with those from another method.

The stakeholder requirements are another potential source of error, being potential killer requirements that lead to an overdesigned UAV. It might be possible that flying at a different altitude or different cruise speed would yield better results in terms of weight.

The equations used for computing the weights of each of the subsystems are presented below.

$$W_{wing} = 0.036 S_w^{0.758} W_{fw}^{0.0035} \left(\frac{A}{cos^2\Lambda}\right) q^{0.006} \lambda^{0.04} \left(\frac{100t/c}{cos\Lambda}\right)^{-0.3} (N_z W_{dg})^{0.49} \tag{4.64}$$

$$W_{horizontal\ tail} = 0.016 \left(N_z W_{dg}\right)^{0.414} q^{0.168} S_{ht}^{0.896} \left(\frac{100t/c}{cos\Lambda}\right)^{-0.12} \times \left(\frac{A}{cos^2\Lambda_{ht}}\right)^{0.043} \lambda_{ht}^{-0.02} \tag{4.65}$$

$$W_{vertical\ tail} = 0.073(1 + 0.2\left(\frac{H_t}{H_v}\right)\left(N_z W_{dg}\right)^{0.376} q^{0.122} S_{vt}^{0.873} \left(\frac{100t/c}{cos\Lambda_{vt}}\right)^{(} - 0.49) \times \left(\frac{A}{cos^2\Lambda_{ht}}\right)^{0.357} \lambda_{vt}^{0.039} \tag{4.66}$$

[86] URL http://www.nasaspaceflight.com/2013/05/ula-delta-iv-launch-wgs-5-satellite/ [June 2016]

$$W_{fuselage} = 0.052 S_f^{1.086} \left(N_z W_{dg}\right)^{0.177} L_t^{-0.051} (L/D)^{-0.072} q^{0.241} + W_{press} \tag{4.67}$$

$$W_{main\ landing\ gear} = 0.095 \left(N_l W_l\right)^{0.768} (L_m/12)^{0.409} \tag{4.68}$$

$$W_{nose\ landing\ gear} = 0.125 \left(N_l W_l\right)^{0.566} (L_n/12)^{0.845} \tag{4.69}$$

$$W_{installed\ engine\ (total)} = 2.575 W_{en}^{0.922} N_{en} \tag{4.70}$$

$$W_{fuel\ system} = 2.49 V_t^{0.726} \left(\frac{1}{1+V_i/V_t}\right)^{0.363} N_t^{0.242} N_{en}^{0.157} \tag{4.71}$$

$$W_{flight\ controls} = 0.053 L^{1.536} B_w^{0.371} \left(N_z W_{dg} \times 10^{-4}\right)^{0.80} \tag{4.72}$$

$$W_{avionics} = 2.117 W_{uav}^{0.933} \tag{4.73}$$

$$W_{electrical} = 12.57 \left(W_{fuel\ system} + W_{avionics}\right)^{0.51} \tag{4.74}$$

Table 4.13: Class I/Class II Comparison

Class I MTOW [kg]	Class II MTOW [kg]	Difference [%]
250.00	298.95	19.58

As it can be seen, in order to perform a Class II weight estimation, all the geometrical properties of the wing (sweep angle, taper ratio, wing span, wing thickness), horizontal and vertical tails (same as wing), fuselage (fuselage length and diameter) and landing gear (wheel track, wheel base, tire diameter, tire width, tire stroke, strut length, strut deflection) need to be available. A preliminary sizing for the wing, fuselage and landing gear is available in the previous sections. For the tail preliminary sizing, it is known that airplanes of similar characteristics have roughly the same volume coefficients so using reference UAVs results in a good first estimation. The size of the aircraft, the type and number of engines and their position (e.g. wing podded, embedded in the fuselage or attached at the back of the fuselage) have an influence on the tail size. This is why, for the final design, the tail size and positioning needs to be determined based on the c.g. range and wing positioning using the methods described in [71].

Figure 4.20 presents the contribution of each of the subsystems. Looking at the percentages alone, the fuel, payload, wing and fuselage weights occupy the largest portions as expected followed by the engine. The wing weight depends also on lift distribution and the presence and integration of the fuel tanks (location in the wing), however Class II methods are unable to capture these differences. Class II methods take in to account the effect of the taper ratio and the sweep angle which actually affects the lift distribution on the wing however parameters such as twist and wing incidence angle are not accounted in most of the Class II methods although they can have a large impact on the lift distribution (hence the wing loading and sizing).

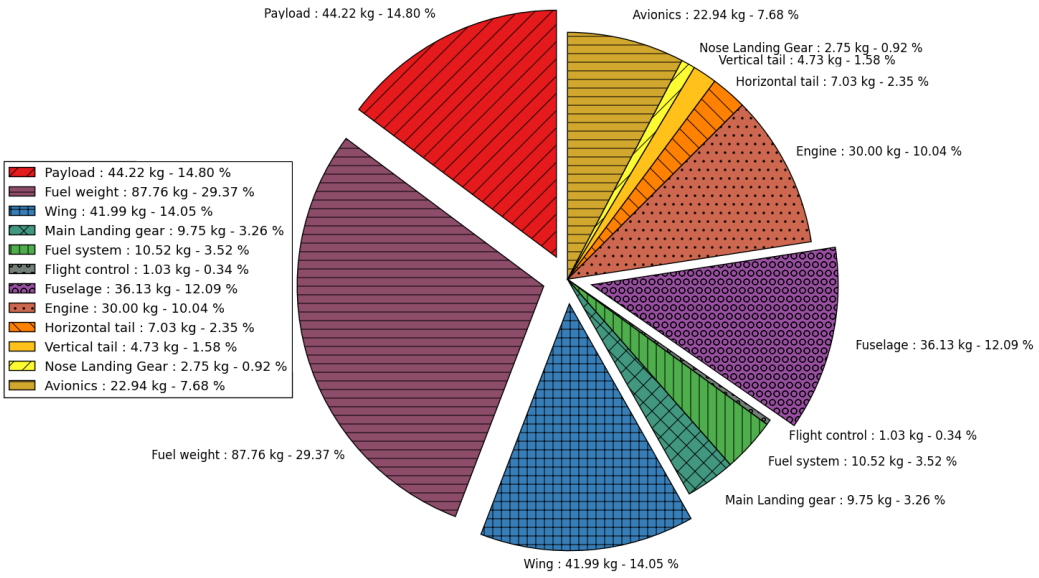

Figure 4.20: Class II: Weight of components (First iteration)

Table 4.14: Summary - Class II weight of components (First iteration)

MTOW [kg]	OEW [kg]	Payload [kg]	Fuel [kg]
298.95	166.87	44.22	87.76

4.5.2. CLASS II SENSITIVITY ANALYSIS

A sensitivity analysis is carried out for the class II weight estimation. Although most elements are related by predetermined equations, some parameters can be changed. The most important ones are the finesse ratio and the length of the fuselage, as well as the weight of the payload. Because the influence of the payload is dominated by the parachute, since it is the heaviest, only the parachute is considered. Each of the parameters was varied with different factors, although the finesse ratio and fuselage length were varied over a smaller range than the parachute weight. This was done because decreasing or increasing the finesse ratio and fuselage length, respectively, yielded a maximum take-off weight which was not feasible. The results are presented in Figure 4.21.

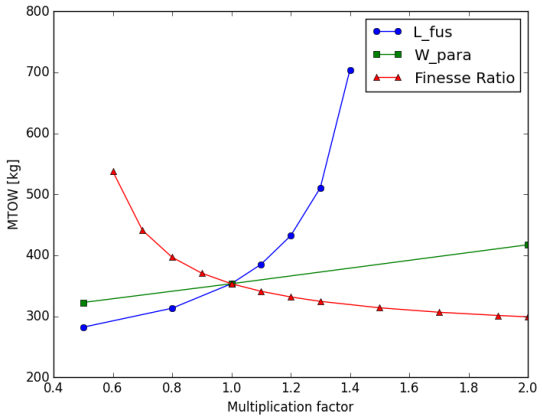

Figure 4.21: Sensitivity analysis for the maximum take-off weight

It can be seen that the most dominant factor is the fuselage length. When multiplying it with a factor of 1.4, the maximum take-off weight already doubles from 353 kg to over 700 kg. The finesse ratio shows a similar effect, although this appears when the finesse ratio decreases. This is because a lower finesse ratio implies a higher fuselage diameter when keeping the fuselage length constant, thus increasing the fuselage weight. The parachute weight shows a much smaller, but still significant effect. The increase in MTOW can be seen to be approximately linear, although the slope is higher than would be expected if only taking into account the parachute weight. The base weight of the parachute is 28 kg, so when multiplying it with a factor of two a 28 kg increase could be expected. Instead, the MTOW increases from 353 to 418 kg, e.g. a 65 kg increase. This results from the fact that a higher MTOW requires the other components to be heavier as well, in order to sustain the loads on the aircraft. This leads to an additional increase which is even higher than the increase in payload weight.

4.5.3. ITERATIONS AND FINAL DESIGN

Iterations are required in order to correct for the 28% discrepancy between the Class I and Class II weight estimations. An acceptable difference between the two methods, as suggested in [41], is less than 1%. The OEW of the Class II method is taken as an input for the Class I and the new estimate obtained is used as an input for a new iteration of the Class II. This process is shown in Figure 4.22 which describes how the maximum take-off weight changes after each iteration. The iterative process stops either when the fuel's percentage of the MTOW is lower than the one calculated with the Breguet range equation (17%, lower than this means that the range requirement for SCULPTUR can not be satisfied) or when the iterations no longer have any significant influence on the final value of MTOW. In the case of SCULPTUR, the latter case is the one limiting. It can be seen in the graph that after around 8 iterations the differences are negligible and the value for the MTOW is more or less final. A 18.46% difference can be observed between the first value of the MTOW and final value after the iterations. This is still within acceptable limits since the design point chosen for the Class I weight estimation is not the optimal one, overdesigning the UAV slightly in order to compensate for any additional weight increases throughout the design process.

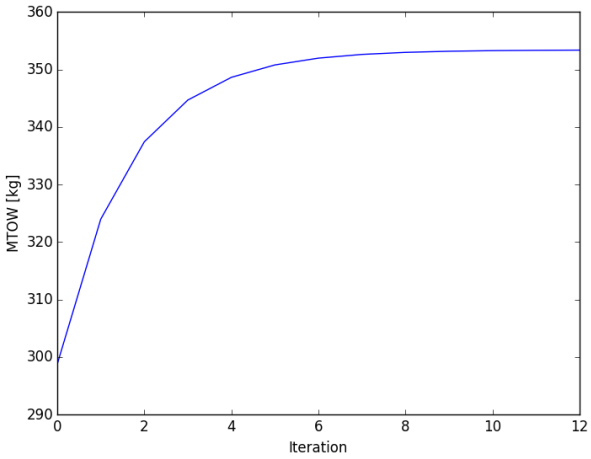

Figure 4.22: Iterations - Class I-II Weight estimation

The final results of the Class II weight are presented in Figure 4.23 and Tables 5.1 and 4.15.

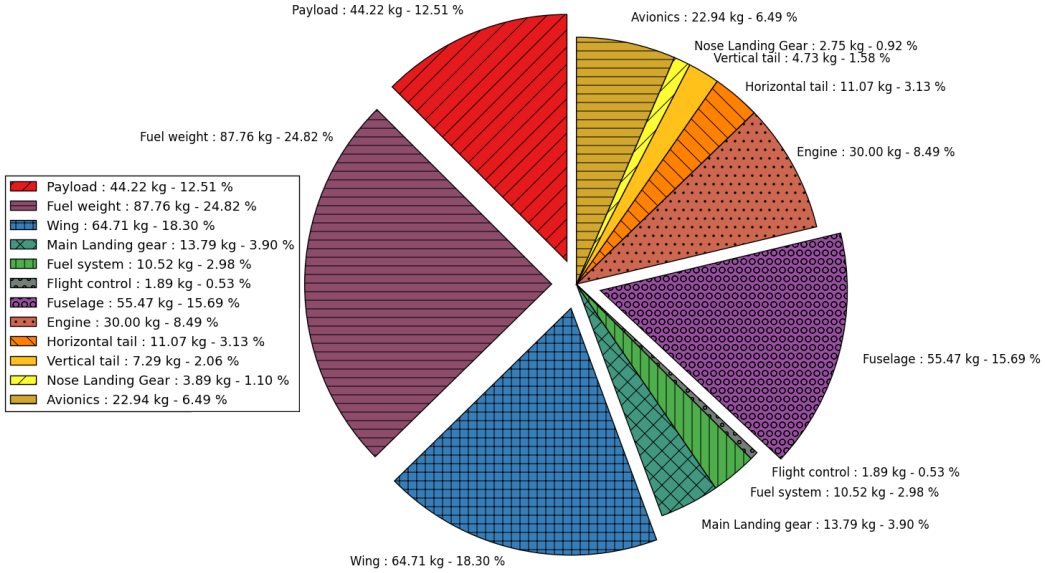

Figure 4.23: Class II: Weight of components (Final iteration)

Table 4.15: Summary - Class II weight of components (Final iteration)

MTOW [kg]	OEW [kg]	Payload [kg]	Fuel [kg]
353.55	221.57	44.22	87.76

The final value of the MTOW from the Class II is 18.37% lower than the permitted budget with the 10% margin determined in Section 3.8. Also, the weights of the OEW, payload and fuel are individually lower than the ones determined in the budgets. It is important that the reader remembers that the Class II weight estimation is only accurate when considering the subsystems together as an OEW, not on an individual subsystem level.

5 UAV ANALYSIS

With the preliminary weight and sizing of the UAV completed, it is essential to go into more detail for each subsystem. Section 5.1 focuses on the performance and stability of the UAV while Section 5.3 presents the aerodynamic analysis done in XFLR5. In Section 5.4 the propulsion subsystem is discussed while Sections 5.5 and 5.6 describe the materials and structural elements of the UAV. The verification strategy used throughout the analysis is shown for each individual subsystem.

5.1. PERFORMANCE ANALYSIS

In order to assess the performance of the UAV, several aspects will be explored in this section. These include payload-range diagram, as well as climb, turning, landing and take-off performance.

5.1.1. PAYLOAD-RANGE DIAGRAM

The payload-range diagram is a visualisation of how far the aircraft can fly with different payload weights. The range of the aircraft is dependent on the fuel consumption per unit range, as well as the fuel on board. The fuel consumption in turn is dependent on the aircraft weight, while the maximum fuel that can be carried depends on the maximum take-off weight and the payload weight, with an upper limit imposed by the capacity of the fuel tanks. Together, these requirements allow for the construction of the payload-range diagram in Figure 5.1. The range is calculated using Breguet's range equation [39], as shown in Equation (5.1). In this equation, η_p is the propulsive efficiency, SFC is the specific fuel consumption, L/D is the lift-to-drag ratio and W_4/W_5 is the weight ratio in cruise.

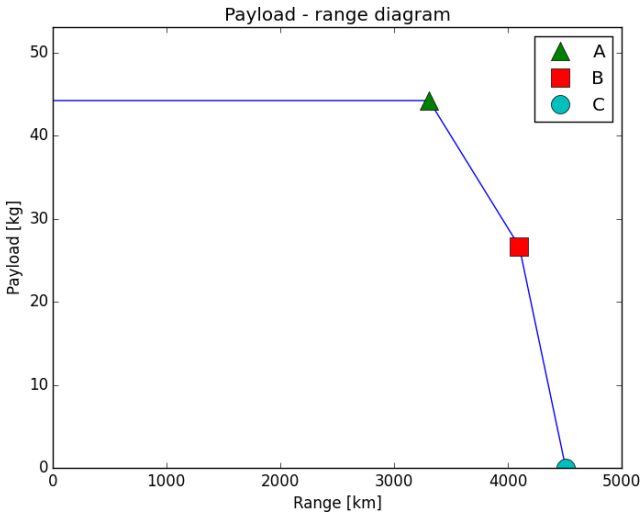

Figure 5.1: Payload-Range Diagram

$$R = \frac{\eta_p}{g \cdot SFC} \frac{L}{D} ln\left(\frac{W_4}{W_5}\right) \tag{5.1}$$

It can be seen that for the first segment, the range increases at a constant payload of 50 kg. In this segment, the additional range is achieved by simply adding fuel. The payload in this case is the maximum payload capacity of the UAV. Point A is at the end of this segment, and is also called the harmonic range, i.e. the maximum achievable range at full payload weight. At this point, W_4 is the maximum take-off weight, and thus no more fuel can be added without sacrificing payload. From the endurance requirement of 20 hours and the SFC as calculated in 5.4.1, the fuel weight was calculated to be 87.8 kg. This gives a harmonic range of 3308 km. Since this is more than the range requirement of 1800 km, no further iterations are necessary.

In the second segment, between point A and point B, payload is sacrificed to allow for a higher fuel weight. This is possible since the fuel tanks have a higher capacity than required for the harmonic range. Since the maximum take-off weight is limited, however, this additional volume can not be used at the full payload capacity. Point B is also called the maximum range[39]. Although the range can be extended slightly after this point, this is not commercially attractive. Using the additional 20% of tank capacity, the maximum range can be calculated to be 4100 km. It should be noted that the ln term in Equation (5.1) imposes a slight curvature on the graph between points A, B and C. However, the difference is at most 0.5%, and thus the line appears to be straight in the graph.

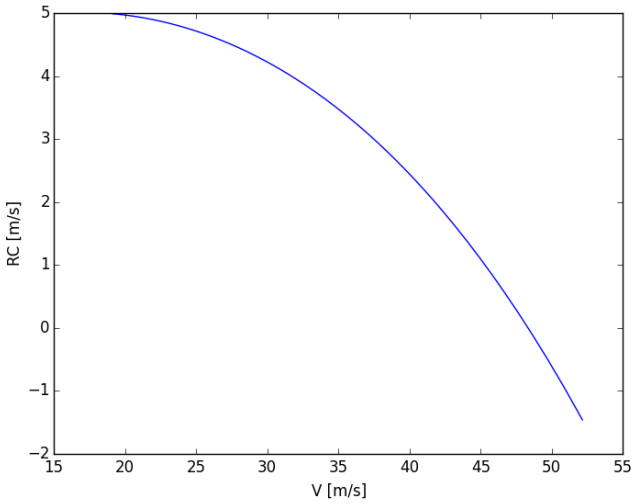

Figure 5.2: Climb rate against airspeed

This additional range is achieved by decreasing the payload weight even further. Although the fuel capacity can not be increased further due to the tank capacity, decreasing the weight will decrease the fuel consumption per unit range, thus extending the range slightly. This can be done until point C, where the payload weight is zero and the aircraft achieves its ferry range of 4508 km.

5.1.2. CLIMB PERFORMANCE

Most of the time, the UAV will fly at a constant altitude of 1000 m. However, if it is flying over mountains, a climb may be required. Additionally, during take-off the climb rate must be known in order to calculate the take-off length.

The climb rate can be calculated using the available and required thrust. Since generally the required power is significantly less than the available power, this excess power can be used to increase the potential energy, mgh, as shown in Equation (5.2).

$$(P_a - P_r)\Delta t = mg\Delta h \tag{5.2}$$

Noting that $\Delta h/\Delta t$ is the rate of climb (RC), and then dividing by $mg = W$ gives Equation (5.3).

$$\frac{P_a - P_r}{W} = RC \tag{5.3}$$

Since the weight and available power are known from the class II estimation, the rate of climb can be computed as a function of power required. The power required is equal to $D \cdot V$, and thus the rate of climb can be plotted against airspeed. This is done in Figure 5.2.

It can be seen that the maximum climb rate of approximately 5 m/s is achieved at the lowest airspeed. This can be explained by noting that when the profile drag is dominant in the drag calculation, the power required strictly increases with airspeed, and as such, a lower airspeed gives more excess power. It should be noted that the curve already flattens near this low airspeed, meaning the induced drag starts to dominate the drag term. Since induced drag increases with a decreasing airspeed, this would yield less excess power and thus decrease the maximum climb rate.

5.1.3. TURNING PERFORMANCE

Although most pipelines are more or less straight, the turning performance of the UAV is still important. The pilot should initiate the turn at the right time in order to keep the pipeline in sight at all times, and thus the turning radius should be known. Additionally, if a potential leak is seen, a second fly-over may be desired. Since every second which is used for this manoeuvre means less pipeline which can be inspected, it is important that the turn is executed as fast as possible. Therefore, the minimum time to turn is also an important parameter to know.

The starting point for analysing the turning performance is the maximum load factor. Since in a turn part of the lift vector contributes as the centripetal force, the lift is no longer equal to the weight, but rather equal to the load factor times the weight. Two equations should be used in order to calculate the maximum load factor. Firstly, force equilibrium in the direction of the lift vector, which results in Equation (5.4).

$$C_L \frac{1}{2} \rho V^2 S = nW \tag{5.4}$$

The maximum lift coefficient is known, as well as the weight and the wing surface area. Thus, the maximum load factor can be determined as a function of airspeed.

Additionally, the required power should be analysed, since the drag is influenced by the lift generated. The power required is equal to the drag multiplied by the velocity, where the drag can be computed using the lift and drag coefficients together with the lift generated. The velocity can be obtained by rewriting Equation (5.4). These results can be combined into Equation (5.5).

$$P_r = \frac{C_D}{C_L} nW \sqrt{\frac{nW}{S} \frac{2}{\rho} \frac{1}{C_L}} \tag{5.5}$$

Since both of these equations impose a limit on the maximum load factor, the actual maximum load factor for every airspeed is the minimum value returned by the two equations. This can be seen in Figure 5.3.

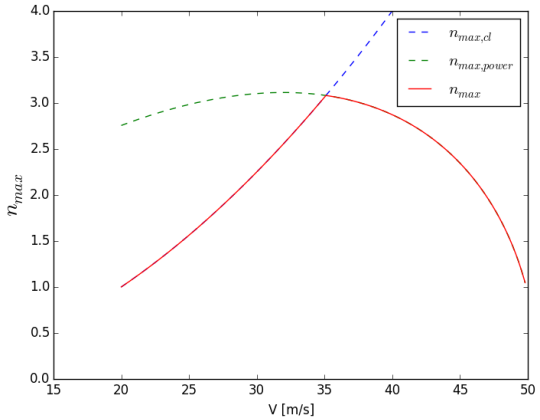

Figure 5.3: Maximum load factor

Now that the load factor is known, the turn radius and time to turn can be calculated using Equations (5.6) and (5.7) respectively[41].

$$R = \frac{V^2}{g\sqrt{n^2 - 1}} \tag{5.6}$$

$$T_{2\pi} = \frac{2\pi R}{V} \tag{5.7}$$

Since R depends on both V and n, and $T_{2\pi}$ depends on R and V, the minimum values for these quantities are not necessarily achieved when using the maximum load factor. For the specific case of SCULPTUR, however, the maximum load factor does yield both the lowest turn radius and turn time. When flying at a speed of 35.1 m/s, a load factor of 3.08 can be achieved. This allows for a turn radius of 43.1 m and a turn time of 7.71 s.

5.1.4. TAKE-OFF AND LANDING PERFORMANCE

In Section 4.3, assumptions were made for the take-off and landing distances in order to determine the preliminary aircraft sizing. These assumptions were only based on statistics, however. Now that more detailed characteristics of the UAV are known, an analytical solution can be found. For the air segments of both landing and take-off, equations from the course Aerospace Design and Systems Engineering Elements II are used [41]. The equations for landing and take-off are shown in Equations (5.8) and (5.9), respectively.

$$s = \frac{\frac{V_A^2}{2g} - \frac{V_T^2}{2g} + h_{scr}}{\frac{1}{2}\left[sin\bar{\gamma}_A + \left(\frac{C_D}{C_L}\right)_T\right]} \tag{5.8}$$

$$s = \frac{\frac{1}{2g} V_{scr}^2 - \frac{1}{2g} V_{LOF}^2 + h_{scr}}{sin\gamma_{scr}} \tag{5.9}$$

The ground sections can be analysed by taking into account the forces which act on the aircraft, as well as looking at the excess power for take-off. This allows to calculate the landing distance to be 340 m and the take-off distance to be 230 m.

5.2. STABILITY AND CONTROL ANALYSIS

A well designed UAV has to be both stable and controllable during all stages of flight. Section 5.2.1 present the centre of gravity locations for all the components of the operational empty weight and the loading diagrams respectively. A description of the scissor plot is presented in Section 5.2.4 and the X-plot is shown in Section 5.2.5. Finally, the dynamic stability of the UAV is described in Section 5.2.6.

5.2.1. CENTRE OF GRAVITY LOCATION

One of the requirements stated in Section 3.5 is that the aircraft must be stable. Static stability depends on the centre of gravity (c.g.) location of this UAV. Hence, it needs to be investigated to be able to comply with said requirement. The c.g. of the empty aircraft can be controlled by moving the wing position with respect to the fuselage. Hence, it is convenient to arrange the various weight components into a fuselage group and a wing group, where the wing group moves with the wing location. The main landing gear has been enforced to follow the wing in order to prevent a configuration that does not allow rotation of the UAV at take-off and to ensure that the tip-back angle constraint is not violated. Furthermore, for the c.g. calculation of the fuselage group, the fuselage and the avionics have a c.g. of 40% of the fuselage length L_f. The rest of the components of the fuselage group, such as the vertical and horizontal tails have specific c.g. location as suggested in [71]. In the case of the wing group, the main gear must always sit behind the max aft c.g. position. Hence, it is assumed that the main landing gear has a c.g. located at 50% of the MAC. The rest of components in the wing group have the same c.g. as the wing itself (40% of MAC).

Table 5.1: Subcomponent weights after last iteration - Wing & Fuselage

Component	Weight [kg]	Percentage of MTOW [%]	Center of gravity from nose of aircraft [m]	Center of gravity from LEMAC [m]	Center of gravity percentage of MAC_{wing} [%]
Fuselage Group	130.65	36.96	1.64	0.65	73.57
Fuselage	55.47	15.69	1.50	0.50	57.10
Engine	30.00	8.49	0.11	-0.88	-100.06
Horizontal Tail	11.07	3.13	4.30	3.31	374.40
Vertical Tail	7.29	2.06	4.35	3.35	379.33
Nose Landing Gear	3.89	1.10	0.35	-0.65	-73.86
Avionics	22.94	6.49	1.50	0.50	57.10
Wing Group	90.90	25.71	1.36	0.37	41.52
Wing	64.71	18.30	1.35	0.35	40.00
Main Landing Gear	13.79	3.90	1.70	0.70	79.55
Flight Controls	1.89	0.53	1.35	0.35	40.00
SCULPTUR OEW	221.55	62.67	1.53	0.53	60.42

In Table 5.1 the weights and the percentage of the MTOW of all the different components are shown as well as their centre of gravity with respect to the nose and with respect to the leading edge main aerodynamic chord (LEMAC). Also, one can see the c.g. of each component as a percentage of the wing MAC. The table first presents the fuselage group and all its components. Then, the wing group and its components are presented. Finally, the UAV as a whole is presented. In this table, one can see that the OEW of the two groups are relatively similar. The fuselage group has a larger weight since the engine and electronics are positioned on the fuselage group in the case of this SCULPTUR UAV, due to the front mounted propeller.

Figure 5.4 shows a sketch of the UAV with the location of the payloads, the landing gears, the wing and the horizontal and vertical tails. This gives an insight on how the design looks like up until this moment. Once the OEW is computed, this analysis can be continued by investigating the change in centre of gravity due to the addition of payload and fuel onto the UAV. This is represented in a loading diagram in the next section.

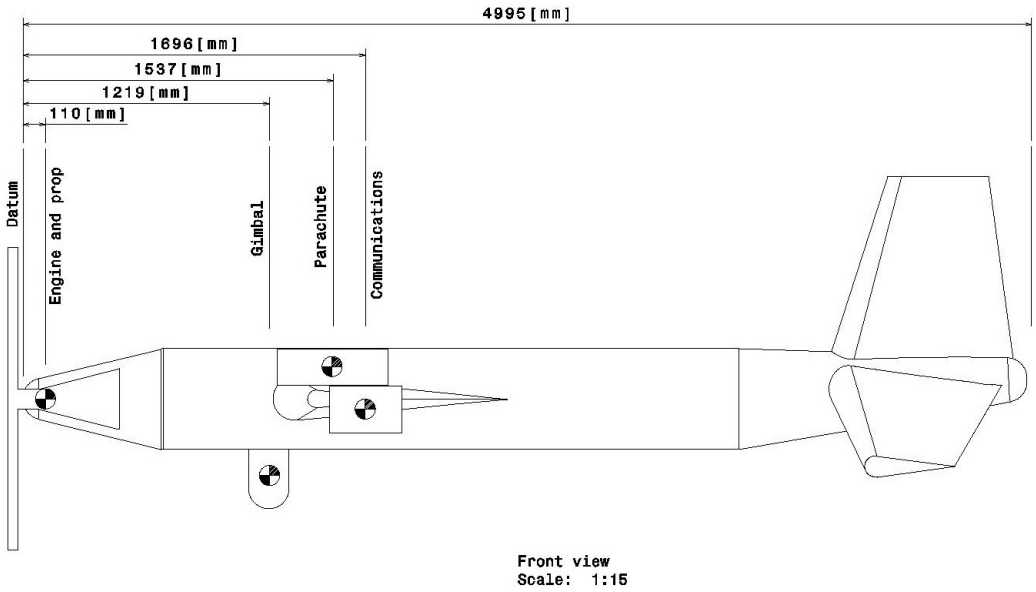

Figure 5.4: Payload location on UAV

5.2.2. LOADING DIAGRAM

Figures 5.5 shows a loading diagrams. These types of diagrams show how the c.g. varies with the addition of payload (communication, gimbal camera and flight data recorder) and fuel. To do this, one needs to set up an order in which the payload and fuel will be added. It was decided that the order was as follows. First the gimbal camera is added to the UAV, followed by the communication payload and finally, the flight data recorder. After all the payload is placed, the fuel is added. In the diagram, the original weight at which cargo weight is added is the OEW and the weight where the fuel weight ends is the MTOW [72]. For the loading diagrams, in order to account for c.g. variations, for example, due to landing gear retracting, a 2% margin on the most aft and forward is imposed as suggested in [71]. Furthermore, in Figure 5.5 one can see that adding the fuel is linear. It does not matter if you start by the front or the back of the aircraft, as it will add up the same way. One can see that while the tank is getting filled the c.g. moves to the right in a quasi-linear fashion.

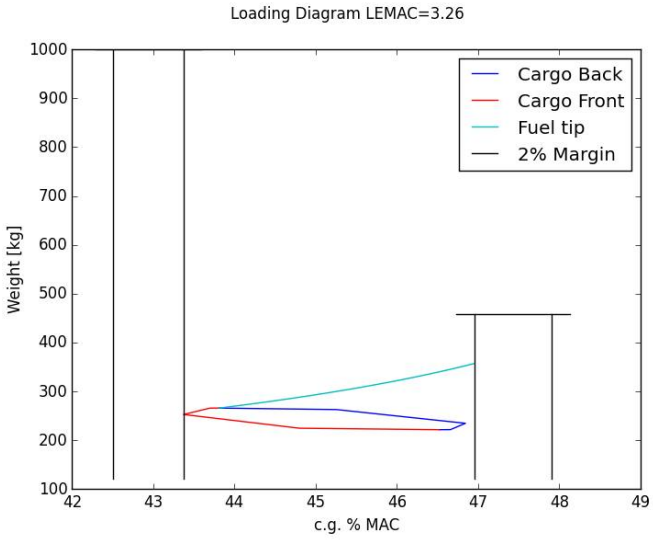

Figure 5.5: Loading diagram at original LEMAC

Figure 5.5 shows a plot of the loading diagram when the leading edge of the wing is at the original x_{LEMAC} distance. One can see the difference on the c.g. when loading onto the aircraft the cargo and the fuel by either starting from the back of the UAV or starting from the front of the UAV. It is logical that when loading onto the aircraft and starting from the back, the c.g. will move backwards (further away from the nose) because there will be more weight at the back of the aircraft first. Analogously to this, when loading from the front, the c.g. will move frontwards (closer to the nose).

5.2.3. CENTRE OF GRAVITY RANGE VS. WING POSITION - PLOT

Modifying the longitudinal position of the wing group with respect to the fuselage allows the designer to change the c.g. range. To study the change of c.g. range with the longitudinal wing group position, different loading diagrams for different wing positions are generated. In this section 2 more diagrams are shown in addition to the one found in the previous section (Figure 5.5). Which is the one used for the initial tail sizing. One can find a wing position 10% more aft and another wing position 10% more forward. One can see in Figure 5.6 that the values on the x-axis are less positive than the values found in the x-axis of Figure 5.5. This result is logical as can be seen from the table in Table 5.1 that the c.g. for the computed OEW is **1.53** meters from the nose of the aircraft. If the LEMAC/l_f is increased by 10%, this means the wing location is moved backwards (further away from the nose) to 3.59 meters. Thus, the c.g. expressed as percentage of MAC is smaller. The c.g. is 0.20 meters away from the LEMAC as comparison to the previous c.g. at 0.53 meters. Moreover, the fuel is added on the wing, hence, if the wing is further aft, the fuel will bring the c.g. further back.

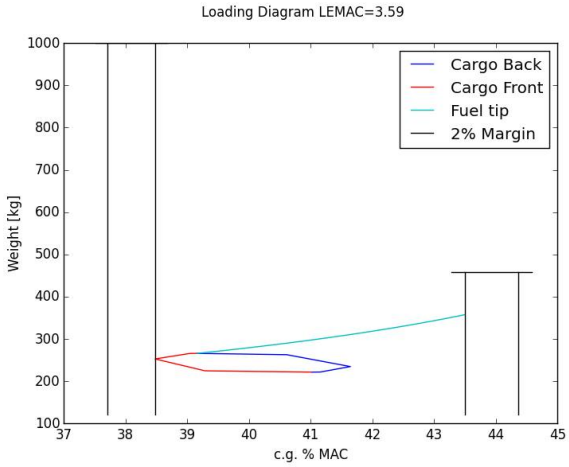

Figure 5.6: Loading diagram at 1.1*LEMAC

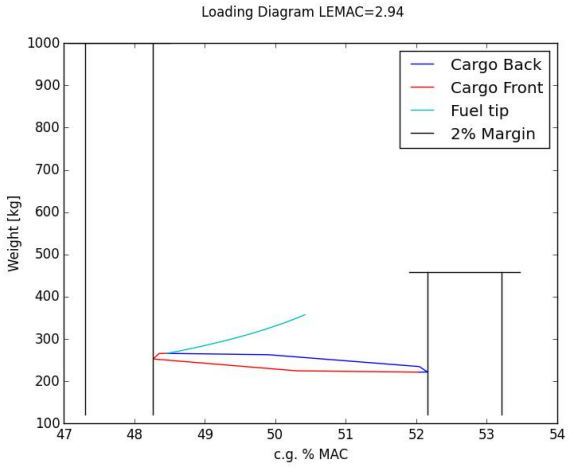

Figure 5.7: Cargo loading at 0.9*LEMAC

In contrast, in Figure 5.7 one can see that the values on the x-axis are positive and bigger than the ones found in the x-axis of Figure 5.5. This is because the LEMAC is moved closer to the nose (at 2.94 m from the nose). This means that the distance between the leading edge of the wing and the c.g. of the OEW will be bigger (0.85 m instead of 0.52 m). Thus, the c.g. expressed in percentage of MAC is also bigger which yields larger values on the x-axis. Also, the fuel does not affect the c.g. much as it is placed with the wing. This can be seen in the diagram as the fuel shifts the c.g. back about 2% of the MAC (from $\approx$ 48.2% to $\approx$ 50.2%.

The change in c.g. % MAC for the three LEMAC locations, can be plotted against the LEMAC/L_f. This will describe the c.g. range variations for different longitudinal position of the LEMAC. Which is the beginning of the so-called "X-plot"[71]. In turn, it will allow to size the vertical and horizontal tails. The other part of the scissor plot is found from the static stability investigation. This will be explored in the following section. This is found in the next sections.

5.2.4. SCISSOR - PLOT

The UAV is designed for stick-fixed static stability and assuming a stability margin of 5% MAC allows, in a large extent, to account for all possible limits (stick-free and manoeuvre force limits) as well. The Stability and Control requirements are to ensure moment equilibrium in steady flight (trim condition), as well as ensuring stability around this state of equilibrium. Also, to generate forces for manoeuvring, to change on demand the aircraft equilibrium state (for instance to rotate the aircraft at take off). Furthermore, certification regulations demand the aircraft to be longitudinally, directionally and laterally stable. Such requirements must be guaranteed for many possible configurations such as: a travel in c.g. location (i.e. changes in landing gear positions); variations in engine operating conditions (including failure of one engine), or failure of any control or trim surface.

STATIC STABILITY CURVE

An aircraft is defined longitudinally statically stable if it is able to react to a disturbance in angle of attack (α) by generating an opposite pitching moment in order to restore the previous state of equilibrium. Moreover, for any change in the angle of attack due to perturbation, the aircraft generates a lift increment. The resultant of said increments in lift are applied on the neutral point of the UAV. Hence, any increase in α should correspond to a pitch down moment. In other words, the aircraft c.g. must always stay in front of the neutral point. For instance, if the c.g. travels beyond the neutral point, an adverse pitching moment is generate due to the lift increments. This yields a further increase of α making the aircraft unstable.

The distance between the neutral point and the c.g. is called the static stability margin (usually expressed as a

percentage of MAC). The relation between the horizontal tail size and the maximum allowable aft c.g. position can be investigated in order to guarantee a set stability margin. Plotting on the y-axis the ratio between the area of the horizontal stabiliser S_h and the wing area S, and on the x-axis, the x coordinate over the MAC. One can deduce the following relations. A larger S_h is needed to allow more aft c.g. positions, for a given aircraft configuration. Moreover, if the stability margin is increased, a larger tail size is needed to allow a certain aft c.g. position. However, enlarging the horizontal tail surface is not the only solution. If one decreases the slope of the stability curve, then it is possible to increase the allowable aft c.g. position without requiring higher S_h values. The most important conclusions that can be drawn are: the more aft x_{ac} is and the lower the slope of the curve, the more stable the aircraft. Hence, any contribution that increases $\frac{x_{ac}}{MAC}$ is stabilising.

CONTROLLABILITY CURVE

In the previous sections, the stability and control requirements were stated. One of this requirement is to ensure trim condition. The aircraft is said to be trimmed, given a certain aircraft configuration, when the total moment coefficient is zero. This achieved when an existing combination of wing-fuselage and tail lift coefficients give a zero moment coefficient. In other words, for different c.g. positions, speed values and wing-fuselage aerodynamic centres, the tail will have to generate different lift coefficient values. This can be achieved either by modifying the elevator angle or rotating the stabiliser. An unstable aircraft can be trimmed, hence, is controllable and unstable. As mentioned previously, the aerodynamic centre is affected by the speed of the aircraft. Hence, for the controllability curve, the most critical condition of lowest speed and flaps out is considered. That is, the landing condition. When adding the controllability curve to the stability curve, the Scissor Plot is generated. From this plot one can see that forward locations of the aerodynamic centre are positive for controllability, yet negative for stability. Moreover, lowering the aerodynamic pitching moment allows improving the controllability of the aircraft without spoiling its stability. One can see that a very stable aircraft is not typically a very controllable one.

Combining the "Scissor - plot" with the "c.g range vs. wing position - plot" one can construct an "X - plot" in order to determine the optimum combination of tail size and longitudinal wing position. This can be found in the next section.

5.2.5. X - PLOT

A so called X-plot (Figure 5.8) is used to asses the static stability and controllability of SCULPTUR. Forward locations of aerodynamic centre are positive for controllability, but negative for stability; the opposite is true for the aft location. The difference between the dashed line and the stability curve next to it is known as the stability margin. The UAV has been designed for stick-fixed static stability; a stability margin of 5%MAC, as suggested in [71], would allow to account for any stability limiting factors such as stick-free and manoeuvre force limits.

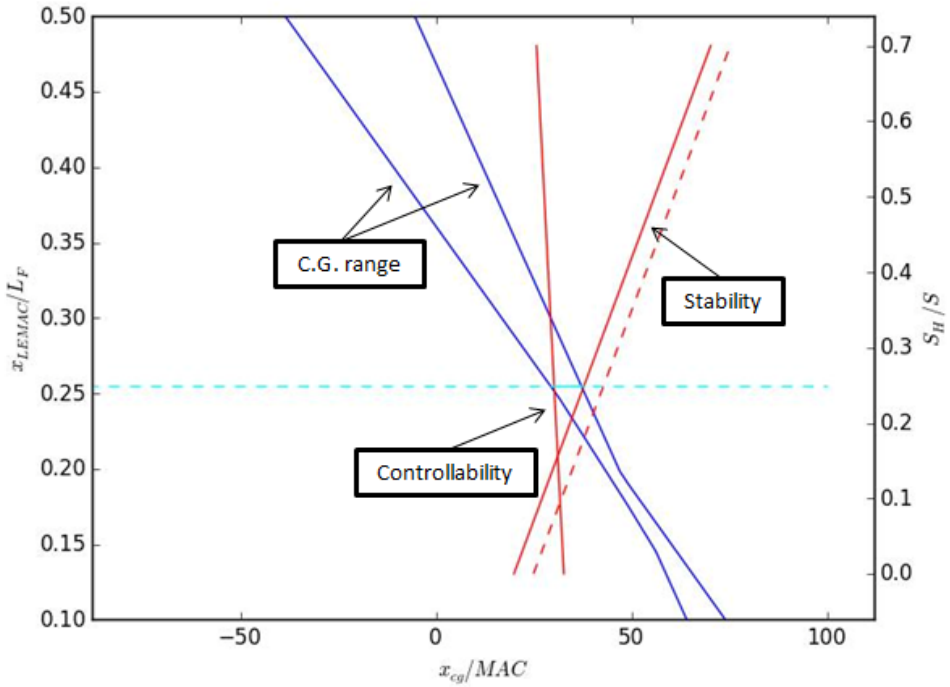

Figure 5.8: SCULPTUR X-plot

The location of the most forward and aft centre of gravity location must be on the same horizontal line in the X-

plot, because they represent the centre of gravity limits for one specific wing location. The wing location where the horizontal tail surface is the smallest possible while at the same time ensuring that both the most forward and most aft c.g. lie within the stability and controllability curves is equal to 27.3%. For this wing location, the most forward c.g. is at 30.3% of the MAC and the most aft is at 37.9% resulting in a tail surface area equal to 24.9% of the wing surface area. If the tail surface area is any smaller, the c.g. would lie outside the stability and controllability curves, meaning that SCULPTUR's requirements can no longer satisfied. If the tail surface area is any larger, the tail would simply be overdesigned, only increasing the weight without any additional benefit.

VERIFICATION

As a verification procedure, several parameters were tested to identify how the stability/controllability characteristics are affected. These were the finding which do correspond to theory.

- UAV's with a large centre of gravity range require a larger tail area.
- A larger stability margin yields a larger tail area since it constrains the allowable centre of gravity range (limited by the stability curve).
- Increasing the negative aerodynamic moment ($-C_{m_{ac}}$) requires a larger effective elevator with a larger deflection.
- The larger the downwash gradient (affected by fuselage geometry, flap angle wing platform and tail position), the less effective the tail. Hence downwash is by nature destabilising.
- A larger value of Low mounted tailplane inside fuselage boundary layer.
- Long tail arm is effective, but increases fuselage weight.

5.2.6. DYNAMIC STABILITY

For the dynamic stability the aircraft is analysed for five eigenmotions: short period, phugoid, aperiodic roll, dutch roll, spiral. Since the UAV's characteristics change for the loaded and unloaded case and also at begin and end of the mission due to the consumed fuel, the UAV will be analysed for the different situations. For the analysis there are a lot of assumptions made. The most important assumptions with the most influence on the outcome are listed below:

1. **Vehicle's mass is constant during the period of one manoeuvre.** The mass of the aircraft is not constant during the flight due to fuel consumption, but the duration of a manoeuvre is short compared to the duration of the whole flight. Therefore, it can be assumed that the vehicles mass is constant during a single manoeuvre. The impact of this assumption is that the center of gravity does not change and also different coefficients.
2. **Neglecting the time-dependency** When doing the linearisation, it is assumed that the time derivatives have a limited influence and can be neglected. With the exception of the influence of $\dot{v}$ on the Y force and N moment and the influence of $\dot{w}$ on the Z force and M moment. With this assumption, the influence of the variation of the parameters trough time is neglected. Only the influence of the speed in Y and Z direction is considered, because they affect the flow that still effects the aerodynamics over time. The impact of this assumption is that the static coefficients either increase or decrease with larger deviations.
3. **Symmetrical and asymmetrical equations can be evaluated independently** It is assumed that there occurs no aerodynamic coupling between the symmetric and asymmetric, as long as the derivatives and disturbances remain small. This assumption makes it possible to analyse the manoeuvre separated as a symmetric and an asymmetric motion. The impact of this assumption is that there is no energy lost into motions that are not considered due to this assumption.
4. **The stability derivatives, except C_L, C_{X_0} and C_{Z_0} are independent of airspeed and pressure altitude in stationary flight condition** The other stability derivatives are also dependent on variables like the centre of gravity, mass, moments of inertia and air density. The influence of these parameters will only act through C_L, C_{X_0} and C_{Z_0}. The other stability derivatives will be adjusted according to the flight data. The impact of this assumption is that all results calculated with stability derivatives affected by this assumption will either be lower or higher than the actual case.
5. **Vehicle is a rigid body** It is assumed the shape of the aircraft does not change during flight under the various forces acting on it. In an aircraft, the fuselage does not distort much in flight, so it can be assumed a rigid body. The wings of the aircraft, however, will be deformed upwards due to the lift force acting on it, which would influence the magnitude and direction of the total lift vector as well as the dihedral angle of the wings. However, the aircraft that is considered in this report is relatively small, so it is assumed the wings do not deform enough to significantly affect those variables in the calculations.

The dynamic behaviour is determined with the equations of motion for symmetric (short period and phugoid) and asymmetric motion (aperiodic roll, dutch roll and spiral) from [45].

For the equations of motion the stability derivatives of the UAV need to be determined. These can be determined in different ways; experimentally determined or estimated with calculations. For conventional aircraft

the derivatives can be calculated and may be expected to show comparable values as the experimentally obtained derivatives [45]. The method to calculate the stability derivatives can be found in [45]. Some additional remarks need to be made, since the described method is not complete and some assumptions were made to simplify the approach.

1. First of all it was the following contributions were left out of the calculation, since there were no available methods to estimate them; the effects of changing trust coefficient, the effects of sidewash.
2. The contributions of the coefficients that were not described; The effect of the propeller on the sideslip derivative for the Y force can be found in [73]. Also for calculating $C_{Y_{p_\alpha}}$ this is used. All the contributions of the wing to the stability derivatives (subscript w) are determined using [74]. The contributions of the tail to the derivatives with respect to the roll rate are determined using the methods from [75]. The determination of the aileron and rudder deflection stability derivatives are computed using the methods from [45] and some additional methods. The equation for $C_{\ell_{d\alpha}}$ is from [76] and $C_{n_{d\alpha}}$ is from [77] where $K_a = 1$ is found in Roskam [78].

The calculated stability coefficients can be found in Table 5.2.

Table 5.2: Stability derivatives

Symetrical		Assymetrical	
C_{X_0}	0	C_{Y_β}	0.4648744335
C_{Z_0}	-0.0600	C_{l_β}	-0.13330842298
C_{X_u}	-0.0916768	C_{n_β}	0.1682273767
C_{Z_u}	-1.5600	$C_{n_{\dot{\beta}}}$	0
C_{m_u}	0	$C_{Y_{\dot{\beta}}}$	0
C_{X_α}	0.5623	C_{Y_p}	-0.4994227182
C_{Z_α}	-5.9924	C_{n_p}	-0.01706542494
C_{m_α}	-9.790782894	C_{l_p}	-0.4403304108
C_{X_q}	0	C_{Y_r}	0.2343690022
C_{Z_q}	-6.113235072	C_{l_r}	0.1872
C_{m_q}	-10.89926921	C_{n_r}	-0.282126096
$C_{X_{\dot{\alpha}}}$	0	Ailreon and rudder	
$C_{Z_{\dot{\alpha}}}$	-0.6823633748	$C_{Y_{da}}$	0
$C_{m_{\dot{\alpha}}}$	-2.211970355	$C_{L_{da}}$	-0.2349
Elevator		$C_{Y_{dr}}$	0.3037
$C_{X_{\delta e}}$	0	$C_{l_{dr}}$	0.0286
$C_{z_{\delta e}}$	-0.6238	$C_{n_{da}}$	0.0286
$C_{m_{\delta e}}$	-11	$C_{n_{dr}}$	-0.1261

DERIVATION OF THE STATE SPACE REPRESENTATION

To analyse the motion of the aircraft in the time domain, a state-space system approach was used. A state-space system can easily facilitate multiple inputs and outputs. The inputs are written in a state vector and this way they can be easily used. In this case a linear time-invariant state-space system is used. To get to a state space system, the 3D equations of motion shown [45] need to be rewritten. They should be rewritten in the form seen in Equation (5.10). The state vector $\bar{x}$ and control vector $\bar{u}$ are defined in Equations (5.11) and (5.12) for the symmetric and asymmetric case respectively.

$$C_1\dot{\bar{x}} + C_2\bar{x} + C_3\bar{u} = \bar{0} \tag{5.10}$$

$$\bar{u} = \begin{bmatrix}\delta_e\end{bmatrix} \quad \bar{x} = \begin{bmatrix}u & \alpha & \theta & q\end{bmatrix}^T \tag{5.11}$$

$$\bar{u} = \begin{bmatrix}\delta_a & \delta_r\end{bmatrix}^T \quad \bar{x} = \begin{bmatrix}\beta & \varphi & p & r\end{bmatrix}^T \tag{5.12}$$

To calculate the matrices C_1, C_2 and C_3 some variables need to be substituted in the equations of motion. The variables that need to be substituted are given in Equation (5.13).

$$\begin{aligned} D_c &= \frac{\bar{c}}{V}\frac{d}{dt} \quad D_b = \frac{b}{V}\frac{d}{dt} \\ \hat{u} &= \frac{u}{V} \end{aligned} \tag{5.13}$$

Substituting these variables in equations of motion, and writing out the left hand side results in the equations for symmetric and asymmetric motion. C_1, C_2 and C_3 can be easily determined by "splitting" the calculated matrices as is also described in [45].

Using linearisation is expected to cause the largest discrepancies between the numerical model and "real world" scenario. While linearisation can be applied for any flight condition, the results from the linearised equation of motions are only valid for that flight condition and for the conditions that are close to that point. If a non-steady or an unstable flight condition is chosen, the aircraft will deviate quickly from this condition, meaning that the set of linearised equations is incapable of describing the motion accurately. As a verification procedure, the equations of motion can be simplified for the five dynamic case as discussed in [45].

Phugoid: The airspeed varies over time for the phugoid motion, slightly decreasing. As the aircraft pitches up, the pitch rate and pitch angle increase as expected. For a very short time, the angle of attack increases.

Short period: The duration of the eigenmotion is relatively short so that no large velocity changes will occurs. The forces in the x-direction can then be assumed in equilibrium as the velocity in that direction is constant.

Dutch Roll: Deflections in the aircraft rudder are used to generate this manoeuvre. Large deviations in the roll angle and yaw rate can be observed however the use of a yaw damper can be used to increase stability.

Aperiodic Roll: The aperiodic roll is initiated by applying a step input to the aileron. This manoeuvre is very fast and the effects of side-slip and yaw are small/neglectful.

Aperiodic Spiral: The spiral motion is induced by an initial roll angle (in the case analysed, 10 degrees). With time, the roll angle increases, forcing the pilot to do something to correct the manoeuvre. The UAV also loses altitude in the process.

The eigenvalues for the different motions are presented in Table 5.3. The stationary conditions present during the actual flight for each manoeuvre are used for both the analytical and numerical model. As a verification step, the eigenvalues from the analytical solution described in [45] are compared to the eigenvalues from the linear model as shown previously. This is done for all the symmetric and asymmetric eigenmotions. Analysing if the solutions converge or diverge, are periodic or aperiodic and seeing if the solution is damped or not also needs to be done.

Table 5.3: SCULPTUR eigenvalues Analytical - Numerical solutions

Eigenmotions	Analytical	Numerical	Difference
Symmetric			
Short period	-0.1378 ± 0.3535 j	-0.1377 ± 0.3537 j	0.073% ± 0.0565% j
Phugoid	-0.0007549 ± 0.004152 j	-0.0007461 ± 0.004335 j	1.795% ± 4.221% j
Asymmetric			
Dutch roll	-0.06271 ± 0.3816 j	-0.02932 ± 0.3934 j	113% ± 2.999% j
Aperiodic roll	-0.6035	-0.6470	-6.723%
Aperiodic spiral	-0.002082	-0.001917	8.607%

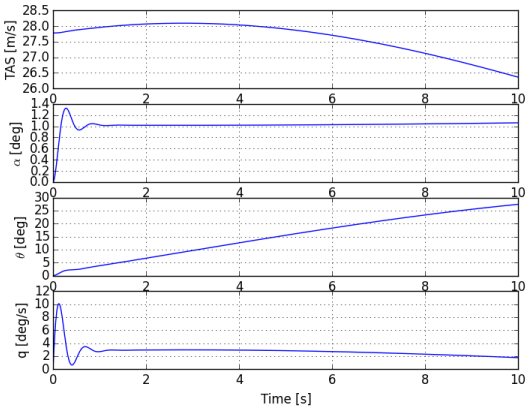

Figure 5.9: Short period - SCULPTUR's response to an input of -1 degree deflection on the elevator

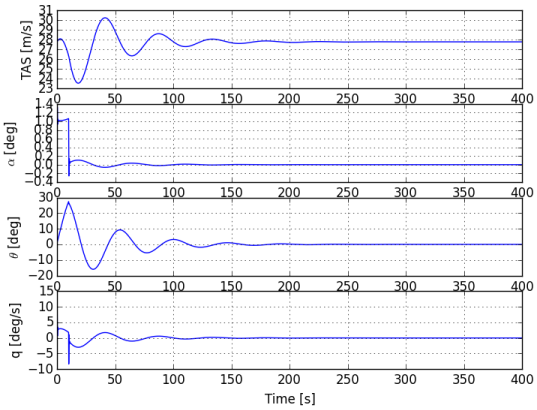

Figure 5.10: Phugoid: SCULPTUR's response to a step input of -1 degree deflection on the elevator

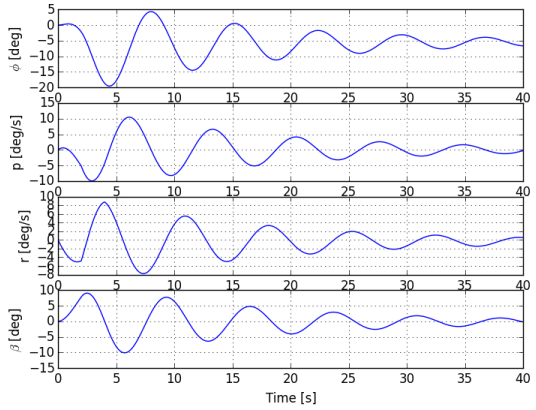

Figure 5.11: Dutch roll - SCULPTUR's response to step inputs of 10 and -5 degrees on the rudder

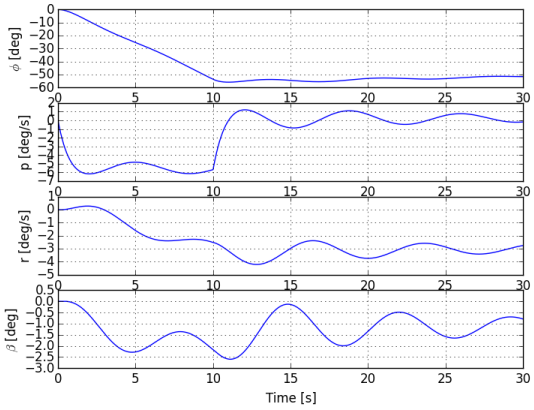

Figure 5.12: Aperiodic roll: SCULPTUR's response to a step input of 3 degrees on the ailerons

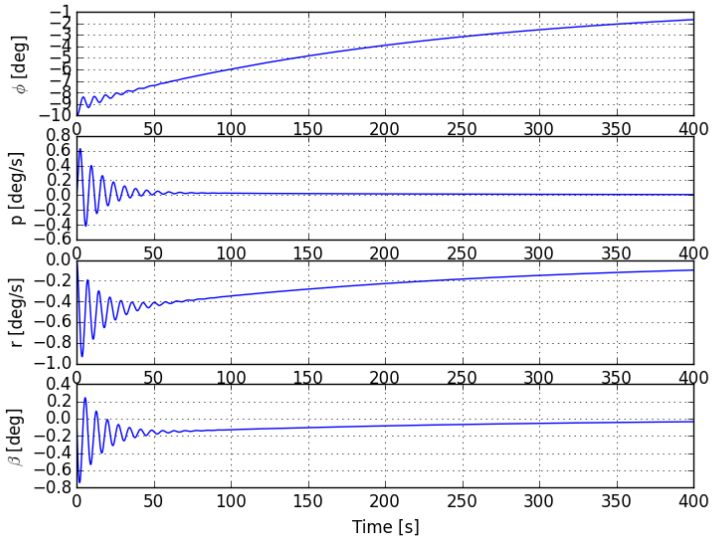

Figure 5.13: Aperiodic spiral - SCULPTUR's response to an initial roll angle of -10 degrees

The signs of the eigenvalues are consistent for both models, indicating that all motions are stable (negative real part). The roll and spiral motions are aperiodic since they only have a real eigenvalue. For the short period and aperiodic roll, the eigenvalues for both models are almost the same, with insignificant errors of 0.073% for the real component of the eigenvalue for the short period (analytical assumes that the airspeed is constant to simplify the symmetric matrix equation by eliminating the first row while there are some small changes during the manoeuvre) and 6.723% for the aperiodic roll (angle of sideslip and yaw rate are assumed to be constant for analytical however they do vary during the manoeuvre). For the aperiodic spiral, a 8.607% difference is observed between the analytical and numerical solutions. This error is addressed to the fact that the stability derivatives C_{Y_r} and C_{Y_p} and that the linear and angular accelerations are ignored for the analytical mode which increase the magnitude of the eigenvalue. Another significant difference can be found in the real part of the eigenvalue for the phugoid which has an error of 1.795% for the real part and 2.999% for the imaginary part. This error inherently also affects the damping ratio and time to half amplitude. The most significant error occurs for the dutch roll, more specifically for the real part. It is concluded that they are due to the fact that the analytical model ignores the rolling component of the motion.

Table 5.4: SCULPTUR eigenmotion Frequency/Damping ratio

Eigenmotions	Natural frequency [Hz]	Damping ratio [-]
Symmetric		
Short period	11.932	0.363
Phugoid	0.138	0.170
Asymmetric		
Dutch roll	0.877	0.074
Aperiodic roll	-	-
Aperiodic spiral	-	-

All the responses are damped as seen in 5.4 and return to the original state. For general aviation aircraft, marginal spiral instability is acceptable as long as the Dutch roll is stable. In the case of UAVs, having a stable spiral mode is more important because if, for example, the communication subsystem fails, the UAV will not be able to recover to its initial state, becoming a potentially safety threat. This is why SCULPTUR is designed with spiral stability in mind.

5.3. AERODYNAMIC ANALYSIS

The aerodynamic analysis has been performed for cruise conditions. The cruise conditions consist out of the cruise speed and cruise altitude as defined by the Requirements **SCULPTUR-SH-04** and **SCULPTUR-SH-05**. The cruise condition is the mission phase with the most extensive fuel consumption, and is thus the phase for which the UAV has to be optimised. All systems will thus be optimised for cruise conditions using the $C_{L_{design}}$ of 0.78 computed in the Mid-Term Report [4], which was computed with half the fuel weight. This will ensure the highest efficiency possible during cruise.

However, because the fuel usage of the UAV changes its weight, the CL_{design} will change during flight. This changes all drag, lift and moment coefficients. Therefore, To be sure all systems depending on the aerodynamic analysis will not be under designed, the coefficients have also been computed for take-off. The take-off condition is namely the condition with the highest loads, since the UAV has the highest lift and highest weight at this mission phase.

All equations and variables used in Subsections 5.3.2, 5.3.1 and 5.3.3 have been taken from Roskam VI [78]. Only the most important and general equations will be mentioned in the following Section. The drag, lift and moment values computed in this Section depend on many values, including the dimensions of the fuselage, wing, landing gear and tail determined in Section 4.4.

Before the analysis can be executed, the oswald factor of the tail has to be determined. Since the tail is unconventional, it is not feasible to base the oswald factor on reference. Equation (5.14) shows how to compute the oswald factor [78].

$$e = 1.1 \cdot \frac{\frac{C_{L_\alpha}}{A}}{R \cdot \frac{C_{L_\alpha}}{A} + (1-R) \cdot \pi} \tag{5.14}$$

Where C_{L_α} is the lift-curve slope, A is the aspect ratio and R is the leading edge suction parameter, as defined in Roskam [78]. The results are presented in Table 5.5.

Table 5.5: Table of Oswald Factors

Oswald Factor	Value
e_w	0.82
e_h	0.89

5.3.1. DRAG ANALYSIS

Table 5.6 shows all final values that have been found during the drag analysis. In these tables, multiple values have been given for several coefficients. These values serve the goal of verification, elaborated on in Subsection 5.3.4.

The drag computations will be used for thrust computations, dynamic stability analysis and can also be useful when designing the aerodynamic shape of the UAV. A sensitivity analysis of the used aerodynamic analysis script will show which parameters influence the drag performance the most, see Subsection 5.3.4. These parameters can be changed to result in a better performing UAV with a minimal drag coefficient.

WING

Equation 5.15 is an expression for the drag coefficient of the wing.

$$C_{D_{wing}} = C_{D_{0_w}} + C_{D_{L_w}} \tag{5.15}$$

$C_{D_{L_w}}$ is the wing drag coefficient due to the lift produced by the wing, and $C_{D_{0_w}}$ is the wing zero-lift drag coefficient. The wing zero-lift drag coefficient can be found using Equation (5.16). This equations contains many variables, some of which can be found using equations from Roskam. Other variables depend on reference data. All of the used reference data has been taken from Roskam [79].

$$C_{D_{0_w}} = R_{wf} \cdot R_{LS} \cdot C_{f_w} \cdot (1 + L'(\frac{t}{c}) + 100(\frac{t}{c})^4) \cdot \frac{S_{wet_w}}{S} \tag{5.16}$$

Here R_{wf} is the wing-fuselage interference factor, R_{LS} is the lifting surface correction factor, C_{f_w} the turbulent flat plate friction coefficient of the wing and L′ is the airfoil thickness location parameter.

The wing drag coefficient due to lift can be found using Equation (5.17).

$$C_{D_{L_w}} = \frac{(C_{L_w})^2}{\pi Ae} + 2\pi C_{L_w} \eta_t v + 4\pi^2 (\eta_t)^2 w \tag{5.17}$$

Where η_t is the wing twist angle, v the induced drag fracture due to linear twist, w is the zero-lift drag fracture due to linear twist. C_{L_w} is the wing lift coefficient. The wing lift coefficient. Since the twist angle is zero in the wing, w and v do not have an effect in this equation.

FUSELAGE

The fuselage drag can be equated using equation (5.18). It consists out of drag resulting from the lift produced by the fuselage, and the zero-lift drag. The fuselage drag coefficient due to lift, $C_{D_{L_{fus}}}$, is equal to zero in the case of the designed UAV. The fuselage is namely placed at an angle of attack of zero, while the wing is placed at an incidence angle to achieve it's $C_{L_{design}}$. The fuselage's angle of attack is chosen to be zero, to minimise drag. While the fuselage would produce a small amount of lift, the drag produced would be significantly higher, which would make this lift production very inefficient[87].

$$C_{D_{fus}} = C_{D_{0_{fus}}} + C_{D_{L_{fus}}} \tag{5.18}$$

$C_{D_{0_{fus}}}$ is the fuselage zero lift drag coefficient. $C_{D_{L_{fus}}}$ is the fuselage drag coefficient due to lift.
$C_{D_{0_{fus}}}$ can be found using:

$$C_{D_{0_{fus}}} = R_{wf} C_{f_{fus}} \left(1 + \frac{60}{\frac{l_f}{d_f}^3} + 0.0025 \frac{l_f}{d_f}\right) \cdot \frac{S_{wet_{fus}}}{S} + C_{D_{b_{fus}}} \tag{5.19}$$

Where $C_{f_{fus}}$ is the turbulent flat plate skin-friction coefficient of the fuselage. l_f is the fuselage length, d_f is the maximum fuselage diameter (equivalent diameter for fuselages with non-circular cross section). $S_{wet_{fus}}$ is the wetted area of the fuselage, and $C_{D_{b_{fus}}}$ is the fuselage base-drag coefficient. This base-drag coefficient is computed by integrating over the surface shape of the fuselage; the equation for this procedure can again be found in Roskam [78].

EMPENNAGE

The drag of the tail can be again be found computing the zero-lift drag and the drag resulting from the tails lift production.

$$C_{D_h} = C_{D_{L_h}} + C_{D_{0_h}} \tag{5.20}$$

$C_{D_{L_h}}$ will be zero for the vertical tail during steady, horizontal flight. The computation for the diagonal tail surfaces of the Y-tail will be done using equation (5.21).

$$\frac{C_{L_d}^2}{A_d \cdot e_d \cdot \pi} \cdot \frac{S_{wet_d}}{S} \tag{5.21}$$

Where A_d is the aspect ratio of the diagonal tail, e_d is the oswald factor of the diagonal tail, S_{wet_d} the wetted area of the diagonal tail and S the reference surface area.

The zero-lift drag has to be computed for both the vertical tails and the diagonal tail. Equation (5.22) will be used for all three tail surfaces.

$$C_{D_{0_h}} = R_{LS_h} \cdot C_{f_h} \cdot \left(1 + L'_h \cdot \left(\frac{t}{c}\right)_h\right) + 100 \cdot \left(\frac{t}{c}\right)_h^4 \cdot \frac{S_{wet_h}}{S} \tag{5.22}$$

[87] URL http://quest.arc.nasa.gov/qna/questions/Angle_of_Attack.htm

Table 5.6: Table of final drag coefficient values

Drag Coefficient	Value from Roskam	Value from XFLR5
$C_{D_{wing}}$	0.022	0.013
$C_{D_{fus}}$	0.002	-
$C_{D_{fus+wing}}$	0.024	0.023
C_{D_h}	0.006	0.003
$C_{D_{gimbal}}$	0.015	-
$C_{D_{total}}$	0.047	-
$C_{D_{total_{TO}}}$	0.072	-
D_{total}	739 N	-
$D_{total_{TO}}$	1250 N	-

Here R_{LS_h} is the tail lifting surface correction factor, C_{f_h} the friction coefficient of the tail surface, L'_h the airfoil thickness location parameter, $\left(\frac{t}{c}\right)_h$ the thickness over chord ratio for the tail surfaces and S_{wet_h} the wetted surfaces of the tail.

OTHER DRAG SOURCES

Several other sources cause the drag coefficient of the UAV to increase. The most important one is the gimbal camera. To compute the drag of the gimbal camera, the equation for a fuselage, Equation (5.19), was used, adding a correction factor described in Roskam [78].

When the total drag coefficient is found, the total drag of the UAV can be found, which then in turn can be used to compute engine thrust for example. To comute the drag, Equation (5.23) is used. The found values can be seen in Table 5.6.

$$D = C_{D_{total}} \cdot S_{total} \cdot 0.5 \rho V^2 \tag{5.23}$$

5.3.2. MOMENT COEFFICIENT ANALYSIS

Table 5.7 shows the results of the moment coefficient computations. The moment coefficients were initially computed without the contribution of the tail, which resulted in the moment of the wing-fuselage combination. This coefficient could then be used to design the tail itself, as can be read in the subsystem design Section; Section 4.4.

The moment coefficient of the UAV will change with the angle of attack. Therefore, it will not suffice to compute one value. Instead, the zero-lift moment coefficient will be computed, together with the slope of the curve.

WING PITCHING MOMENT COEFFICIENT, C_{M_w}

The wing zero-lift pitching moment coefficient can be found from Roskam [78]:

$$C_{M_{0_w}} = \frac{A}{A+2} \cdot C_{m_{airfoil}} \tag{5.24}$$

Where $C_{m_{airfoil}}$ is the pitching moment of the airfoil and A is the aspect ratio of the wing. The slope of the graph (w.r.t. the lift coefficient of the wing, C_{L_w}) can then easily be found using Equation (5.25).

$$\frac{dC_{M_w}}{dCL_w} = \frac{x_{ref} - x_{ac_w}}{c_r} \cdot \frac{c_r}{MAC} \tag{5.25}$$

Here x_{ref} is the reference position, which is in this case taken to be the average c.g. position during flight. x_{ac_w} is the aerodynamic centre position of the wing, c_r is the root chord of the wing, and MAC is the Mean Aerodynamic Chord of the wing. When adding the fuselage to the result from the above mentioned equations, the total fuselage-wing moment coefficient can be found.

Table 5.7 shows a positive moment coefficients slope. According to the Flight Dynamics course, a negative slope is required for static stability [45]. However, this moment coefficient slope is the slope without including the tail. The tail has thus been designed to decrease the slope below zero, and thus make the UAV statically stable, see Subsection 4.4.

WING-FUSELAGE PITCHING MOMENT, $C_{M_{w+f}}$

$$C_{M_{0_{w+f}}} = C_{M_{0_f}} + C_{M_{0_w}} \tag{5.26}$$

$C_{M_{0_f}}$ can be found using a lengthy integration process over the complete process. The equations for this process can be found in Roskam [78]. The slope of the moment coefficient plot can then be found by equation:

Table 5.7: Table of final moment coefficient values

Moment Coefficient	Value from Roskam	Value from XFLR5
$\frac{dC_{M_{w+f}}}{dCL}$	0.09 $[\frac{1}{rad}]$	0.56
$C_{M_{0_{w+f}}}$	-0.92	-0.98
$\frac{dC_{M_{w+f}}}{dCL}$	0.12	0.79
$C_{M_{0_{w+f_{TO}}}}$	-0.92	-0.98

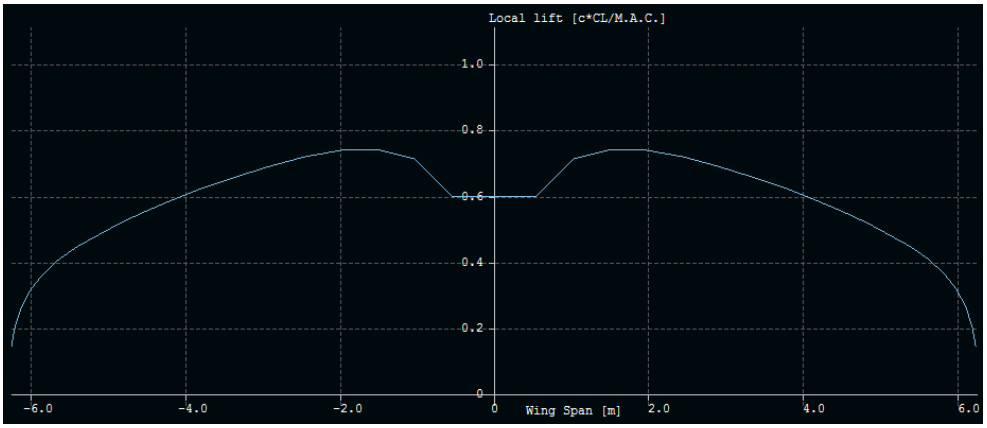

Figure 5.14: Lift Distribution of the wing and at sea level and an angle of attack of 3.5 degrees.

$$\frac{dC_{M_{w+f}}}{dC_L} = x_{ref} - x_{ac_{w+f}} \tag{5.27}$$

Where $x_{ac_{w+f}}$ is the aerodynamic centre position of the wing-fuselage combination. Again, lengthy iterations are required to compute the addition of the fuselage to the aerodynamic centre. The results are presented in Table 5.7.

5.3.3. LIFT DISTRIBUTION

The C_L produced by the tail and the wings has been described in the sections elaborating on the wing and tail airfoil design; Subsection 4.4.3. The lift distribution over the wing itself is an important factor when computing structural loads on the wingbox. To provide accurate estimations for present loads, the lift distribution of the wing during take-off has been estimated using the software program XFLR5 [80]. The lift distribution during take-off was chosen, since the UAV weight, and therefore the lift, will be highest. This ensures that the wingbox will be able to withstand the maximum loads present during a nominal mission. Section 5.6 will elaborate on the wingbox design.

The wing lift distribution can be seen in Figure 5.14. The horizontal axis here gives the span in meters, while the vertical axis gives the lift coefficient of the wing, normalised using the chord length of the wing. The figure shows the decrease in lift where the fuselage is present, and also shows that the lift distribution is resembling an elliptical distribution.

XFLR5 is not accurate for large angles of attack, since it used the Vortex Lattice Method to analyse the lift distribution. However, since the UAV flies at low angles of attack, namely an α of 3.6°, the VLM method can safely be used. XFLR5 can also use the Lifting Line Theory, which is accurate for large angles of attack. This method was used to verify the VLM values. XFLR5 does not take into account viscosity of the air, therefore rendering the results less accurate. However, including the viscosity would be out of the scope of this aerodynamic analysis[81]. To account for discrepancies between the generated data and real-life, safety factors have been introduced in the structural analysis.

5.3.4. AERODYNAMIC VERIFICATION & VALIDATION

VERIFICATION

The verification of the aerodynamic analysis is done by verifying that all requirements have been met. However, no aerodynamic requirements were stated, thus verification cannot be executed. Instead, the method will be validated and a sensitivity analysis will be performed.

VALIDATION OF THE METHOD

The validation of the aerodynamic analysis equations and software an be done using different programs to compute the same value. In this case, XFLR5 has been used together with equations from Roskam [80] wel[78]. Looking at Tables 5.7 and 5.6, one can see the two columns giving the values resulting from both computation methods. In these tables, the most left column presents the value used in further computations and analysis,

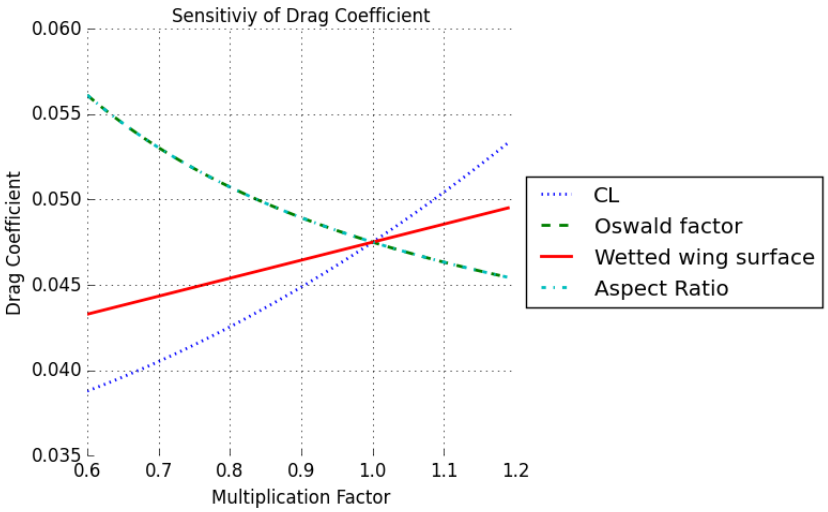

Figure 5.15: Figure showing the sensitivity of the drag coefficient to the change of several parameters

while the most right column presents the value used for validation.

XFLR5 is a program originally designed for airfoils, and can do 3D analysis for small wings and tails. A combination can be made, combining the fuselage and the wing, but the analysis of this combination is generally less accurate [80]. A full analysis, combining the tail, fuselage and wing, is not possible in XFLR5. For this reason, many values in the tables have not been found using XFLR5.

When looking at Table 5.6, three values could be verified. XFLR only produces values when a wing is present, making it impossible to analyse the drag coefficient of the fuselage or the gimbal. Furthermore, the program cannot analyze the full UAV, therefore the total drag coefficients could not be verified with XFLR5 either. The values for the wing drag coefficient, $C_{D_{wing}}$, differ by roughly 20 %, which is an acceptable range when verifying two different programs, keeping in mind the program flaws stated above. The values for the wing-fuselage combination drag coefficient, $C_{D_{fus+wing}}$, are very close, which is quite surprising. Again, this value is verified. However, the tail drag coefficient, C_{D_h}, differs by 50 %. This value is not acceptable, and thus both programs should be checked for errors or wrong assumptions.

Table 5.7 shows that the XFLR5 values for the zero-lift moment coefficient are relatively close to the values found in Roskam; a difference of 6 %. This is an extremely good result for the validation of the zero-lift moment coefficients. However, the values for the moment coefficient slopes differ enormously; both differ by roughly 84 %. This reason of this difference is not yet clear. The percentages of difference are however similar, indicating that the program computes the slope in the right way, but a wrong value is used somewhere. Therefore, before moving on to a more detailed design phase, this difference should be thoroughly researched.

Since Roskam cannot simulate the lift distribution over the wing, the lift distribution in Figure (5.14) cannot be verified using Roskam. Another 3D-analysis program should therefore be used when verifying the lift distribution. This could be performed during a more detailed design phase.

VALIDATION OF THE RESULTS

The validation of the aerodynamic analysis of the SCULPTUR UAV can only be done when a working prototype is produced. This prototype can then be tested in a low-speed wind-tunnel, such as the one situated at the Delft University of Technology. Since no working prototype can yet be produced, the validation cannot yet be executed.

5.3.5. AERODYNAMIC SENSITIVITY ANALYSIS

The sensitivity analysis of the drag coefficient can be seen in Figure 5.15. After varying all input variables, it was found that the four variables that influenced the drag coefficient the most, were the lift coefficient, C_L, the oswald factor, e, the wetted wing surface, S_{wet}, and the aspect ratio, A. Therefore, these variables are the most favourable to change when an in- or decrease of the drag coefficient is required. As can be seen in the graph, the drag coefficient increases when the wing surface and/or the C_L is increased. This is intuitive, since an increased wing surface will directly cause more drag, and indirectly cause more lift, therefore again increasing drag. An increase in C_L means an increase in lift, and thus also, in drag. The graph shows that the aspect ratio and the oswald factor follow the exact same line, decreasing the drag coefficient when their value is increased. This can easily be explained when looking at the equations for the drag coefficient. In these equations, oswald factor and aspect ratio always appear as the fraction; $\frac{1}{\pi Ae}$. Therefore, their change in value has the same effect on the drag coefficient: when their values increase, the fracture decreases, decreasing the drag coefficient.

The two variables influencing the moment coefficient slope, $\frac{C_{M_{w+f}}}{C_L}$, the largest, are the wing aerodynamic centre and the centre of gravity position. The wing aerodynamic centre is, in case of the SULPTUR UAV, in front of the c.g. position of the wing-fuselage combination. Increasing the wing aerocynamic centre position (moving it further aft, away from the nose) naturally decreases the moment coefficient slope. Namely, the aerodynamic centre is the point where an incremental change in lift will act, so by moving the aerodynamic centre, the moment arm is changed. Moving the aerodynamic centre more towards the reference point, will decrease the moment coefficient, since the arm is decreased. Since C_{M_0} will not change when the a.c. changes, C_{M_0} is namely the moment without lift present, the slope of the moment coefficient graph will decrease. The opposite happens when the c.g. is moved more aft. The c.g. position is namely the reference position; the point about which the moment is calculated. Moving it more aft, thus moving it away from the aerodynamic centre, will increase the moment coefficient. Again, C_{M_0} stays the same, thus the moment coefficient slope increases.

The zero-lift moment coefficient, C_{M_0}, is influenced the most by the aspect ratio of the wing, and the airfoil moment coefficient. Both variables decrease C_{M_0} when they themselves are increased. This is intuitive for the airfoil moment coefficient, since the zero-lift moment coefficient of the wing is linearly dependant on the airfoil moment coefficient, see Equation (5.24).Therefore, increasing the airfoil moment coefficient's absolute value, increases the wing zero-lift moment coefficient's absolute value. Increasing the aspect ratio also increases the zero-lift moment coefficient absolute value, since an increase in aspect ratio increases the wing weight[88], therefore increasing the moment generated around the c.g. at zero lift.

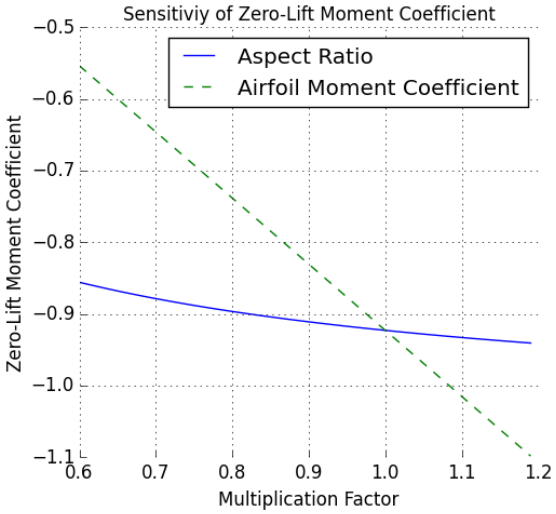

Figure 5.16: Figure showing the sensitivity of the zero-lift moment coefficient to the change of several parameters

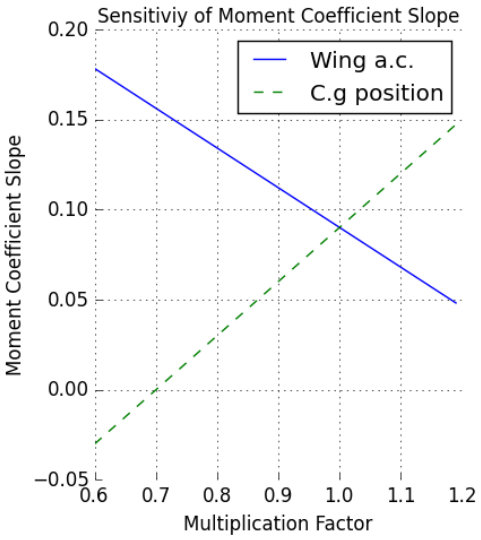

Figure 5.17: Figure showing the sensitivity of the moment coefficient slope to the change of several parameters

5.4. PROPULSION SYSTEM ANALYSIS

The design and analysis of the propulsion system were performed simultaneously with the use of the Gas Turbine simulation Program (GSP). Initially, Subsection 5.4.1 will provide an overview of the program and the model implementation, then a point of design and input conditions will be reasoned in Subsection 5.4.1 based on the requirements and restrictions listed in 4.3, 4.4.7 and 5.3. Following, Subsection 5.4.2 will discuss the results found from the analysis and the off-design performance of the engine. Finally, sensitivity analysis and Verification & Validation are performed in Subsections 5.4.3 and 5.4.4.

5.4.1. GSP IMPLEMENTATION

The GSP cycle code is used to perform the analysis of the engine under development and predict its performance at different flight stages. GSP is mainly based on zero dimension modelling of the thermodynamic gas turbine cycle, whereas the gas model is based on NASA's CEA program for the thermodynamic properties of gas chemical composition. As a 0-D model, in GSP the flow properties are averaged over the flow cross section areas at the interface surfaces of the component models (inlet and outlet). GSP utilises component model stacking to create the thermodynamic cycle of the engine being developed[89]. In this analysis, only the design and steady state series conditions have been used to iterate and modify the parameters of the engine until a design point is reached. Next to that, off-design calculations were performed to obtain an overview of the steady state performance of the engine when the ambient and operational conditions are altered.

[88] URL http://www.wainfan.com/wingdes.pdf

[89] URL http://www.gspteam.com/about.html [cited June 17 2016]

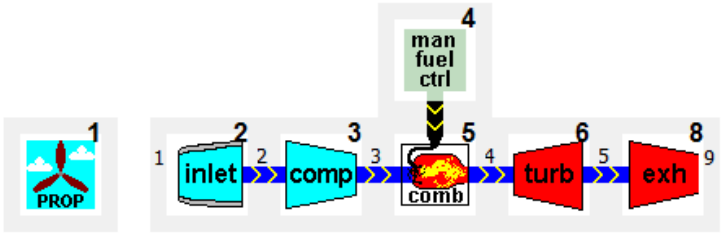

Figure 5.18: Reference turboprop model

The reference model implemented in GSP is the basic initial cycle that includes a propeller, inlet, a single compressor, combustor, a single turbine and exhaust stages (see Figure 5.18). This model was used as an initial point of iteration; then the configuration was adjusted in order to meet the required output parameters set by the flight performance calculations, certifications and regulations (see Subsection 4.4.7).

ESTIMATION TECHNIQUES USED BY GSP

GSP calculates engine performance and gas composition changes across the components using the following equations:

- Conservation of mass equations
- Conservation of energy equations
- Equations for conservation of momentum of gas flow
- Gas state equations
- Isentropic flow equations
- Equation for rotor inertia effects
- Equations for heat flux change between the gas path, material and ambient environment

From these equations, a set of non-linear differential equations is arranged and solved by the GSP solver [82].

DESIGN POINT, INPUT PARAMETERS AND GSP MODEL REDESIGN

The first step taken in the turboprop engine design is to develop a design point which represents the engine's desired performance at a specified operating point. It must be noted that only the maximum take-off and normal cruise conditions have been considered for this analysis, as being critical. Table 5.8 shows the design conditions, the required shaft power output, required thrust generation, required fuel consumption and the dominant exhaust emissions limit for both take-off and cruise conditions.

The challenge with the design was found to be the generation of the required shaft power and excess thrust (with respect to aerodynamic drag) at take-off conditions (sea level, zero velocity) and to be able to generate enough thrust to overcome the drag during cruise. The values for total drag during take-off and cruise have been obtained from Section 5.3 and can be found below. The rest of the ambient condition values, such as density, operating temperature and pressure are standard values estimated by ISA, while the relative humidity input was acquired to be 70% based on the average relative humidity in Australia[90].

Table 5.8: Take-off and cruise design conditions and required output parameters

Description	Symbol	Value	Unit	Description	Symbol	Value	Unit
Altitude take-off	H_{TO}	0	[m]	Altitude cruise	H_{cr}	1000	[m]
Initial speed	V_0	0	$[\frac{m}{s}]$	Cruise true airspeed	V_{cr}	27.8	$[\frac{m}{s}]$
Rel. Humidity take-off	RH_{TO}	70[91]	[%]	Rel. Humidity cruise	RH_{cr}	70	[%]
Inlet pressure take-off	Pt0	101325	[Pa]	Inlet pressure cruise	Pt0	89875	[Pa]
Inlet temperature take-off	Tt0	288.15	[K]	Inlet temperature cruise	Tt0	281.7	[K]
Air density take-off	ρ_{SL}	1.225	$[\frac{kg}{m^3}]$	Air density cruise	ρ_{cr}	1.111	$[\frac{kg}{m^3}]$
Total drag during take-off	D_{TO}	1250	[N]	Total drag during cruise	D_{cr}	739	[N]
Thrust required take-off	T_{TO}	»1250	[N]	Thrust required cruise	T_{cr}	>739	[N]
Design propeller power	$PW_{pr,TO}$	>21.03	[kW]	Design propeller power	$PW_{pr,cr}$	>7.6	[kW]
Design SFC take-off	SFC_{TO}	≈ 0.35	$[\frac{kg}{kWh}]$	Required SFC cruise	SFC_{cr}	<0.572	$[\frac{kg}{kWh}]$
Fuel consumption take-off	$W_{f,TO}$	<0.0094	$[\frac{kg}{s}]$	Fuel consumption cruise	$W_{f,cr}$	<0.0012	$[\frac{kg}{s}]$
NO_x emissions take-off	$NO_{x,TO}$	<0.04	$[m\%]$	NO_x emissions cruise	$NO_{x,cr}$	<0.04	$[m\%]$
CO_2 emissions take-off	$CO_{2,TO}$	<10	$[m\%]$	CO_2 emissions cruise	$CO_{2,cr}$	<10	$[m\%]$

For the design point, an optimum pressure ratio, air mass flow and engine component maximum efficiencies were estimated based on the take-off conditions as the power output is critical, while the propeller sizing and

[90] URL http://www.bom.gov.au/jsp/ncc/climate_averages/relative-humidity/ [cited June 18 2016]

required rotational speed setting is mainly dependent on the thrust, shaft power and SFC requirements for cruise. This is the reason why the analysis was performed simultaneously and iteratively for both conditions. It is important to note that all the input parameters of each engine component were based on reference existing technology data and they do not account for future development predictions (future level effects will be treated in Subsection 5.4.3). Most of the input parameters were varied via the use of the GSP 'LoopCtrl' feature until the design point was reached. The input and design parameters for each component stage will be explained below.

Propeller and Gear Box

As the UAV is designed to operate at similar speeds throughout all flight stages, it has been decided to use a fixed-pitch propeller. This means that the propeller pitch would not be possible to be adjusted during flight. The decision complies to the results in the trade-off presented in the Mid-term report [4].

As a starting point of iteration, the propeller has been idealised to operate at an efficiency of $\eta_{pr} = 90\%$, which was determined to be possible with existing technology[92]. This efficiency was based on the reference Turboprop model and the Generic propeller map, provided by GSP for propeller conceptual design purposes. The diameter, rotational rate and gear ratio of the propeller & reduction gear box were varied in the Design series via the usage of the LoopCtrl feature until the required amount of thrust and torque have been reached. The resultant values for these, as well as the determination of number of propeller blades will be treated in Subsection 5.4.2.

Inlet & Compressor

Based on the reference Turboprop model implemented in GSP and the reference Capstone C-30 turbogenerator [59], a MGT with similar power output, it has been assumed that the ambient conditions do not change through the inlet. This is considered a reasonable assumption since these effects would be extremely small for the rather low airspeed.

Table 5.9: Reference Micro Gas Turbine parameters [83] [59]

Parameter	$MGTI$	$MGTII$	$MGTIII$	Capstone C-30
Output [kWe]	25	10	5	30
Air mass flow [kg/s]	0.22	0.15	0.07	0.31
Pressure ratio [-]	3.5	3.5	3.0	3.5
Compressor efficiency [-]	0.775	0.765	0.753	0.76
Turbine efficiency [-]	0.852	0.85	0.838	0.82-0.85
Speed [RPM]	100,000	130,000	150,000	96,000
Thermal efficiency [-]	0.27	0.26	0.225	0.261
Radial compressor diameter [mm]	150	114	92	147
Radial turbine diameter [mm]	-	-	-	169.5

To continue with the compressor stage, a reference maximum efficiency value was taken from Capstone C-30, being $\eta_{c,max} \approx 0.76$ (see Table 5.9). The input mass flow was altered in GSP and the optimal pressure ratio was determined to be $PR_{tot,max} = 8.7$ for a limited Turbine Inlet Temperature (TIT) at $1350K$ according to Subsection 4.4.7 (see Figure 5.19).

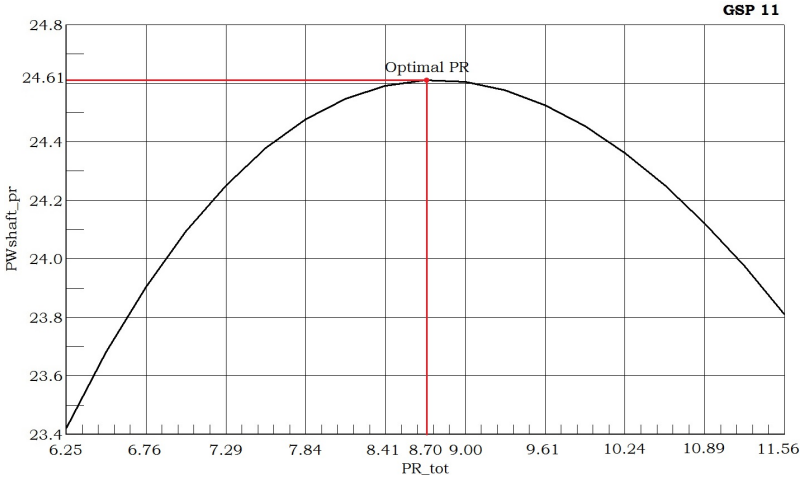

Figure 5.19: Total pressure ratio vs. propeller power quadratic plot - take-off conditions

[92] URL http://hartzellprop.com/the-history-behind-airplane-propeller-design/ [cited June 18 2016]

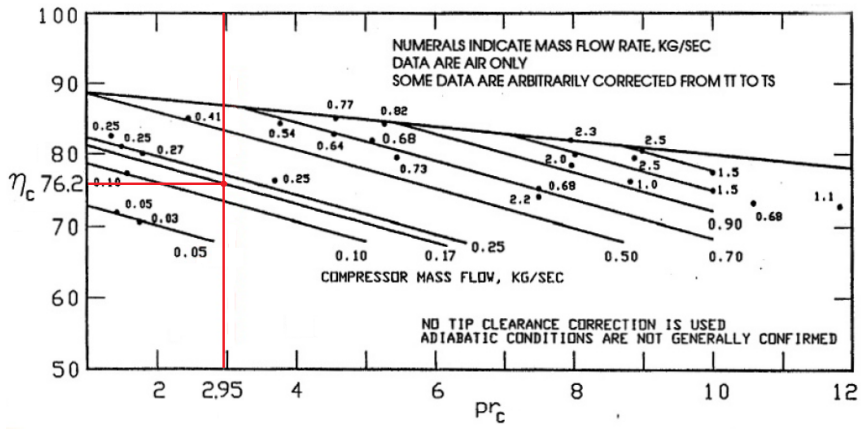

Figure 5.20: Single-stage pressure ratio vs. compressor efficiency reference data [84]

Following the trade-off criteria defined in [4], it has been chosen to use either single-stage or multi-stage centrifugal (radial) compressors. The radial compressors are relatively simpler, lighter, cheaper to produce/buy and maintain, and more efficient for small-scale applications than axial multi-stages [84]. Since the efficiency of the radial turbomachinery drops with an increase of pressure ratio (see Figure 5.20) and the mass flow is required to be as low as possible for a given fuel-to-air ratio, the optimal compressor configuration has been determined to be two-stage centrifugal. This is also because of the high total pressure ratio required and the fact that an extremely large cross sectional area would be required for a single-stage radial turbomachinery to achieve it.

Neglecting any pressure losses through the diffusion and U-turn channels for preliminary design purposes (see Figures 5.21 and 5.22 for an overview of the channels between the two radial stages)[93][94], it follows that each stage should be capable of operating at a maximum single-stage pressure ratio of $PR_{c,max} = 2.95$. This pressure ratio was deemed possible to use based on the reference micro-gas turbines shown in Table 5.9, particularly $MGTI$, $MGTII$ and Capstone C-30 [59].

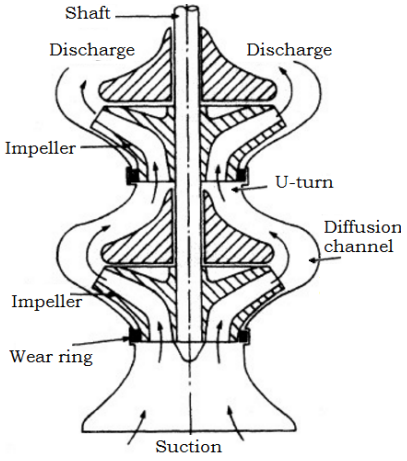

Figure 5.21: Two-stage radial compressor

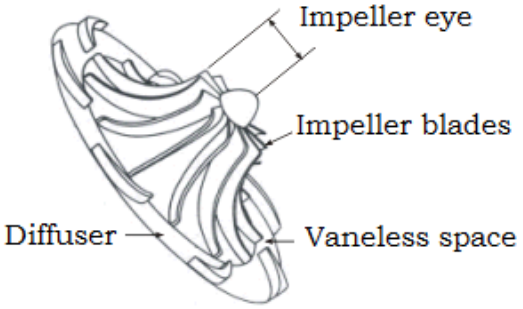

Figure 5.22: Schematic view of a radial compressor

Keeping the acquired optimum pressure ratio and the reference compressor efficiency in mind, it is estimated using Figure 5.20 that to operate at these conditions the inlet air mass flow shall be $\dot{m}_{air,max} = 0.17 kg/s$, according to reference data provided by [84]. These maximum provided values are assumed to be used for take-off conditions. They have been verified to be within appropriate boundaries on account of the reference $MGTII$ given in Table 5.9, as having similar mass flow and even higher single-stage pressure ratio.

The air mass flow during cruise is, however, desired to be as low as possible to keep a similar optimum lean-burn fuel-to-air equivalence ratio. This cruise air mass suction is adjusted by decreasing the rotational speed of the turbine stage. It follows from Figure 5.20 that decreasing the mass flow decreases the efficiency at which the compressor and turbine stages operate. The mass flow is dependent on the pressure ratio, as well, hence an optimum pressure ratio was determined for the cruise conditions via the use of GSP. Figure 5.23 shows the cruise pressure ratio being varied with different TIT. The design point is circled and was chosen so that it minimises SFC_{cr} and maximises PW_{cr}, while keeping the air mass flow as low as possible. Based on this optimal cruise

[93] URL http://strictlynorules.blogspot.nl/2011/10/centrifugal-pumps-for-general-marine.html [cited June 18 2016]
[94] URL http://nptel.ac.in/courses/Webcourse-contents/IIT-KANPUR/machine/ui/Course_home-lec6.htm [cited June 18 2016]

pressure ratio of $PR_{tot} = 2.7^2 = 7.29$, the values for air mass flow, compressor and turbine operating isentropic efficiencies at cruise conditions were varied and adjusted according to the $MGTIII$ and Capstone C-30 turbo-generator (See Tables 5.9 and 5.10 for a full overview). The $\dot{m}_{air,max}/\dot{m}_{air,cr} = 2.83$ fraction was compared with the Pratt&Whitney $PW120A$ turboprop engine which operates at $\dot{m}_{air,max}/\dot{m}_{air,cr} \approx 1.51$ [85]. The reason for the higher value of the engine under development is the large fraction difference of shaft power output between the cruise and take-off conditions.

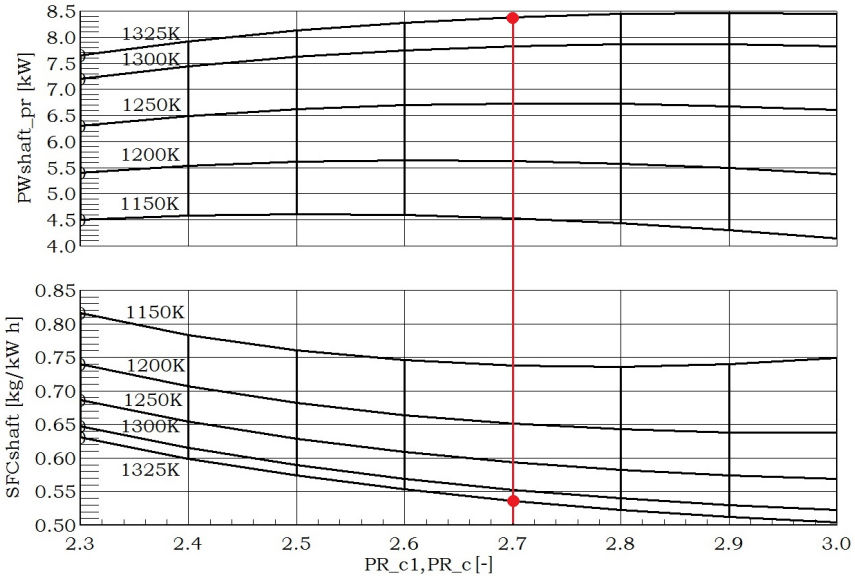

Figure 5.23: Single-stage pressure ratio vs. compressor efficiency reference data [84]

Another point of design is that bleed air is required entirely for cooling of the turbine stage due to the high TIT and the rapid heat transfer occurring between the relatively small-sized components when compared to large gas turbines. For this reason, a bleed valve is determined to allow extraction of up to $W_{bl,TO} = 4\%$ fraction of the air mass flow at take-off conditions. During cruise this fraction is taken to be $W_{bl,cr} = 3\%$ because of the lower TIT_{cr} as fuel consumption is lower. These values were normalised based on reference turboprop engines, especially the $PW120A$ (2.5% minimum and 4.4% maximum bleed fraction [85]). Even with the limited bleed air usage of the designed engine, a slightly higher bleed fraction is still needed because of the extremely low inlet air mass flow. It must be considered that these optimum values were obtained via the $BleedControl$ loop feature in GSP' Steady State series. Essentially, for an increase in power output these fractions are wanted to be kept as low as possible.

Finally, comparing the mass flow, pressure ratio and compressor efficiency of the provided $MGT\ I$ and II reference data, it has been determined that the radial compressor diameter would be within the [114;150] mm range. This means that the compressor will be easily implemented within the fuselage.

Combustor

For the design of the engine, a lean-burning annular reverse-flow combustor has been chosen based on the trade-off matrix selection provided in [4]. This combustor is commonly used in reference turboprop engines (e.g. PBS TP-100 [2] and Pratt&Whitney PT6A [86]) and MGTs (e.g. Capstone C-30 [59]) mainly because of its excellent performance with low flame residence time (due to the small size of the combustor), and the fact that lower CO, NO_x and particulate matter emissions can be achieved. Additionally, the configuration is relatively simple, easily maintainable, it allows for lower engine longitudinal size and it has a high combustion performance for small-sized applications (see Figure 5.24) [87]. As inputs, a combustion efficiency of 0.995 and relative pressure loss of 2% have been implemented in GSP based on the Capstone C-30's combustion chamber, according to Table 5.9. Exact estimation of these parameters is beyond the scope of this MGT's preliminary design.

Turbine

Given the relatively high overall pressure ratio achieved through the two stages of compression, a high expansion ratio is also in order through the turbine stage, thus a power turbine on a separate shaft designed to only drive the propeller through a reduction gear box has been implemented. The power turbine concept was also reasoned in the Mid-term report [4] to be preferable because of its better starter performance (during start-up only one of the shafts has to be rotated and this requires less starter power) and the possibility to use a smaller clutch system for propeller RPM adjustment [88].

Both of the turbines were determined to be radial single-stage, again, based on the same criteria as for the compressor stage (refer to the turboprop engine trade-off matrix in the Mid-term report for additional information [4]). All input parameters of the High-Pressure Turbine (HPT), Power Turbine (PT) and the two shafts are en-

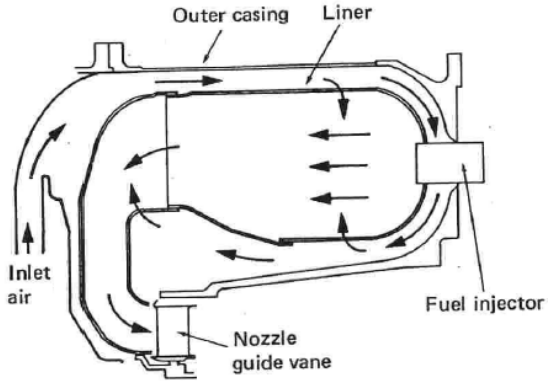

Figure 5.24: Annular reverse-flow combustor [87]

tirely based on the Capstone C-30 turbogenerator. The values were verified to be suitable for the decreased air mass flow with respect to Capstone C-30 using the reference $MGTII$ data in Table 5.9.
During take-off, both HPT and PT are being cooled, using a 75% fraction of the bleed air flow for post-combustion dilution and cooling of the HPT, while the remaining bleed air fraction for cooling of the PT, due to the lower resultant temperatures after the first expansion stage. During cruise, all the bleed air flow is supplied for dilution and HPT cooling.

Finally, because of the decreased mass flow and expansion ratios compared to the Capstone C-30, it is only logical that the radial turbine diameter would be also lower ($< 169.5\ mm$). This range of values is suitable for the engine to be fit into the fuselage. A more exact sizing is beyond the scope of the project, thus only recommendations will be given in Chapter 11.

Exhaust

At the exhaust stage, the 'fixed area nozzle' GSP feature is checked, and all default values are kept, neglecting all pressure changes 5.10.

For an overview of all design and fixed input parameters into the GSP simulation refer to Table 5.10. Further on, Figure 5.25 shows the complete redesigned configuration that is implemented in GSP.

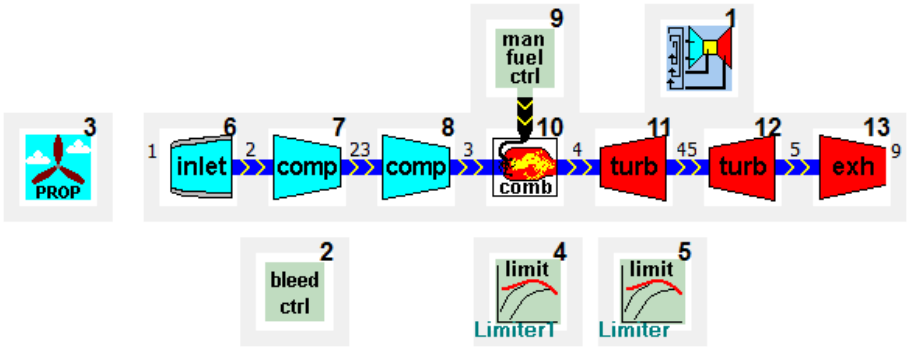

Figure 5.25: GSP model redesign

Table 5.10: Design and fixed input parameters based on existing technology

Description	Symbol	Value	Unit	Description	Symbol	Value	Unit
Des. air mass flow	$\dot{m}_{air,max}$	0.17	$[\frac{kg}{s}]$	Spool inertial moment	I_{spool}	0.7578	$kg\ m^2$
Inlet pressure ratio	PR_{in}	1.0	[-]	Des. mech. efficiency	η_m	0.99	[-]
Max total pressure ratio	$PR_{tot,max}$	8.7	[-]	Des. max HPT eff.	$\eta_{hpt,max}$	0.85	[-]
Comp. heat transfer fraction	HT_c	0.50	[-]	HPT rotor speed	ω_{hpt}	96,000	[rpm]
Design comp. eff.	$\eta_{c,max}$	0.76	[-]	Des. PT efficiency	$\eta_{pt,max}$	0.85	[-]
Comp. rotor speed	$\omega_{c,max}$	96,000	[rpm]	PT rotor speed	$\omega_{pt,max}$	96,000	[rpm]
Des. TIT limit	TIT_{max}	1350	[K]	Velocity coefficient	CV	1.0	[-]
Des. comb. efficiency	η_b	0.995	[-]	Thrust coefficient	CX	1.0	[-]
Comb. rel. pressure loss	ΔP_{comb}	0.02	[-]	Throat	CD	1.0	[-]
Cruise conditions							
Cruise air mass flow	$\dot{m}_{air,cr}$	0.06	$[\frac{kg}{s}]$	Cruise HPT efficiency	$\eta_{hpt,cr}$	0.84	[-]
Cruise total pressure ratio	$PR_{tot,cr}$	7.29	[-]	Cruise HPT rotor speed	$\omega_{hpt,cr}$	<vary>	[rpm]
Cruise comp. efficiency	$\eta_{c,cr}$	0.74	[-]	Cruise PT efficiency	$\eta_{pt,cr}$	0.84	[-]
Cruise TIT	TIT_{cr}	1325 K	[K]	Cruise PT rotor speed	$\omega_{pt,cr}$	<vary>	[rpm]

FUEL SELECTION

Referring back to the trade-off in the Mid-term report [4], the fuel selection is based on the capability of the fuels to provide sufficient energy, assure safe engine combustion and operation of the UAV, their ability to self-lubricate, the cost and the capability to flow (viscosity).

For exhaust emission reduction purposes, mostly "green" fuels and combinations of biofuels with other long-chained hydrocarbons were examined. The relatively low cruise altitude and the intentions to carry out the mission in Australia, a place with high average temperatures throughout the year, ruled out the cloud, pour and freeze points of the fuels as not critical for the selection. Even in case of flying at elevated altitude regions, the temperatures would still be high enough to sustain the fuel at the appropriate liquid state. Additionally, additives can be used prior to flight in order to enhance the fuels and prevent gelling at cold weather conditions [89] [90].

To be exact, the fuels that were looped in GSP were the Hydrogeneration-Derived Renewable Diesel Type I ($HDRD\ I$) and two soybean biodiesel blends (combined with petroleum diesel) - $B20\ SME$ and $B50\ SME$. Overview of the fuel characteristics implemented in GSP can be found in Table 5.11. The cost of all fuels considered were found to be similar[95].

Table 5.11: Fuel properties [90] [91] [92] [89] [93]

Liquid fuel	LHV [kJ/kg]	Density @ 21° C $[kg/dm^3]$	H/C ratio	O/C ratio	Lubricity	Viscosity $[\frac{mm^2}{s}]$
B20 SME	43,230	0.851	1.87	0.02	Excellent	$\approx 4-5$
B50 SME	41,930	0.862	1.88	0.02	Excellent	$\approx 4-5$
HDRD I	**43,563**	**0.749**	**1.65**	**0**	**Excellent**	$\approx 3-4$

A comparison of the engine's performance on the three different fuels can be seen in Figure 5.26. It is only logical that $HDRD\ I$, the fuel with the highest LHV, shows the most optimal performance when minimisation of SFC is required. Moreover, lowering the fuel consumption also lowers the exhaust emissions per mass basis.

[95] URL http://www.government-fleet.com/article/story/2016/03/what-you-need-to-know-about-renewable-diesel.aspx [cited June 26 2016]

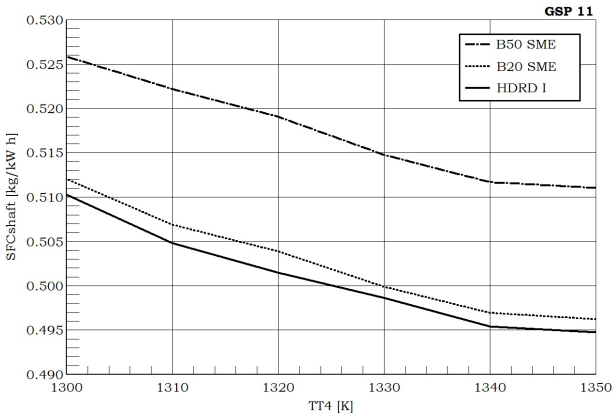

Figure 5.26: TIT vs. SFC for different fuels - take-off

Because of the relatively low density, high Lower Heating Value (LHV), high lubricity and medium viscosity (with respect to petroleum diesel and biodiesel), $HDRD\ I$ has been chosen for a design fuel. Further reasons for the choice are its superior emission profile (reduced particulate matter, hydrocarbons, and CO_2 emissions) and its lower production cost as it uses existing hydro-treatment process equipment in petroleum refineries[96].

FLIGHT OPERATING ENVELOPE

Before the simulation is run it has to be considered at what ambient conditions the engine is designed to operate. This is why a flight envelope was developed in GSP to show the range of Mach number and altitude of engine operation. Note that the flight envelope assumes ISA conditions with 0° temperature offset.
According to Section 5.1, the minimum UAV airspeed was estimated to be $V_{min} = 20m/s$ while the maximum airspeed was found $V_{max} = 48m/s$. These limits restrict the boundaries of the flight envelope to the left and right, especially above $1km$ altitude. Having an altitude boundary limit of $7.2km$, and an extension to zero speed up to $1km$ altitude for climb purposes, the engine's operating envelope can be observed in Figure 5.27.

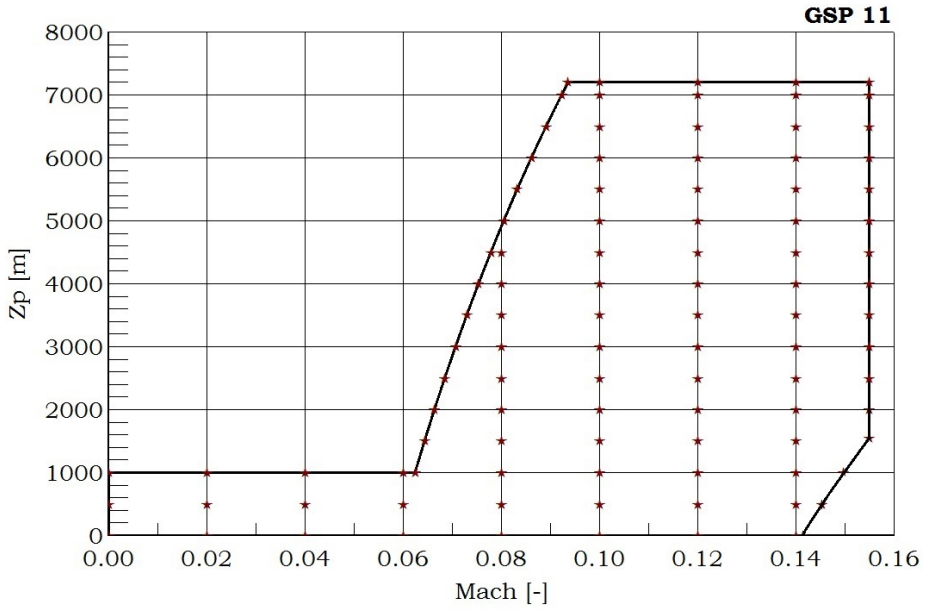

Figure 5.27: Flight operating envelope

5.4.2. DESIGN ANALYSIS RESULTS AND OFF-DESIGN ENGINE PERFORMANCE

This subsection will explain and show what iterations were performed to obtain the final results of the analysis. The propeller stage will be sized, then the two design condition results will be presented.

To get an overview, before the steady state series calculations are performed, a Temperature-Entropy graph is presented in Figure 5.28 for both take-off and cruise based on GSP Design calculations, which are only dependent on the thermodynamic cycle and do not take into account any rotational rate variations for example. For both conditions, there are two slope changes between sections 2 and 3, mainly due to the fact that the processes are not ideal. The reason for having the take-off condition to be steeper is the higher operating isentropic compressor efficiency because of the higher air mass flow and higher pressure ratio. The change in slopes within

[96] URL http://www.betalabservices.com/biofuels/renewable-diesel-hdrd.html [cited June 24 2016]

each flight condition is resultant from the fact that air is bled in the first compressor stage only, hence the slope from section 23 and 3 is slightly steeper. A slight non-linearity in the combustion stage is shown; however, because of the high combustion efficiency used and the low relative pressure loss (according to input conditions - 2%), the results are almost optimal. As for the turbine stages, two slopes are observed, again having the slope at cruise to be less negative, because of the slightly decreased turbine efficiency (lower mass flow). The change in slopes between sections 4 and 5 (between HPT inlet and exhaust) within a flight stage is dependent on the cooling fraction and the fact that most of the bleed air is provided for cooling at the HPT (75%), hence the air mass flow that enters the power turbine is higher and PT operates at a higher isentropic efficiency. Lastly, a constant-pressure line is observed between sections 9 and 1, since pressure changes at the exhaust were neglected.

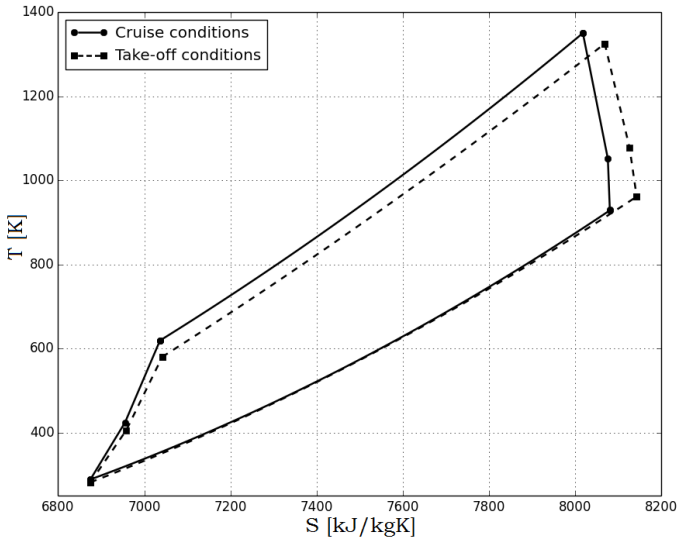

Figure 5.28: Temperature-entropy diagram

PROPELLER SIZING

Concerning the size and number of blades of the propeller, important factors to consider are performance, cost, weight, noise, diameter limits and durability. Since a large amount of the turboprop engine's thrust generation was found to result from the conservation of momentum at the propeller stage, the propeller size was iterated and adjusted appropriately based on both cruise and take-off conditions in order to meet the requirements for thrust.

Regarding the number of blades selection, only two-bladed and three-bladed propellers were examined mainly because of the relatively low amount of thrust that is needed to be generated when compared to larger aircraft. Propellers with four or more blades would add too much weight and the budget would be exceeded. The most important consideration is that a three-blade propeller requires a smaller diameter than a two-blade configuration; this lowers the blade tip speed which also reduces noise emissions. Regarding weight and cost, both configurations are comparable because the three-blade concept has an extra blade which adds weight, but since the diameter is smaller, it is possible to have a lighter structure than for the two-blade configuration. Concerning noise, a two-blade propeller produces two pressure pulses per revolution, while a three-blade one generates three smaller pulses per revolution for the same amount of output thrust. The latter is inherently smoother and consequently quieter[97]. Because of these reasons and the high fraction of propeller-to-exhaust thrust $F_{Nprop,cr}/F_{Ge,cr}$ that the turboprop engine is needed to produce, a three-blade propeller was chosen.

Using GSP's simulation results, it was found that a propeller having three blades, a diameter of $1.91m$ and rotational speed of $1500RPM$ at cruise conditions will generate the required total thrust of $F_{N,cr} = 739N$ ($F_{Nprop,cr} = 712N$ and $F_{Ge,cr} = 27N$). At take-off the thrust generation was found to be $F_{N,TO} = 1447N$, also meeting the requirement to be in excess of the aerodynamic drag.

It must be however noted that appropriate design for the blade angle β_{blade}, advance ratio $J = \frac{V}{ND}$, power coefficient (C_{pw}) and thrust coefficient C_t is not yet considered at this preliminary design stage. Instead, the 'prescribed efficiency' feature in GSP was used as it allows for assumptions that achieving the output parameters is possible by appropriate variation of the rotational rate.

[97] URL http://hartzellprop.com/faq/technical-questions/ [cited June 24 2016]

TAKE-OFF ENGINE PERFORMANCE

The final resultant output parameters regarding the thermodynamic cycle of the simulation under design take-off conditions can be observed in Table 5.13 and Figure 5.19. Figure 5.29, on the other hand, is provided via a steady-state simulation, meaning that some of the input parameters were adjusted automatically by the program to examine the engine's Off-Design performance. To limit these adjustments, GSP 'limiter' features are set on the turbine inlet temperature and rotor RPM. The first figure shows a linear behaviour of the change in propeller shaft power with TIT_{TO} and parabolic behaviour for the change in thrust. It is observed that for TIT_{TO} above $1300K$ the thrust requirement is met, and at the limit of $TIT_{TO} = 1350K$, both propeller shaft power and thrust requirements are fulfilled, while the SFC remains well below the maximum value specified by regulations according to Table 5.8. These values were obtained at $2000RPM$ propeller rotational rate and $\omega_{hpt,TO} = \omega_{pt,TO} = 96,000RPM$ (see Table 5.12). This invokes for the necessity to use a reduction gear box, having a maximum gear ratio of approximately $48:1$. This gear ratio is deemed possible to be obtained according to [94]. A more thorough analysis on the reduction gear box is recommended to be done only after the detailed design of the engine is completed.

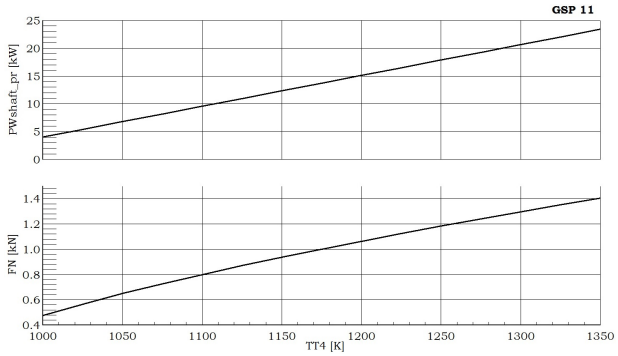

Figure 5.29: TIT vs. Shaft power output and Overall Thrust

To get a better overview of the emission control and to check if the values obtained are reasonable, the fuel-to-air equivalence ratio is calculated using Equation 5.28, based on the resultant fuel-to-air ratio found by the GSP simulation.

$$\phi_{TO} = \frac{F/A_{actual}}{F/A_{stoichiometric}} = \frac{0.0206}{0.0696} = 0.296 \tag{5.28}$$

Now Figure 5.31 presents that CO_2 emissions are being dominant and orders of magnitude higher than NO_x exhaust emissions. This is mainly because of the extremely low equivalence ratio that was used in order to meet the turbine inlet temperature limit and cruise fuel consumption requirement (take-off and cruise are interrelated as the configuration remains the same). Even so, the CO_2 emissions are still low when taking into account the relatively small mass flow rate when compared to reference turboprop engines, e.g. PBS TP-100 [2]. Taking the limit of $1350K$ at $W_F = 0.0034kg/s$, only about $6.5\% \cdot 0.17kg/s = 11g/s$ of CO_2 is being produced. Concerning NO_x exhaust emissions, they were found to be within the range $[0.02, 0.04]m\%$. As stated previously in Subsection 4.4.7 the limit mass-fraction-based values for CO_2 and NO_x exhaust emissions are provided to be $10m\%$ and $0.04m\%$. It follows that both NO_x and CO_2 emission requirements have been met. Other radicals of the combustion reaction such as unburned or partially-burned hydrocarbons, N_2O and CO emissions were found to be extremely small and they were neglected.

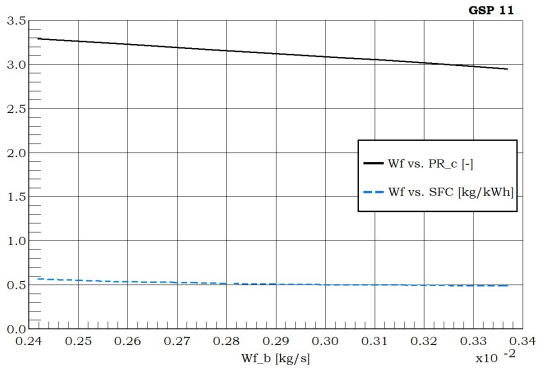

Figure 5.30: Fuel flow vs. PR_c and SFC

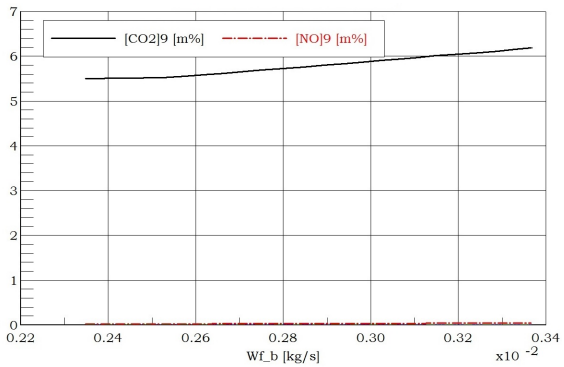

Figure 5.31: Take-off fuel flow vs. exhaust emissions @ $\phi \approx 0.29$

CRUISE PERFORMANCE

The Design performance results regarding the thermodynamic cycle during cruise were iterated by GSP until a convergence occurred and the output parameter requirements specified in Table 5.8 were met. These Design results are presented in Table 5.13 and Figure 5.23. It can be seen that the all the of fuel consumption, SFC, power output and thrust requirements have been fulfilled for cruise conditions at 1325K turbine inlet temperature.

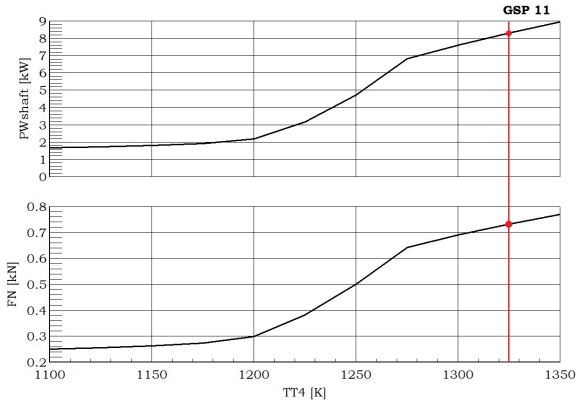

Figure 5.32: Steady State simulation of increase in TT4 with LoopCtrl during cruise

Figure 5.32 shows the Steady State simulation results with change of TIT_{cr} for a range of 1100K to 1350K. After several iterations performed in steady state series, it has been determined that the rotational rate of the propeller will remain 1500RPM, as already discussed previously, while the cruise rotational rate of both turbines was iterated and optimal output parameters were found at 70,000RPM (see Table 5.12). The gear ratio for the cruise conditions (46.7 : 1) is determined not to be critical as it is lower than for take-off conditions.

Table 5.12: Take-off and Cruise Performance settings

Performance setting	$\dot{m}_{air}$	PR_{tot}	W_f	$\omega_{hpt} = \omega_{pt}$	PW_{prop}	F_N	SFC
Maximum take-off	0.17 kg/s	8.7	0.0034 kg/s	96,000 rpm	24.61 kW	1447 N	0.493 kg/kWh
Normal cruise	0.06 kg/s	7.29	0.0012 kg/s	70,000 rpm	8.4 kW	739 N	0.537 kg/kWh

Moving on to the steady state generated Figures 5.33 and 5.34, it is presented how the shaft power output, SFC, compressor pressure ratio and polluting emissions are varied with fuel flow. Similar to the take-off, at an equivalence ratio of 0.3, the mass fraction of CO_2 is dominant and ranges from 5m% at $TT4 = 1100K$ to around 6.5m% at $TT4 = 1325K$, orders of magnitude higher than NO_x emissions which are found to be in the range $[0.015 : 0.03]m$%. This shows that for both cruise and take-off, the sustainability requirement has been met.

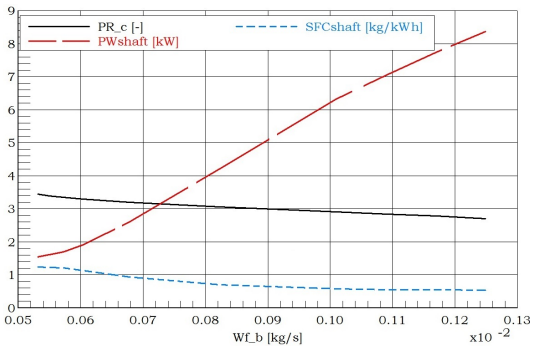

Figure 5.33: Steady state Fuel flow vs. PWshaft, SFCshaft and PR_c

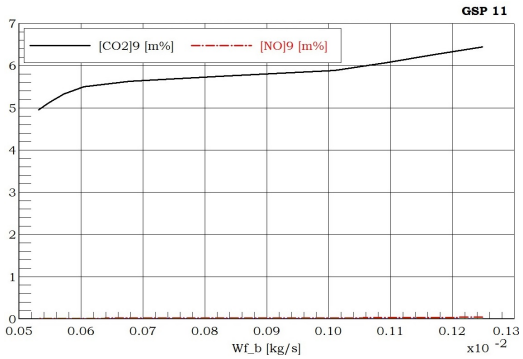

Figure 5.34: Cruise fuel flow vs. exhaust emissions @ $\phi_{cr} \approx 0.3$

5.4.3. SENSITIVITY ANALYSIS AND TECHNOLOGY LEVEL EFFECTS

The sensitivity of the design is investigated for a change in major engine parameters. It was chosen to investigate the change in pressure ratio, efficiency of the compressor and turbine inlet temperature, while keeping all other engine parameters the same. This was based on the fact that the choice for these was based on reference data and they may be subject to change when it is continued to the detailed design of the engine.

TAKE-OFF CONDITIONS

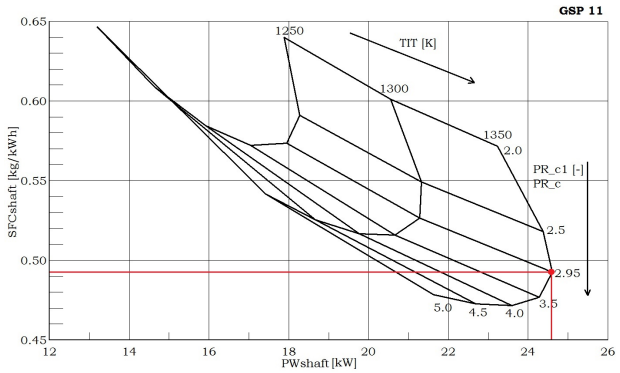

Figure 5.35: Shaft power vs. SFC take-off carpet plot

Using the simulated in GSP steady state results, carpet plots were generated so that multiple variables can be varied in the same time and the change in multiple engine output parameters can be observed. Figure 5.35 shows a carpet plot of varying TIT and single-stage compressor pressure ratio (both compressors were assumed to operate at the same efficiency). It is clear that increasing TIT has the direct effect of increasing the shaft power, while increasing PR_c has the strongest influence on the reduction of SFC.

To continue, Figures 5.36 and 5.37 present the power output and thrust generation against specific fuel consumption (SFC and TSFC) for take-off conditions. For both carpet plots the TIT and compressor efficiency have been varied, accounting for future technology improvements. It can be seen that by increasing TIT, the power and thrust generation increase, while the SFC decreases. The combination of both TIT and compressor efficiency increase can yield much more efficient values for the engine's performance, especially by reducing SFC and increasing power & output during take-off.

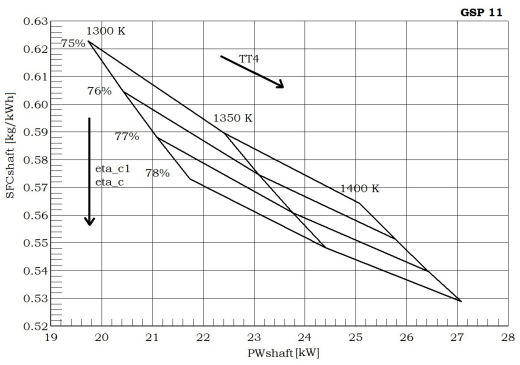

Figure 5.36: Take-off PWshaft vs. SFC for change in compressor efficiency and TIT

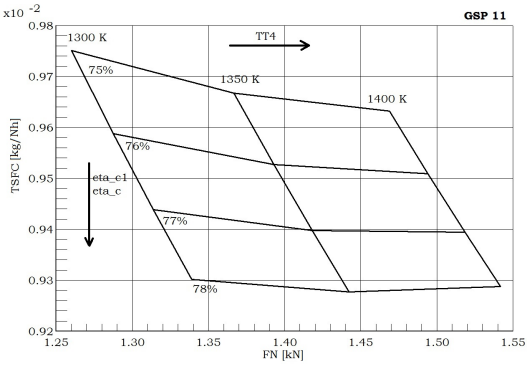

Figure 5.37: Thrust vs. TSFC for change in compressor efficiency and TIT

CRUISE CONDITIONS

At cruise conditions, the pressure ratio is optimised for minimising specific fuel consumption. Since the thrust generation was determined to be critical during the design analysis, a F_N-SFC carpet plot is generated by GSP for an adjustment of TIT and Total pressure ratio at idle conditions (see Figure 5.38). Increasing the pressure ratio for a given TIT results in a decrease of SFC up to a peak total pressure point. This phenomenon is explained with Figure 5.23 showing the optimum pressure ratio for SFC during cruise.

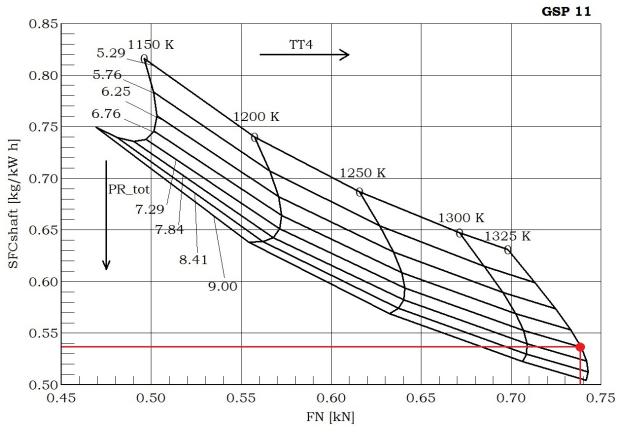

Figure 5.38: Thrust output vs. SFC cruise carpet plot

Lastly, Figures 5.39 and 5.40 show similar cruise power and thrust behaviour as 5.36 and 5.37. It is seen that with a slight increase in compressor efficiency and turbine inlet temperature, significant SFC reductions can be achieved.

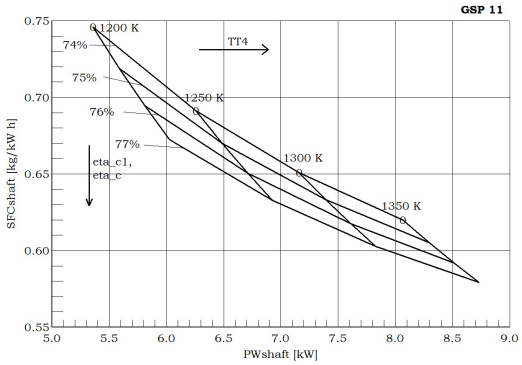

Figure 5.39: PWshaft vs. SFC for change in compressor efficiency

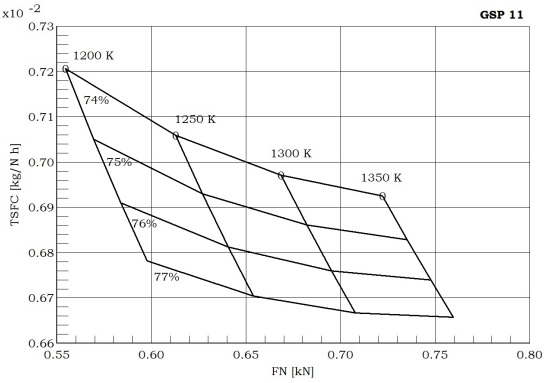

Figure 5.40: Thrust generation vs. TSFC for change in compressor efficiency

5.4.4. VERIFICATION AND VALIDATION

In order to verify the design points produced with the GSP tool, a system test was performed. This system test analyses the thermodynamic cycle as produced by GSP against a simplified analysis of a simple thermodynamic cycle using the equations as provided in [55]. In this model it was assumed that the influence of pressure on the specific heats C_p and C_v is negligible, but the temperature effects not. For this reason two sets of main specific heats were used during the calculations, one for the cold part of the engine (before combustion) and a different, higher value for the hot part (after combustion).

No unit tests were performed on the GSP program, as the units are tested simultaneous with the system. This is visualised in Table 5.13 by the individual components of the inlet, compressor, combustor, turbine and the engine nozzle. Table 5.13 presents the input parameters of the system test, together with the analysis of both the take-off and cruise thermodynamic cycles. The values of the simple cycle calculation together with the output value of the GSP program is shown, after which the error percentage is determined. An overview of the stage numbering is given in Figure 5.28.

Table 5.13: System test - thermodynamic cycle

Input Parameters			Take-off				Cruise			
Variable	Value	Unit	Output	Ideal Cycle	GSP	Error%	Output	Ideal Cycle	GSP	Error%
η_t_takeoff	0.85	[-]	Inlet				Inlet			
η_c_takeoff	0.762	[-]	T0.2	288.15	288.15	0,0	T0.2	281.6	281.6	0,0
T_amb (Take-off)	288.15	K	P0.2	101350	101350	0,0	P0.2	89875	89875	0,0
P_amb (Take-off)	101350	Pa	W_prop	24610.1	24090.1	2.1	W_prop	8380.1	8160.4	2.7
PW_sh (Take-off)	24.61	kW	Compressors				Compressors			
Cp_gas (Take-off)	1248	J/(kg K)	T0.25	425.1	424.1	0.2	T0.25	406.2	405.6	0.2
k_gas (Take-off)	1.3	[-]	P0.25	298982.5	298909.1	0.02	P0.25	242662.5	242661.7	0,0
PR_c_takeoff	2.95	[-]	T0.3	627.2	618.8	1.3	T0.3	585.9	580.1	1.1
M_takeoff	0.17	kg/s	P0.3	881998.4	881781.1	0.02	P0.3	655188.8	655186.1	0,0
η_t_cruise	0.84	[-]	Combustor				Combustor			
η_c_cruise	0.74	[-]	T0.4	1350	1350	0,0	T0.4	1325	1325	0,0
P_amb (Cruise)	89874.6	Pa	P0.4	868768.4	868554.1	0.02	P0.4	645360.9	645358.1	0,0
T_amb (Cruise)	281.6	K	M_fuel	0.00337	0.0034	0.1	M_fuel	0.00127	0.0012	2.4
PW_sh (Cruise)	8.38	kW	Turbines				Turbines			
Cp_gas (Cruise)	1242	J/(kg K)	T0.45	1080.9	1051.5	2.7	T0.45	1082.7	1077.4	0.5
k_gas (Cruise)	1.3	[-]	P0.45	262077.1	264596.1	1.1	P0.45	225922.3	224944.1	0.4
PR_c_cruise	2.7	[-]	T0.5	966.1	929.3	3.8	T0.5	971.5	961.1	1.1
V_cruise	27.8	m/s	P0.5	146921.5	144750.1	1.5	P0.5	129281.2	128392.3	0.7
M_cruise	0.06	kg/s	W_ct	58214.6	57140.2	1.8	W_ct	18436.7	18540.3	0.6
LHV	43.563	MJ/kg	W_pt	24858.6	24860.1	0.006	W_pt	8464.6	8470.2	0.1
Cp_air	1000	J/(kg K)	Nozzle				Nozzle			
k_air	1.4	[-]	Ts.9	886.8	850.3	4.1	Ts.9	893.3	880.2	1.5
η_mechanical	0.99	[-]	V8	445.1	427.6	3.9	V8	440.7	434.6	1.4
η_combustion	0.995	[-]	T_jet	77.2	74.1	4.1	T_jet	26.1	27.1	3.4
η_propellor	0.9	[-]	T_prop	1475.1	1447.8	1.9	T_prop	719.3	712.1	1.1

From this system test is is found that the GSP program produces accurate results for both design points. It was found that only small differences between the ideal cycle and the actual cycle were present, as all values are within 5% of another. The differences found between both models are caused by limitations on the simple cycle model, as it does not take bleed air, pressure losses and heat losses into account. For this reason, differences were especially found after the combustor stage, where the gas composition changed significantly. However, as determined by [55], the results can still be considered accurate enough to verify the GSP model with when within the 5% margin.

Validation of the engine model and design is conducted by comparison with reference engines. Due to the lack of test data during conceptual design, validation is performed using references to investigate whether the retrieved values are feasible in an actual designs. The reference engine and values used for this validation are the values retrieved from the TP100 engine as described by [2]. Similar input values were used in the GSP program, and compared with the actual output values as stated by the manufacturer[98]. The results of the validation procedure were, as expected, similar to the original values. No additional validation procedures of the GSP program were carried out, as the program has been validated by several institutions (NLR, TU Delft) before.

Finally, it is recommended for future preliminary analysis that also transient analysis (e.g. altering fuel flow with time) is estimated in GSP to check take-off acceleration and landing performance. It is suggested that additional engine performance settings are set to account for minimum take-off performance, climbing performance, and landing performance. Using the figures generated in Subsection 5.4.3, additional adjustments in the component design can also be performed if the engine is used to account for future technology improvements.

5.4.5. SUSTAINABILITY ANALYSIS

After the propulsion analysis described in section 5.4, a short overview of the sustainability characteristics of the engine is presented in this section. The sustainability of the engine design was focused on reducing engine noise, emissions and vibrations, with the purpose of elongating the lifetime of the engine and UAV, together with reducing the environmental impact of surveillance missions. Below each of the three parameters are described together with their results and further required analysis.

UAV NOISE

Four main aspects contribute to the noise level of SCULPTUR. Namely the propeller, aerodynamic noise, engine exhaust and engine vibration. Three of those are thus depending on the engine characteristics of the UAV which

[98] URL http://www.pbsvb.com/customer-industries/aerospace/aircraft-engines/tp-100-turboprop-engine [cited June 20 2016]

is therefore the main noise emitter[99].
In order to keep the noise as low as possible certain measures can be taken. It is important to reduce the noise with a minimum of performance, weight and economic disadvantages [95]. This includes reducing the the tip speed of the propeller, orienting the exhaust upwards and damping vibrations. Nonetheless is not possible to perform a noise level analysis of the UAV as part of the conceptual design. By means of extensive noise models and finally testing of the engine the requirement in the detailed design and development phase the **SCULPTUR-SH-21** noise requirement can be checked and validated. During testing also the aerodynamic noise will be included.

ENGINE EMISSIONS

The emissions of the engine were determined using the GSP model, of which the results are presented in the section before. From this engine analysis it was found that the required fuel consumption of the engine varied between 0.0012-0.0034 kg/s, showing fuel consumption which is more than 27 times lower than the fuel consumption of a general aviation aircraft. Similar results in exhaust gas composition were found compared to general aviation aircraft, with a maximum masspercentage of 6.5% CO_2 and 0.003% NO_x. With the reduction in both masspercentage and fuel consumption it can be safely stated that the ICAO advisory requirement has been met. Future analysis might be required on environmental impact of the engine emissions due to the low cruise altitude of the SCULPTUR UAV, this is recommended to consider during the detailed design phase.

ENGINE VIBRATIONS

As described in section 4.4.7, no quantifiable information is available on the vibrations of reference engines. It was therefore decided to not include engine vibrations in the conceptual design phase. In order to make an accurate determination of the engine vibrations, frequency and amplitude, a prototype will have to be produced and tested with the help of accelerometers and other specialised equipment. More detailed engine vibrations models might be used to provide an initial estimation, however detailed design is necessary to provide the parameters of the model. This was therefore found to be out of the scope of this project.

5.5. MATERIAL ANALYSIS

In this section the process that was used to choose the material for the UAV is explained. The material was chosen for the main structural components of the fuselage, the wing and the skin. First a study of different materials was performed, to give a good insight in their behaviour. In this study the focus was mainly on Aerospace variants of the different main material classes. With this behaviour the final materials for the UAV were chosen, which will be explained in the final section.

5.5.1. MATERIAL STUDY

The material study was mainly focused on materials that are optimised for aircraft structures. These materials require a combination of high stiffness, strength, fracture toughness, fatigue endurance and corrosion resistance[100], which optimally should be achieved with a low density. Furthermore it is important to know the cost, availability, manufacturing and environmental properties in order to make a well reasoned material selection [96]. The material study was performed in the two material classes that are used in aircraft structures; metals and advanced composites.

METALS

Metals and especially their alloys are the classic aerospace material since the 1930s. The main metal groups currently used in aerospace structures are aluminium alloys, titanium alloys and steels. Starting with the raw material their properties are changed by changing the alloy components and metal treatments. A general advantage of metal alloys is that most of them have existed for many decades, therefore their properties and long term behaviour is known and the material and the production processes have been optimised.

The most common aluminium alloys in aviation are Aluminium-Copper, Aluminium-Zinc-Magnesium and Aluminium -Lithium; the mixture influences the behaviour of the material during different load cases. During treatment, copper, zinc and magnesium react with the raw aluminium to create intermetallic precipitates which increase the strength and fatigue resistance. Furthermore small parts of manganese and chromium restrict the grain growth which increases the yield strength and traces of titanium reduce the grain size of the alloy. Finally silicon and iron reduce the viscosity and hot cracking respectively but their intermetallic particles with aluminium lower the fracture toughness and therefore its percentage is kept relatively low.
Al-Cu alloys (2000 series) are characterised by high strength, toughness and fatigue resistance which are especially useful in tension. Therefore, they are currently often used for fuselage skins, lower wing panels and control surfaces. Al-Cu-Zn alloys (7000 series) enriched with traces of other materials show higher strength performance than the 2000 series. Due to their better performance they are often used in high stress locations like the top panel of the wing but also stringers in the fuselage and floors. The added lithium in Al-Li alloys (8000 se-

[99] URL http://www.wolf-aviation.org/aircraft_noise.htm [cited June 20 2016]
[100] URL http://www.sciencedirect.com/science/article/pii/B9781855739468500030 [cited June 1 2016]

ries) reduces the density of the metal while increasing the Young's modulus. Adding too much lithium however influences the producability negatively.

Another common metal choice for aircraft are titanium alloys. Especially its specific strength, good fatigue resistance, creep resistance at high temperature and excellent oxidation resistance. Furthermore titanium can be used at higher temperatures than aluminium alloys. A major disadvantage however is the relatively high density and the high cost. Similar to the aluminium alloys, different titanium alloys also show different properties.
α titanium alloys are strengthened by work hardening, solid solution hardening and grain-size refinement. Aluminium is its main alloy element which is used to stabilise the α phase and to increase the creep and tensile strengths. Low creep resistance at high temperatures however can be found in β titanium alloys but the strength and fatigue properties are better than α alloys. α + β titanium alloys contain both α-Ti and β-Ti grains and its advantage are the combined positive properties.

Finally steel alloys are used as metal components in aircraft. Usually it is used in highly loaded locations of the structure since its material properties show high qualities with respect to strength, stiffness, fatigue and stainless steel furthermore has the advantage of being resistant to corrosion [96].

ADVANCED COMPOSITES

Advanced composites are composite materials in which fibrous materials are embedded in a resin matrix. Fibres are the primary load carrying element, but are only strong and stiff in the direction of the fibres. To approach quasi-isotropic behaviour, the orientation of the fibres can be adjusted. The resin matrix bonds all the fibres and transfers the loads. It keeps the fibres positioned, oriented, gives the composite environmental resistance, and determines the maximum service temperature[101]. Firstly different fibres will be discussed, followed by different matrices.

Although there are a lot of different types of fibres, the two most common are carbon fibres and fibreglass[102]. Between carbon fibres a distinction into five categories based on mechanical properties can be made. The categories range from low to ultra elastic moduli. In aircraft structures mostly intermediate and high modulus fibres are used[103], which is defined as an elastic modulus of at least 280 GPa and a tensile strength of 2500 MPa or higher. A benefit of carbon fibres is their very good fatigue and heat resistance[104].
Fibreglass composites are categorised based on their mechanical, electrical and chemical performance. To improve mechanical performance, S-class is the commonly used fibre, especially the S2-class. It has an elastic modulus of 86.9 GPa and a tensile strength of 4890 MPa [97]. However, it is difficult to improve the fatigue performance to acceptable level for aerospace applications [98].

Different materials can be used as a matrix in composites. Generally they can be divided into metal or polymer matrices. Furthermore thermoset of thermoplastic polymers can be chosen. For aircraft applications mostly polymer composites are used.
Using thermoset polymers as a matrix is already often done in current aircraft structures[105]. A lot of thermoset composites are made with epoxy resins as the matrix with the benefit of high strength and stiffness for low weight[106].
Using thermoset composites also has some drawbacks with respect to the production and end-of-life processes due to their characteristic of forming one molecule and shape after curing in an autoclave. Production is more difficult and more expensive because curing takes a long time, about 3 hours, and a lot of energy in the autoclave which results in a definite shape which can not be changed. Furthermore recycling those materials at the end-of-life is problematic since the matrix sets into one molecule when cured. Using certain techniques it is possible to recycle parts of the material but still a lot of material waste is produced [99]. A final production disadvantage is the machining because the shapes can not be changed and fibres would be deformed[107]. Finally the fatigue properties of thermoset composites allow for 25.000 load cycles before losing the main material properties. Adding nanoclay can increase this to around 35.000 load cycles [100].

Using thermoplastic polymers as a matrix in aircraft structures is a relatively new method of the last decade[108]. The material properties of thermoplastic composite are similar to thermoset composites[109], however there are differences in producability, operations and end-of-life, dictated by the thermoplastic behaviour of the matrix. Using thermoplastic polymers results in the following benefits. The production time and effort can be reduced

[101] URL http://www.faa.gov/regulations_policies/handbooks_manuals/aircraft/amt_airframe_handbook/media/ama_ch07.pdf [cited June 1 2016]
[102] URL http://www.automateddynamics.com/article/thermoplastic-composite-basics/types-of-fiber-reinforcement [cited June 1 2016]
[103] URL http://www.hexcel.com:82/pdf/Product%20Selector%20Guides/Aerospace_SelectorGuide [cited June 1 2016]
[104] URL http://www.carbonfiber.gr.jp/english/material/feature.html [cited June 1 2016]
[105] URL http://www.mhi-global.com/news/story/1212191607.html [cited June 1 2016]
[106] URL http://www.performance-composites.com/carbonfibre/mechanicalproperties_2.asp [cited June 1 2016]
[107] URL http://www.apexdesigns.net/carbon-fiber-manufacturing.html [cited June 1 2016]
[108] URL http://www.fokker.com/sites/default/files/media/Files/Brochures/Fokker_Thermoplastics.pdf [cited June 1 2016]
[109] http://www.tencate.com/advancedcomposites/product-compare-tool/TC1200.aspx [cited June 1 2016]

since the thermoplastic composites do not need to be cured in a autoclave which reduces the time to set the material and it is easier to produce into different shapes as it can be formed multiple times by reheating the material. Also combining different subparts is easier as simpler welding techniques can be used. Furthermore its recyclability is preferable over the one of thermoset composites. This can be done for thermoplastic composites by reheating them again, resulting in only 20% decrease in material behaviour[101]. Although they are still in development, already different applications of the thermoplastic materials can be found[110].
But there are also negative aspects of using thermoplasic composites. Their operating temperature range is limited and has immediate influence on the performance. Temperatures above the glass transition temperature will make the matrix soft. This influences positioning, orientation and loading of the fibres. This needs to be taken into account during designing to ensure the structural integrity of the UAV. Another downside is the limited knowledge due to the few existing applications in flying aircraft.
The most used thermoplastic matrices are PEI (Polyetherimide), PEEK (Polyetheretherketone) and PEKK (Polyetherketoneketone), depending on the application. A benefit of using PEEK is the fatigue behaviour. When exposed to many cycles, the material properties do not decrease too fast[111].

5.5.2. MATERIAL SELECTION

Choosing between those different materials and their combinations more than one solution could solve the problem of providing structural integrity by providing the necessary material behaviour for aircraft structures. In order to make a decision the design cost, sustainability and weight were chosen to be the main drivers. The weight also influences since lower weight results in lower thrust and emissions. As composites can give better strength and stiffness to weight ratios[112], composites instead of metals were chosen.

Choosing fibres needed to be done based on cost, fatigue and stiffness. Fibreglass is the cheaper option but carbon fibre has better fatigue properties. Their structural performance is similar but carbon fibres have better stiffness properties whereas the strength of fibreglass is higher[113]. The structural loads of SCULPTUR are relatively low, but stiffness is important to provide good flying characteristics. Since cost does not only depend on the fibres but also the matrix and the production methods, carbon fibres were chosen.

Finally the resin needed to be chosen. Again metals were discarded as their density is too high. So the choice could be made between thermoset and thermoplastic polymers. As explained in Section 5.5.1, thermoplastics have better production properties which also results in better recyclabiltiy at the end-of-life. With respect to fatigue resistance thermoset and thermoplastic polymers perform similarly. Initially the operating temperature of thermosets is higher than the one of thermoplastics but depending on the manufacturing and treatment the service temperature of thermoplastics can also be increased to handle in flight temperatures. A final criterion is the knowledge about the matrix. A lot more is known about thermosets, while the knowledge of thermoplastic composites in aircraft structures knowledge is not very extended. But as this design focuses a lot on sustainability and economic pricing, the advantages of the thermoplastic polymers weight up against the downside of not having extensive knowledge. Therefore a thermoplastic matrix was chosen which had to be optimised for temperature and structural integrity. The chosen polymer is PEEK[114].

To conclude, the main structural components of the fuselage and the wing and the skin will be made of Carbon Fibre Reinforced Polyetheretherketone (CF PEEK). The volume percentage of fibres can be determined for the amount of loads that have to be carried. In order to analyse the material properties the Ten Cate CETEX-TC1200 with AS-4 fibres was chosen. This is the CF PEEK that has enough stiffness to be a structural material. The material properties are given in Table 5.14[115].

[110] URL http://www.composites.nl/products/aerospace-structures/# [cited June 1 2016]
[111] URL https://ab-div-bdi-bl-blm.web.cern.ch/ab-div-bdi-bl-blm/Radiation/radiation_hardness/Victrex%20PEEK%20Properties_Guide.pdf [cited June 2 2016]
[112] URL http://machinedesign.com/materials/basics-aerospace-materials-aluminum-and-composites [cited June 2 2016]
[113] URL http://gwcomposites.com/carbon-vs-fiberglass/ [cited June 2 2016]
[114] URL http://www.ptonline.com/products/materials-peek-compounds-with-high-modulus-carbon-fiber [cited June 3 2016]
[115] URLhttp://www.tencate.com/emea/Images/CETEX-TC1200_DS_071515_Web_tcm28-3782.pdf [cited June 3 2016]

Table 5.14: Material properties Ten Cate CETEX-TC1200 PEEK AS-4

Property	Result
Tensile Strength (0°)	2280 MPa
Tensile Modulus (0°)	130 GPa
Poisson's Ratio	0.33
Tensile Strength (90°)	86 MPa
Tensile Modulus (90°)	10 GPa
Compressive Strength (0°)	1300 MPa
Compressive Modulus (0°)	124 GPa
In-Plane Shear Strength (±45°)	152 MPa
In-Plane Shear Modulus (±45°)	5.2 GPa
Density	218 gsm
Density (calculated)	1630 kg/m^3
Layer thickness (calculated)	0.134 mm
Glass Transition Temperature	143 °C
Melting Temperature	343 °C

5.5.3. PRODUCTION METHODS

As stated before, using thermoplastics has many advantages during the production process. Compared with thermoset composites the production requires higher but shorter temperatures to form the material. This section elaborates on the different production methods of the chosen material.

Ten Cate CETEX-TC1200 PEEK AS-4 can be obtained as carbon unitape with widths of 75 mm or 305 mm[116] which can then be manufactured differently. During fibre placement in situ consolidation the tape is heated and then applied with pressure by a roller onto the tool. The tool is beforehand produced with the correct shape of the final part. Once the material has cooled down it can be removed and it is ready to use. Furthermore it is possible to similarly produce a simple sheet of laminate by heating and applying the tape to an even surface and after cooling it can be heated again and pressed into the final form. The forming can be done using various methods like using vacuum or rubber forming. Finally compression molding can be used to produce internal beam structures. During molding multiple unitape layers are heated and pressed in a form. The laminate can then be thermoformed into the desired profile. During production different methods will be used for different sub parts of the UAV. Skin panels should be produced using fibre placement in situ consolidation whereas smaller parts and stringers and ribs can also be formed or molded.

Furthermore thermoplastic characteristics enable easier assembly techniques namely welding of different structural parts. Welding does not require intensive preparations like adhesive bonding nor does it have high stress concentrations due to mechanical fasteners[117]. Fusion welding is a promising assembly technique for thermoplastic structures. Especially resistance welding, induction welding and vibration welding produce strong welds [102].

The final production methods will be decided during the detailed design phase as part of the post-DSE steps as explained in Section 7.6.1 and Chapter 9.

5.6. STRUCTURAL ANALYSIS

To ensure the UAV will be able to cope with all the different loads during flight and ground operations, a numerical tool was used to determine how the loads act on the structure and which stresses they introduce. This information was used to design the structure of the UAV and ensure the structural integrity. In this section the methods to accomplish this are explained and the results are shown.

5.6.1. METHODS

To have good insight in the structural behaviour of the UAV, different steps have to be taken. These are explained in the sections below.

LOAD, SHEAR AND MOMENT DIAGRAMS

To be able to find the different loads, first a two dimensional model was made on which all the vertical forces during flight were analysed both in the fuselage and the wing. These were used to come up with the shear and moment diagrams of both wing and fuselage. For these two dimensional models several assumptions were made which are listed below:

- Only vertical forces are take into account
- Lift was taken from the Aerodynamic analysis, see Section 5.3.3

[116] URL http://www.tencate.com/emea/Images/CETEX-TC1200_DS_071515_Web_tcm28-3782.pdf [cited June 10 2016]
[117] URL https://tprc.nl/research-overview/welding-technologies/ [cited June 13 2016]

- Lift acts at quarter chord
- Lift acts over the whole span
- Lift is exactly equal the weight
- Weight of the wing is distributed with area ratio of the wing
- Weight of the fuel is distributed with area ratio of the wing
- Fuel tanks span from root to 80% of the span
- Weight of the fuselage is distributed equally
- Maximum endured load factors are -1 and 2.5, raised to -1.5 and 3.8 with a safety factor for ultimate loads
- No shear or moment is present at the tips of the wing or of the fuselage
- Components are assumed to be point loads

To analyse the wing the load diagram was integrated to come up with the shear diagram, as there is an elliptical distribution. For the fuselage the shear diagram can be made using locations and weights of the different components. For wing and fuselage the shear diagrams were integrated to come up with the moment diagrams. This is valid as can be seen in Equations (5.29) and (5.30) when using the proper boundary conditions. The fact that at the tips of both the fuselage and the wings no shear or moment can exist is used as a boundary condition. This results in the following diagrams (Figures 5.41, 5.42, 5.43, 5.44 and 5.45), shown for a load factor of 3.8.

$$\frac{\mathrm{d}V}{\mathrm{d}x} = q \tag{5.29}$$

$$-\frac{\mathrm{d}M}{\mathrm{d}x} = V \tag{5.30}$$

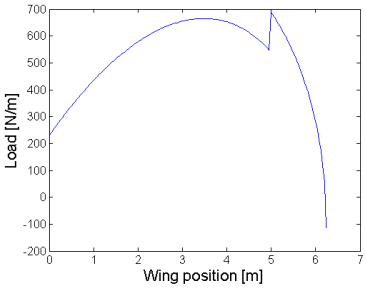

Figure 5.41: Load diagram wing

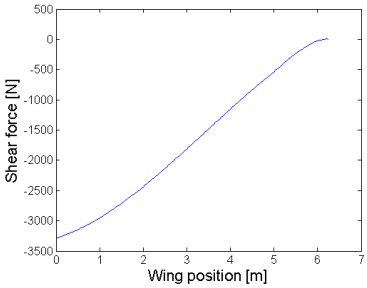

Figure 5.42: Shear diagram wing

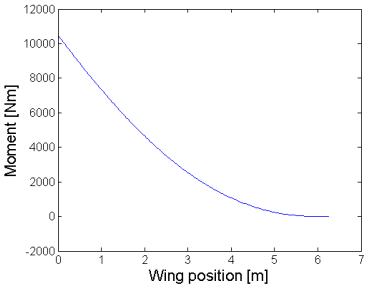

Figure 5.43: Moment diagram wing

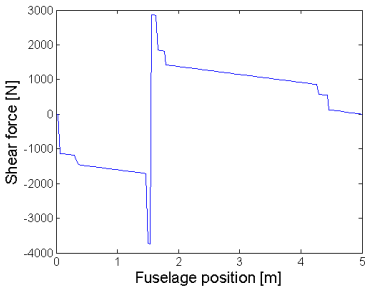

Figure 5.44: Shear diagram fuselage

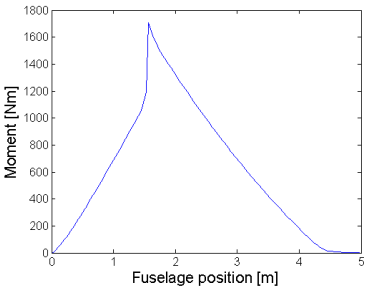

Figure 5.45: Moment diagram fuselage

This first part of the program is verified with hand calculations. To verify the wing loads, the lift is averaged and the order of magnitude of the shear and moment and their sign is checked. These turn out to be complying with the numerical model. Also the fuselage is verified. The shear shear diagram goes to 0 at the tips, and also all the forces sum up. The moment also goes to 0 on both tips and the order of magnitude and sign is correct. This verifies this part of the program.

Sensitivity is as expected for this part. By changing input loads, the structural behaviour changes, but always the program calculates the lift in such a way that the loads are carried. Depending on where loads increase, the distribution and maximum values will differ. Only the moment calculations in the fuselage are more sensitive to different inputs. Again it will calculate what will happen and includes a compensating moment to keep balance, only now the results are not correct, as this moment is not representative for what can be achieved in reality. The program will always try to solve, but when the inputs make no realistic sense, this solution is incorrect although matematical correct. The balance of the fuselage is calculated with the Class II estimation and changing this will give strange and wrong results. Thus, changing inputs gives no problems and as can be seen later the margins are so high that they will not influence the design. However, the set of loads has to be correct to give good results.

3D ANALYSIS

To do the 3D analysis different stresses have to be found and combined to determine the maximum stress in the structure and see if this is possible within the ranges of the material. Bending, shear and torsion were taken into account in this analysis. After the first iteration, the information was used to optimise the structure with respect to the weight.

To be able to model in 3D another set of assumptions was used to approach the problem. These are stated below:

- The wingbox is a rectangular box fitting the airfoil, with a height of 0.07 chord and a length of 0.5 chord
- The thickness varies stepwise along the wingspan
- The fuselage has a circular cross section with constant thickness
- Thicknesses are multiples of 4 material layers to ensure quasi-isotropic behaviour
- Quasi-isotropic material behaviour enabling use of Von Mises stress
- Torque induces a constant shear flow
- X runs along the fuselage, Y runs along the wing and Z runs down the aircraft
- The shear and moment diagrams are used as an input

Now the structural analysis can be done. This is an iterative process in which the output is the final weight and used as a new input for the following iteration. Structural performance is optimised for weight, by playing with skin, spars, stiffeners and ribs. The program is used to come up with the final design shown in the following section.

The program contains several sections. All different locations of the fuselage are defined in X, Y and Z. This was verified by plotting the points and checking visually if the shapes of the fuselage and wing are as designed. Next the moments of inertia of all the sections were calculated. For this the wing and fuselage were sliced in length directions to comply with the shear and moment diagrams. For every slice the moment of inertia was calculated with Equation (5.31). This was verified by calculating the moment of inertia by hand at different locations, with thin-walled approximations. All locations turned out to have the right moment of inertia within 5% margin, verifying this part of the program.

$$I = \int r^2 dA \tag{5.31}$$

After this was done, the different stresses could be calculated. First the bending stress was calculated. This was done with the general bending formula given in Equation (5.32), in which both the fuselage and the wing bend in the Z-direction. Also this part had to be verified and this was done with a simpler 2D program in which the stresses are plotted along the span and the fuselage. Both the shape of the stress distribution and the maxima were compared. Since these were approximately the same, the program was verified. Also on the 3D plot, visually it was checked if the 3D pattern of the stress distribution was as expected and this was indeed the case.

$$\sigma = \frac{Mz}{I} \tag{5.32}$$

The next part of the program calculated the shear flow through the fuselage and the wing. In addition, it included the torque on the wing resulting from the lift not acting at the centre of gravity of the wingbox. The shear was calculated with Equation (5.33) for shearflow and torque was added as a constant shearflow onto that, by use of Equation (5.34). This was divided by the thickness to give the resultant shearstress. This program was again verified with a 2D model that calculates the maximum shearstress at spanwise and fuselage locations. The 3D model was within a 5% margin of the 2D model and the shape and location of the peaks was completely similar. This verified the shear part of the program.

$$q_b = -\frac{S_y}{I_{xx}} \int_0^s t y ds \tag{5.33}$$

$$T = 2Aq_c \tag{5.34}$$

The following step of the stress analysis was summing up the stresses with the Von Mises equation as can be seen in Equation (5.35). Looking at the locations of the maxima and checking their magnitudes verified the 3D Von Mises model. The fact that Von Mises was used, although the structure is made of composite is reasonable, as the composite is in a quasi-isotropic configuration.

$$\sigma_{VonMises} = \sqrt{\sigma^2 + 3\tau^2} \tag{5.35}$$

Sensitivity of the stress calculations is similar to the shear and moment diagrams. As they serve as an input for the shear forces and moments used for the stresses, changes in the inputs influences the stresses in a similar matter.

The last step of the program was to calculate the buckling load. This buckling load is dependent on the moment of inertia and will later be used to see how much the moment of inertia has to be raised to keep the loads within the buckling loads. The formula used for buckling is for one sided clamping and can be seen in Equation (5.36). This was verified by a hand calculation of the buckling load for a given moment of inertia and gives indeed the same result.

$$P_{cr} = \frac{\pi^2 EI}{4L^2} \tag{5.36}$$

5.6.2. FINAL PRELIMINARY DESIGN

With this information of the stresses the more in depth design can be made. First this section will focus on the wing and the important design parameters there and then it will continue with the fuselage. In this section the final results of the iterations are presented, which were used as a final input to the 3D model to show final behaviour.

The wing was designed as a rectangular box which is load carrying. The thickness of the wingbox varies over the span. As more thickness is necessary at the root, the thickness is the highest at this position. The variation is in discrete steps as composites with quasi-isotropic behaviour have four layers or multiples of this[118]. The wing is divided in four equal parts, on which between section 2 and 3, and 3 and 4 there is a decrease in thickness. This results in a variation of the thickness from 0.535mm at the tip to 2.140mm at the root, which can be seen to be enough to deal with the loads. This is presented in Table 5.15. Although a constant thickness of 0.535mm would be sufficient, then the impact resistance would go down enormously, which is not wanted at parts where fuel tanks are. The difference in weight would be around 20kg for the both wings combined. So although the total weight is high, still this option of variable thickness is preferred to protect the fuel tanks. The reason the 3rd section has slightly thinner skin than 1 and 2 is to make the increment not to big to avoid to much stress concentrations. The thickness of more than 2mm is determined based on impact testing as can be seen on 2mm plate impact tests [103].

The following thickness that has to be determined is of the airfoil outside of the wingbox. This is not load carrying but should still be able to remain shape. For the trailing edge, with no risk of impact, it can be calculated that the minimum thickness of 0.535mm is enough for this function. The leading edge has most risk on impact. This is why a thickness of 2.140mm is used.

The next part of the design is the amount of stiffeners. Although the structure of the wingbox is strong enough to manage the loads, the compression will induce buckling. To ensure structural rigidity, the amount of stiffeners that deal with the buckling has to be determined. Stiffeners are added to enlarge the moment of inertia, getting the whole wing stiffer and more resistant against buckling. For this a part of the program compares the loads in the wingbox with the buckling load and optimises the moment of inertia with the amount of stiffeners to be stiff enough. This ensures good behaviour in terms of buckling. Again loads at the root are much higher, so more stiffeners are necessary. The area of a single stiffener is $2.568*10^{-4}$ m^2 (6cm length with 32 layers of composite). Combining this all results in the following amount of stiffeners, shown in Table 5.15. For the top panel this is much more as for the bottom panel, as the maximum load factor is 3.8 and the minimal -1.5.

The last that has to be determined is the rib spacing. The ribs do not cross the wingbox, but ensure the shape of the wing for the leading and trailing edge. The spacing is mostly dependent on the speed and wing loading of the aircraft as it influences the amount of tension in the skin by the pressure differences of the lift generating surface. It is because of this reference can be used for the ribspacing. A ribspacing of 38cm is appropriate for this UAV's speed and weight [104].As the stresses will not go close to the yield strength, and no impact resistance is necessary for the ribs, the thickness is chosen to be the minimum, namely 0.535mm. The total design of the wing can be found in Table 5.15.

The result is a total wing weight of 124.1 kg. This is much higher than the Class II weight estimation and because of the big difference this should be explained more. The problem is that the Class II weight estimation is based on commercial aircraft and in this case with this small take-off weight, namely Cessna like aircraft. These have small wingspans which give different wings. Although the total weight of the skin and wingbox is low, still the weight goes up enormous because of the stiffeners. Because the wing is so long and slender, stiffeners are necessary to help against the buckling and over this length this immediately increases the weight a lot. To keep the aircraft flying, this is necessary, but the weight does not compare to the Class II weight estimation. Furthermore, the reader needs to keep in mind that the Class II weight estimation gives an initial overview of the weights of the main components of the UAV. The stability calculations are now based on said Class II estimation. However,

[118] URL http://www.compositesworld.com/blog/post/qiso-fabric-for-tooling [cited June 13 2016]

more precise weights are found in this structural analysis. For the stability, the new weights have an influence. In the detailed design phase stability should be computed again based on this last iteration.

Table 5.15: Wing design parameters

Section	Wing box thickness [mm]	Leading edge thickness [mm]	Trailing edge thickness [mm]	Amount of stiffeners top / bottom panel [-]	Area of stiffeners [m^2]	Rib spacing [m]	Rib thickness [mm]
1	2.140	2.140	0.535	17 / 7	$2.568*10^{-4}$	0.38	0.535
2	2.140	2.140	0.535	12 / 5	$2.568*10^{-4}$	0.38	0.535
3	1.605	2.140	0.535	6 / 3	$2.568*10^{-4}$	0.38	0.535
4	0.535	2.140	0.535	2 / 1	$2.568*10^{-4}$	0.38	0.535

The final Von Mises stress can be seen in Figure 5.46. It can be seen that the torque of the wing bends the stress lines a little. Also the stress gets distinctively lower at the part where the wingbox increases thickness. With a load factor of 3.8 the stresses are well within the allowed stresses of the material, with a peak value of 37.8 MPa.

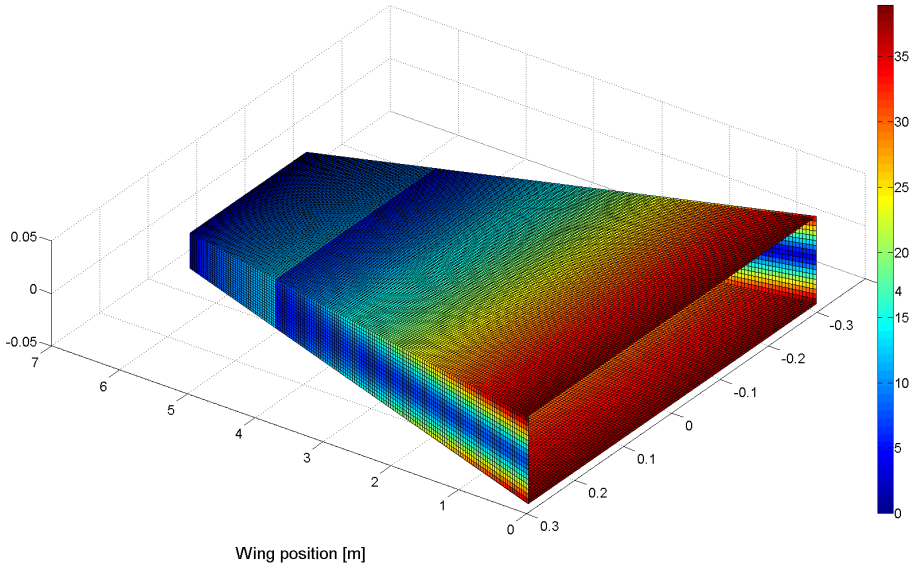

Figure 5.46: Von Mises stress wing [MPa]

For the design of the fuselage two distinctive cases have to be considered. The first is when the aircraft is in flight and the lift is generated at the wing. The second is when the aircraft is on the runway, supported by the landing gear, with maximum loading. The design is done as follows. First a proposal is made, and this is checked whether or not the both cases are structural integer.

For the "fuselage during flight" analysis the thrust is assumed to be maximum, so during an acceleration. As the fuselage has a circular shape, the first parameter that has to be designed is the thickness of the fuselage. To be able to give some impact resistance, the fuselage is chosen to be a total of 8 layers, so 1.070mm in total thickness. This is not complete impact resistant, but this is allowed as the fuselage has no extreme risk of getting impacted directly. Only the bottom and the nose will have more thickness, as there the chance on impact is higher. When the analysis was performed it turned out this thickness is sufficient to deal both with the loads and provide enough stiffness against buckling. So impact resistance is driving the thickness and no more extra stiffeners are necessary. The fuselage only gets an additional four tracks inside of 4 cm^2 each, to which different components can be attached.

Now the stress analysis can be done, and this results in the following Von Mises stress through the fuselage as can been seen in Figure 5.47, with a load factor of 3.8. Again the stresses stay well within the range of allowable stresses, with a highest stress of 4.2 MPa.

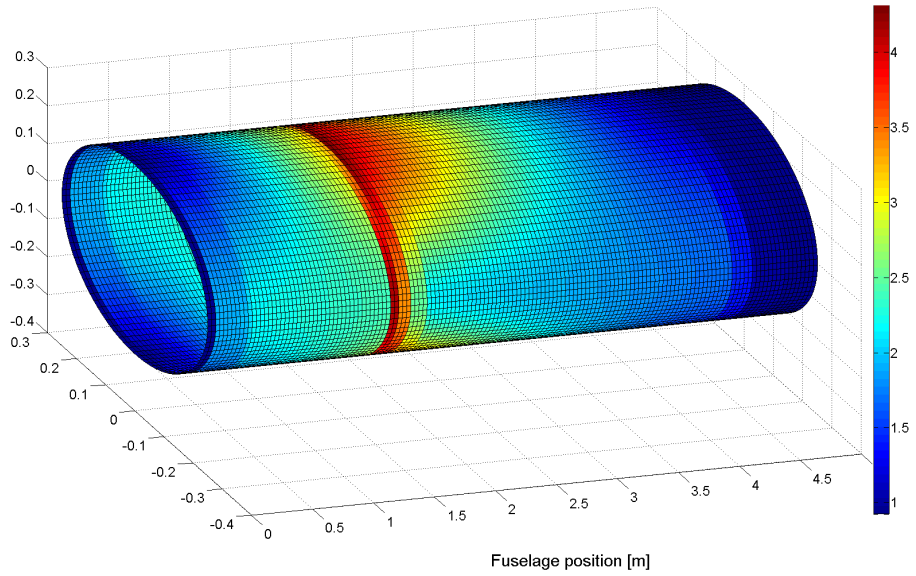

Figure 5.47: Von Mises stress fuselage in flight [MPa]

It can be seen that for the fuselage shear stress is more dominant in some parts of the structure than for the wing. This goes in very discrete steps because of the model, but the maximum values still give good insight on the behaviour of the fuselage. As expected near the wing there is most bending and also the most shear as there the lift acts to counter all the other downwards forces.

The next is checking if the fuselage is still structural integer when the loads are different, because of the landing gear. This has to be checked for strength and stiffness. A load factor of 3.8 is assumed to comply with the requirements. And again maximum thrust is assumed for the tension of the engine during take-off. This results in the following distribution of the stress as can be seen in Figure 5.48.

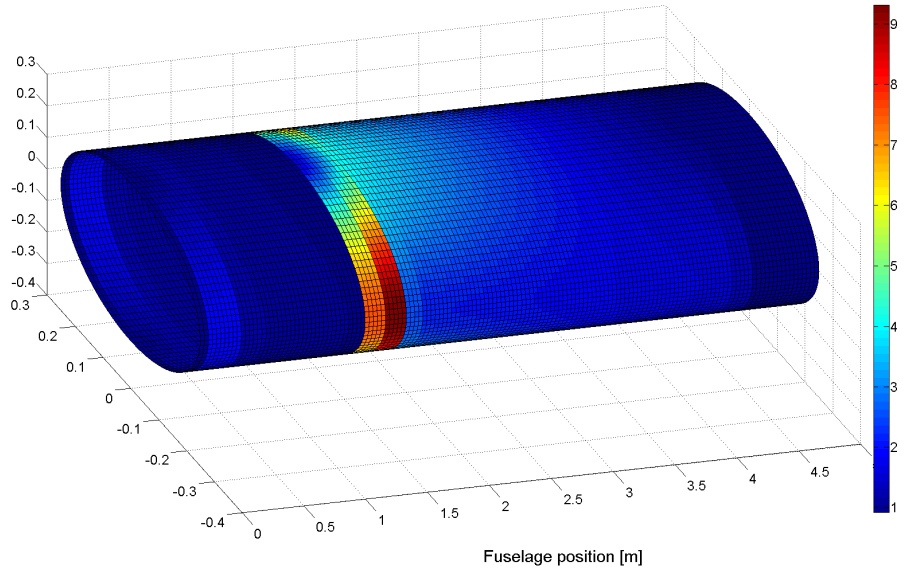

Figure 5.48: Von Mises stress fuselage with gear [MPa]

Also here it performs well within the material properties. Now the shear is completely dominant. Between the wing and the main gear there is a lot of shear as the whole weight of the wing and the fuel is transported to the main gear. But these stresses are still within the material properties easily, with a highest value of 9.1 MPa.

The total weight of the fuselage is 30.7kg, well within the budget of the Class II estimation. This is wanted, because now the total weight of the structure is not deviating a lot from the Class II estimation. As can be seen indeed the estimation is more precise for the combined weights than for a single subsystem weight. An overview of all the design parameters of the fuselage can be found in Table 5.16.

Table 5.16: Fuselage design parameters

Parameter	Value
Fuselage thickness [mm]	1.070
Nose thickness [mm]	2.140
Bottom thickness [mm]	2.140
Amount of rails [-]	4
Area of rails [cm^2]	4

FATIGUE

Now that all the maximum stresses are know it is important to check how long the material will be able to deal with these loads. Because of all the cycles, fatigue will become a factor in the life time of the UAV. These cycles are not introduced by pressurisation Because the stresses are reasonably low the material will not endure a lot of fatigue. As can be seen on the graphs of the fatigue behaviour [105] the material will be able to endure more than 10^5-10^6 cycles. This is for stresses of 400 MPa, insinuating that this structure will live even longer.

5.6.3. DETAILED DESIGN

For further design in the next phase still some more aspects have to be taken into account. In this section a small future proposal is done of what still has to be designed.

For the fuselage and the wing it is important to look at how the forces are transported between them, so how the wing is integrated in the fuselage. Now everything is assumed to be point loads to get a preliminary approximation of the all the forces and moments, but this has to be designed more in depth. As can be seen the loads that have to be transported are low and well within the margin of the material, so no problems are expected for this part.

Another part that still has to be designed is the tail. This is quite general, but the hard part is that it is quite big, which can result in a higher weight than expected. Already a part of the weight is accounted for, but if it is increased it has some influence on the balance and the stresses. But as the fuselage is mainly driven by impact resistance and the thickness is easily thick enough to hold a lot more loads, within the structures no problems are expected when the tail is added.

Next that has to be designed is the integration of the gear. The weights of the gear are approximated well, so only the integration has to be designed. This should be possible and also here no major problems are expected as the margins are high.

The last that has to be looked into is the separation of the wing. This is necessary for the operations and will be possible, as it is possible on glider aircraft with similar weights [119].

Also in the following phase the validation will become a big part of the process. Until now all the parts are verified, but this is still done on other analytical methods. During the detailed design parts will be produced and validation tests will be performed to test if the parts indeed perform as calculated.

[119] URL http://www.alexander-schleicher.de/en/flugzeuge/ask-21/ [cited June 24 2016]

6 Budget Analysis

When a new customer enters an undeveloped market, he will be presented with multiple solutions, all of which can fulfil the design requirements. The customer is thus faced with a dilemma, meaning he can not only base his decision on the actual performance of each of the designs. While there will be clear differences between the designs, the credibility and amount of data available for each of them, it is often the case that his final decision will be based on cost. This Chapter deals with cost estimation which is a largely statistical process, the final cost being dependant on the actual costs of prior UAVs.

6.1. Financial Analysis

The ideal stages of the life-cycle of an UAV are development, manufacturing, operations and disposal. Their relative contribution to the life-cycle cost is presented in Figure 6.1. The contribution of the airframe size and the maximum take-off weight on the cost in the case of small UAVs is generally low: software and avionics are more significant. It is a usual approach during cost modelling to not consider the disposal stage therefore it will also be neglected during this analysis. A good estimate for the disposal costs would most likely be obtained from the company that bought the UAV; various companies will replace the SCULPTUR with a new model after a different amount of time.

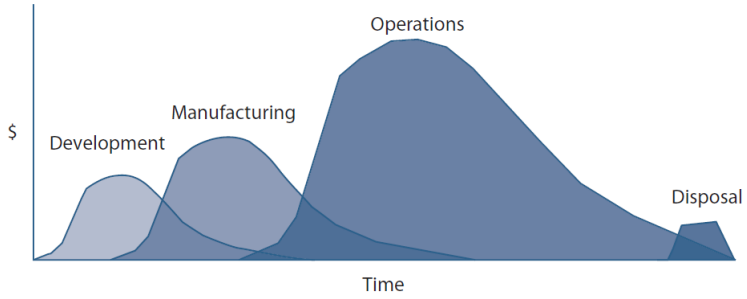

Figure 6.1: UAV life-cycle cost phases [18]

6.2. Budgets & Resources

It is essential to recognise that initial bottoms-up cost estimates should never under any circumstances be considered to be correct. These estimates are generally focused on the best-case scenario without taking into account uncertainties that might arise. For this conceptual design phase, it is advisable to use so called realism factors to account for these uncertain cost drivers (typical values in order of 2-3)[18]. Even with such a factor, it is difficult to take into account things such as inflation, fuel price increases, requirements changes as the design matures or other external factors. All the costs presented in this chapter for all the phases are notional, though they can be considered to be representative for the design phases of typical UAV programmes.

6.2.1. Development costs

Development costs refer to the capital invested during the conceptual, preliminary and detailed design stages. It is considered a “non-recurring” cost, meaning that after the development phase, there will be no additional costs involved unless any improvements are required. This stage is meant to mature the design such that it is ready for production and to demonstrate that its capabilities are adequate to perform the mission.

- Design
- Procurement
- Materials
- Tooling
- Parts fabrication
- Assembly
- Development tests
- Integration
- Documentation and drawings

It is very difficult to obtain an accurate value for the development costs as it differs from company to company based on the resources available. As an initial estimate, the development cost can be calculated using the method from [106], the Eastlake model. All the main contributions to cost are estimated using Equations (6.1) - (6.5) which depend on the empty weight, maximum velocity, number of flight test aircraft together with the

wrap rates of the employees (hourly salary + benefits, overhead and administrative costs).

$$C_{ENG} = 2.0969 \cdot H_{ENG} \cdot R_{ENG} \cdot CPI_{2012} \tag{6.1}$$

$$C_{DEV} = 0.06458 \cdot W_{airframe}^{0.873} \cdot V_H^{1.89} \cdot N_P^{0.346} \cdot CPI_{2012} \cdot F_{CERT} \cdot F_{CF} \cdot F_{COMP} \cdot F_{PRESS} \tag{6.2}$$

$$C_{FT} = 0.0096463 \cdot W_{airframe}^{1.16} \cdot V_H^{1.3718} \cdot N_P^{1.281} \cdot CPI_{2012} \cdot F_{CERT} \tag{6.3}$$

$$C_{MFG} = 2.0969 \cdot H_{MFG} \cdot R_{MFG} \cdot CPI_{2012} \tag{6.4}$$

$$C_{QC} = 0.13 \cdot C_{MFG} \cdot F_{CERT} \cdot F_{COMP} \tag{6.5}$$

The total research, development, test and evaluation costs can be summarised in Equation (6.6). It is composed of the engineering costs, development support (overhead, facilities, administration), flight test operations, manufacturing costs and quality control. F_{CERT} is the certification constant, being equal to 0.5 in the case of SCULPTUR which can be classified as a LSA (Light-sport aircraft) since it has a MTOW lower than 600 kg. F_{CF} describes the complexity of the flap system (=1 in the case of a simple flap system) while F_{COMP} is a factor to account for the use of composites. Finally, F_{PRESS} is also equal to 1 since SCULPTUR is an unpressurised UAV. A typical wrap rate for engineering (R_E) is \$59.10 and for manufacturing the test prototype (R_M) \$50.10 [40]. A significant additional cost during the development stage included in this analysis as well is the cost of the avionics (typically \$4500 for LSA) [106].

$$RDTE = C_{ENG} + C_{DEV} + C_{FT} + C_{MFG} + C_{QC} + C_{avionics} \tag{6.6}$$

Table 6.1 summarises the results of the development cost. A detailed design for SCULPTUR in order to make it certifiable will cost around \$739,890. The only stakeholder requirement regarding cost for SCULPTUR (SCULPTUR-SH-31) is that it should have a development cost lower than 3000 €/kg (empty weight cost per unit mass). With an operational empty weight of 221.7 kg and with a current euro to dollar conversion factor of 1.14, this results in a maximum development cost of \$758,344. This means that the requirement is satisfied, the actual development cost being 2.50% less than the one specified by the requirement. It is also important to keep in mind that this method was developed for General Aviation aircraft and not for UAVs; the actual development cost could even be lower since the number of tests required. The type and amount of tests could also be reduced in some cases if already proven off-the shelf items (payload - cameras, radars) are used.

Table 6.1: Development cost

Cost	Symbol	Price [$]
Engineering	C_{ENG}	447820
Development support	C_{DEV}	36350
Manufacturing	C_{MFG}	230070
Quality control	C_{QC}	14950
Flight test	C_{FT}	6200
Avionics	$C_{avionics}$	4500
Total	**RDTE**	**739890**

6.2.2. MANUFACTURING COSTS

The unit flyaway price (UFP) is the amount of money that a customer has to pay for everything that has to leave the ground with the exception of fuel. Remembering that the OEW includes everything with the exception of fuel and payload, it is known that the cost per pound of empty weight in the case of UAVs is \$1,500/lb in \$FY04 (according to the OSD UAV roadmap [18]). With that known, the total cost of the OEW can be estimated using Equation (6.7).

$$C_{AV} = \$1,500 \cdot W_E \cdot CEF \tag{6.7}$$

When using older cost data it is important to account for inflation by using a cost escalation factor (ratio of the costs of today to the cost of back then). It can be computed using Equation (6.8).

$$CEF(TY) = \frac{CPI(NOW)}{CPI(TY)} \tag{6.8}$$

The annual average consumer price index in 2004 was 188.9 [18] while as of January 2016, the CPI is equal to 236.916 [120]. This means that the cost escalation factor is equal to 1.25. With the CEF now known and the OEW already determined during the Class II Weight Estimation (Section 4.5), it is now possible to calculate the cost of the OEW using Equation (6.7), arriving to a final value of \$ 1,034,846.

[120] URL http://inflationdata.com/Inflation/Consumer_Price_Index/HistoricalCPI.aspx?reloaded=true [cited April 26 2016]

As a verification step for this simple analysis, the method from Technomics [107], a more precise alternative, can be used to estimate the cost of the entire UAV, including the fuel and payload costs. There are two way to compute the unit flyaway price: first the more traditional method where the cost depends on the maximum takeoff gross weight (Equation (6.9)) and second a method where the cost is dependant on the payload capacity and endurance (Equation (6.10)).

$$C_{AV1} = \$12,550 \cdot W_{TO}^{0.749} \cdot f_{Prod} \cdot CEF \tag{6.9}$$

$$C_{AV2} = \$118,750 \cdot \left(E_{Max} \cdot W_{PL}\right)^{0.587} \cdot e^{[-0.010 \cdot (FF_{Year} - 1900)] \cdot f_{Prod}} \cdot CEF \tag{6.10}$$

where FF_{Year} is the year when the first flight will occur, E_{Max} is the maximum endurance calculated in hours and f_{Prod} is a factor which distinguishes between a production unit or a demonstration unit. With the first method, a production cost of $3,181,807 is obtained while the second gives a final value of $5,495,544. Since these statistical methods are based largely on military UAVs where the payload used (weapons, sensors, cameras) is much more expensive than for civil UAVs, it can be concluded that the first method can be considered more accurate since it is dependant more on the maximum take-off weight rather than on the payload weight. A profit margin of 5% is a typical value used for UAVs and can be used as a first order estimate hence the price that SCULPTUR will be marketed at is $3,341,000.

6.2.3. OPERATING COSTS

It is important to also analyse what are the cost estimates from a potential buyer's point of view in order to highlight SCULPTUR's competitive market position. Such an analysis can help them determine whether or not SCULPTUR is a viable solution. The cost of ownership is in almost all situations much higher than the purchase price, especially when considering the entire life cycle of the product, as can be seen in Figure 6.2. Good management understands that there are both visible and hidden costs to take into account when ultimately making a decision on a product; this section serves as an indication of what these hidden costs might be. Operating costs can be broken down into direct and indirect operating costs.

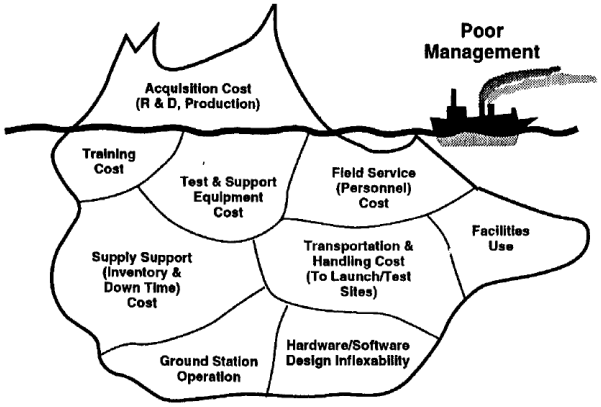

Figure 6.2: Designing for life cycle - Purchase vs Ownership Costs [34]

DIRECT OPERATING COST

Direct operating costs (DOC) includes all costs which are associated with and are dependent on the type of UAV being used and would change for different aircraft. These can be subdivided in three main parts [108]:

- Flight operation costs
  - Fuel and oil
  - Airport and en-route charges
  - UAV insurance
  - Flight crew salaries and expenses
  - Rental/lease of flight equipment/crews
- Maintenance and overhaul costs
  - Engineering staff costs
  - Spare parts consumed
  - Maintenance administration
- Depreciation and amortisation costs
  - Flight equipment
  - Ground equipment and property
  - Development cost and flight crew training amortisation
  - Extra depreciation (to account for any potential deviation from the historic cost depreciation)

All of these will be elaborated upon below together with an initial estimate.

MAINTENANCE COSTS ($ PER YEAR)

The most important part of this category is the maintenance personnel direct labor cost which can be calculated using Equation (6.11).

$$C_{AP} = F_{MF} \cdot R_{AP} \cdot Q_{FLGT} \tag{6.11}$$

where F_{MF} is the maintenance to flight hour ratio (Equation (6.12)), R_{AP} the hourly rate for a Airframe & Powerplant mechanic (maintenance engineer from Table 6.2) and Q_{FLGT} the yearly flight hours.

$$F_{MF} = 0.30 + F_1 + F_2 + F_3 + F_4 + F_5 + F_6 + F_7 + F_8 \tag{6.12}$$

where the F coefficients describe certain features of the UAV (integral fuel tanks, complexity of the flap system, UAV weight, type of landing gear etc). All the values are taken from [106] with SCULPTUR's design in mind.

STORAGE COSTS ($ PER YEAR)

The yearly storage cost can be calculated using Equation 6.13.

$$C_{STOR} = 12 \cdot R_{STOR} \tag{6.13}$$

where the storage rate for general aviation aircraft is approximately $250 per month [106].

FUEL COSTS ($ PER YEAR)

Fuel and oil costs play a major role for the flight operation costs; they vary depending on the type of UAV, the thrust and number of engines. It is also not entirely correct to assume a constant fuel consumption since, during operation, factors such as wind conditions, cruise altitude, changing routes etc frequently change. Besides fuel, there is also oil to consider however the oil consumption is negligible. These can be calculated using Equation (6.14).

$$C_{FUEL} = \frac{BHP_{CRUISE} \cdot SFC_{CRUISE} \cdot Q_{FLGT} \cdot R_{FUEL}}{6.5} \tag{6.14}$$

INSURANCE COSTS ($ PER YEAR)

Insurance cost is difficult to estimate and is only disclosed to individuals by the insurance companies. It usually depends on factors like the type of UAV, pilot credentials, price of aircraft etc. For an initial estimate, Equation (6.15) can be used.

$$C_{INS} = 500 + 0.015 \cdot C_{AV1} \tag{6.15}$$

where C_{AV1} is equal to the marketing price of the UAV.

INSPECTION COSTS ($ PER YEAR)

Inspection cost is mainly dependant on the engine which requires regular overhaul. It is generally accepted that inspection can be amortised (spreading of capital expenses related to intangible assets over a specific period of time) over the amount of time the UAV flies [106].

$$C_{INSP} = \$500 \tag{6.16}$$

FLIGHT CREW COSTS ($ PER YEAR)

Typical salaries are listed in Table 6.2. Equation (6.17) presents the flight crew costs.

$$C_{Operators,Dir} = N_{Operator} \cdot Q_{FLGT} \cdot R_{Operators} \tag{6.17}$$

It is assumed that three operators are hired per day in order to account for the 20 hour long endurance missions.

Table 6.2: UAS support labor rates, 2001-2006 [18]

Labor category	GSA rate, $/hr
Operations director	126.47
Operations engineer	95.70
Mission manager	119.85
UA operator/pilot	89.90
UA maintenance technician	59.91
Sensor operator	77.90
Program manager	154.50
Project leader	125.86
Technical specialist III	128.52
Technical specialist II	95.72
Technical specialist I	73.33
Technical editor	90.39
Technical media specialist II	82.05
Technical media specialist I	49.68

SPARES COSTS ($ PER YEAR)

Besides the general costs for labor and the cost of spare parts, consumable materials (engine filters, spark plugs, composite repair materials etc) also need to be taken into account as it can bee seen in Equation (6.18).

$$C_{spares} = F_{spares} \cdot C_{ops} \tag{6.18}$$

where F_{spares} can be taken as 12% according to Roskam [79].

The total direct operational cost of a SCULPTUR UAV is the sum of all the previously mentioned components. Table 6.3 summarises the results of the direct operational cost.

Table 6.3: Direct operational costs

Cost	Symbol	Price [$/year]
Maintenance	C_{AP}	6614
Storage	C_{STOR}	3000
Fuel	C_{FUEL}	830
Insurance	C_{INS}	48227
Inspection	C_{INSP}	500
Operator	$C_{Operators,Dir}$	45310
Spares	C_{SPARES}	14042
Total	**RDTE**	**839720**

INDIRECT OPERATING COST

Indirect operating costs (IOC) concerns costs that are not dependent on the type of aircraft being used. They also depend very little upon the aircraft design and thus are harder to estimate with statistical relationships (better to obtain from the company itself). These could be divided as follows:

- Station and ground expenses
  - Ground staff
  - Building, equipment, transport
  - Any handling fees paid to other third parties
- General and administrative
- Other operating costs

A rough approximation according to [40] is to take indirect operating costs equal to the direct operating costs.

6.2.4. BREAK EVEN POINT

A typical development phase is presented in Figure 6.3. For any aerospace project, whether it is related to aircraft or UAVs, there are significant costs involved before even the first revenues are received. The design, development and the arrangement of the manufacturing processes and assembly lines is a very costly phase. This means that the company also develops a huge deficit, and only after a couple of years (4 years in the case presented in Figure 6.3) revenues start coming in.

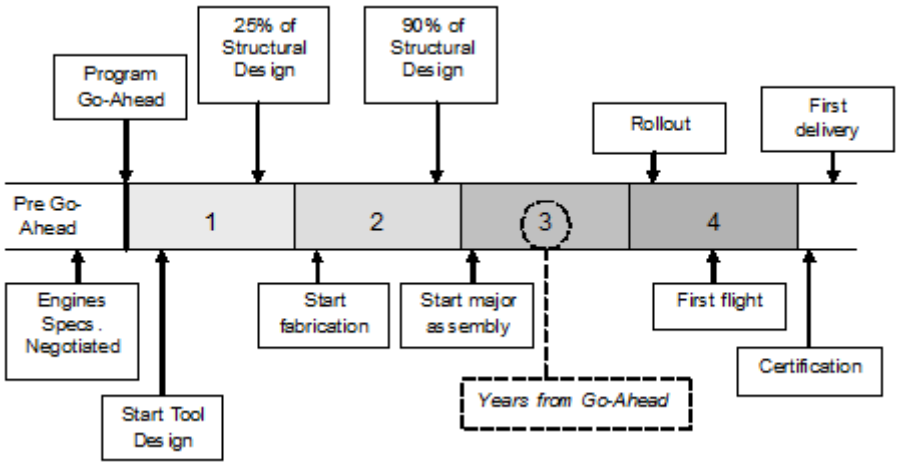

Figure 6.3: Schematic picture of milestones in the development of a new aircraft [109]

After the first UAV is sold, many years still have to go by in order to cover all the costs. The point where the expenses (development cost + production cost) and revenues are equal, the so-called Break Even Point (BEP), can be used to identify this milestone. It is shown in Figure 6.4.

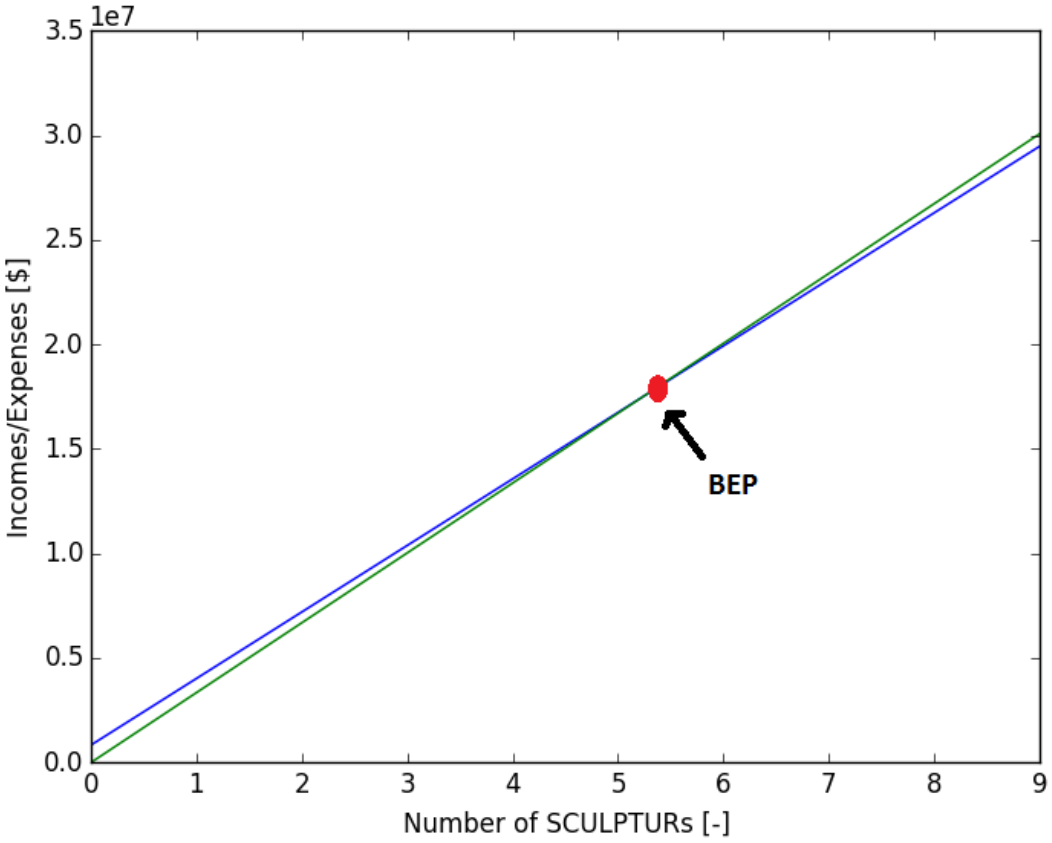

Figure 6.4: Incomes/Expenses for number of SCULTPURs sold

The first line with the lower slope represents the costs that are incurred from the development and production of SCULPTUR. It does not start at zero due to the development costs that are non-recurring and arise even before the first UAV is sold. The second line represents the income received from the sales of SCULPTUR. After six UAVs (break-even point), profits starts coming in (income greater than expenses).

6.2.5. RETURN ON INVESTMENT

A Benefit Cost Analysis (BCA) is done not only to determine if a certain policy is a sound investment but also to provide a basis for comparing different options. In order for a policy to be approved and accepted by shareholders, the total discounted benefits must cover the total discounted costs (investment, maintenance, construction, operation costs). A BCA, which for company managers represents a basis for comparing projects, is a very detailed analysis and is beyond the scope of this report. An important parameter however that can be calculated at this stage is the return on investment (benefits that an investor receives from spending resources on a particular product). It can be used to determine if the profits outweigh the amount of money invested thus the efficiency of an investment. This can help potential buyers determine if SCULPTUR is a viable solution for them.

An annualised rate of return can be calculated using the online calculator from [121] which allows for the comparison of different investments. It is assumed that within the first year after development, the first ten SCULPTUR UAVs will be sold to petrol companies in Australia, which results in a rate of return of 2.0%. This is a positive value, meaning that the business concept is profitable.

6.2.6. COST BREAK-DOWN STRUCTURE

The Cost Break-down Structure (CBS) is an AND tree that can be used to identify all the post-DSE contributions to the overall cost. This includes the detailed design phase, assembly costs, all the tests required for verification and validation, essentially everything that follows after the preliminary design phase which has been performed during the DSE. All the required steps for each stages are listed followed by the final milestone at the end. During the detailed design phase, a more in depth analysis of the characteristics of SCULPTUR (structural/stress analysis - FEM/CAD model for thickness distribution, lift, drag - CFD analysis) needs to be performed finalised by a verification and validation procedure. The construction phase starts shortly afterwards: the parts for building the UAV, a factory needs to be bought or rented, all the tools required during the construction etc; the first

[121] URL https://financial-calculators.com/roi-calculator [cited June 14 2016]

SCULPTUR prototype UAV is ready for testing at the end of this phase. The testing and production phases are interrelated, taking place simultaneously. Several test flights ensure that all the requirements (range, endurance, noise, emission etc) are fulfilled. Finally, there is a marketing phase in which SCULPTUR is promoted and presented to potential buyers. A demonstration flight is required in order to prove to buyers that SCULPTUR can accomplish its ultimate goal: pipeline surveillance. The final milestone for this stage is the first product sold. All the stages imply also staff costs: first three mainly require technical staff while the last one is focused mostly on the managers and the promoters. The CBS for SCULPTUR is presented in Figure 6.5.

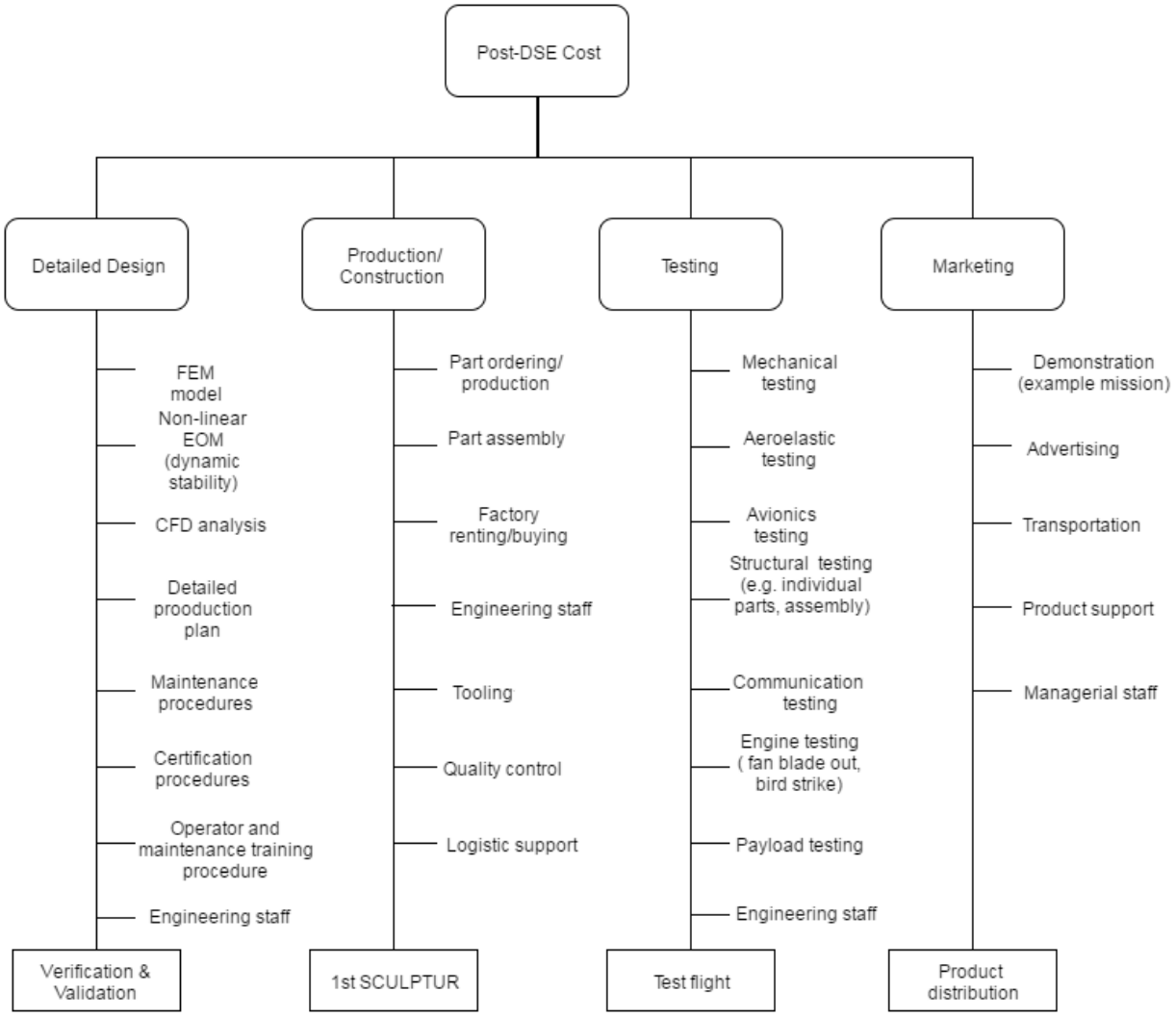

Figure 6.5: Cost breakdown structure

7 Operations and Logistics

Once the external, structural and payload design is finalised it is furthermore important to design the operations and logistics of SCULPTUR. The logistics needs to fulfil sustainability and ground control requirements as stated in Section 3.5. Section 4.1 Operations and logistic concept which elaborates on the steps which need to be taken to prepare and finish a mission. A reliability, availability, maintainability and safety analysis is made in Section 7.2. The software and hardware diagrams are presented in Section 7.3 and Section 7.4 respectively and together with the data handling procedures in Section 7.5 the electronical subsystems are designed. Section 7.6 finally explains the manufacturing, assembly and integration plan of SCULPTUR.

7.1. Operation and Logistic Concept Description

Not only has the UAV to perform the mission, it is also necessary to look at what operations and logistics are necessary to accomplish the mission. For this an operation and logistic concept description is made. This can be seen in Figure 7.1, the operation and logistic flow diagram, and will be elaborated on in this section. The concept has as main goal to give good insight in steps that have to be taken other than know from the functional flow diagram. Also it is important which steps are taken by companies out of this group or parties that are within the company of this group.

The concept assumes that all the trained mechanical personnel is stationed on the airport and its surroundings together with the ground station, but the longer storage is at a warehouse located somewhere else. Also only the trained personal and ground station personal is within the company of this group, while other parties are outside of this company. With this in mind 8 distinct steps can be taken to get the UAV in flight and retrieve it back in storage. First it has to be retrieved from the storage, next it has to be transported and delivered at the airport, where it can be assembled an pre flight checks can be done. When those are performed the mission itself can be performed. After touchdown, the UAV has to be checked again, data has to be handled and maybe some maintenance has to be done. When this is done the UAV can be packed again, transported and put back in storage.

Now there will be some more in depth explanation of these different steps. The first is at the warehouse where the disassembled UAV has to be prepared for transportation. Warehouse employees will search for the different parts, collect them and make them ready for transportation. Always before handing over to another party, transportation tickets have to be signed to check if indeed all parts are packed. This is done by the warehouse personnel and checked by the supervisor, which has final responsibility. When this is done it will be handed over to the truck driver. The warehouse and personnel is not part of this company. This is why good checked documentation is demanded, as it always has to be clear which party is liable for the parts.

The truck is loaded and now also the truck driver, who is now responsible, signs the form. The driver will bring all the parts to the airport and there they will be unpacked again. Now the maintenance supervisor will receive all the parts, check if indeed everything is there and and sign the ticket as accepted. This acceptance is again important for liability. Now the parts are in hands of people of this company. Only if everything is correct signing will take place to ensure safety of the parts of this company.

Now the maintenance crew will prepare the UAV for flight. This means first assembling all the different parts to build it. When this is done it can be fuelled. After fuelling the communications are started with the ground station. This is where the UAV operator controls the whole UAV. He will collaborate with the maintenance crew to do all the pre flight checks. They check both the control surfaces and the engine, and when this is fine this is communicated and the pre flight check form is signed. The UAV operator operates from the ground station located at the airport, to make communications between maintenance crew and ground station much easier.

Now the UAV is ready to take off and will be positioned on the runway to take off. When in flight, the operator controls the aircraft, and the UAV will perform its flight and surveillance. Other ground station personnel will monitor the data incoming from the UAV and analyse it. They will use this later to report to the customer. When the mission is performed the UAV lands again and is shutdown and handed over to the maintenance crew.

They will bring the UAV back to the ramp and check the status of it, to see if there are any abnormalities. Now the post flight form can be signed, with this information, both by the maintenance crew and the operator. Also the analysed data will now be reported to the customer to tell them how their pipeline is doing. Now the UAV can be disassembeled again and transported to maintenance.

Here the post flight form will be checked and all irregularities on the form will be dealt with by the maintenance. When the UAV is back to supposed status, it can be packed for transport. Again all parties check and sign the transportation ticket to be able to distinct the responsibility in all the phases.

The truck driver brings all the parts back to the warehouse, where the warehouse supervisor will check all the content and signs the transportation ticket accepted. Now the warehouse employees can store all the parts on

the assigned locations and fill in the documentation going with that.

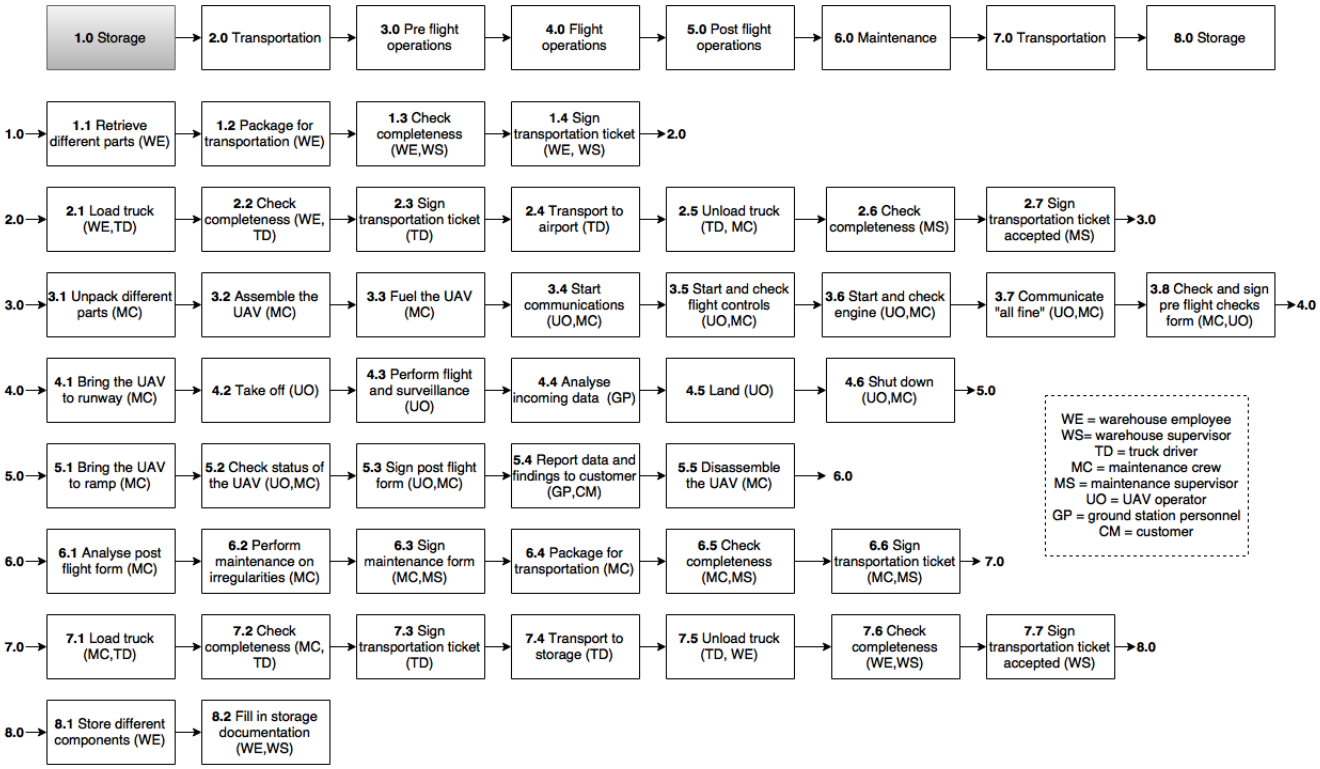

Figure 7.1: Operation and logistic concept flow diagram

7.2. RELIABILITY, AVAILABILITY, MAINTAINABILITY & SAFETY

This section will discuss the RAMS; Reliability, Availability, Maintainability, and Safety of the whole UAV system. Since many aspects of RAMS has already been discussed when discussing emergency systems and risks, this section will be a summary referring to all chapters covering the aspects of RAMS.

7.2.1. SAFETY CRITICAL FUNCTIONS

To ensure the success of the UAV's mission, its critical functions should always be operative. Therefore, the safety of these systems should be ensured.

The critical subsystems in the UAV are the systems which, in case of of a failure in the system, result in a mission failure or an inability to execute the mission. These critical functions are presented in Table 7.1. Many of these functions have already been described when mitigating UAV system development and mission risks, see Section 3.6. According to requirement **SCULPTUR-SR-SH18-2**, the UAV shall have a high level of redundancy. This requirement ensures the safety of all critical functions. Table 7.1 shows the Minimum Equipment List for the SCULPTUR UAV. It also shows the redundancy level of the critical subsystems.

Table 7.1: Table of critical functions of the UAV

Subsystem	Installed	mission need
Communication system	1	1
Autopilot	2	1
Extra avionics	2	1
Fuel system	2	1
Power supply	2	1
Engine	1	1
Landing gear system	1	1
Collision avoidance system	1	1
Parachute	1	1

The M.E.L. shows which subsystems need to be operative before the start of the system. The systems needed for mission success cannot be inoperative before the flight, although the redundant system can be inoperative, as long as it is restored after the mission has been performed. However, not more than one of the redundant systems on the M.E.L. can be inoperative.

The communication subsystem is not installed with redundancy. The antenna combined with the receiver sys-

tem has a large weight, making a redundant system infeasible. Instead, when the communication system fails, the UAV will fly autonomously to a preset landing site, as prescribed in Requirement **SCULPTUR-SH-SH18**. For this purpose, the autopilot is used. The autopilot, as can be seen in Table 7.1, contains a single redundant on-board computer (see Section 4.2, thereby increasing the reliability and complying with Requirement **SCULPTUR-SR-SH18-2**.

The avionics system is the full electrical system of the UAV. The most important subsystems of the avionics are the communication system and the autopilot. Other subsystems consist of GPS, data gathering instrumentation for air, inertial and meteorological characteristics, and the Air collision avoidance system, see Section 4.2. Furthermore, all connections between these systems, i.e. wiring and transfer processors, are also included with avionics. The wiring and the data acquisition systems have been installed redundantly. Therefore, a failure in one system will never result in a lack of flight data (i.e. airspeed, air pressure etc.).

The fuel system is installed redundantly. Booster pumps are installed together with jet pumps, where the booster pumps serve as an emergency for when the jet pumps fail, see Subsection 4.4.8. This ensures fuel is at all times fed to the engines.

The power supply of the UAV is a critical system, since a power outage would result in loss of communication, imaging capabilities, UAV control etc. Therefore, this system is made redundant by adding a RAT; a Ram Air Turbine, see Subsection 4.4.9. This RAT deploys whenever the installed power system fails.

The landing gear and the engine are critical systems of the UAV. Adding an extra engine or an extra landing gear system for redundancy would however be infeasible. For this reason, the parachute was added to the UAV. When the landing gear does not deploy, or if the engine fails, the UAV can land safely using the parachute. This emergency system will ensure that the UAV can land mainly undamaged, in accordance with Requirement **SCULPTUR-SH-SH18**, see Subsection 4.2.3 To further decrease the risk of damaging the UAV, an aircraft collision avoidance system is installed in the UAV. On top of this electronic system, lights are installed on the top and bottom of the UAV, increasing its visibility. This mitigates mid-air collision risks as described in the risk analysis; Section 3.6, and also complies to the certification requirements described in Section 3.3.

As can be seen in Table 7.1, the critical functions of the UAV have been installed so that they are redundant. If one system fails, the other system will take over. This ensures the safety of all critical functions of the UAV. On top of this redundancy concept, the maintenance schedule will include constant check ups on these critical systems, ensuring they are regularly checked for problems. This will be further elaborated upon in Subsection 7.2.3

7.2.2. EXPECTED RELIABILITY

The reliability of a system can be defined as the probability that a system will perform in a satisfactory manner for a given period of time when used under specified operating conditions [110]. In the case of the SCULPTUR UAV, a 'satisfactory manner' would mean a mission success without UAV damage.

Since the UAV has not yet been constructed and operated, the reliability of the complete UAV cannot be computed. Instead, the reliability can be estimated using reference UAVs. As described in Section 2.3.3, research into the field of UAV reliability showed an average reliability of military UAV's is 87 % [111]. This means that for a specified time, the UAV will be without critical subsystem malfunctions for 87 % of that time. A more accurate reliability estimate would include multiplying reliability values of separate subsystems. However, this data is not available, making it impossible to estimate the reliability of the complete UAV accurately.

7.2.3. MAINTENANCE ACTIVITIES

Unlike commercial manned aircraft it is not yet compulsory to have predefined maintenance schedules for UAVs. Nevertheless is it important to ensure the reliability of SCULPTUR by regular checks of the system. This is done by different maintenance activities. Maintenance is divided into different categories which can be seen in Figure 7.2. Firstly a distinction between corrective (repair) and preventive (service) maintenance can be made. It can also be seen when the maintenance will be done [110].

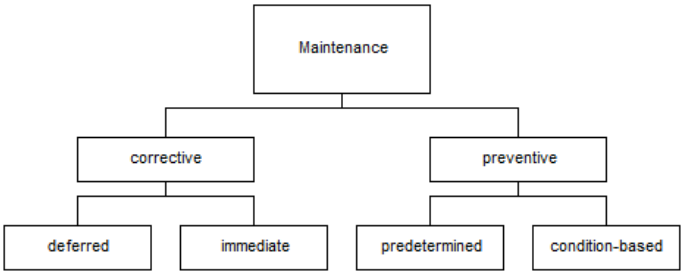

Figure 7.2: Maintenance Categories [112]

Different activities can be used to fulfil the maintenance requirement namely continuous monitoring, planned

and unplanned inspections, routine maintenance service, unplanned repairs, planned overhaul and planned rebuilding.

Most aspects of the maintenance schedule of a commercial aircraft can be used for SCULPTUR as well. However small aspects need to be adapted. Due to the fact that the UAV does not have any windows and less cut-outs, crack growth is less likely to occur. Since there is no pressurisation of the fuselage there is no pressure system which needs to be part of the maintenance schedule. Furthermore special attention needs to be put on the engine. It is placed within the nose of the UAV which makes maintenance more difficult but also more important since failure would have a bigger impact. It also The payload, communication and auto pilots are also crucial to check carefully. Without those the UAV would not be able to fly safely and to perform the mission. Finally the unmanned factor of SCULPTUR results in a high importance of preventive maintenance since there is no pilot to recognise and handle in-flight failures[122].

Table 7.2: Maintenance schedule

Checks	When	Activities	Out of service
Daily checks	every 24-60 hours	- check fluid levels - test communication system - check emergency systems	0.5 hours
A checks	after 250 flight hours	- incl. daily checks - check lights - lubricate gear retract actuator - visual inspection of the structure - visual inspection of the engine	1 day
B checks	6 months	- incl. daily and A checks - detailed checks of components and systems	1-2 days
C checks	20-24 months	- incl. daily, A and B checks - engine inlet inspection	3-5 days
D checks	6 years	- incl. daily, A, B and C checks - detailed inspection on the wingbox structure	20+ days

The scheduled maintenance in Table 7.2 is based on the current maintenance plan for commercial aircraft[123] and it is extended to meet SCULPTUR specific needs.

Furthermore unscheduled maintenance will be needed during the lifetime of the UAV when unexpected failures occur. Depending on the severity of the failure a quick repair between missions is possible or SCULPTUR needs to be transported to a main maintenance sight in order to perform appropriate overhaul.

7.2.4. EXPECTED AVAILABILITY

Availability is often used as a measure of system readiness. The degree, percent, or probability that a system will be ready or available when required for use. Availability can be seen as the result of reliability and maintainability [110].

The availability of SCULPTUR is dependant mainly on scheduled and unscheduled maintenance sessions. Other reasons for the unavailability of the UAV could be the absence of the ground crew and/or the pilots, or problems with the Air Traffic Control (ATC). However, these occurrences are expected to have a small effect on availability, since the UAV will fly in empty airspace and there will be spare personnel available at all times. The expected availability can thus be derived from the expected reliability and the routine maintenance schedule. Using a reliability of 87 % and the out of service time from Table 7.2 the initial availability will be 1695 out of 2190 days per 6 year interval which equals an initial availability of 77 %. After the detailed design phase, which includes a detailed reliability and maintainability analysis, the final availability can be calculated.

7.3. SOFTWARE LAYOUT

In order to have an overview of how the software layout of the UAV, a software diagram will be presented in this section. This diagram is made based on the Unified Modelling Language (UML) standard for software design[113].

Each block in the diagram represents a class as used in the software. The first line in bold is the name of the class, giving an indication of the function of the class. The second and third areas in the box represent the most important variables and methods in the class respectively, if applicable. Each variable or method is on a separate line, with the type of the variable or of the return value indicated after the colon. A plus in front of the name indicates that the variable is public and thus can be accessed by other classes, while a minus indicates that it is private.

[122] URL http://www.roboticskies.com/wp-content/uploads/2016/03/Hayden-ROTORWinter2016.pdf [cited June 18 2016]
[123] URL http://www.aviationpros.com/article/10388655/whats-this-a-check-c-check-stuff [cited June 18 2016]

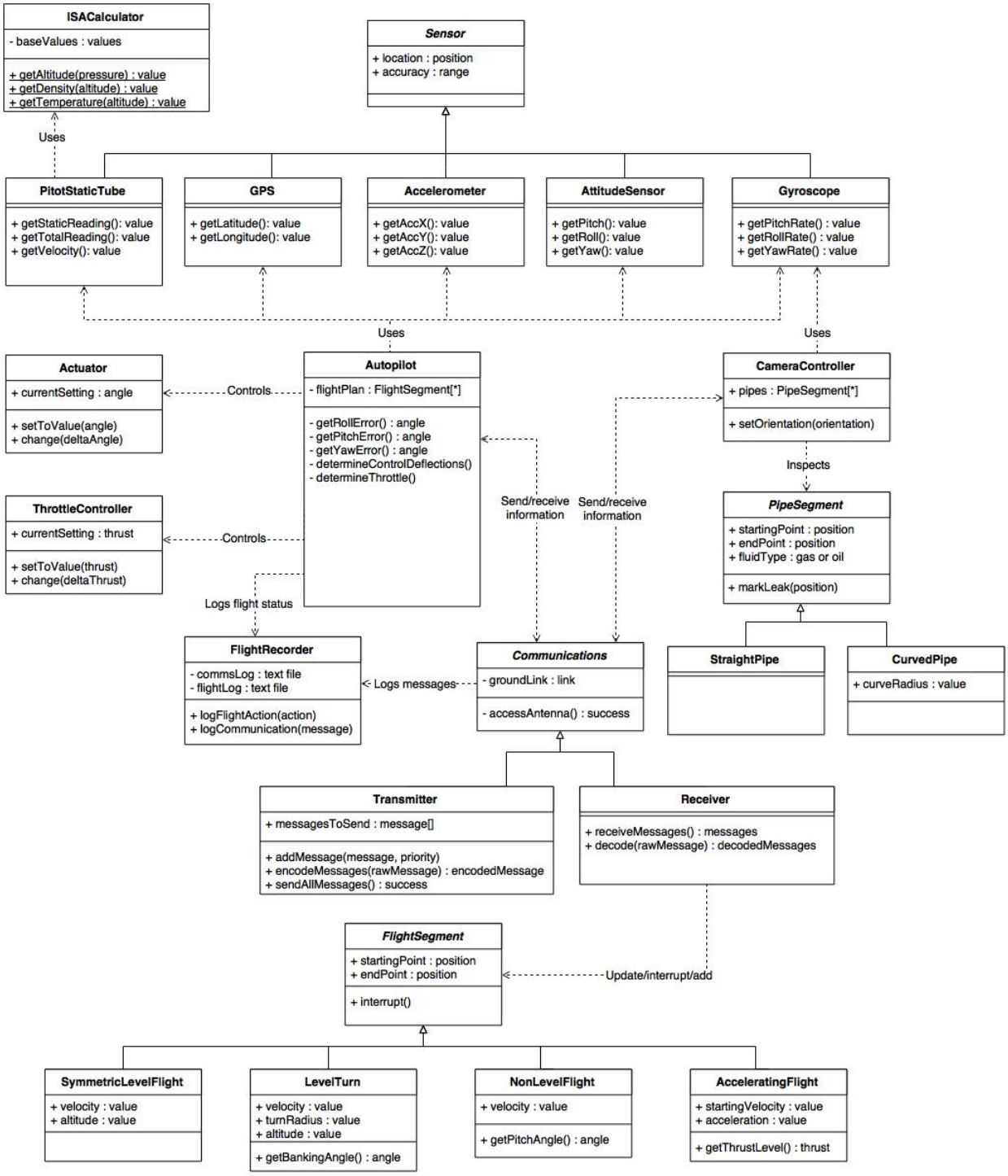

Figure 7.3: Software UML diagram

Some of the classes are derived from a parent class. This is indicated by solid lines. The child class inherits all all variables and methods of the parent class, although the value or implementation may differ between different child classes. Other relations between classes are visualised using dashed lines, with some text describing the exact relationship. The complete software diagram is presented in Figure 7.3.

The main software component is the autopilot. The autopilot is in charge of the direct control of the UAV, and uses the sensors in order to make sure the right commands are given to the flight control actuators and the engine. In addition, it logs its actions to the flight recorder. The autopilot gets input from the communications class, and returns any required information to the ground station. In addition, the autopilot keeps track of the flight path that is to be flown, which is subdivided in different categories of flight. This allows for easier determination of the settings which are required to fly this flight path.

The only system which is not directly related to the autopilot is the camera controller. The camera controller retrieves input from the communications system, and stores a list of the pipe segments which need to be in-

spected. Additionally, it sends the images of the camera back to the ground station.

7.4. HARDWARE LAYOUT

The hardware diagram shows the interaction between several parts of the UAV. Although the aircraft of course includes more parts like the wingbox and the fuselage, only the parts which show interaction are depicted, as can be seen in Figure 7.4.

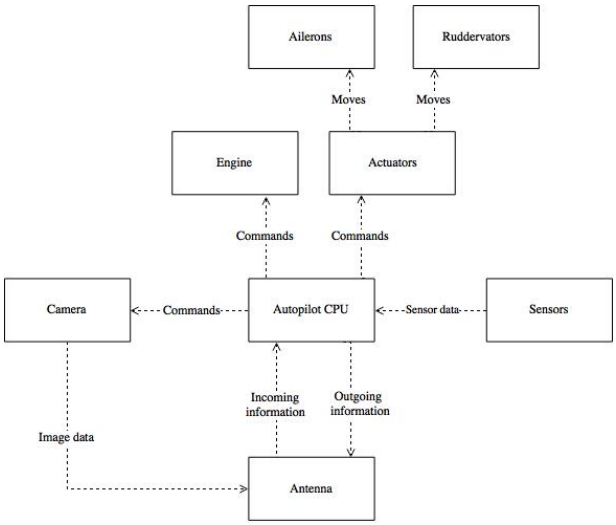

Figure 7.4: SCULPTUR hardware diagram

The central part of the hardware is the central processing unit (CPU) of the autopilot. Data from the sensors and the antenna is transmitted to this CPU, where it is processed. Then, commands are sent to the camera, engine and actuators, as well as back to the antenna which then transmits to the ground station. The actuators, in turn, move the control surfaces.

7.5. DATA HANDLING

In Figure 7.5 the data handling diagram can be seen, in which all the data systems are connected in the way they interfere with each other. The diagram is divided in six main categories. The first is the central computing units, which communicate with all the other subsystems. This includes the autopilot, navigation unit and is mostly driven by the onboard computer. The central computing units keep track on all the different processes that take place during flight and to perform the mission and control the UAV by sending commands. All information necessary to do this comes from all the different sensors and systems that measure the environment or provide information. This is the second category of the diagram. Thirdly is a separate category for the communication, as not only here a lot of information is received but also transmitted. Part of the footage of the surveillance is directly linked to the communications, while higher resolution footage is sent and received by the onboard computer and stored on the data recorded. All data is always recorder in high detail in the fourth category, the data recorder. The fifth category is taking care of all the electric power necessary to ensure operations. The onboard computer drives all the commands to ensure electrical power. In case of engine failure the system will switch to the Ram Air Turbine. The final category is for commands in flight. The onboard computer and navigation unit are in a loop with the autopilot. Here all commands to keep the UAV on track are sent to the engine for providing thrust, to the fuel system to give fuel and to the flight actuators to drive all the movements. The air collision system is a hard input on the autopilot, to ensure safety. The navigation unit gets the position based on GPS data.

The onboard computer chosen is the EagleEye Online Onboard Computer[124]. It allows GPS-Based flight plans, operations with absent ground datalink and live image recognition. Also, the mission can be conducted based on sensor/camera live data and the data transition can be encrypted.

[124] URL http://www.eagleeyesys.com/technology-on-board-computer.aspx [cited 17 June 2016]

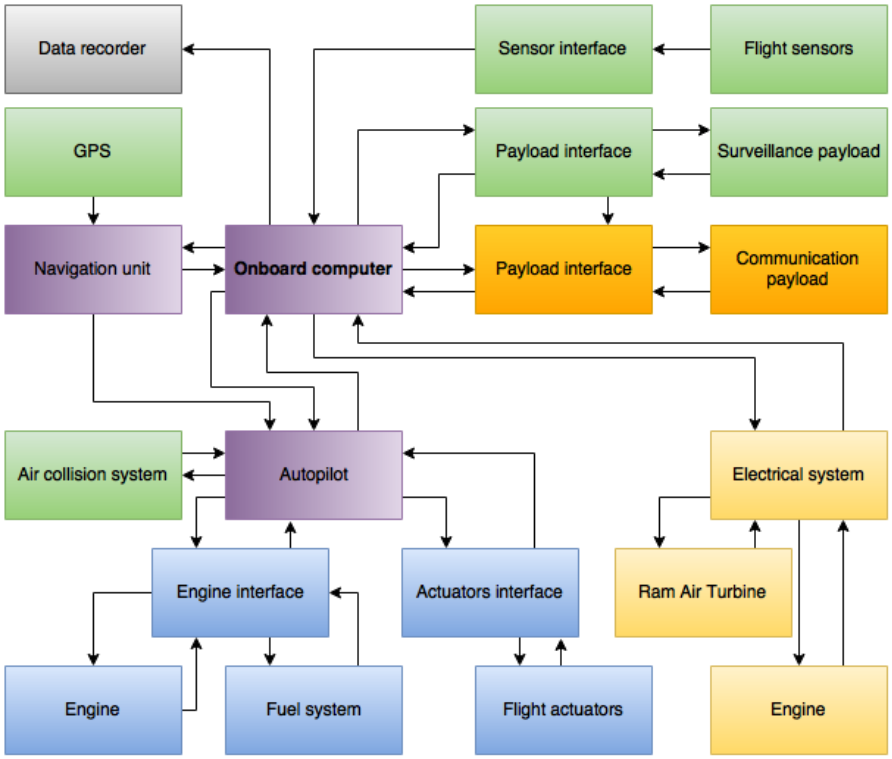

Figure 7.5: Data Handling Diagram

7.6. MANUFACTURING, ASSEMBLY AND INTEGRATION PLAN

The manufacturing, assembly and integration plan is an important step in order to plan the production of the surveillance UAV. A crucial factor in the MAI plan is lean manufacturing to ensure an optimal assembly line which minimises waste and increases efficiency and added value.

7.6.1. PRODUCTION PLAN

An initial production plan was constructed for the SCULPTUR UAV. This version of the plan focuses on the assembly and assumes that subcontractors follow the given production methods as stated in Section 5.5. Initially the plan was developed for a medium-sized production scale of approximately 50-100 UAVs which ensures profit to the company and at the same time is a reasonable market volume.

The goal is to achieve a lean manufacturing process which is defined as: 'Lean thinking is the dynamic, knowledge driven and customer-focused process, through which all people in a defined enterprise continuously eliminate waste with the goal of creating value' [114]. Therefore reducing non value adding steps is the main focus point. This includes limiting material waste but also reducing overproduction, waiting time, work in progress or inventory, processing waste, transportation, movement or motion, rework and under-utilising people [115]. The six sigma method was used to design an efficient production process. It covers all DMAIC phases (Design-Measure-Analyse-Improve-Control)[125] in order to produce an optimal result. Part of this method is a SIPOC tool[126] which was used to define the suppliers, inputs, process, outputs and customers, which could then be used to construct the MAI plan as shown in Figure 7.6.

As can be seen in the MAI plan, the final assembly line consists of six main parts namely assembling the fuselage and adding the landing gear, wings, tail, engine and payload. In order to reduce the above mentioned reduction of waste it is important to keep storage and waiting time to a minimum. Using the 'Just-in-time'[115] procedure means sub-assembling the landing gear, wings, tail and engine in parallel to the final assembly line in a way that they arrive at the final assembly location at the same moment they are needed. Parts needed for the sub-assembly, such as skin panels, struts, engines, tail surfaces will be manufactured by subcontractors. Ordering small manufacturing parts will also be done to keep storage of those to a minimum. Initial subcontractors like Fokker Aerostructure, Fokker Landing Gear, Dutch Thermoplastic Composites and MTU Aero Engines were chosen to produce the wings/tail, landing gear, skin panels and the engine respectively. During the detailed design phase the definite suppliers will be decided and a detailed production plan will be made. After assembly the UAVs will be transported to the customers abroad.

[125] URL https://www.isixsigma.com/new-to-six-sigma/dmaic/six-sigma-dmaic-roadmap/ [cited June 14 2016]
[126] URL https://www.isixsigma.com/tools-templates/sipoc-copis/sipoc-diagram/ [cited June 14 2016]

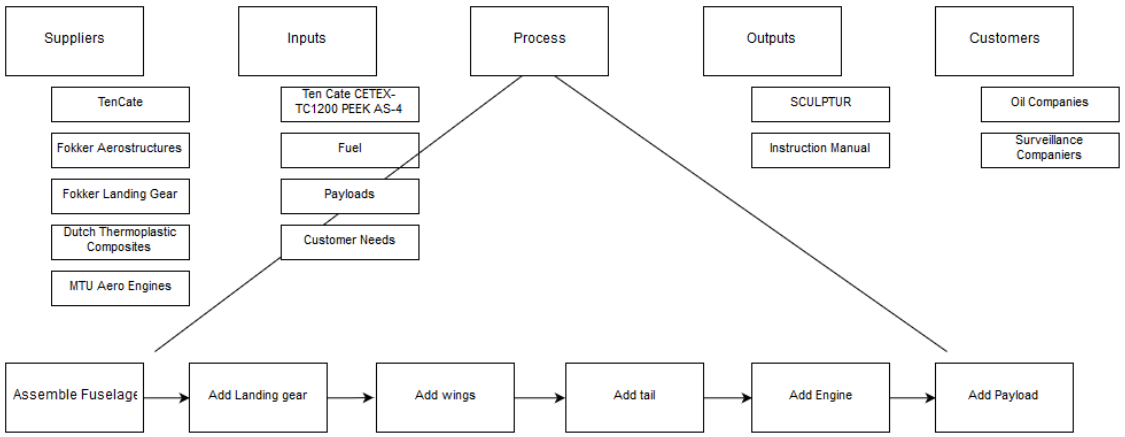

Figure 7.6: Manufacturing, Assembly and Integration Plan

7.6.2. END-OF-LIFE RECYCLE STRATEGY

It is not only important to design the production but also the disposal at the end-of-life of SCULPTUR. This includes the structure of the UAV but also the propulsion and payload system. As stated in Section 5.5, using thermoplastic composites offers new and better recycling methods than thermoset composites. The recycling methods comply with the current European waste regulations[127].

Two main procedures are possible to recycle the UAV at the end of his life cycle. Firstly reforming parts of the structure which means cutting parts of the wing or the fuselage and heating it until the processing temperature in order to press it into a new form. This method does not reduce the material properties of the used thermoplastic composite [116]. Secondly grinding the material into small parts and reusing them in different production processes. Depending on the chosen grind size the recycled material can be used for injection molding or compress moulding production methods. This procedure shortens the fibres which results in lower material properties in the newly produced parts [117].

The value of the engine is higher than most parts of the aircraft. Therefore direct recycling in form of re-usage is mostly an option. Depending on the status of the engine at the end-of-life the whole engine can be reused in a different SCULPTUR UAV or its parts can be reused to built a new engine [118]. Remaining fuels and oils in the UAV will also be recycled in order to use them again in new aircraft.

Finally similar to the engine, the payload can be reused in different UAVs if they are still working. After their lifetime their materials and electronics can be recycled. Cameras and electronics include many valuable but also hazardous materials which should be taken care of[128].

7.6.3. IMPACT ON SUSTAINABILITY

Using the chosen lean manufacturing methods and the improved end-of-life strategy not only results in an economical and time benefit but also in a positive effect on sustainability. Lean manufacturing reduces overproduction and storage and the final assembly and suppliers are chosen to be in the Netherlands or Germany which results in high quality and improvement of the Dutch economy but furthermore also shorter transportation times. Furthermore materials and parts are reused of recycled appropriately. Following effects can be expected [119]:

- **Minimising overproduction**. Less production means less energy needed to produce materials and parts, less emissions during unneeded transportation.
- **Minimising storage**. Less storage buildings are used which reduces the amount of energy needed. Also less packaging waste is needed to store parts.
- **Shorten waiting time**. Less energy for heating, cooling, lighting during production downtime
- **Reducing transportation**. Less energy and emissions are needed for transporting part and sub-assemblies during shorter transportation times. Less expected damage and less packaging and protection material needed.
- **Recycle appropriately**. No hazardous material will enter the environment uncontrollably. Partially energy can be obtained from old material which can be sold or reused to produce new material.
- **Reuse material**. Minimal energy input for optimal re-usability. Furthermore less unuseable waste which needs to be taken care of.

[127] URL http://ec.europa.eu/environment/waste/legislation/ [cited June 14 2016]
[128] URL http://www.ksewaste.org/ewaste_why.htm [cited June 17 2016]

8 Final Design Summary

In this chapter the final conceptual design will be summarised to show all the results found in this study and how this influences the characteristics of the UAV. First, the layout of the UAV in Section 8.1 will be shown and based on that the system characteristics will be summarised in Section 8.2.

8.1. Design Lay-Out

The major parts of the final layout are presented in this section. The layout is conventional. This is chosen for its performance in stability, weight, drag, development risk and design complexity. All the components are located at positions which in the end results in a stable configuration and ensures satisfying the surveillance. The wing is slender, tapered but has no sweep, optimised for drag and the low cruise speed. The wings structure is affected most by impact resistance, because of the fuel tanks, and buckling of the top panel due to compression. The tail can be seen to be an inverted Y-tail in order to have the yaw moment positively affecting the rolling moment. The engine is located on the nose which is important for the noise emissions. The gear is located and designed such that it has the best stability performance on rough terrain and better performance during ground operations. The fuselage is slender, optimised for drag while still having enough space for the payload. Its structure is mainly driven by impact resistance. All this can be seen in Figure 8.1. The final dimensions and characteristics will be shown in the following section.

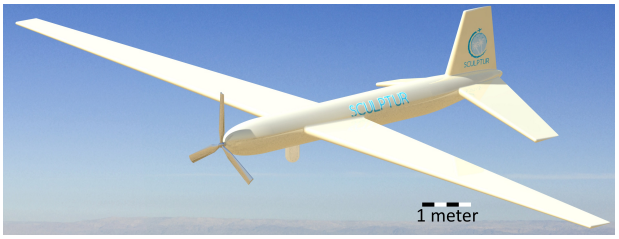

Figure 8.1: SCULPTUR Render

8.2. System Characteristics

The most important characteristics of this design will now be presented. First, the relevant weights are given in Table 8.1. Next, the final dimensions are given in Table 8.2.

Table 8.1: Weights final preliminary design

Component	Wing	Fuselage	Tail	Engine	Gear	Payload	Fuel	Rest	MTOW
Weight [kg]	124.1	30.7	18.4	45.3	17.7	44.2	87.7	35.4	**403.5**

Table 8.2: Dimensions final preliminary design

Wing	Span	Rootchord	Tipchord	Surface area	Structure	Airfoil
Dimension	12.5 [m]	1.19 [m]	0.48 [m]	10.4 [m^2]	Table 5.15	NACA 4409
Fuselage	Length	Diameter	Thickness			
Dimension	5.0 [m]	0.5 [m]	1.070 - 2.140 [mm]			
Tail	Surface (Horizontal)	Surface (Vertical)	Span (Horizontal)	Span (Vertical)	Airfoil (Horizontal)	Airfoil (Vertical)
Dimension	6.24 [m^2]	1.54 [m^2]	3 .48 [m]	0.86 [m]	NACA 0012	NACA 0012

The selected payload is summarised in Table 4.4. This is chosen to comply with the different requirements of the mission. The cameras chosen are LWIR (long wavelength infrared), to be able to see the pipelines that are underground which for this mission is mostly the case and the electro-optical camera coming with the chosen gimbal. The communication payload, the Gilat BlackRay 1000, is chosen for its capability of sending large amounts of data efficiently. The UAV is controlled by an autopilot along waypoints and this is done with the VECTOR autopilot, both light and power efficient. The emergency payload is there to ensure safe landing even during an engine failure. It consists of a ballistic parachute which is large enough to cope with the required loads. This is accompanied by a flight data recorder to always have data about what is happening during flight.

To have a reliable, stable aircraft the locations of the different components can be seen in Table 5.1. With this, the final c.g. range is determined, which is between 30.3% to 37.9% MAC. This is not yet iterated for the final design values and should be performed again in the detailed design. The dynamic analysis shows that all the eigenmotions are stable.

The aerodynamic design is optimised for total drag during cruise, the values of which can be found in Table 5.6. The tail is designed to counter the moment calculated in the aerodynamics section of which the tail sizing can be found in Table 8.2. The lift distribution can be found in 5.14.

The engine is designed to minimise specific fuel consumption, provide the required thrust to overcome the drag and propeller power output. The performance settings have been determined and can be found in Table 5.12. As far as sustainability is concerned, the engine has been designed to run on Renewable Diesel I and thus reduce NO_x, CO and particulate matter emissions (Section 5.4.2 shows emission results). For the start-up system and power generation to onboard systems, a starter-generator has been connected via a small reduction gear box to the high-pressure turbine.

The material choice is mostly dominated by production costs and sustainability. Polyetheretherketone, a thermoplastic polymer, with AS-4 carbon fibres is traded-off to be the best suited solution. The resin matrix is easy to produce, can be recycled almost completely, has a suited operating temperature range and can endure more than enough cycles to perform the requirement of structural integrity for the lifespan of the UAV. The carbon fibres are stiff, which for aircraft applications is preferred. TenCate CETEX-TC1200 is chosen for the final material properties, which can be found in Table 5.14.

With the material and the loads known, the structure is designed. The wing has a wingbox, with 0.5 chord length and 0.07 chord height. To ensure safe operations, buckling load turns out to be dominant; stiffeners are added to solve this issue. Rib spacing is determined and all the skin thicknesses, for which impact was taken as one of the driving requirements. All this resulted in the wing design which can be found in Table 5.15. The highest endured stress in the wing is 37.8 MPa. The fuselage design is mainly driven by impact resistance. Stresses are rather low, but still a minimum thickness of 1.070 mm is required. For two distinct load cases, during flight and on the gear, the stress analysis is done. The maximum stress found is 9.1 MPa. The final design can be found in Table 5.16. Finally, fatigue is checked, but with these stresses and the chosen material, 10^5-10^6 cycles can be achieved easily which is sufficient. Because of the impact resistance and buckling loads, the stresses are well within the maximum yield stress of the material.

A timeline showing how SCULPTUR's weight changed throughout the design process is presented in Figure 8.2. The line with pluses shows the weight estimation using the Class I and Class II methods while the other line indicates the weight budget derived through statistical methods. Everything above the full line means that the design is over budget and is not competitive enough for the current UAV market since lighter solutions exist. It is interesting to observe how the design evolved in order to meet the required budget and how a good market analysis and well planned verification procedures impact the final product.

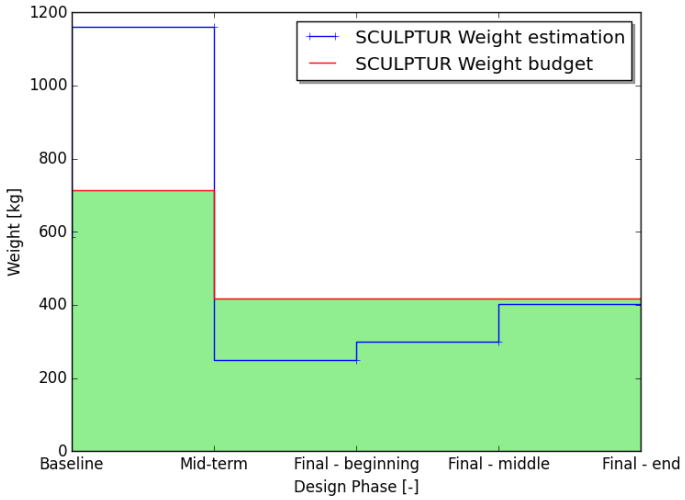

Figure 8.2: SCULPTUR Weight evolution

9 Project Design and Future Development Strategy

This project is not finished with the conceptual design of the UAV as stated in Chapter 8. Further steps need to be taken in order to deliver a final product. This chapter elaborates on the project design and development logic (PD&D) and the project Gantt chart.

9.1. Project Design & Development Logic

The activities following the conceptual design stage of the DSE project are shown in Figure 9.1, where the blocks and their connections visualise the logical connection between the activities. Furthermore some sub-tasks of bigger activities are mentioned. It includes the main phases namely the detailed design phase, the development phase and the final implementation and close-up phase of the SCULPTUR project. The PD&D logic diagram focuses on the needed activities to produce a working and flying surveillance UAV.

After the preliminary design review the detailed design stage starts. It consists of design analyses and verification but also construction of maintenance and production plans which includes choosing contractors and designing the construction processes. In order to assemble SCULPTUR the design needs to be revised and parts need to be ordered and produced. During the test phase all subsystems need to be tested before full scale testing and validation can take place. Certification includes test flights and the flight readiness review which will then be followed by launching and selling SCULPTUR.

9.2. Project Gantt Chart

The post-DSE Gantt chart puts the logical connections of the PD&D diagram activities of the upcoming phases into a chronological order. All activities are included and a rough time frame is added in order to construct a better planning of the different phases and their interrelation.

Similar to the logical relation the three main phases are detailed design, development and close-up. Their duration and predecessors can be found in Figure 9.2. The detailed design phase includes the actual design, optimising, prototyping and revising which is then followed up by the development phase which can be divided into manufacturing, testing and certification of SCULPTUR. Finally the close-up phase where the UAV is presented and sold to the public.

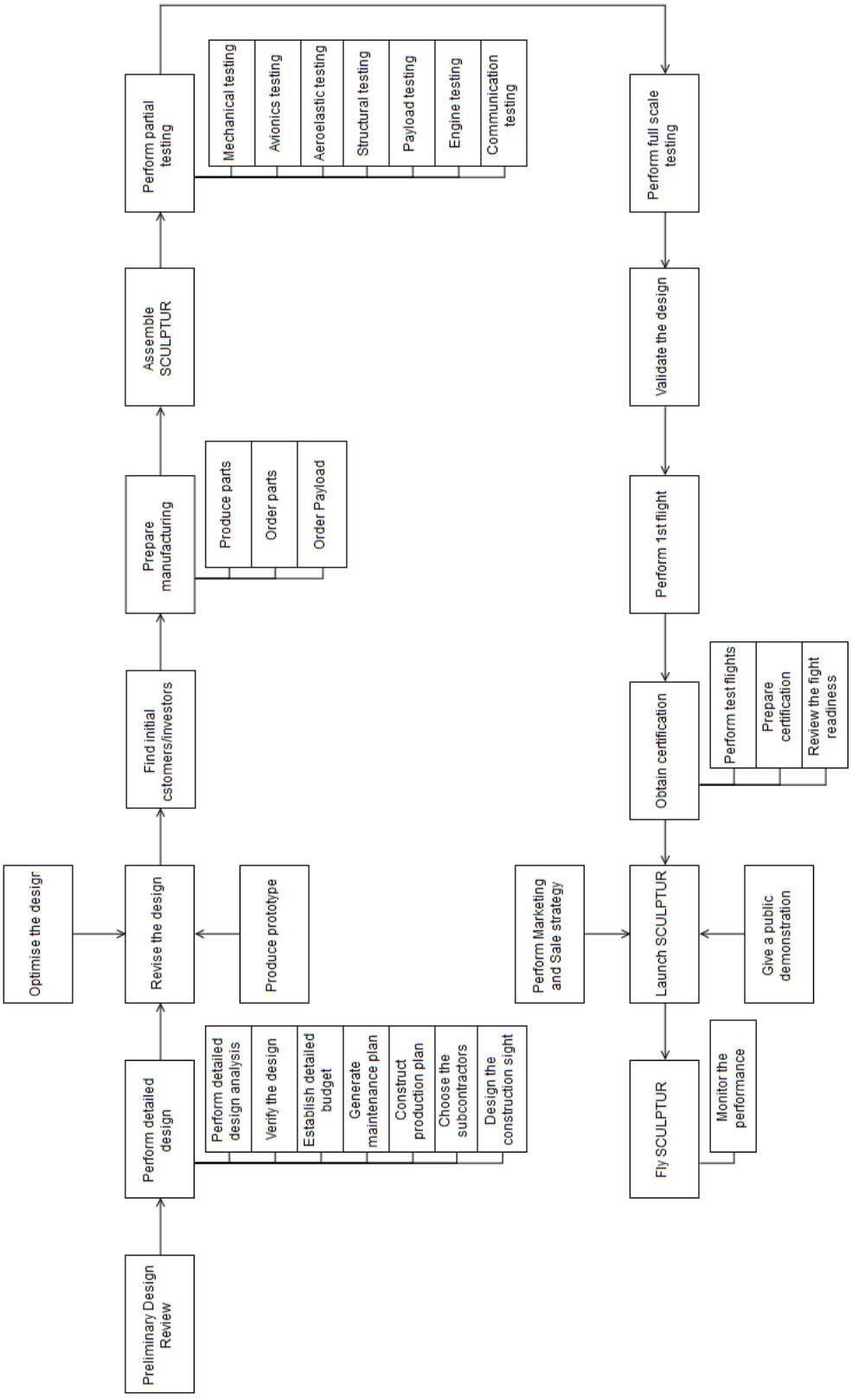

Figure 9.1: Project Design and Development logic

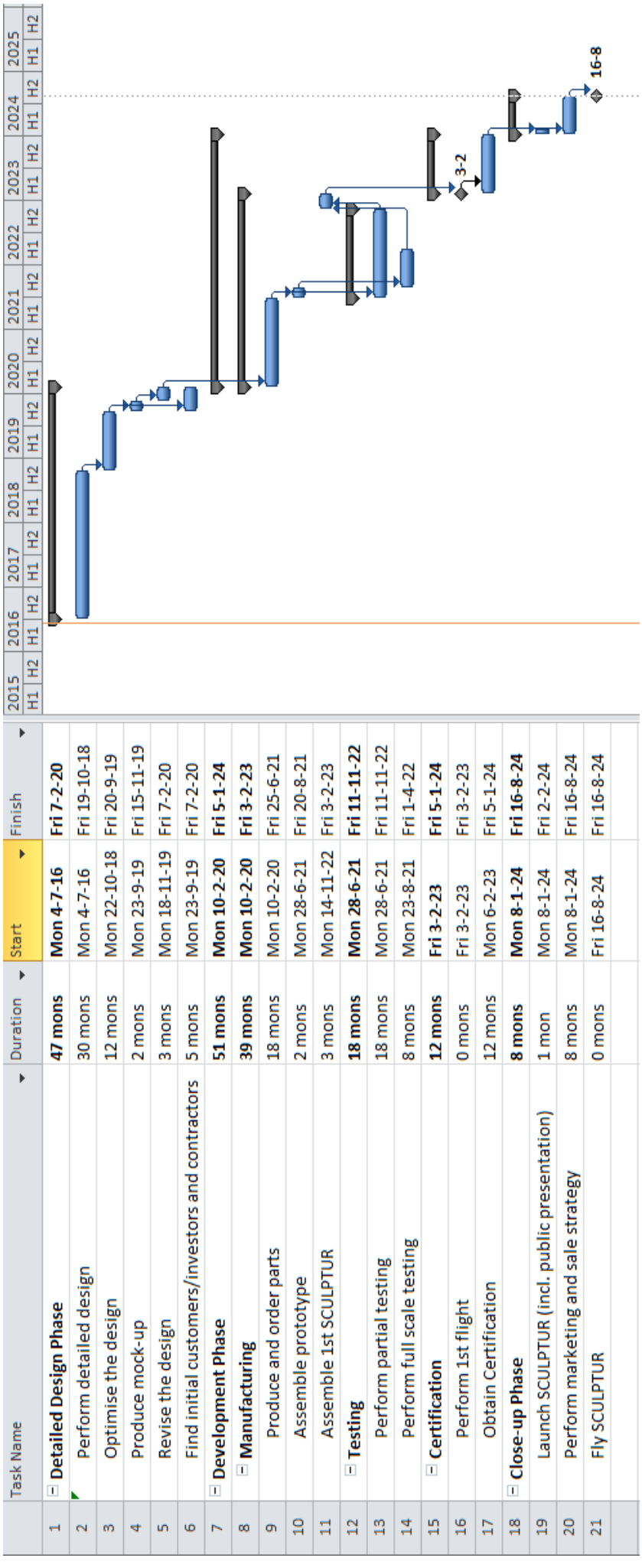

	Task Name	Duration	Start	Finish
1	**Detailed Design Phase**	**47 mons**	**Mon 4-7-16**	**Fri 7-2-20**
2	Perform detailed design	30 mons	Mon 4-7-16	Fri 19-10-18
3	Optimise the design	12 mons	Mon 22-10-18	Fri 20-9-19
4	Produce mock-up	2 mons	Mon 23-9-19	Fri 15-11-19
5	Revise the design	3 mons	Mon 18-11-19	Fri 7-2-20
6	Find initial customers/investors and contractors	5 mons	Mon 23-9-19	Fri 7-2-20
7	**Development Phase**	**51 mons**	**Mon 10-2-20**	**Fri 5-1-24**
8	**Manufacturing**	**39 mons**	**Mon 10-2-20**	**Fri 3-2-23**
9	Produce and order parts	18 mons	Mon 10-2-20	Fri 25-6-21
10	Assemble prototype	2 mons	Mon 28-6-21	Fri 20-8-21
11	Assemble 1st SCULPTUR	3 mons	Mon 14-11-22	Fri 3-2-23
12	**Testing**	**18 mons**	**Mon 28-6-21**	**Fri 11-11-22**
13	Perform partial testing	18 mons	Mon 28-6-21	Fri 11-11-22
14	Perform full scale testing	8 mons	Mon 23-8-21	Fri 1-4-22
15	**Certification**	**12 mons**	**Fri 3-2-23**	**Fri 5-1-24**
16	Perform 1st flight	0 mons	Fri 3-2-23	Fri 3-2-23
17	Obtain Certification	12 mons	Mon 6-2-23	Fri 5-1-24
18	**Close-up Phase**	**8 mons**	**Mon 8-1-24**	**Fri 16-8-24**
19	Launch SCULPTUR (incl. public presentation)	1 mon	Mon 8-1-24	Fri 2-2-24
20	Perform marketing and sale strategy	8 mons	Mon 8-1-24	Fri 16-8-24
21	Fly SCULPTUR	0 mons	Fri 16-8-24	Fri 16-8-24

Figure 9.2: Post-DSE Gantt chart

10 Conclusion

The aim of this report was to design a micro-gas turbine propelled UAV with a payload of up to 50kg. As well as having a range of 1800 km and an endurance of 20 hours at a cruise speed of 100 km/h, the UAV will be remotely controllable at long distance. Followed by an investigation on the socio-economic benefits, the environmental footprint and the sustainability connected to the life-cycle of the UAV.

A market analysis was conducted in order to investigate how UAVs perform in the present. By searching for the ones with similar range, propulsion system and endurance, it was found that a wing-tail configuration would be the most suitable. The micro-turboprop engine is situated at the front of the fuselage in a tractor configuration since it less noisy and more efficient than the pusher configuration. The use of renewable diesel type I (SuperCetane) fuel, a 100% renewable variant of petroleum diesel, contributes further to the sustainability of the aircraft, substantially reducing greenhouse gas emissions. Furthermore, the required payload to perform the mission has also been determined with the aid of the market analysis: a gimbal turret containing a high-definition electro-optical camera and multiple infra-red cameras for surveillance, communication payload, a parachute used for emergency situations and a flight data recorder.

The UAV has been designed with the implications of being unmanned in mind, meaning that all collateral damage from any system failures is prevented (through the use of a parachute for example). When assessing the risks of designing a UAV, it was found that the propulsive subsystem has the highest risk of failing, flight control having the second highest risk. Risk mitigation was applied to the events that had a high chance of occurrence and a catastrophic effect. These events were mid-air collision, terrain impact and payload failure for the operational risks. For design risks, these events were certification issues, killer requirements, noise risk, emissions, fatigue analysis and cost risks.

This final report introduced the conceptual design phase, focusing on the main components of the various subsystems. With a final MTOW of 403.5 kg and an estimated selling price of only $3,341,000, it is believed that SCULPTUR is an attractive product for all oil and natural gas companies in Australia. As time passes, it could be available for sale also in different countries, as certifications for UAVs develop further.

To conclude, SCULPTUR complies with all the stakeholder requirements as well as with almost all the system requirements set by the design team. It is the first UAV of its kind, being the only one capable of long-range pipeline surveillance. With the conceptual design phase now finished, it is time to move on to the next step: detailed design. Some suggestions on how to proceed further and improve the design are stated in the next chapter.

11 RECOMMENDATIONS

With the preliminary design phase now coming to a close after ten weeks, it is imperative to look back and evaluate what could be improved or be done differently for the detailed design phase. Even though the team has always been driven to find the best design, it was found that it might not always be possible. Finding the optimum solution is difficult due to the many interrelationships between the subsystems. This means an iterative procedure is required for which the DSE simply does not allocate enough time to be done in its entirety. With more time available during the next design phase, any errors due to insufficient iteration can be removed.

Some recommendations can be given on a subsystem level. For the structures & materials subgroup, a detailed FEM model can be constructed which would allow for an accurate representation of the loads the UAV has to cope with. It would also offer a visual representation of a wide variety of physical parameters such as stress or temperature, allowing the group to have a definite idea of the failure modes encountered. Furthermore, it would be interesting to perform real tests to ensure that the values from the model correspond to the real life scenario. Using a semi-analytical or FEM based method, it is possible to compute the thickness distributions and weights of main structural elements (skin panels, spars, ribs, frames). This is also known as a Class III weight estimation. Since a well-defined breakdown of component weights and centre of gravity locations on a subsystem level is required for the Class III weight estimation, it was not jet possible to perform such an analysis.

For the aerodynamics subgroup, computational flight dynamics (CFD) analysis is a must have. With such a study, the overall value of the design can be greatly improved. It is possible to investigate difficult problems such as turbulence, allowing for determining more realistic values for the aerodynamic coefficients. Performing wind tunnel experiments was not possible during the DSE due to the time allocated and available budget. Measurement time and effort are also significant factors when dealing with wind-tunnels. Whereas a numerical program can be run within a few seconds and give reasonable results, wind tunnel testing usually takes many hours, not to mention even more hours prepping the testing subjects. Also, the tested subjects, such as airfoils, have to be carefully manufactured or else the entire test is invalidated. Thus, for preliminary designs of airfoils especially or entire wings in general, it is probably better to at least start with computational methods first. The main advantage of a wind-tunnel is that it still produces the most accurate data possible (next to full-scale testing).

For the performance subgroup, in general, it can be concluded that the chosen theories and idealisations are correct. It should be mentioned however that these are still used within the framework of the linear model. This means that despite the fact that all the used theories are valid, they are still relatively general, however the results obtained with this numerical model correctly predict the behaviour and stability of the different manoeuvres, albeit with a degree of error. Better, more accurate simulation of aircraft response can be done through other numerical integration routines and by using non-linear theory. It becomes a trade-off between the degree of accuracy, and the time and finances. Also, the stability and control of the UAV should be checked for the very final configuration as the design has slightly changed after the iterations from the Class II weight estimation.

Concerning the propulsion design, further analysis in the preliminary design stage should be carried out. This involves a consideration of other engine performance settings, specifically during normal take-off, climbing and landing conditions. A recommendation is to also examine the engine's performance during take-off acceleration using GSP's Transient performance series. In addition, the propeller sizing might undergo some changes when other contributing factors are considered, such as the blade angle, optimum thrust & power coefficients and structural issues. Hence, it is recommended that the propeller is further iterated in the detailed design phase. Furthermore, a particular speed reduction unit should be chosen and its losses due to friction between the rotating gears should be taken into account for future analysis. Lastly concerning the preliminary design optimisation, appropriate size estimations should be considered for the turbomachinery and combustion chamber. The design can be taken a step further by utilising software packages like *COMPAL*®, *RITALTM* and *AxCent*® whereby geometry design and CFD analysis can be undertaken. Finally, regarding the future detailed design, it is recommended to perform an appropriate FEM and material selection analysis for each component.

In the case of the financial analysis, it would be preferred to contact different manufactures and see how the prices vary between the required off-the-shelf products. For the development costs, it would be efficient to find a way to adapt the Eastlake model such that it is applicable specifically for UAVs and not for general aviation aircraft. This would lead to a better estimate, presumably smaller than the current one since a development stage for a UAV is generally shorter than for an aircraft. After a few years since the first UAV is sold, it would be interesting to explore how SCULPTUR changed the market. It might be the case that a combination of manned and unmanned aircraft perform pipeline surveillance or that manned aircraft are completely phased out.

To conclude, it is highly recommended to investigate if it would be possible to fly at higher altitudes and still be able to perform the surveillance mission with the available payload. This will make it possible to have a lower fuel consumption and operating costs at the expense of decreased longitudinal static stability.

BIBLIOGRAPHY

[1] T. Chis, *Pipeline leak detection techniques,* Andrei Saguna University (2009).

[2] A. Marcellan, *An exploration into the potential of microturbine based propulsion systems for civil unmanned aerial vehicles,* Delft University of Technology (2015).

[3] NASA, *Earth observations and the role of uavs: a capabilities assessment,* Civil UAV Assessment Team (2006).

[4] B. Dorca, A. Engelke, E.M.Fernandez-Santoro, T. Haex, L. Hikspoors, N. Kirov, R. Molenaar, R. Riepe, D. Risselada, and M. Smeenk, *Midterm report - group 9,* Delft University of Technology (2016).

[5] C. Achebe, U. Nneke, and O. Anisiji, *Analysis of oil pipeline failures in the oil and gas industries in the Niger delta area of Nigeria,* Hong Kong (2012).

[6] C. Gomez and D. Green, *Small-scale airborne platforms for oil and gas pipeline monitoring and mapping,* University of Aberdeen (2005).

[7] J. Wilson, *Worldwide uav roundup,* AIAA, American Institute of Aeronautics and Astronautics (2013).

[8] R. Austin, *Unmanned aircraft systems: UAVs design, development and deployment* (John Wiley and Sons Ldt., 2010).

[9] J. Gundlach, *Designing unmanned aircraft systems a comprehensive approach* (Reston, 2012).

[10] N. Xue, *Design and optimization of lithium-ion batteries for electric-vehicle applications,* University of Michigan (2014).

[11] S. Beuselinck, *Exploration of the potential of civil unmanned aerial vehicles powered by micro gas turbine propulsion system,* Delft University of Technology (2015).

[12] P. Pilavachi, *Mini- and micro-gas turbines for combined heat and power,* Applied thermal engineering (2002).

[13] E. I. H. Tan and W. Liou, *Microgas turbine engine characteristics using biofuels,* Western Michigan University **Volume 5** (2011).

[14] C.Rodgers, *Turbofan design options for mini uav's,* AIAA (2001).

[15] K. Williams, *A summary of unmanned aircraft accident/incident data: Human factors implications,* Federal Aviation Administration (2004).

[16] *2014 statistical summary of commercial jet airplane accidents,* Boeing (2015).

[17] W. Crowther, *Perched landing and take-off for fixed wing uavs,* Applied Vehicle Technology Symposium (2000).

[18] J. A. Schetz, *Designing unmanned aircraft systems:a comprehensive approach,* Virginia Polytechnic Institute and State University (2015).

[19] A. J. Chaput, *Aircraft design resources - air vehicle geometry,* University of Southampton (2003).

[20] C. Gomez and D. R. Green, *Small-scale airborne platforms for oil and gas pipeline monitoring and mapping,* University of Aberdeen .

[21] M. Toyoshima, *Trends in satellite communications and the role of optical free-space communications,* The Optical Socitety (2005).

[22] G. S. Dieter Hausamann, Werner Zirnig, *Monitoring of gas transmission pipelines – a customer driven civil uav application,* German Aerospace Center (DLR) (2015).

[23] P. L. Robin Higgons, *Unmanned aerial vehicles,* Qi3 Insight (2014).

[24] A. S. de Joode, *Pipeline leak detection and theft detection using rarefaction waves - 6th pipeline technology conference,* ATMOS (2011).

[25] Civil Aviation Safety Authority Australia, *Part 101 unmanned aircraft and rocket operations,* (1988).

[26] Civil Aviation Safety Authority Australia, *Unmanned aircraft and rockets: Unmanned aerial vehicle (auv) operations, design specification, maintenance and training of human resources,* (2002), advisory Circular AC 101-1(0).

[27] Civil Aviation Safety Authority Australia, *Design standards: Unmanned aerial vehicles- aeroplanes,* (2010), version 2.2.

[28] I. C. A. Organization, *Unmanned aircraft systems (uas),* (2011), circular 328.

[29] L. Broers, *Engineering for sustainable development: Guiding principles,* The Royal Academy of Engineering (2005).

[30] M. Pini, *SCULPTUR: Surveillance Civil UAV Led by Propeller-based Gas Turbines* (Delft University of Technology, 2016).

[31] R. Austin, *Unmanned aircraft systems* (John Wiley & Sons Ltd, 2010).

[32] M. P. Huerta, *Integration of Civil Unmanned Aircraft Systems (UAS) in the National Airspace System (NAS) Roadmap* (U.S. Department of Transportation, 2013).

[33] R. Clothier, *The safety risk management of unmanned aircraft system,* RMIT University (2015).

[34] R. Curran and W. Verhagen, *AE3221-I Systems Engineering and Aerospace Design - Lecture 8 - Risk Management & Reliability* (TU Delft Aerospace Engineering, 2015).

[35] E. Mooij and Z. Papp, *Simulation, verication and validation - lecture notes,* Delft University of Technology (2014).

[36] J. Vanderover and K. Visser, *Analysis of a contra-rotating propeller driven transport aircraft,* .

[37] Ascent Vision, *CM202 brochure,* Ascent Vision (2008).

[38] J. Melkert, R. Vos, and T. Zandbergen, *AE211-II Aerospace Design & Systems Engineering Elements Course slides lecture 2* (Delft University of Technology, 2015).

[39] R. Vos, *AE1222-II Aerospace Design & Systems Engineering Elements,* (2013).

[40] D. P. Raymer, *Aircraft Design: A Conceptul Approach* (American Institute of Aeronautics and Astronautics, 1992).

[41] N. Timmer, *Ae2111-i systems design,* (2014).

[42] S. Gudmunsson, *General Aviation Aircraft Design: Applied Methods and Procedures* (Elsevier, 2014).

[43] W. R. Donovan, *The Design of an Uninhabited Air Vehicle for Remote Sensing in the Cryosphere* (University of Kansas, 2007).

[44] E. Gill, *AE3221-I Systems Engineering and Aerospace Design - Extra 2 - Design of Unconventional Solutions for Stability and Control (V-tail, Canard)* (TU Delft Aerospace Engineering, 2015).

[45] J.A. Mulder, W.H.J.J. van Staveren, J.C. van der Vaart, E. de Weerdt, C.C. de Visser, A.C. in 't Veld and E. Mooij, *Flight Dynamics Lecture Notes* (Delft University of Technology, 2013).

[46] M. H. Sadraey, *Aircraft Design: A Systems Engineering Approach* (Wiley, 2012).

[47] J. Roskam, *Airplane Design* (Roskam Aviation and Engineering Corp., 1985).

[48] A. Jha, *Landing gear layout design for unmanned aerial vehicle,* (2009), (Visited on 05/17/2016).

[49] *Global Aviation Tires* (Goodyear-aviation, 2015) (Visited on 05/18/2016).

[50] J. Bennett, *Fault Tolerant Electromechanical Actuators for Aircraft* (Newcastle University, 2010).

[51] S. Boughcum, J. Begin, and e. a. F. Franko, *Aircraft emissions: Current inventories and future scenarios,* University of Pensylvania (1999).

[52] G. A. M. Association, *General aviation: Statistical databook & industry outlook,* Federal Aviation Administration (2010).

[53] T.Ford, *Engine vibration analysis,* Aircraft Engineering and Aerospace Technology, Vol. 69 Iss 2 pp. 126 - 128 (1997).

[54] M. Levit and Y.A.Kolosov, *Eliminating aircraft engine vibrations,* (1961).

[55] W. Visser, *Gas Turbines, Propulsion and Power: AE2203* (TU Delft, 2011) first Edition.

[56] S. Spearing, *Materials selection, modelling and mechanical design,* University of Southampton (2005).

[57] S.Tin and T.M.Pollock, *Nickel-based superalloys for blade application: Production, performance and application,* Encyclopedia of Aerospace Engineering (2010).

[58] R. V. den Breambussche, *Mirco gas turbines - a short survey of design problems,* Micro gas turbines (2005).

[59] A. Head, *Conceptual Design and Simulation of a Microturbine* (The University of Queensland, 2011).

[60] Pilatus, *PC-7(PWC PT6A-25A) Technician Training Manual* (Pilatus, 2015).

[61] H.Gavel, *On aircraft fuel systems: Conceptual design and modeling,* (2007).

[62] R. Langton, C. Clark, M. Hewitt, and L. Richards, *Aircraft Fuel Systems* (Wiley, 2009).

[63] V. Bites, *Basic technical information turboprop engine tp-100,* (2014), (Visited on 05/19/2016).

[64] G. aviation CZECH s.r.o, *Installation Manuel Walter M601E Turboprop Engine* (GE Aviation, 2008).

[65] Informal South Pacific Air Trafic Services Coordinating Group, *Fans-1/a datalink communications environment,* (2008).

[66] J. B. Masferrer, D. C. Vuilleumier, and J. Cherkaoui, *Satellite-uav cooperative missions: Status and outlook,* ESTEC (2009).

[67] Leon W. Couch II, *Digital and Analog Communication Systems* (Pearson Education Limited, 2013).

[68] G. Cuypers, *Noise in satellite links,* Katholieke Universiteit Leuven (2001).

[69] A. DS, *x-band brochure,* Airbus Defense Systems (2014).

[70] *Blackray 1000 satcom solution for uav / uas - specification sheet,* Gilat Satellite Networks (2014).

[71] E. Gill, *AE3221-I Systems Engineering and Aerospace Design - Lecture 2 - Systems Engineering Methods* (TU Delft Aerospace Engineering, 2015).

[72] G. L. Rocca, *Weight estimation and iterations in a/c design aircraft balance,* (2016), aE2111-II, Delft University of Technology.

[73] H. Ribner, *Formulas for propellers in yaw and charts of the side-force derivative,* Technical report, NACA Report 820 (1945).

[74] D. Hoak and J. Carlson, *USAF Stability and Control Handbook* (Douglas Aircraft Company Inc., 1960).

[75] W.H. Michael Jr., *Analysis of the effects of wing interference on the tail contributions to the rolling derivatives,* Technical report, NACA Report 1086 (1952).

[76] M. Sadraey, *Aircraft Design: A Systems Engineering Approach* (Wiley Publications, 2012).

[77] J. Grasmeyer, *Stability and control derivative estimation and engine-out analysis,* Virginia Polytechnic Institute and State University (1998).

[78] J. Roskam, *Airplane Design, Part VI: Premliminary calculation of aerodynamic, thrust and power characteristics* (Roskam Aviation and Engineering Corp., 1987).

[79] J. Roskam, *Airplane Design, Part VIII: Airplane Cost Estimation: Design, Development, Manufacturing, and Operating* (Roskam Aviation and Engineering Corp., 1990).

[80] A. Deperrois, *Analysis tools for airfoils, wings and planes* (GNU General Public License, 2007 - 2016).

[81] J. Anderson, *Fundamentals of Aerodynamics* (McGraw-Hill, 2001).

[82] *GSP 11 User Manual* (National Aerospace Laboratory NLR, 2016).

[83] C. Rodgers, *25-5 kWe microturbine design aspects,* ASME TURBOEXPO 2000-GT-0626 (2000).

[84] R. Braembussche, *Micro gas turbines - a short survey of design problems,* Karman Institute for Fluid Dynamics (2005).

[85] *Parametric specific fuel consumption analysis of the pw120a turboprop engine,* Specific Range Solutions Ltd. : SRS-TSD-002 (2009).

[86] *Know your pt6a turboprop,* Pratt & Whitney Canada (Visited on 05/19/2016).

[87] R. Tuccillo and M. C. Cameretti, *Combustion and Combustors for MGT Applications* (Universita di Napoli).

[88] CAST, *Introduction to Turboprop Engine Types* (2011).

[89] N. Lambert, *Study of hydrogenation derived renewable diesel as a renewable fuel option in north america,* Eco Resources Consultants (2012).

[90] *Engine performance and exhaust emissions from a diesel engine using soy bean oil biodiesel,* ASABE 084942 (2008).

[91] Y. Zhong, *Pollutant emissions from biodiesels in diesel engine tests and on-road tests,* University of Kansas (2012).

[92] *Biomass energy data book appendix a,* U.S. Department of Energy (2011).

[93] A. Munack and C. Pabst, *Lowering of the Boiling Curve of Biodiesel by Methathesis* (Fuels Joint Research Group, 2012).

[94] *Standard Worm Gear Speed Reducers* (Altra Industrial Motion, 2013).

[95] J. Mixson, G. Greene, and T. Dempsey, *General Aviation Aircraft Design: Applied Methods and Procedures* (NASA, 1981).

[96] A. P. Mouritz, *Introduction to aerospace materials* (Woodhead Publishing Limited, 2012).

[97] D. Hartman, *High strength glass fibres,* agy (1996).

[98] C. S. Grimmer and C. K. H. Dharan, *Journal of Materials Science* (2008).

[99] S. Pickering, *Recycling technologies for thermoset composite materials—current status,* The 2nd International Conference: Advanced Polymer Composites for Structural Applications in Construction (2006).

[100] S. U. Khana, A. Munirb, R. Hussainb, and J.-K. Kima, *Fatigue damage behaviors of carbon fiber-reinforced epoxy composites containing nanoclay,* Composites Science and Technology (2010).

[101] M. Roux, N. Eguéman, L. Giger, and C. Dransfeld, *High performance thermoplastic composite processing and recycling: From cradle to cradle,* Fachhochschule Nordwestschweiz and Institut für Kunststofftechnik (2010).

[102] A. YousefPour, M. Hojjati, and J. Immarigeon, *Fusion bonding/welding of thermoplastic composites,* Journal of Thermoplastic Composite Materials Vol.17 (2004).

[103] M. Wedekind, L. Khoun, P. Krempl, H. Baier, and P. Hubert, *Impact behavior of thin thermoplastic composites dependant on manufacturing parameters and layup,* Technische Universität München (2012).

[104] E. D. M. Field, *Structural Analysis and Design of Airplanes* (2005).

[105] N. Tai, C. Ma, and S. Wu, *Fatigue behaviour of carbon fibre/peek laminate composites,* Composites (2003).

[106] S. Gudmundsson, *General Aviation Aircraft Design - Applied methods and procedures* (Elsevier, 2014).

[107] J. Cherwonik, *Unmanned Aerial Vehicle System Acquisition Cost Estimating Methodology* (Technomics, 2004).

[108] R. Doganis, *Flying off course: The economics of international airlines,* (2015).

[109] J. Sinke, *AE3211-II production of aerospace systems,* Delft University of Technology (2016).

[110] R. Hamann and M. van Tooren, *SYSTEMS ENGINEERING AND TECHNICAL MANAGEMENT TECHNIQUES* (TU Delft, 2006).

[111] S. A. Cambone, *Unmanned aircraft systems roadmap* (Office of Secretary of Defence, 2005).

[112] G. J. van Busse, *Maintenance concepts and maintenance activities* - (AE3512 Asset Management TU Delft Aerospace Engineering, 2015).

[113] G. Booch, J. Rumbaugh, and I. Jacobson, *The unified modeling language user guide,* Addison-Wesley Professional (2005).

[114] E. Murman, *Lean enterprise Value: Insights from MIT's Lean Aerospace Initiative* (Basingstoke: Palgrave, 2002).

[115] J. Sinke, *Lean Manufacturing, Chapter 10* (AE3211-II: Production of Aerospace Systems (Delft University of Technology), 2014).

[116] G. Schinner, J. Brandt, and H. Richter, *Recycling carbon-fiber-reinforced thermoplastic composites,* Journal of Thermoplastic Composite Materials Vol.9 (1996).

[117] F. L. Mantia, *Handbook of Plastics Recycling* (Rapra Technology Limited, 2002).

[118] E. Asmatulu, M. Overcash, and J. Twomey, *Recycling of aircraft: State of the art in 2011,* Journal of Industrial Engineering Volume 2013 (2013).

[119] M. Mitsuishi, K. Ueda, and F. Kimura, *Manufacturing Systems and Technologies for the New Frontier* (Springer, 2008).

A Requirement Compliance Matrix

After the design was completed a requirement compliance matrix was created to provide a final overview of the met requirements. Table A.1 shows all requirement identifiers together with a checkmark or cross in the column next to it. A checkmark indicates that the requirement has been met, a cross indicates that a requirement has not been met. The requirement belonging to each identifier can be found in Section 3.5.

Table A.1: Compliance matrix

Requirements	Compliance	Requirements	Compliance
Performance		**Sustainability**	
SCULPTUR-SH-01	✓	SCULPTUR-SH-20	✓
SCULPTUR-SH-02	✓	SCULPTUR-SUST-SH20-1	✓
SCULPTUR-SH-03	✓	SCULPTUR-SUST-SH20-2	✓
SCULPTUR-SH-04	✓	SCULPTUR-SH-21	×
SCULPTUR-SH-05	✓	SCULPTUR-SUST-SH21-1	×
SCULPTUR-SH-06	✓	SCULPTUR-SH-22	×
SCULPTUR-SH-07	✓	SCULPTUR-SUST-SH22-1	×
SCULPTUR-SH-08	✓	SCULPTUR-SH-23	✓
SCULPTUR-PERF-SH08-1	✓	SCULPTUR-SH-24	✓
SCULPTUR-PERF-SH08-2	✓	**Ground Control**	
SCULPTUR-SH-09	✓	SCULPTUR-SH-25	✓
SCULPTUR-PERF-SH09-1	✓	SCULPTUR-GC-SH25-1	✓
SCULPTUR-SH-10	✓	SCULPTUR-GC-SH25-2	✓
SCULPTUR-SH-10-1	✓	SCULPTUR-GC-SH25-3	✓
SCULPTUR-SH-11	✓	SCULPTUR-GC-SH25-4	✓
SCULPTUR-SH-12	✓	SCULPTUR-SH-26	✓
SCULPTUR-PERF-SH12-1	✓	SCULPTUR-GC-SH26-1	✓
SCULPTUR-SH-13	✓	SCULPTUR-GC-SH26-2	✓
SCULPTUR-PERF-SH13-1	✓	SCULPTUR-GC-SH26-3	✓
SCULPTUR-SH-14	✓	SCULPTUR-GC-SH26-4	✓
SCULPTUR-PERF-SH14-1	✓	SCULPTUR-GC-SH26-5	✓
SCULPTUR-PERF-SH14-2	✓	SCULPTUR-SH-27	✓
SCULPTUR-PERF-SH14-3	✓	SCULPTUR-SH-28	✓
SCULPTUR-SH-15	×	SCULPTUR-SH-29	✓
SCULPTUR-SH-16	✓	SCULPTUR-SH-30	✓
SCULPTUR-SH-17	✓	SCULPTUR-GC-SH30-1	✓
SCULPTUR-PERF-SH17-1	✓	SCULPTUR-GC-SH30-2	✓
SCULPTUR-PERF-SH17-2	×	SCULPTUR-GC-SH30-3	✓
SCULPTUR-PERF-SH17-3	×	**Cost**	
Safety and Reliability		SCULPTURE-SH-31	✓
SCULPTUR-SH-18	✓	**Structure**	
SCULPTUR-SR-SH18-1	✓	SCULPTUR-SH-32	✓
SCULPTUR-SR-SH18-2	✓	SCULPTUR-SH-33	✓
SCULPTUR-SH-19	✓	SCULPTUR-SH-34	✓
		SCULPTUR-SH-35	✓

B Task Division

Table B.1: Task Division Final Report

Section	Student
Preface	Elias
Jury Summary	Bogdan, Elias
Summary	Thomas
1. Introduction	Elias, Lars
2. Exploration Study	
2.1. UAV Definition and Classification	Elias, Roos
2.2. Existing Energy Pipeline Surveillance Missions	Elias
2.3. Current UAV Market	Bogdan, Elias, Nikolay, Roos
2.4. Current Payload Market	Dirk, Elias, Lars, Thomas
2.5. SWOT Analysis	Bogdan, Elias
2.6. Outlook on UAV Technology	Bogdan
2.7. Prediction of Future UAV Market	Elias
3. Mission Definition & Design Strategy	
3.1. Mission Analysis	Elias
3.2. Functional Diagrams	Nikolay, Thomas
3.3. UAV Certification	Roos
3.4. Sustainability Strategy	Roos
3.5. Requirements	Bogdan, Rick, Roos
3.6. Risk Assessment	Bogdan, Lars, Nikolay
3.7. Verification & Validation Strategy	Bogdan
3.8. Initial Budget & Resources	Bogdan, Lars
4. UAV Design Methodologies and System Characteristics	
4.1. Conceptual Designs	Roos
4.2. Chosen Payload	Elias, Lars
4.3. Preliminary Class I Estimations	Bogdan, Rick
4.4. Preliminary Subsystem Design	Anna (.8), Bogdan (.1, .2), Dirk(.3, .4, .10), Lars(.6, .9, .10), Nikolay(.5), Roos (.7, .8)
4.5. Preliminary Class II Weight Estimation	Bogdan, Rick
5. UAV Analysis	
5.1. Performance Analysis	Rick
5.2. Stability & Control Analysis	Bogdan, Elias, Lars
5.3. Aerodynamic Analysis	Mirthe
5.4. Propulsion System Analysis	Anna (.5), Nikolay (.1, .2, .3), Roos (.4, .5)
5.5. Material Analysis	Anna, Thomas
5.6. Structural Analysis	Thomas
6. Budget Analysis	
6.1. Financial Analysis	Bogdan
6.2. Budgets & Resources	Bogdan
7. Operations and Logistics	
7.1. Operations and Logistic Concept Description	Thomas
7.2. Reliability, Availability, Maintainability & Safety	Anna, Mirthe
7.3. Software Layout	Rick
7.4. Hardware Layout	Rick
7.5. Data Handling	Elias, Lars, Thomas
7.6. Manufacturing, Assembly and Integration Plan	Anna
8. Final Design Summary	
8.1. Design Lay-Out	Thomas
8.2. System Characteristics	Bogdan, Thomas
9. Project Design and Future Development Strategy	
9.2. Project Design & Development Logic	Anna
9.2. Project Gantt Chart	Anna
10. Conclusion	Bogdan
11. Recommendations	Bogdan

C FUNCTIONAL BREAK-DOWN DIAGRAM

This appendix shows the second and third level activities of the functional break-down diagram. This is visualised by the top level, under which the second and third level are shown for this particular function. To have a complete functional break-down diagram, the top levels should all be connected to the "perform mission" block. Figure C.1 shows a detailed view of the first three functions of, figure C.2 shows the detailed view of the last three functions.

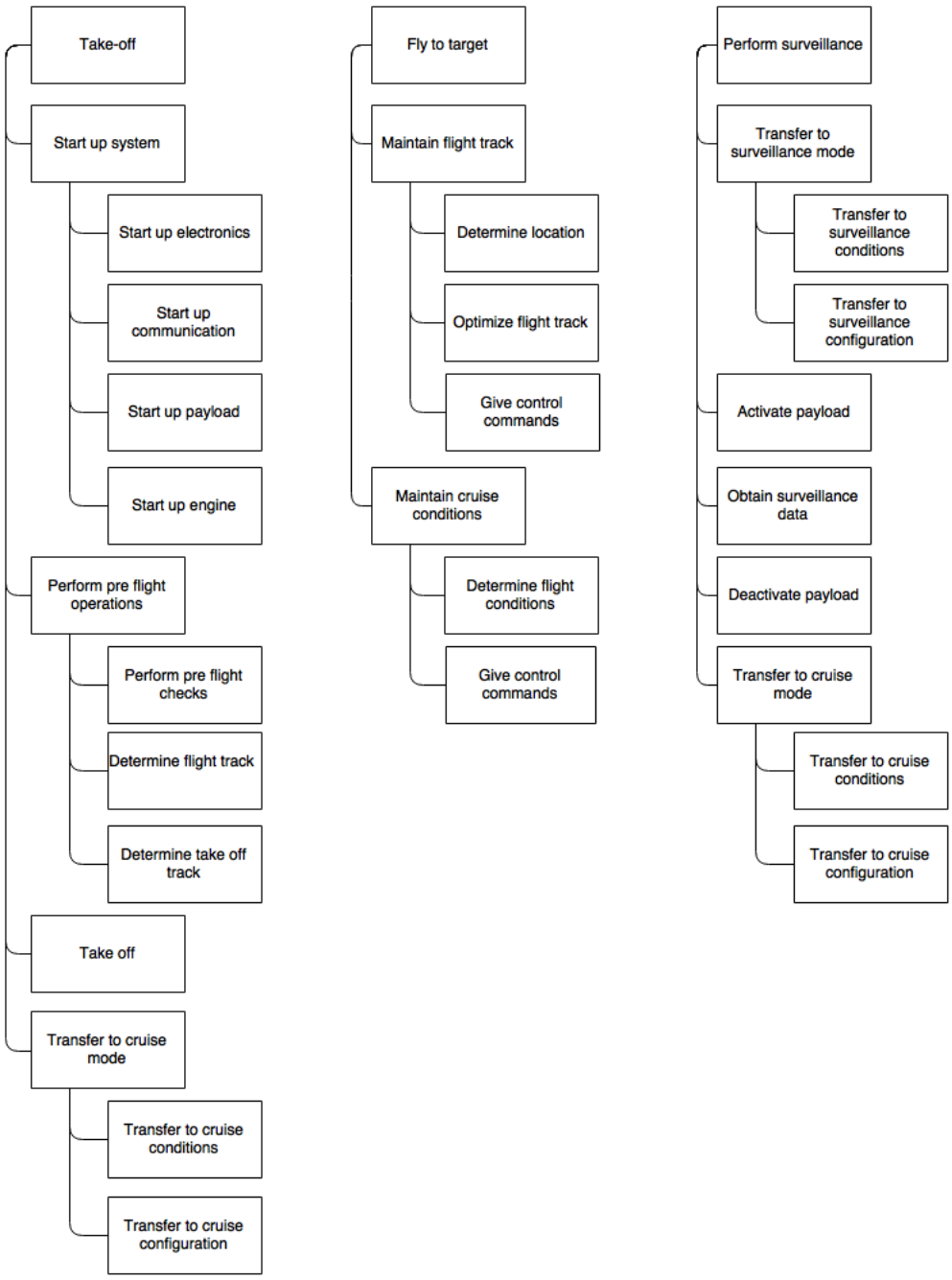

Figure C.1: Detailed View of first 3 functions from Functional Breakdown Diagram SCULPTUR

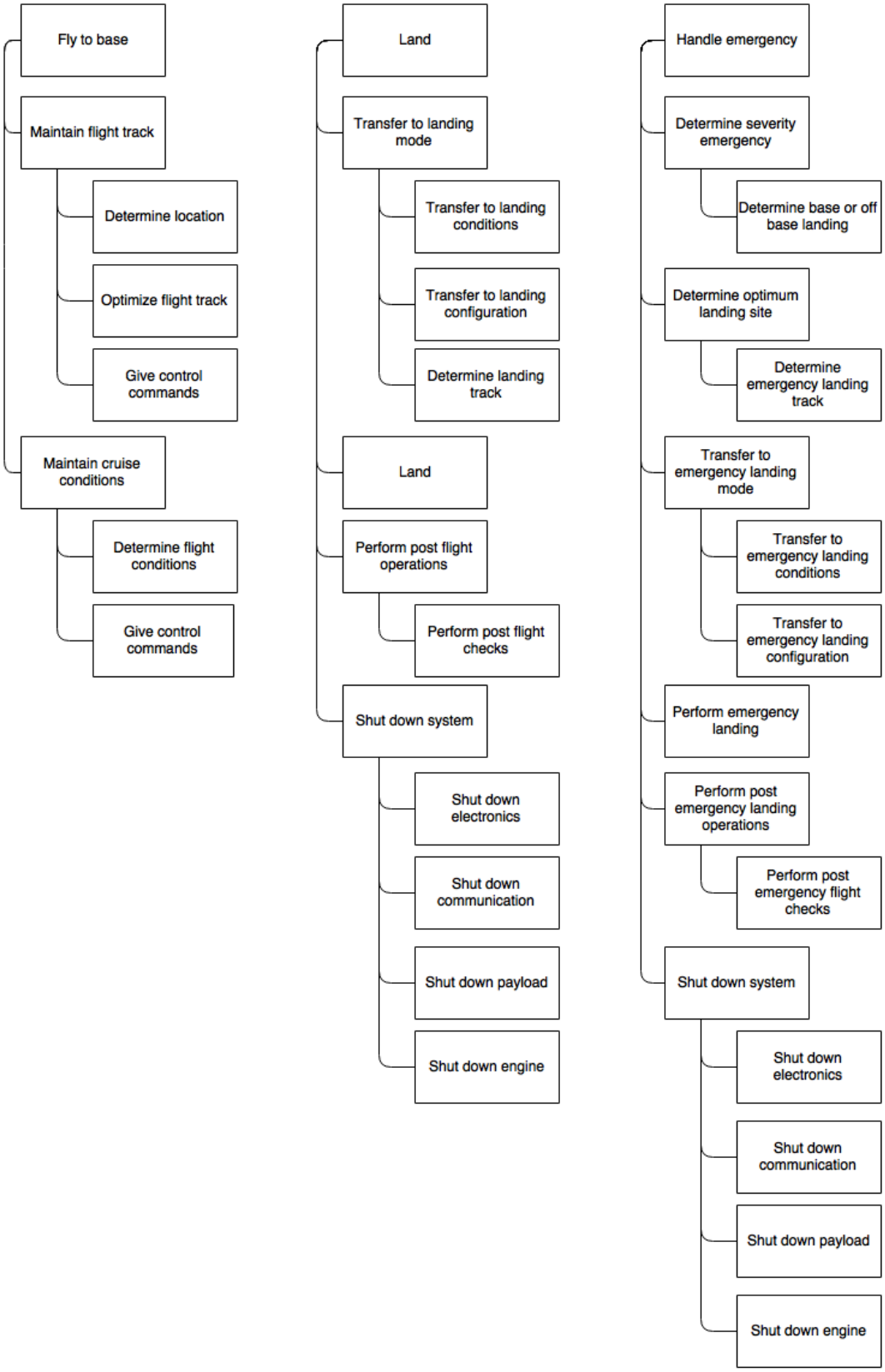

Figure C.2: Detailed View of last 3 functions from Breakdown Diagram SCULPTUR